UNIVERSITEIT VAN PRETORIA
UNIVERSITY OF PRETORIA
YUNIBESITHI YA PRETORIA

UNIVERSITEIT VAN PRETORIA
UNIVERSITY OF PRETORIA
YUNIBESITHI YA PRETORIA
Denkleiers • Leading Minds • Dikgopolo tša Dihlalefi

Energy optimisation for mine cooling systems through flow control

BY

WALDO BORNMAN

Thesis submitted in partial fulfilment of the requirements for the degree
PHILOSOPHIAE DOCTOR in Mechanical Engineering
in the
Faculty of Engineering, Built Environment and Information Technology

UNIVERSITY OF PRETORIA

Promoter: **Prof J Dirker (internal)**
Prof JP Meyer (internal)
Dr DC Arndt (external)

Date: **June 2017**

Publications resulting from this investigation:

Published journal articles:

W. Bornman, J. Dirker, D. C. Arndt and J. P. Meyer, "Operational energy minimisation for forced draft, direct-contact bulk air cooling tower through a combination of forward and first-principle modelling, coupled with an optimisation platform," *Energy*, vol. 114, pp. 995–1006, 2016.

W. Bornman, J. Dirker, D. C. Arndt, and J. P. Meyer, "Integrated energy simulation of a deep level mine cooling system through a combination of forward and first-principle models applied to system-side parameters," *Applied Thermal Engineering*, vol. 123, pp. 1166–1180, 2017

Journal articles prepared for publication:

W. Bornman, J. Dirker, D. C. Arndt, and J. P. Meyer, "Deep level mine cooling system operational energy minimisation through an integrated simulation model coupled with an optimisation platform – Case Study," *Applied Energy*.

Conference proceedings:

W. Bornman, J. Dirker, D. C. Arndt, and J. P. Meyer, "Bulk air cooler energy optimisation through simulation coupled with an optimisation platform," *South African Conference on Computational and Applied Mechanics (SACAM)*, 2016.

Abstract

The mining sector in South Africa accounted for 14.3% of all electricity supplied by Eskom in 2016. Up to 25% of this energy was consumed by mine cooling systems, suggesting that more focus should be placed on the energy consumption of cooling systems. Notwithstanding previous significant reductions obtained through energy efficiency in mine cooling systems, it was found that the current initiatives were not necessarily optimised to achieve their full potential. Through a review, several variable-flow energy-saving strategies were identified in the literature with the objective of ultimate integrated optimisation.

In this semi-empirical investigation, an integrated simulation model was developed to fully quantify the overall cooling system's integrated energy consumption. This model was subsequently coupled to a commercial optimisation platform to arrive at a globally optimised system. The novelty of the current study lies in the development of a mathematically optimised mine cooling system which is not currently found in the literature.

The optimisation-friendly simulation model was constructed and verified through suitable component models and a component-based calibration process as a case study. For these verifications, modelling accuracies with root mean square of relative error (RMSRE) values between 0.0114 and 0.0651 were obtained. The components were subsequently coupled to form the integrated cooling system simulation model that was validated through a baseline simulation conducted on various isolated weekly datasets to confirm its integrity for simulation during and outside of the system calibration period. For these validations, RMSRE values in the range of 0.0362 to 0.0704 were obtained with average absolute error values between 2.44% and 4.61%. The baseline simulation validation was concluded with an hourly annual simulation that obtained an RMSRE value of 0.860 with an average absolute error of 6.22%.

During the case study, it was found that the use of an integrated optimised mine cooling system has the potential to reduce the total average annual energy consumption by roughly 18%. This translates to an annual energy saving of more than 7.1 GWh for the particular mine. Because the majority of underground mines in South Africa utilise similar cooling systems, the adoption of integrated mine cooling optimisation systems could result in significant reductions of energy consumption in this sector.

Acknowledgements

- I would like to thank God for affording met the opportunity to conduct the study.
- My wife, Sunél Bornman, for all her love and support throughout the study.
- My supervisors Dr Deon Arndt, Prof Jaco Dirker and Prof Josua Meyer for their guidance and insight.
- Kopanang Mine for making the cooling system data available for the purposes of this study.
- Frontline Systems Inc. for providing a student licence for its optimisation platform.
- All my friends and family who supported me during the time of the study.

Table of contents

Nomenclature

Symbol	Description	Unit
C	Loss coefficient	-
C_p	Specific heat capacity	J/kgK
D_h	Hydraulic diameter	m
f	Friction factor	-
g, C	Constraints	-
h	Specific enthalpy	J/kg
k	Flow admittance	m^4
L	Length	m
$\dot{m}$	Mass flow	kg/s
N	Dataset length	-
N	Fouling factor	m^2K/W
P	Pressure	Pa
$\dot{Q}$	Cooling	W
Q	Variable in Equation 14	
T	Temperature	°C
V	Velocity	m/s
$\dot{W}$	Work input	W

Greek letters

Symbol	Description	
Γ	Variable in Equation (7)	
β	Effective heat transfer coefficient	W/K
ζ	Variable in Equation (7)	
η	Efficiency	
ρ	Density	kg/m³
σ	Variable in Equation (17)	
ϕ	Variable in Equation (12)	

Subscripts and super-scripts

Symbol	Description
a	Air
AMB	Ambient
c	Cooling
calc	Calculated value
cond	Condenser
DB	Dry bulb
evap	Evaporator
ex	Excess
f	Fan
i	Inlet
j	Index number
L	Heat removal
min	Minimum
mine	Underground mine
n	Index number
o	Outlet
p	Pump
plant	Total integrated cooling plant
real	Measured value
ref	Refrigeration
s	Saturation
w	Water
WB	Wet bulb

Abbreviations

Abbreviation	Description
ASHRAE	American Society of Heating, Refrigeration and Air-Conditioning Engineers
BAC	Bulk air cooler
BLAST	Building load analysis and system analysis
CC	Cooling capacity
CCT	Condenser cooling tower
COP	Coefficient of performance
DOE	South African Department of Energy
HVAC	Heating ventilation and air conditioning
L/G	Liquid-to-gas
MS	Microsoft
NLP	Non-linear programming
NTU	number of transfer units
ODE	ordinary differential equation
OQNLP	OptQuest non-linear programming
PCT	Pre-cooling tower
RH	Relative humidity
RMSE	Root mean squared error
RMSRE	Root mean square of relative error
SCADA	Supervisory control and data acquisition
USD	United States Dollar
VBA	Visual Basic for Applications
VFD	Variable frequency drive

List of tables

List of figures

UNIVERSITEIT VAN PRETORIA
UNIVERSITY OF PRETORIA
YUNIBESITHI YA PRETORIA

1 Introduction

1.1 Background information

With the ever-increasing need and escalating cost of electrical energy, the necessity for energy-efficiency initiatives on the demand side rises, especially when there are restrictions on the supply side. The mining sector in South Africa accounted for 14.3% of all electrical energy supplied by Eskom (South Africa's electrical energy utility) in 2016, of which up to 25% is used by mine cooling systems [1, 2]. It is evident from the utility's electricity distribution results summary in Table 1 that the mining sector, with more than 1 000 customers, is among the largest consumers based on the percentage per customer scale [2].

Table 1: Eskom electricity sales distribution for 2016

	Percentage of total sales	Number of customers	Percentage per customer
Municipal	41.8%	801	0.052185%
Industrial	23.4%	2 733	0.008562%
Mining	14.3%	1 013	0.014116%
International	6.3%	11	0.572727%
Residential	5.6%	5 550 307	0.000001%
Commercial	4.7%	50 816	0.000092%
Agriculture	2.7%	82 450	0.000033%
Rail	1.2%	509	0.002358%

The mining industry is faced with a number of challenges. For instance, the energy required to extract a unit of gold from the earth increased by a factor of four from 1970 to 2001. This results from mines becoming deeper and more energy being required to process the higher weight of ore for each ton of gold mined due to, among other things, higher hoisting, milling and cooling energy consumptions [3, 4].

Many energy-saving initiatives have been studied. Some of these initiatives were successfully implemented in the mining industry and primarily comprised load-shifting and energy-efficiency strategies implemented on large energy-consuming equipment typically found on mines, including compressed air, dewatering and cooling systems [5-20]. Energy recovery has

also been implemented in the form of turbine systems, which became popular during the 1970s [21].

With the continued and growing strain on the energy utility and the high energy-consuming nature of the mining industry, every effort to realise additional energy savings in any of the previously implemented strategies or the suggestion of new strategies would be of valuable support to the sustainability of electricity in South Africa and elsewhere in the world. Energy savings achieved by controlling auxiliary equipment in mine cooling systems have been investigated [18, 19]. These cooling systems consist of surface refrigeration plants, which include pre-cooling towers, chillers, condenser cooling towers, bulk air coolers and all the associated pumps and fans.

Although some statements of optimisation were made, it appears that these statements merely suggest manual trial-and-error optimisation in which the system's operational parameters were varied to obtain a more energy-efficient operation of the cooling system. This was done as a manual iterative process for several iterations until acceptable energy-saving results were obtained. Du Plessis, Liebenberg and Mathews [18] and Bornman [19] suggest that the savings achieved by the mine's cooling systems were significant, although one cannot claim that the integrated optimal operation had been achieved with energy consumption minimised as the objective function.

It is important to consider the integrated cooling system by means of a simulation model. This allows one to observe the effect of energy consumption on the overall integrated cooling system when applying one strategy to a part of the system. It is therefore important to consider the complete, integrated cooling system when applying the optimisation in order for the global optimum set of parameters to be determined for each set of boundary conditions, instead of optimising each component of the system in isolation without interpreting its effect on the overall cooling system. It has been suggested that a slight increase in one component's energy consumption could realise a more significant energy reduction elsewhere in the system in some cases [22].

It is clear from these concluding remarks that there is an opportunity to investigate the possibility of determining the optimum energy-minimised operational parameters for the integrated cooling system. Although many models and energy improvements have been considered and implemented before, none were found where the integrated mine cooling system's energy consumption was minimised.

If this minimisation is successfully achieved, these optimal parameters can be used to operate the mine's cooling system at its minimum energy consumption in real time, as the demand and other boundary conditions change dynamically, based on mining requirements and ambient climate conditions.

1.2 Problem statement

Many mine cooling system energy models have been considered in the past, but none of them simulated and quantified the complete integrated system on a component level. Therefore, it is necessary to construct a suitable integrated mine cooling system model that will simulate the cooling system on an integrated component basis to allow a holistic view of the system's behaviour and energy consumption to variations in the system's operational parameters.

Although several mine cooling system energy-saving initiatives were previously investigated and some implemented, they did not include the mathematical optimisation of an integrated cooling system to operate at its energy minimum for all permutations of demand and ambient conditions. It is therefore necessary to couple a suitable simulation model to an optimisation platform to minimise the total energy consumption of the system.

1.3 Research objectives

The following research objectives were identified:

- Investigate the state of the art relating to cooling system modelling and optimisation through an extensive literature review.
- Construct an integrated cooling system model based on several subcomponent models.

- Model the integrated cooling system of a deep level mine, as a case study, by combining the system models in such a way as to ensure easy optimisation application. This should be successfully incorporated while maintaining acceptable accuracy in comparison to the real system.
- Verify the case study simulation model through system calibrations on the subsystem components. The integrated simulation model will be validated through a baseline simulation in order to compare the simulation model with the current operation.
- Minimise the integrated cooling system energy while still meeting the cooling demand.
- Estimate the annual energy-saving potential that is realised by the integrated mine cooling system optimisation.

1.4 Methodology

Following from the problem statement and research objectives, in order to determine the possibility of arriving at a matrix of energy-minimised system operational parameters, the cooling system considered as a case study will be simulated by the various modelling methods and strategies available and presented in the literature. This simulation model will be compared to the measured data that was obtained from the mine to determine the model's accuracy and acceptability.

The optimisation-friendly simulation model will be coupled with a commercially available optimisation platform, which will optimise the boundary control variables of the cooling system in an integrated fashion in order to arrive at the energy-minimised matrix of operational parameters for an entire year if feasible.

These parameters along with the simulation model by which they are optimised, will be used to determine the system output at the energy-minimised operation, while ensuring that the demand requirements are still met and that the optimisation yields acceptable output results.

Finally, the optimised energy consumption of the system will be compared to the system's measured performance at current operating conditions to determine the energy savings that can be achieved by implementing the optimisation to the system.

The study's hypothesis is therefore summarised as: **Determining the energy minimum operational system parameters with an integrated system simulation and corresponding optimisation**.

1.5 Delineation and limitations

Annual optimised results will only consider hourly time steps due to computing power limitations. This can be refined for practical applications with increased computing power. To investigate the effect of refined time-step optimisations, weekly models for shorter time steps will be considered and the results will be compared to those of the hourly model to determine whether the hourly model is acceptable to predict the annual saving potential.

Only one commercially available optimisation software package, for which a research licence was made available to the author, will be considered for this study. The global optimisation of this package will be verified to ensure that the proposed results yield global optimal solutions inside the defined constraints.

Only simulation and optimisation solutions obtained inside the practical operational boundaries of the system equipment, which will form part of the optimisation constraints, will be considered. The simulation model's calibration and verification will only be considered for one dataset.

Only Kopanang Mine, which gave the author permission to use its system data for research purposes, will be considered as a case study.

This study will only consider surface mine cooling systems. Only plant-level cooling system components will be considered, and the study will therefore not include any further downstream demand equipment, such as spot coolers, drills, dewatering pumps and energy-recovery devices.

Only the thermal performance effects due to the change of flow and other operational parameters of the system will be considered for the cooling machines and cooling towers,

including their associated auxiliary equipment, such as pumps and fans, in order to obtain the impact on the energy consumption for variations in the parameters. Internal machine or tower components, such as compressor efficiency and expansion valve performance, will not be considered. Rather, the total performance of the machine or component will be considered, as this is what the study investigates. Pump and fan power consumption and subsequent model calibration will only be based on name plate design information as these parameters are not individually logged. For this reason, only plant level power data will be compared for the purposes of the integrated simulation model verification.

1.6 Overview of the thesis

The thesis commences in Chapter 1 with an introduction of mine energy consumption and a brief overview of energy-saving initiatives that have been implemented before. The problem statement, research objectives, methodology, as well as the delineation and limitations, are also presented. An investigation into the state of the art relating to mine cooling system simulation and optimisation is considered as part of the literature review in Chapter 2. The mine cooling system that is considered to form the research instrument as a case study is introduced in Chapter 3. Subsystem models are also developed for the primary energy-consuming equipment of the cooling system. These models are calibrated according to the mine's cooling system under consideration and verified against measured data. The baseline simulation and validation results of the case study are presented in Chapter 4 for various sets of measured data in order to determine the simulation accuracy and robustness inside and outside of the model training data. The case study optimisation results in Chapter 5 commence with a validation of the optimisation platform used before the optimisation results are presented. Chapter 6 summarises the conclusions drawn from the study by consolidating the mine cooling system and energy-saving potential that were identified. This chapter includes recommendations for further investigation. The thesis is concluded with appendixes A and B, which contain alternative coefficient of performance models for chillers in Appendix A, and additional figures in Appendix B that have been obtained as part of the results presented in Chapter 5.

2 Literature review

2.1 Preamble

Mine cooling systems contribute significantly to the overall mine energy consumption as shown earlier. This chapter reviews and discusses typical deep-level mine cooling systems. The development of an integrated energy optimisation approach is supported by reviewing the state of the art through the investigation of relevant existing systems and strategies implemented previously. Subsequently, potential energy-saving opportunities are identified based on the energy consumption behaviour of the major components of a typical mine cooling system.

As the current study's intention is to arrive at an energy-minimised cooling system through integrated optimisation applied to a simulation model, it is beneficial to briefly provide background on mathematical optimisation, its limitations and suitable platforms that are available. A section on optimisation is therefore included in the literature review.

2.2 Typical mine cooling system layout and components

The early development of mine cooling systems commonly consisted of underground systems, comprising chillers, cooling towers and air coolers. These systems require the rejected heat to be removed through the ventilation system [23]. The limited heat rejection potential via the ventilation system leads to more frequent use of surface cooling systems over time. The primary requirement for cooling systems in the deep-level mining industry is to provide safe underground working conditions for miners through sufficient mine ventilation and air conditioning. Mines exceeding depths of 2 500 m to 3 000 m reaches the critical ventilation depth and rely completely on the air conditioning system to remove heat [24]. Below these depths, virgin rock temperatures could reach more than 70 °C [25]. Further requirements for mine cooling systems include chilled water for drilling machine cooling, dust suppression and underground spot coolers [26].

Each mine cooling system is unique in its design, based on the specific mine's requirements. These systems are governed primarily by the mine depth, underground temperatures and the

scale of mining operations. Mine cooling systems that operate with vapour compression refrigeration cycles date back to the 1920s when they were used in mines such as the Morro Velho mine in Brazil [23]. Further methods of air cooling were implemented in deep-level gold mines in South Africa and India during the 1930s. Significant increases in installed cooling capacity on mine cooling systems were seen in the 1960s.

Typical mine cooling systems are operated by refrigerating process water through the chiller machines to produce chilled water from where it is distributed to the air conditioning units, as well as to the process components that require cooling. The design of these cooling systems has not changed substantially since they were introduced in the 1960s [22]. Mine surface cooling systems are installed as fundamental parts of typical semi-closed loop water reticulation systems [27]. Figure 1 gives a schematic representation of a typical deep-level mine surface cooling system. These systems comprise installed cooling capacities of up to 30 MW*c*, with the electrical energy consumption of individual components ranging between 25 kW and 3.5 MW, although it is most commonly around 1 MW [7].

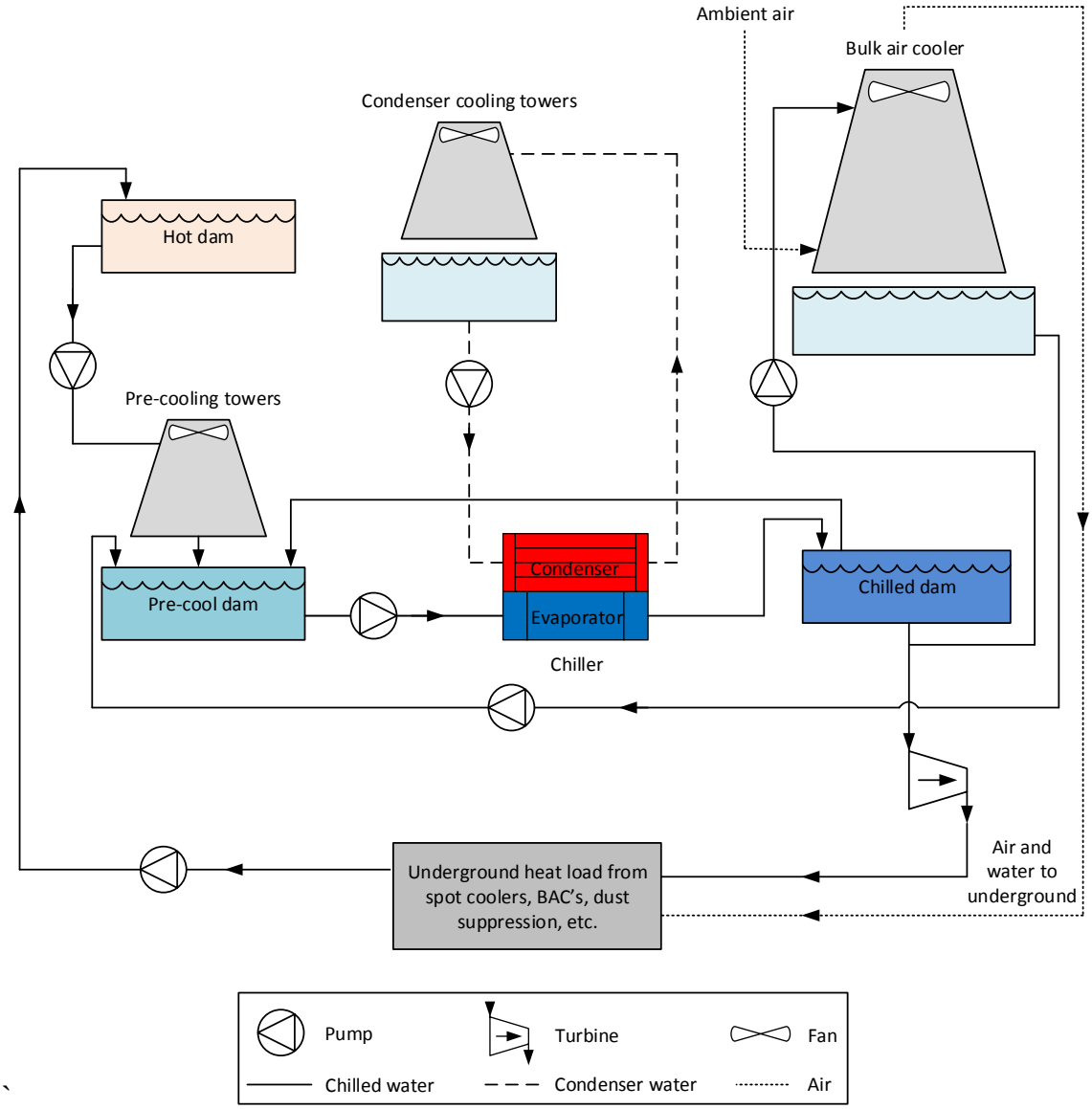

Figure 1: Typical surface mine cooling and chilled water supply schematic layout

In a typical surface mine cooling system accumulated hot water in underground hot-water dams, with temperatures ranging between 25 °C and 35 °C, is pumped to the surface hot-water dam [19, 22]. From there, the water is usually circulated through direct-contact pre-cooling towers into the pre-cooled dam, which reduces the hot-water temperature to just above the ambient wet bulb temperature [27].

Pre-cooled water entering the evaporator at around 14 °C, depending on the pre-cooling tower performance, ambient conditions and the specific system configuration used, is cooled to

chilled-water temperatures of between 2 °C and 6 °C, depending on the application, by pumping it through the chiller evaporator and into the chilled-water dam. Generally, there are arrangements of multiple chillers to satisfy the substantial cooling loads and allow fractional cooling loads for annual climatic changes [28]. Chilled water is supplied to the various end users, as described earlier, from the chilled-water dam. The use of a chilled-water dam allows the storage of chilled water to enable the system to satisfy the intermittent demand for chilled water, while the chillers could run more continuously instead of cycling on and off according to the demand, as these are traditionally operated at constant evaporator water flow rates [22]. This method of operation calls for the recirculation or back-passing of some of the chilled water back to the pre-cooled dam, as shown in Figure 1, in order to maintain chilled-water dam levels and an overall system balance.

A portion of the chilled water is used to cool and dehumidify ambient air through the bulk air cooler (BAC) [1]. The conditioned air, typically at around 7 °C wet bulb, is circulated through the mine along with the main ventilation fan. The return water from the BAC outlet is recirculated to the cooling system by introducing it between the hot-water dam and the chiller evaporators, where it performs additional pre-cooling.

The remainder of the chilled water is sent underground as required by various end consumers which include spot coolers, dust suppression and rock drill cooling, as stated earlier. This is typically controlled by means of actuated valves controlling the flow. The water demand of a typical deep-level mine ranges between 200 kg/s to 600 kg/s depending on the specific operational requirements.

The high static pressure of water reaching various levels of the mine underground, due to the potential energy of supplying it from the surface, has to be overcome [23]. This is most frequently achieved through energy-recovery devices, including turbines, hydro-lift systems or pressure-reducing valves. The latter has the downside that no energy is recovered and the cooling capacity of the water is compromised, as some energy is added to the water, which increases the temperature of the chilled water.

Heat rejection from the cooling system is achieved through direct-contact condenser cooling towers that eject the heat extracted from the chilled water to the ambient air. The condenser cooling towers are typically designed to allow a 5 °C to 7 °C condenser temperature differential [22].

From the cooling system operation discussed and shown in Figure 1, it can be determined that the cooling system consists of the following major components: chillers and cooling towers, comprising pre-cooling towers, bulk air-cooling towers and condenser cooling towers, as well as pumps and fans. Each of these major components will be discussed in more detail below.

Other component configurations and system integrations with series and parallel chillers and multiple chilled-water dams are also employed and summarised in literature but are not discussed in length here, as the strategies considered and examined in this study could be adapted for integration into these systems, although this falls outside the scope of this study [22].

2.2.1 Chillers

The most commonly used chillers in the mining industry are water-cooled vapour compression chiller machines [23, 28]. This is based on the principle that a boiling liquid remains at the same temperature if the pressure is maintained. If the pressure is increased additional heat would be required to vaporise the liquid. Transporting a pressurised vapour to another environment where it can be condensed allows the heat to be rejected through condensation. Finally, reducing the pressure of the high-pressure condensed liquid causes it to extract heat from its surroundings to create a cooling effect. Figure 2 shows the basic components of the vapour compression refrigeration cycle.

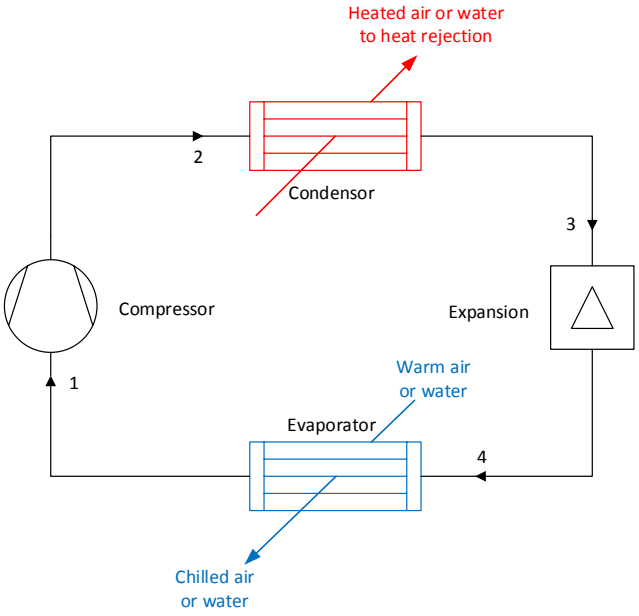

Figure 2: Basic components of a simple vapour compression chiller machine

From Figure 2, the basic components of a typical chiller can be identified as the evaporator, compressor, condenser and expansion valve. The evaporator and condenser on mine chillers are most commonly shell and tube heat exchangers where the refrigerant is circulated inside the shell and externally to the tubes, while the liquid to be cooled or heated flows through the tubes [29]. The heat extraction produced by the evaporation of the refrigerant results in heat flowing from the water inside the tubes to the refrigerant in the evaporator shell. Contrariwise, the heat from the high-temperature refrigerant inside the condenser shell is transferred to the cooling water of the condenser.

The compressor raises the refrigerant pressure after it is released from the evaporator through shaft input work, which is most frequently achieved by means of electrical motors. The compressor motor's power input is the largest single power-consuming part of the mine cooling system. Chiller compressors are commonly found in various arrangements, including reciprocating, screw and centrifugal, of which the latter is the most common in the mining industry due to the size of the units. The cycle's thermodynamics are revealed by the typical pressure enthalpy diagram, as shown in Figure 3.

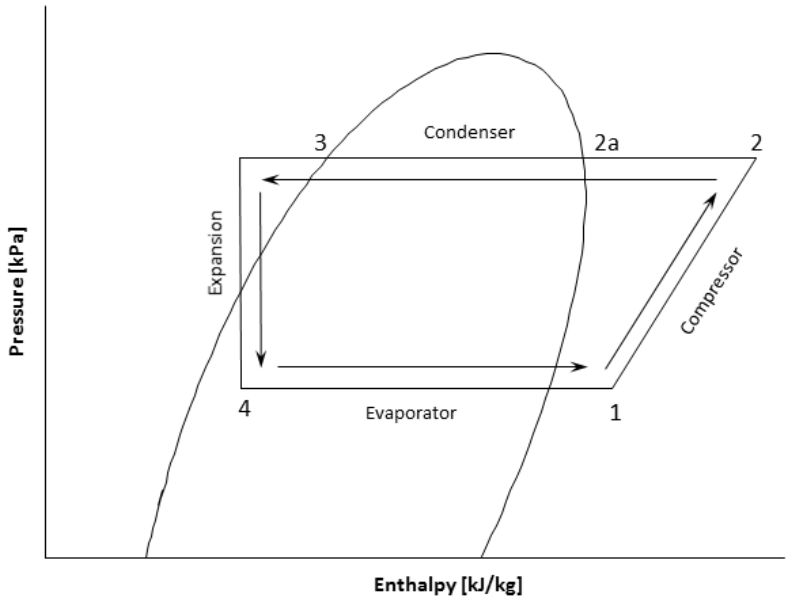

Figure 3: A pressure enthalpy diagram of a typical simple vapour compression refrigeration cycle

In Figure 3, the compressor raises the pressure of the superheated refrigerant, which also increases the temperature, as shown from point 1 to point 2. The high-temperature and high-pressure refrigerant then de-superheats from point 2 to point 2a and condenses at a constant pressure in the condenser, as indicated from point 2a to point 3. The high-pressure and lower-temperature condensed refrigerant then passes through the expansion valve, where the pressure reduces from point 3 to point 4, while it finally passes through the evaporator where it evaporates at a constant pressure, as indicated from point 4 to point 1 before entering the compressor again.

The amount of cooling performed by the chiller (or chiller cooling load) is commonly controlled by means of guide vanes integrated with the centrifugal compressor that controls the refrigerant's mass flow rate through the compressor [30]. Other means of capacity control are achieved via compressor speed reduction with variable frequency drives (VFDs) [31].

2.2.2 Cooling towers and bulk air coolers

Cooling towers are commonly used to pre-cool a deep-level mine's process water and to supply cooled water to the chiller condensers. BACs are used to cool ambient air for circulation

through the mine as stated earlier. Both operate on the same fundamental principles of heat and mass transfer between a wetter surface and an air stream. Depending on the operating conditions, the effect is to cool down the water or air [32, 33]. Both cooling towers and BACs can typically be forced-draught counter-flow devices where the air stream comes into direct contact with the water [23]. The electrical energy consumption of these devices primarily occurs through their fans, which typically consume energy between 25 kW and 120 kW [19]. A further indirect energy consideration for BACs would be the chilled-water consumption due to the significant cooling demand. Previous studies suggest that BACs could consume up to 50% of a typical deep-level mine's cooling capacity [26].

In a cooling tower, as shown in Figure 4, the water is distributed through the tower by means of spray nozzles at the top, while the water surface area is increased by means of splash bars or film fill materials. A fan at the top of the tower draws the ambient air through the tower introduced from the bottom, which is at a lower temperature than the cooling water for the pre-cooling tower, as well as condenser cooling applications [32]. For the BACs, ambient air is cooled by means of circulating chilled water in order to obtain acceptable air psychrometric conditions for underground mining.

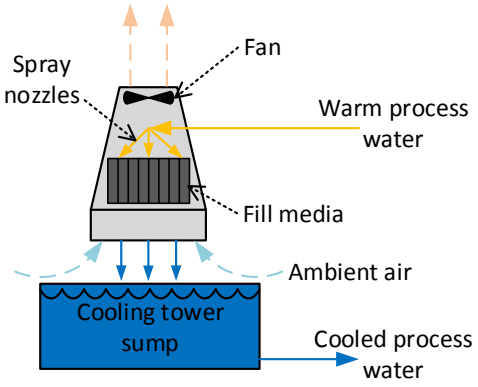

Figure 4: A schematic layout of a typical direct-contact forced-draught cooling tower

Through the operation of this type of cooling tower, a portion of the water is evaporated into the air stream because the moisture content of the air is not saturated at the water temperature. The evaporation process yields additional cooling as this process requires energy to change the state of the liquid to vapour whereby heat is transferred from the liquid [34].

The performance of a cooling tower depends on the water flow rate, water inlet and outlet temperatures, air flow rate, air inlet and outlet psychrometric state, as well as the power consumption of the pump and fan [14]. From these parameters, the performance of the cooling tower can be expressed in various ways including, including the range, which is the difference between the water inlet and outlet temperature, the approach, which is a represented by the difference between the water outlet temperature and the ambient wet bulb temperature, and the effectiveness, which is the ratio between the range and the ideal range. These parameters can be calculated by Equations (1) to (3) [22] respectively. Most commonly, only the waterside efficiency is considered, as the air outlet conditions are often not recorded. Therefore Equation (3) only considers the said efficiency.

$$Range = T_{w,i} - T_{w,o} \quad \textbf{(1)}$$

$$Approach = T_{w,o} - T_{a,i(WB)} \quad \textbf{(2)}$$

$$\eta_w = \frac{T_{w,i} - T_{w,o}}{T_{w,i} - T_{a,i(WB)}} \quad \textbf{(3)}$$

Another important cooling tower parameter to consider is the liquid-to-gas (L/G) ratio, which is the ratio of water-to-air mass flow rates. This ratio is typically determined during the cooling tower design, although seasonal variations call for adjustments and tuning in order to obtain the optimum effectiveness [14]. Variations of the L/G ratio and its limitations will be discussed in Section 2.5.

2.2.3 Energy-recovery devices

Energy-recovery devices could be summarised as devices that extract energy from a fluid [35]. Energy recovery is commonly done in deep-level mining where the potential energy of the chilled water supplied from the surface to underground is utilised to assist with the dewatering pumping energy required. The consumed chilled water, or return chilled water, is pumped back to the surface level for refrigeration. Although these systems are not considered as part of the

integrated energy considerations of this study, the basic working is included here for continuity of the basic layout and principles of the entire cooling system.

Two methods of energy recovery are commonly used in the mining industry. These include water-propelled turbines, as shown in Figure 1 and hydro-lift systems (also known as three-pipe systems) [36]. Various turbine arrangements yielded confirmed efficiencies between 40% and 54% previously, depending on the type of turbine and configuration used [37].

The hydro-lift system is shown in Figure 5. In this arrangement, the hot water is pushed out via valve arrangements and a chamber that allows the pressure of the chilled water to be sent underground to drive the hot water from underground to the surface level. This system's intermitted operation could be overcome by utilising three chambers, whereby a constant flow in both directions could be obtained, as would typically be the requirement for mining operations. Hydro-lift systems could typically reach an effectiveness of over 80%. The effectiveness of these systems consists of the product of the availability factor, utilisation factor, hydraulic efficiency, mechanical efficiency and thermodynamic efficiency of the system. The downfall of these systems is the significantly high capital cost and large space requirements [23].

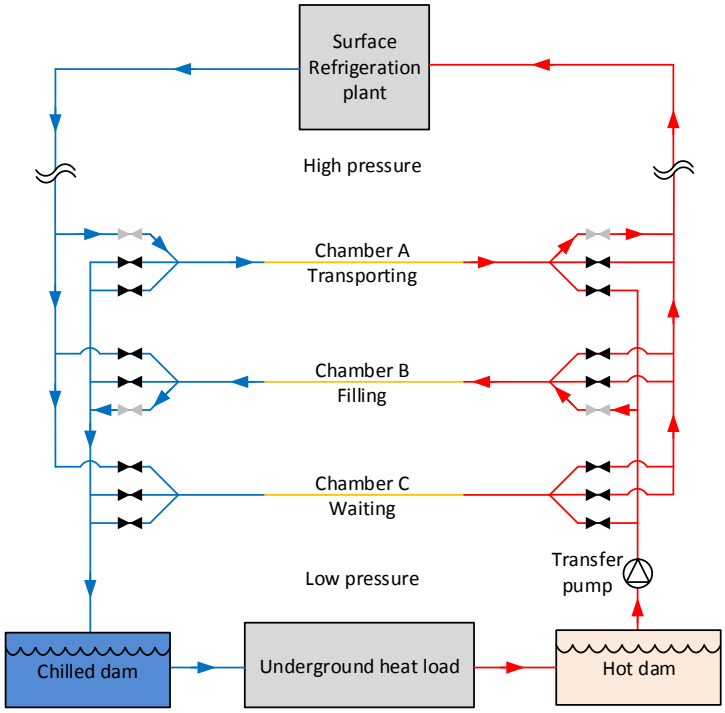

Figure 5: A mine cooling system with a surface refrigeration plant employing a typical hydro-lift energy-recovery device

2.2.4 Pumps and fans

As opposed to energy-recovery devices, pumps and fans add energy to a fluid [35]. In hydronic cooling systems pumps are employed to transport fluids throughout the system as can be seen in Figure 1. The most common pumps are those used to circulate water through the condensers, evaporators, cooling towers, secondary heat exchangers and other auxiliary equipment. These pumps typically range between 15 kW and 250 kW on mine cooling plants. Dewatering pumps are also included. However, these do not form part of the energy considerations of the current study, and are only mentioned for the continuity of the entire cooling system. These pumps could consume more than 4 MW due to the significant depths of some mines [7].

Of the various types of pumps, centrifugal pumps are employed most frequently for cooling and heating systems [38]. Pumps are selected based on the volume and pressure head that is required. Based on these parameters, the pump's power source (most commonly an electrical motor) could be selected at the appropriate size and power rating.

Fans are used to move air for various cooling system components, such as the cooling towers and BACs of large mine cooling systems. This is achieved through a power source that drives a rotating impeller, which performs work on the air, providing it with static and kinetic energy in various proportions, depending on the fan type. Large cooling towers for the cooling system are usually operated by means of axial fans that are driven by electrical motors. Similar to pumps, fans are selected based on the volume flow and pressure differential of the air that is required.

2.3 Existing energy-saving initiatives

A previously conducted review study reports on several energy-saving initiatives that have been implemented in the mining industry since the early 1970s [5]. Initiatives such as substituting air agitation with mechanical agitation, replacing air with oxidising compounds, physically covering process tanks to reduce heat losses and the implementation of heat recovery measures have been considered. Other initiatives, including preventative maintenance, reducing fuel spills, repairing air leaks, equipment scheduling and efficient lighting, were implemented during the late 1970s. By implementing heat recovery and compressed air reductions, energy savings of roughly 6% and 5% respectively were achieved in terms of total energy consumption for the mine.

Around the late 1990s various load-shifting initiatives were motivated by the introduction of Eskom's real-time pricing, whereby the energy tariff structure was varied according to supply and demand. A load-shifting initiative implemented on one of the South African deep-level mines' cooling and ventilation systems yielded load-shifting potential in the range of 13.5%, with an increase in the maximum load of 2.6% due to the requirement to cool and pump more water during off-peak times [6].

Mine dewatering pumps typically constitute around 14% of the mine's energy consumption. Load-shifting of the dewatering pumps was implemented and reductions of 65% were achieved during peak demand. An overall electricity reduction of 2% was suggested by the implementation of a new control strategy [7]. Operational cost reductions of 13% were achieved. Energy efficiency was achieved by installing control valves on the water supply lines

to each mining level, yielding a reduction in total water consumption, which resulted in a decrease in the dewatering pumping energy requirement as well as a reduction of the water cooling load requirements [8]. With the aid of investigations and feasibility studies conducted on five mines, an average energy-efficiency saving of 8.1% was suggested.

The use of turbines became popular during the 1970s. Most commonly, Pelton wheel turbines are used for these applications and the driving shaft can either be connected to an electrical generator or to a pump that can pump out water as the chilled water that is sent underground is directed through the turbine [21]. During the early 1990s, three-chamber pumps were introduced to the deep-level mining industry. Savings in the range of 15% to 20% on the dewatering pumping energy consumption were reported [21].

In addition to the methods already mentioned, it has been proposed that VFDs should be implemented on the main ventilation fans of deep-level mines in South Africa [9]. Savings of up to 20% were suggested through simulation on the airflow and cooling, while additional savings of between 2% and 4% were suggested on the clear-water pumping system at one of the mines examined, due to the reduced air flow. Another suggested method to implement fan energy savings is by replacing oversized fans with smaller fans based on the required air flow rates and by optimising the blade angles and rotary velocities [10]. These methods, which are called “hermit crab technologies” suggest energy savings of about 10% on the main ventilation fan system [11, 12].

An alternative study suggested a plausible 24% energy saving on auxiliary fans. This can be achieved by implementing fan efficiency initiatives, including fan blade angle, aerodynamic designs and motor efficiency improvements [13]. The same study suggests a saving potential of 30% on the main fans, although practical implementation has not confirmed this.

Another approach that has been considered is the use of energy-efficiency strategies involving cooling towers [14]. It is suggested that the correct cooling tower size should be determined before installation for the specific application as it is difficult to significantly alter the performance once it has been installed. An additional opportunity was suggested by considering the fill material used inside the cooling tower. Efficiencies of 85% to 92% could

be achieved on the fans when introducing optimum aerodynamic fibre-reinforced blades on the cooling tower fan, with energy savings reported in the range of 20% to 30%.

Energy-saving possibilities on compressed-air mine systems have been investigated where various initiatives, including compressor control by varying the inlet guide vane angle, compressor scheduling and prioritisation, repairing air leaks, as well as compressed air line control valves, were considered and implemented [15]. Load-shifting results between 22% and 26% were achieved, whereby the load was shifted outside the utility peak time [16, 17].

Lastly, further energy-efficiency strategies were identified for the mine refrigeration system whereby some of the auxiliary equipment of the cooling system including the evaporator, condenser, pre-cooling towers and BAC flows, were controlled to realise energy consumption at the cooling plant [18–20]. The replacement of a cooling tower was also included as part of one of the case studies, and presented significant energy reductions of around 25% on the cooling system [19]. All three these studies on cooling system flow control reported average savings of approximately 30% on the cooling system. One of the mines previously considered for flow control was used for the current case study to further investigate energy-efficiency opportunities through optimisation.

2.4 Cooling system modelling

In order to further reduce the energy consumption of mine cooling systems after typical energy considerations that had been implemented previously, a holistic view or integrated investigation of the system's major energy-consuming components would be required to quantify the contribution of each component to the energy reduction. To achieve this, an integrated simulation model would be required, whereby the complete cooling system can be modelled to determine the integrated effect on the system's energy consumption when one or more parameters of any combination of cooling system components vary.

The successful implementation of such an integrated model would facilitate the coupling with an optimisation platform to determine the overall energy minimum operational parameters of the entire system for any given set of climate and boundary demand conditions.

This section reviews previous work performed on cooling system modelling and optimisation. It further identifies the opportunity and subsequent novelty of the current study.

2.4.1 Cooling system models

Various models for cooling system component modelling were found in the literature, most of which only consider specific subsystem components and therefore do not provide a fully integrated system approach [20, 39–62]. Modelling refrigeration system components of large heating ventilation and air conditioning (HVAC) applications were also considered due to the similarities between the two systems that typically employ large vapour compression refrigeration machines. Romero, Navarro-Esbrí and Belman-Flores [41] used a black box modelling approach to determine the water outlet temperature of a HVAC cooling system when constant condenser conditions were assumed. The study states that the cooling capacity of a refrigeration machine changes as the inlet temperature varies, while the other parameters remain unchanged. It was reported that the quality of the model predictions were in the range of 68.5% to 76.3%.

Li, Li, Seem and Li [45] and Ali, Vukovic, Sahir and Fontanella [48] used the Modelica© modelling language-based dynamic simulation models for their cooling systems used in commercial buildings. Li *et al*. [45] only modelled the cooling tower while, Ali *et al*. [48] considered more components of the cooling system in addition to five variables as part of an optimisation, including the number of chillers and cooling towers in operation, building load demand, the temperature difference across the condenser, and the cooling tower fan speed. Li *et al*. [45] used the cooling tower fan speed as the control variable input into the optimisation controller, while the condenser water flow rate was assumed to be constant. Subsequently the chiller compressor and condenser cooling tower fan speed were used as the performance objectives. Both these studies reported significant energy-saving potential, although neither explicitly reported on the modelling accuracy.

Various studies used the TRNSYS© modelling tool as part of simulation-based optimisation approaches to model their cooling systems. Fong, Hanby and Chow [58] considered the chiller water inlet temperature set point and the supply air temperature set point as control variables

to achieve annual energy consumption savings of between 0.15% and 6.74% on HVAC systems. Here the TRNSYS© simulation was used as an optimisation tool and did not report on its simulation accuracy. Vakiloroaya, Khatibi, Ha and Samali [60] considered the cooling tower, cooling coil, evaporative cooling system and air-to-air heat exchanger as part of their HVAC model to achieve modelling accuracies where 24% of the predicted data deviated by more than 5% from the actual data. They reported a savings potential of 52% by replacing the central cooling plant with a hybrid evaporative cooling system. Chow, Fong, Chan, Yau, Au and Cheng [49] included water-cooled chillers, constant-speed primary chilled-water pumps, variable-speed secondary chilled-water pumps, heat exchangers and straight pipes as part of their model. Another study included refrigerant mass flow, chilled-water temperature and supply-air temperature as part of their control variables, while the cooling demand and ambient air dry bulb temperature were considered uncontrolled variables [51]. Their model achieved similar accuracies to the one presented by Vakiloroaya *et al*. [60].

Jing, Jiang, Wu, Tang and Hua. [54] considered steady-state chiller models where the start-up and shutdown transients were neglected along with a range of other system-simplifying assumptions to model the cooling system. The system consisted of a district cooling and heating facility for six residential homes. No report on the integrated simulation accuracy was found. However, correlations having coefficients of determination in the range of between 0.8 and 0.97 were obtained when various climatic zones were modelled.

Ding [55] and Afram and Janabi-Shari [40] reviewed various cooling-system modelling methods and concluded that simple component models should be considered. These models can then be integrated for larger cooling systems to achieve acceptable stability, rapidness and accuracy, as these parameters are often in conflict with each other when simulation models are attempted. Ding [55] states that many attempts have been made to improve these parameters in simulation applications, although the effects were not adequate, and therefore suggests that further research is required. Afram and Janabi-Shari [40] and Lee and Lu [39] categorised cooling-system modelling into three different categories: a data-driven (black box) approach, a physics-based (white box) approach and a grey box approach, which is a combination of the first two. Afram and Janabi-Shari [40] suggests that there is a trade-off between the white box and black box approaches: although the white box approach is more generic, accuracy is

reduced, and vice versa for the black box approach. Lee and Lu [39] advise that, although black box models are easier to set up, they cannot be used to extrapolate performance beyond the data range for which they were developed.

Mofet and Zmeureanu [61] propose two types of models as a benchmark, one of which is correlation based, while the other is an artificial neural network. These models were used to model the energy performance of water-cooled electric chillers. They achieved modelling accuracies with root mean squared error (*RMSE*) values below 7% for the remainder of the summer (the same summer used to train the model) and below 8% for the following summer. Their study suggests that the primary reason for the deterioration of the modelling accuracy when applying it to time spans further away from when the training data was collected is due to the cooling demand and ambient conditions being significantly different from those during the training period.

Du Plessis, Arndt and Mathews [20] modelled the effects of variable water flow on mine cooling systems by examining the impact of evaporator, condenser and BAC water flow rate adjustments. Although no quantification of the various system component models' accuracies were given, an integrated simulation accuracy with an average error of 4.1% on the modelled system energy consumption for one summer month was achieved. They also used the model as part of an energy-efficiency initiative whereby water flow rates were controlled to maintain chilled dam levels, as well as pre-determined temperature differences across the condenser. Furthermore, the BAC water flow was controlled linearly according to ambient climate fluctuations. The result suggested energy savings of 33% on the cooling system.

From the studies considered above, no component-based integrated energy simulation model, based on system-side parameters, has been constructed and quantified for a deep-level mine cooling system. The successful development of such a model would allow a holistic analysis of variations in any subcomponent's operational parameters and its effect on the integrated system's energy consumption. This would be of great value because the effects that alterations to one component would have on all the others are often not considered during the operation and maintenance of these systems. It would furthermore facilitate the possibility to couple such a model to an optimisation platform granting the opportunity to determine the overall

energy optimal operation of the integrated system for variations in demand and other uncontrollable external parameters.

2.4.2 Cooling tower models

The study and performance modelling of cooling towers (and BACs) are not novel, as various methods with several levels of accuracy and relevance have been proposed in the literature [14, 32, 63–94]. The first formally documented work in this field was done by Merkel in the early 19th century. Kloppers and Kröger [90] indicated that the Merkel, e-NTU (electronic number of transfer units) and Poppe methods are among the most popular models used to predict the performance of cooling towers. Although these models are extensively used in cooling tower design, they are not ideally suited for optimisation as they require iterative computation.

Khan, Qureshi and Zubair [81] highlight the importance of suitable variable selection when modelling cooling towers to ensure a transparent and robust model. They considered a sensitivity analysis and reported that the two most important parameters influencing the performance of counter-flow cooling tower design are the air inlet wet bulb temperature, $T_{a,i,wb,}$ and the water outlet temperature, $T_{w,o}$. These models were based on the steady-state energy and mass balance of incremental volume sections with the solution obtained through iterative computation with respect to the air humidity ratio and temperatures. These are also iterative in nature and are not ideal for optimisation purposes.

Various studies have considered part-load cooling tower operation. In some studies, the air flow rate was held constant and varying water flow rates were considered, while in other studies, the water flow rate was held constant and varying air flow rates were considered. The water-to-air mass flow ratio, $\dot{m}_w/\dot{m}_a$, also known as the liquid-to-gas ratio, has a significant effect on cooling tower performance. Söylemez [87] performed optimisation in terms of $\dot{m}_w/\dot{m}_a$ and found that the optimum ratio increased as the water inlet temperature increased. From this, it was suggested that the water mass flow rate be increased for locations with lower ambient pressures in order for $\dot{m}_w/\dot{m}_a$ to remain in the optimum range. The model used was based on the e-NTU method, which requires iterative computation. Lemouari, Boumaza and

Mujtaba [72] confirm that the cooling water range increases with an increase in the air flow rate, while it decreases with an increase in the water flow rate. They also conclude that the best water cooling is achieved with any combination of higher water inlet temperatures and lower water flow rates. Both these models were based on numerical methods, which also require iterative computation.

A paper by Pan, Shieh, Jang, Tseng, Wu and Ou [75] suggests that several of the existing non-linear cooling tower studies are black box approaches with limited transparency. Their study also considered methods comprising a data-driven approach of modelling the performance of cooling towers during regular operation. This is in contrast to the detailed methods described earlier, which require a large number of geometrical parameters to define the system. These may not always be available. Heidarinejad, Karami and Delfani [77] developed models that incorporate a detailed analysis of the various zones inside the cooling tower, namely the spray, fill and rain zones. Earlier modelling approaches often only considered the fill zone, while the consideration of adding the spray and rain zones yielded improvements of approximately 1.25% in the calculation error of determining the effective volume of a cooling tower. The model by Pan *et al*. [75] is based on a multi-model approach method by iterating and adding various local solutions in order to obtain a global solution. This modelling method is described in detail by Xue and Li [95]. The modelling approach by Heidarinejad *et al*. [77] is also based on the steady-state energy and mass balance of incremental volume sections similar to Khan *et al*. [81]. Therefore these models may be somewhat unsuitable for operational optimisation.

Chargui, Sammouda and Farhat [85] studied the effect of incorporating water loss due to evaporation and suggest that modelling, where the inlet and outlet water flow rate is assumed to remain constant, may incur errors in the range of 1 ºC in the water outlet temperature. They also found that between 1% and 4% of the water entering the cooling tower is lost through evaporation. The modelling method they used in their study was based on the e-NTU method, which, as stated earlier, would not be ideally suited for operational optimisation.

According to Wang, Shieh, Jang and Wu [78], the complex models constructed to model the various components of the cooling tower in refined detail are not always practical. Therefore, the research team suggests that the measured actual process data could reflect the actual process

parameters and performance with more ease and simplicity. The objective of the study was to develop a model with which the outlet water temperature, $T_{w,o}$, can be calculated in terms of variables that include the water inlet temperature, $T_{w,i}$, the inlet air psychrometric state and the water mass flow rate, $\dot{m}_w$. The model was therefore simplified and limited by neglecting air flow as a variable, since there was no air flow variance. Similar to Pan *et al*. [75], this model was also based on the multi-model modelling method described by Xue and Li [95] and therefore also requires iterative computation to obtain the solution.

Operational cost minimisation, where various optimisation algorithms were used to determine the optimum operational cost parameters of cooling systems and cooling towers, has previously been considered. Wei, Xu and Kusiak [96] considered optimisation models for a cooling system that included cooling towers with the objective of minimising the total cost of the chilled-water plant. The results obtained suggested energy savings of 14%. Unfortunately, the individual components' contributions to the savings were not quantified. The cooling tower used as part of their study was based on a model presented by Fisenko, Petruchik and Solodukhin [97], which states that the model consists of nine ordinary differential equations, which would also require iterative computation. Serna-González, Ponce-Ortega and Jiménez-Gutiérrez [70] suggested using Merkel's method, while Rubio-Castro, Serna-González, Ponce-Ortega and Morales-Cabrera [88] considered the Poppe model, both coupling their models with a mixed-integer, non-linear programming algorithm to minimise the total annual cost. Although yielding satisfactory results, these methods are also not ideally suited for real-time optimisation due to the iterative computation requirement of the models. However, they contain valuable insight for cooling tower design considerations. Serna-González *et al*. [70] achieved operational cost savings of 19.65% on the cooling tower considered.

In a summary of the three most common cooling tower models (the Merkel, e-NTU and Poppe methods), Klimanek and Bia [89] confirmed the iterative requirement of these models to determine the solutions. Jin, Cai, Lu, Lee and Chiang [65] proposed a new, simple and relatively accurate cooling tower modelling method, which is based on heat resistance and energy balance principles. The distinguishing feature of this modelling method, in comparison with other presently available models, is that it predicts cooling tower performance without the requirement of iterative computation when the operational parameters change. Their model

obtained root mean square of relative error (RMSRE) values ranging between 0.056 and 0.143 as part of their verification. Huang, Pan and Wu [93] referred to the modelling method of Jin *et al.* [65], where the cooling tower model was used as part of a HVAC cooling system optimisation model. Apart from this modelling method, Arndt [98] also presented an alternative explicit method to model cooling towers based on heat balance and heat transfer rate.

From the literature considered relating to cooling system modelling and optimisation, it is concluded that numerous different strategies and approaches had previously been considered. From these, none were found where the integrated cooling system was modelled via explicit non-iterative equations. Furthermore, it was established that no mathematical optimisation application had previously been performed on mine cooling systems based on system-side parameters. Although statements of optimisation were used, these were only trial-and-error user-optimised control strategies. Therefore, the state of the art condenses to the current study that aims to couple a mathematical optimisation platform to an integrated mine cooling system simulation model to determine the global energy minimum operational parameters for variations in the uncontrolled boundary variables. The novelty of the current study thus firstly lies in the construction of a suitable simulation model and secondly in coupling it to an optimisation platform to determine the optimal energy minimum system.

2.5 Variable-flow energy-saving potential of a mine cooling system

Many traditional mine cooling systems circulate water and air by constant speed electric motors that require either bypass or recirculation pipes or throttling valves and flow reduction dampers to balance and control the flow [27]. Typically, chillers are operated at constant design evaporator and condenser flow rates, often balanced by means of valves while cooling towers are run at constant water and air flow rates [1, 19].

The efficiency of a chiller is often represented by the coefficient of performance (COP), which states the ratio of cooling achieved at the evaporator, $\dot{Q}_L$, to the energy input in terms of work, $\dot{W}_{ref}$, and can be calculated by Equation (4).

$$COP = \frac{\dot{Q}_L}{\dot{W}_{ref}} \quad (4)$$

Factors that influence the actual COP include the condensing temperature, which depends on the ambient conditions, as well as the evaporator inlet water temperature that relates directly to the cooling demand, as the outlet temperature is usually at a fixed set point [99]. Reductions in the ambient temperature will result in lower condensing temperatures, which would increase the COP as a result. This phenomena is shown in Figure 6, where the COP of a typical centrifugal chiller, operated on HFC-134a refrigerant, is given as a function of the part-load ratio at various outdoor temperatures [100, 101]. The refrigeration capacity of a chiller is furthermore also suggested to be a function of the condensing and evaporating temperatures [102]. The response is similar to the COP, where the refrigeration capacity increases with a decrease in condensing temperatures, as well as increased evaporator temperatures.

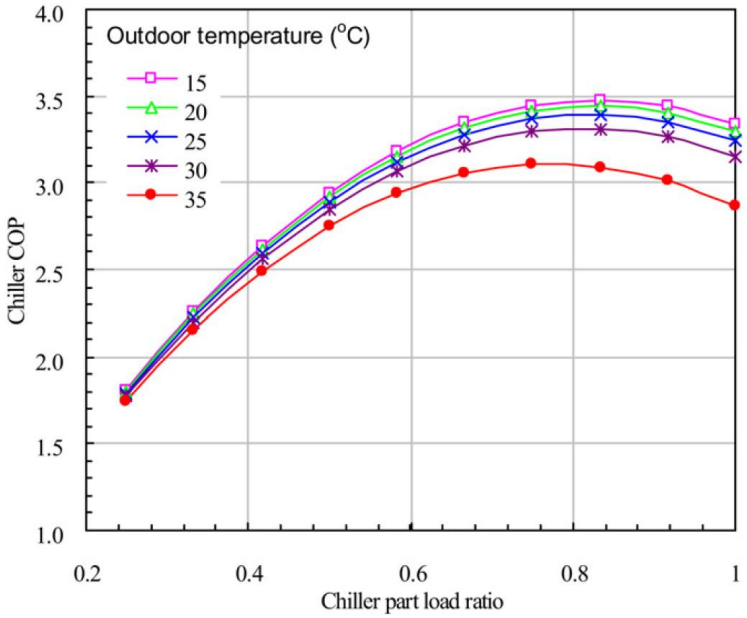

Figure 6: Chiller COP for various ambient temperatures and part-load ratios [100]

The effect of variations in the evaporator water inlet temperature on the COP of a typical centrifugal chiller previously considered is shown in Figure 7. The COP is given as a function of the evaporator water inlet temperature with a constant water outlet temperature. From this

figure, it is evident that the COP decreases as the evaporator water inlet temperature decreases. Lowering evaporator water inlet temperatures result in the chiller operating at lower part loads, which results in lower COP values that are also evident from Figure 6 [28].

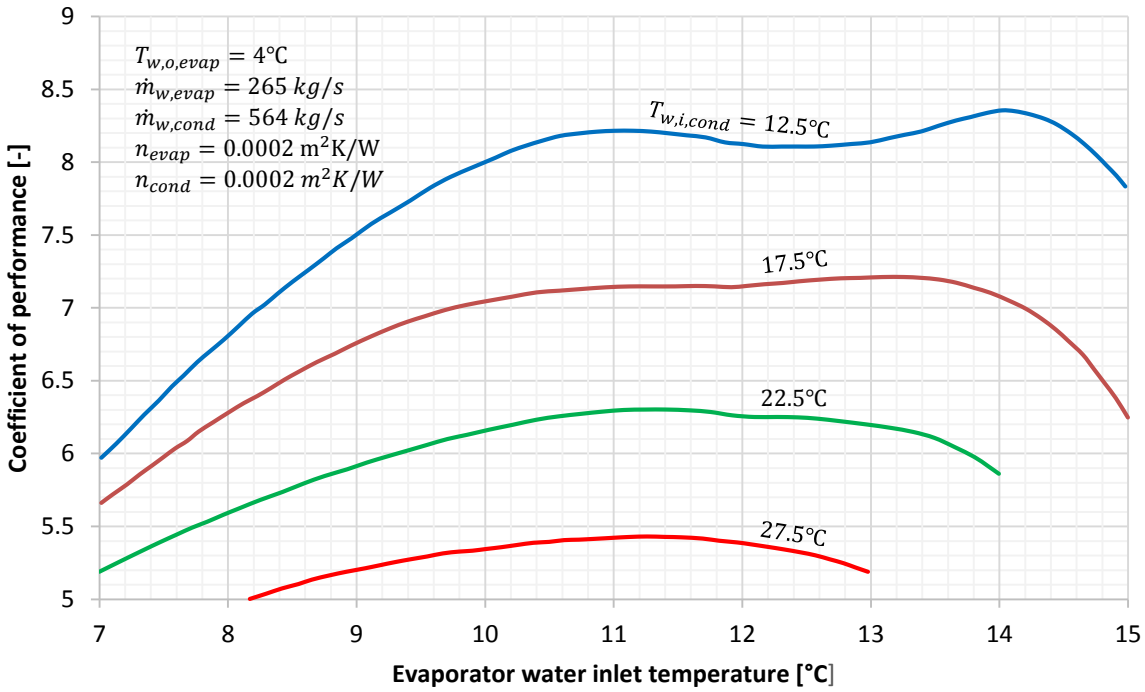

Figure 7: The effect of variations in the evaporator water inlet temperature on the chiller COP [28]

2.5.1 Variable water flow in evaporators

In typical mine cooling systems, water is circulated through evaporators at a constant flow rate, as mentioned earlier. This results in the recirculation of chilled water from the chilled-water dam into the pre-cooled dam to maintain a balanced system. This ultimately leads to reductions in the water inlet temperature of the evaporator. The reduction in water inlet temperature causes the chillers to reduce their cooling load to maintain a constant set point water outlet temperature [41].

From the energy consumption phenomena of chillers, it is obvious that centrifugal chillers that operate at partial loads lead to reduced COPs, as shown in Figure 6 and Figure 7. It is therefore suggested that reductions in evaporator water flow rates during reduced cooling demand

periods result in improved COPs under these circumstances [103]. Evaporator flows could be controlled to match demand more closely by using VFDs on the evaporator water pumps. The chiller load control will automatically adjust accordingly to maintain a fixed chilled-water outlet temperature.

In some instances, chilled water is intentionally recirculated due to the chillers not being able to perform enough cooling to achieve the desired outlet temperatures [22]. Reduced evaporator flow rates would assist higher water inlet temperatures, as the same amount of cooling would be able to achieve a higher temperature difference on a smaller volume of water [31]. Avoiding recirculation and obtaining increased evaporator water inlet temperatures will result in the chiller running at a higher load and increased COPs for reduced durations, which ultimately leads to an overall increase in energy efficiency and cooling capacity, as suggested by previous studies.

Evaporator pumps are often oversized for their application due to safety factors during the design, which results in the use of throttling valves to maintain the required constant evaporator flow rate [19]. The utilisation of VFDs allows the relief of this arrangement by opening these valves fully and controlling the flow entirely with the pump speed. This realises additional energy savings apart from the reduced chiller load that was described above, as the pump energy consumption would also be reduced due to the cubic relation between pump energy and flow, as discussed in more detail later. However, minimum pump speeds will be governed by the minimum allowable flow and the cooling demand, as explained below.

Manufacturer guidelines on minimum and maximum evaporator flow rates should also be considered when implementing variable evaporator flow strategies. The lower limit would be critical to avoid chilled-water freezing in the evaporator tubes and reduce scale formation inside the tubes as this would adversely affect heat transfer through the tubes over time [103]. Trane©, a chiller manufacturer, suggest that the typical minimum water flow velocity is around 1 m/s, while the upper limit is around 3.6 m/s. It should be noted that these values will vary if a glycol mixture is added to the water. It also varies among manufacturers [31].

Further considerations to consider during the control design of this strategy is the maximum allowable rate of change of the evaporator flow [104]. Trane©, suggests that it remains below

50% per minute, while the effect of the evaporator-leaving temperature's response should also be considered [31].

2.5.2 Variable water and air flow in the condenser

Similar to flows in the evaporator, water and air flow rates in the condenser are also traditionally operated at a constant rate in the cooling systems of mines. This is often achieved by means of throttling valves and constant-speed cooling tower fans [22]. This method of operation, along with a relatively constant cooling load, would lead to the ambient temperature being the primary factor to influence the energy consumption of the chiller and subsequent COP [103]. A reduced refrigerant pressure is required in the condenser at lower condenser temperatures, which reduces the electrical energy input required from the compressor, as shown in Figure 8 [105]. Lower ambient temperatures enable the condenser cooling tower to achieve lower water temperatures in the condenser, which results in the suggested savings. A typical saving of 3% is proposed for each reduction of 1 °C in the water temperature of the condenser [24].

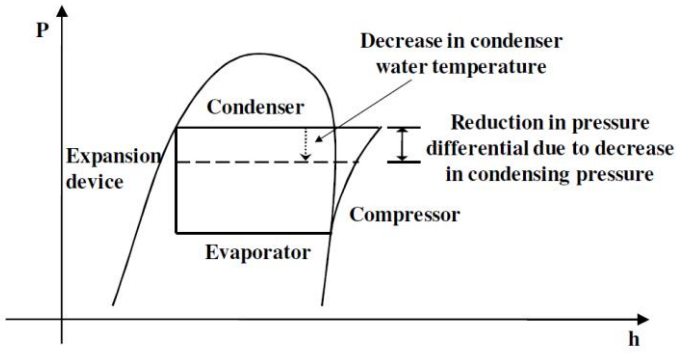

Figure 8: The pressure enthalpy diagram indicating pressure reduction due to lowered condenser temperature [105]

The introduction of variable condenser water flow enables condenser temperature control, whereby the temperature difference across the condenser could be controlled during variations in ambient temperatures or during changes in cooling loads [100]. This would be particularly useful for the implementation of the variable evaporator flow that was discussed in the previous

section, as this strategy would introduce significant variations in the chiller load, based on the system's cooling demand.

Similar to evaporators, condenser pumps are frequently oversized and therefore significantly throttled by valves to maintain design flow rates [19]. Further energy savings could be achieved by opening all the valves and utilising VFDs to control and maintain flow through the condenser. In addition to the pumps, variable air flow via VFDs could be included on the cooling tower fan motors. This will allow the fan's speed to be controlled, as well as its effect on the condenser temperature during variations in the cooling load, ambient temperature and water flow rates. It has been suggested that there is an optimal point in terms of the power consumption of the fan and chiller, as shown in Figure 9 [106].

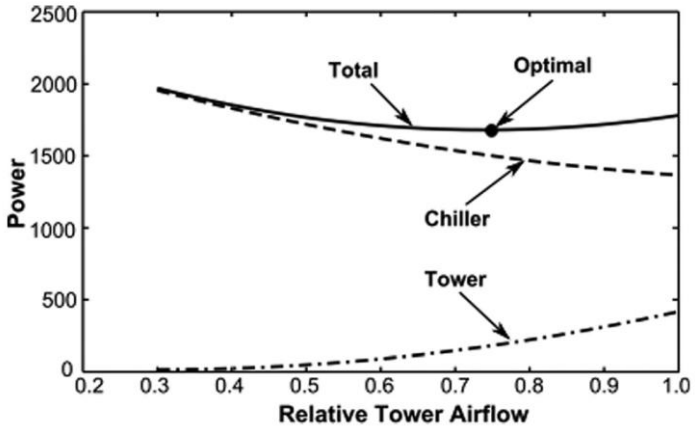

Figure 9: The optimal chiller and condenser cooling tower fan speed operation [106]

The performance of the condenser cooling tower should also be considered to determine the outlet temperature that would be achieved for variations in the air and water mass flow rates, as the relation to variation in the L/G ratio is typically non-linear (see Figure 10) [64].

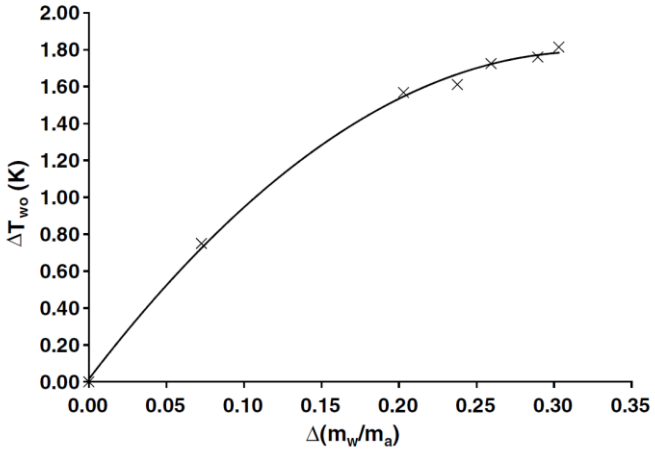

Figure 10: Change in the cooling tower outlet temperature as a function of change in the L/G ratio [64]

Manufacturer limitations should also be adhered to for variable condenser water and air flows along with reduced condenser temperatures. Temperatures typically below 20 °C could lead to oil return problems on the compressor, and it could be difficult to maintain the required oil viscosity for adequate compressor lubrication [107, 103]. Furthermore, the minimum flow would also be governed by the specific cooling tower used, as flows below a certain value would greatly deteriorate the cooling towers' efficiency due to spray pattern deterioration and scale formation inside the tower [108].

All factors considered, it is suggested that there are optimal operating water and air flow rates for variations in the ambient conditions and cooling loads. As previously suggested, depending on the specific chiller's response to variations in the condensing temperature and the size of the pump and fan, this optimal point might result in significantly reduced condenser flow rates with a marginal increase in compressor energy although the pump and/or fan power saving outweighs the increase in compressor energy [22]. An accurate and clear model of the chiller's COP as a function of the condenser parameters would therefore be required to simulate this integrated subsystem.

2.5.3 Flow control in the bulk air cooler

BACs are employed to maintain acceptable underground ventilation air conditions for a safe work environment, as discussed earlier. Ambient air is cooled to wet bulb temperatures of around 8 °C to maintain underground temperatures below 27 °C [1, 19].

Similar to other cooling system components discussed earlier, BACs are traditionally operated at constant design conditions that cater for extreme summer ambient temperatures [63]. This method of operation is often achieved through throttling valves with constant speed pumps, which results in frequent overcooling as the daily ambient conditions are often lower than the design conditions [22]. The opportunity exists to reduce the cooling demand imposed on the refrigeration plant by implementing water flow control via variable speed water supply pumps. This allows reduced chilled-water flow requirements during lower ambient temperatures caused by climate fluctuations throughout the day, as well as during seasonal cycles [63]. Further savings can be achieved through the reduced pumping power that would be realised by the suggested method of operation. This is accomplished by ensuring that satisfactory air outlet psychrometric conditions are maintained through the BAC.

There is a variation on BAC air flow where the air flow through the towers is directly controlled by the mine's main ventilation fans, while other arrangements employ their own BAC tower fans. The installation with dedicated fans would furthermore be able to incorporate air flow control as part of the subsystem.

As stated earlier, variations in the water and air flow rates of cooling towers and BACs would result in a non-linear response on the outlet conditions. Similar to the condenser cooling tower, this would require a suitable model whereby the outlet conditions could be determined for any given set of input conditions with acceptable accuracy.

This strategy could be implemented by simplified forward-loop control, whereby the water flow rate supplied to a BAC is linearly varied according to the ambient enthalpy [22, 19]. Alternatively, more accurate control would be achieved by implementing feedback control,

whereby the outlet air enthalpy of the BAC is monitored and provided to the controller in order to maintain a specified air outlet enthalpy [63].

2.5.4 Flow control in the pre-cooling tower

Pre-cooling tower flow control would be required for integration with the evaporator flow control strategy to maintain a balanced system in steady state [22]. Further saving opportunities come along with this requirement, as reductions in water and air flow would yield savings in pump and fan energy. Variations in water and air flow would have performance implications for the cooling tower, which would have to be considered.

As suggested by the phenomena shown in Figure 10, a decrease in the water flow rate (or increase in the air flow rate) would yield lower water outlet temperatures, although it is evident that the sensitivity of the water outlet temperature near the design water and air flow rates is less than for significantly reduced flow rates. Similar to condenser cooling towers, where it is suggested that there is a global optimal operational point, it is suggested that pre-cooling towers would also have a global optimal point of operation for variations in the ambient conditions, as well as the cooling demand. This is true, as the water outlet temperature of the pre-cooling tower would directly influence the pre-cooled dam temperature, and in turn, the water inlet temperature of the evaporator.

2.5.5 Pump and fan energy consumption due to flow control

As all strategies discussed in sections 2.5.1 to 2.5.4 involve either pump or fan control, or a combination of both, it is beneficial to briefly discuss the effect of flow control on the energy consumption of these components.

Pumps consume electrical (or other) input energy in order to impart a velocity to a fluid that ultimately converts the velocity energy to pressure energy [38]. The input power, $\dot{W}_{p,}$ which is required to drive the pump, can be calculated as stated in Equation (5) [32].

$$\dot{W}_p = \frac{\Delta P_p \cdot \dot{m}_w}{\rho_w \cdot \eta_p} \quad \textbf{(5)}$$

Similar to pumps, the electrical energy consumed by fans $\dot{W}_f$ could be expressed by Equation (6).

$$\dot{W}_f = \frac{\Delta P_f \cdot \dot{m}_a}{\rho_a \cdot \eta_f} \quad \textbf{(6)}$$

Due to the squared relation between the pressure differential ($\Delta P_{p,f}$) and the fluid flow ($\dot{m}_{w,a}$), it could be concluded, as suggested by the Dracy Weishbach equation and shown in Figure 11, that there is a cubic relation between the power ($\dot{W}_{p,f}$) and the fluid flow (see Figure 12).

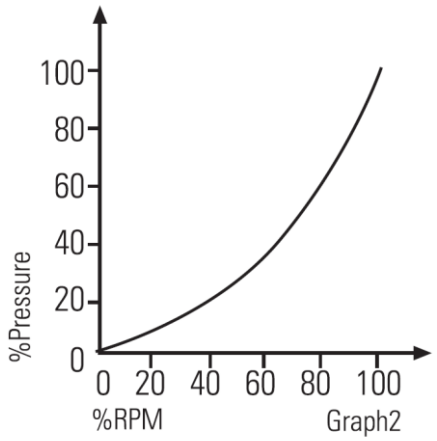

Figure 11: The pump pressure as a function of motor speed [109]

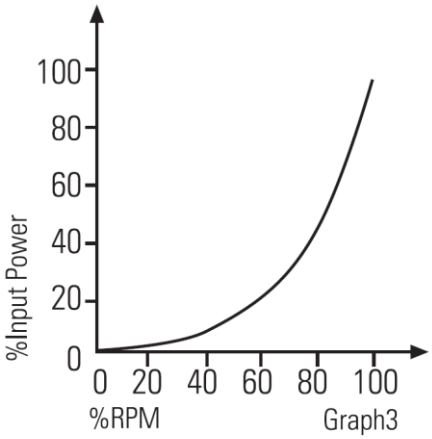

Figure 12: The pump power as a function of motor speed [109]

2.5.6 Economic considerations

The identified strategies all depend on certain components to be incorporated into the cooling system. These include VFDs, flow meters, thermometers and weather stations. In some instances, some or all of these components might already be in place with no requirement for additional capital expenditure to implement the flow control strategies. In these events, the system control would only need to be adapted to integrate the optimised parameters.

For other cooling systems where the necessary infrastructure is not yet in place, detailed economic considerations, as well as a cost-benefit analysis, were previously performed on the installation of these components and the VFDs were found to be the most expensive [22]. Therefore, only the effect of the VFDs will be briefly discussed.

It is suggested that the increase in the popularity of VFDs has resulted in overall cost reductions over the last few years. Based on March 2013 rates, low-voltage pump and fan VFDs cost (USD, $) in the region of $ 92/kW for smaller units around 35 kW. The cost reduces to roughly $ 80/kW for units in the region of 750 kW. Table 2 indicates typical VFD costs that relate to the installation of medium-voltage applications. These costs are inclusive of the installation, cabling, programming, control adjustments and commissioning of the VFDs.

Table 2: Typical medium-voltage VFD costs in USD ($) (According to March 2013 rates) [22]

	Voltage (V)	800 kW	1 000 kW	1 500 kW	Average
Company A	6 600	$148 327.68	$174 846.02	$230 151.58	
Company B	6 600	$157 262.97	$186 473.11	$239 380.47	
$/kW		$191.04	$180.64	$156.49	**$176.10**
Company A	11 000	$212 885.53	$239 401.48	$321 099.97	
Company B	11 000	$214 588.87	$253 689.18	$319 130.97	
$/kW		$267.18	$246.60	$213.46	**$242.38**
Installation	6 000 – 11 000	$9 227.16	$9 227.16	$9 227.16	
$/kW		$11.59	$9.21	$6.17	**$8.99**
$/kW (6 600 V total)		$202.63	$189.85	$162.67	**$185.08**
$/kW (11 000 V total)		$278.76	$255.80	$219.63	**$251.36**

Table 3 indicates typical VFD costs that relate to low-voltage applications. These costs also include the installation, cabling, programming, control adjustment and commissioning of the VFDs.

Table 3: Typical low-voltage VFD costs in USD ($) (According to March 2013 rates) [22]

	Voltage (V)	75 kW	132 kW	160 kW	200 kW	275 kW	Average
Company A	525	$16 677.77	$22 213.41	$25 286.43	$30 118.77	$43 030.84	
Company B	525	$9 744.73	$13 138.31	$15 105.36	$16 801.66	$21 135.83	
Company C	525	$8 075.82	$12 472.91	$14 266.47	$18 224.40	$22 000.06	
Company D	525	$10 026.09	$13 468.73	$14 398.16	$17 459.91	$23 946.21	
$/kW		$148.37	$116.10	$107.87	$103.21	$100.07	**$115.12**
Installation	525	$3 207.63	$3 207.63	$3 207.63	$3 207.63	$3 207.63	
$/kW		$42.78	$24.26	$20.04	$16.03	$11.70	**$22.96**
$/kW (total)		$191.15	$140.36	$127.90	$119.24	$111.77	**$138.08**

It is evident From Table 2 and Table 3 that the costs of VFDs per kW of installed capacity decreases as the power increases. It is also evident that the medium-voltage drives are significantly more expensive than the low-voltage ones, which suggests that the application of low-voltage equipment is more financially viable. The payback period for medium-voltage VFDs controlling chiller compressors is suggested to be in the region of 4.2 years, while the payback on low-voltage VFDs controlling pumps and fans is suggested to be roughly 1.4 years

[22]. It is thus concluded that the application of low-voltage VFDs on pumps and fans provide a more cost effective option.

2.6 Optimisation overview

Optimisation is used in many applications such as business transaction decision making, investment analysis and engineering design, and industrial manufacturing [110]. The last couple of decades have seen significant advances in the field of optimisation, while it has reached a certain level of maturity in recent years [111, 112]. Mathematical optimisation can be traced back to some of the pioneering mathematicians such as Newton, La Grange, Cauchy, Leibnitz, Euler, Bernoulli and Weirstrass [111].

In order to fully utilise and obtain the minimum energy consumption of an integrated mine cooling system for any given set of demand and ambient boundary conditions a suitable optimisation algorithm or platform is required. The requirement would be to couple the integrated simulation model to the optimisation platform with relative ease and accuracy.

As optimisation is an in-depth study and a research field on its own. It should be noted that the objective of this study is not to derive a new optimisation method or algorithm, but rather to apply a suitable existing strategy to the simulation model. Successfully coupling the simulation model with a suitable optimisation platform would assist in satisfying the hypothesis of determining the overall minimum energy operational set of parameters for a mine cooling system using an integrated system simulation and corresponding optimisation.

This chapter briefly examines various optimisation algorithms and platforms that are available in the literature and in the commercial market. The background considered would facilitate the choice of a suitable platform to be coupled to the integrated simulation model.

2.6.1 Optimisation classifications and algorithms

Optimisation problems could be broadly classified based on the nature and objective under consideration [111]. These could firstly be classified as constrained or unconstrained,

depending on the presence or absence of constraints imposed on the optimisation algorithm. Furthermore, the nature of the design variables dictates the problem as static or dynamic. A static optimisation problem represents a set of design parameters that would yield the minimum of a prescribed function subject to some constraints. A dynamic optimisation problem consists of design parameters that are all continuous functions of another parameter, which minimises some objective function subject to certain constrains.

Optimisation problems could further be classified as linear, non-linear, geometric or quadratic programming problems, based on the nature of the equations utilised. It is therefore useful to first determine the class of problem under consideration to select the most appropriate type of optimisation procedure.

If any of the optimisation problem's objective or constraint functions contain non-linear equations, it would form part of the non-linear classification, which is commonly known as a Non-linear Programming (NLP) problem. NLP problems are deemed to be the most general problems, while all other classifications apart from linear programming could be considered as special cases of the NLP problem. With most expressions for the energy consumption of mine or industrial cooling system components consisting of non-linear equations, it is obvious that the resulting optimisation problem would form part of the non-linear classification.

Geometric programming problems are considered when the objective and constraint functions can be expressed as the sum of power terms of polynomials. A quadratic programming problem is one where the optimisation problem is formulated through non-linear equations with a quadratic objective function, while the constraints are represented through linear functions.

A specific optimisation problem could be categorised by various other classifications and sub-classifications according to the permissible values of the design variables, the deterministic nature of the variables, the separability of the functions and the number of objective functions. These classifications are not considered in detail here and are well documented in the literature [111, 112].

2.6.2 Non-linear global optimisation, constraints and objective functions

Constraints

Most practical engineering optimisation problems would be subject to certain constraints that are imposed on the decision variables. Constraints that influence the system's performance or behaviour are called behavioural or functional constraints, while those that represent physical limitations to the decision variables are called geometric or side constraints [111]. The optimisation of a mine or industrial cooling system through flow control would result in a constrained optimisation problem due to the physical limitations of the infrastructure, such as the maximum and minimum flow rates.

Figure 13 shows the constraint functions for a hypothetical two-dimensional problem. From this figure, it is clear that the acceptable solution would have to remain inside both the behavioural and side constraints, which dictate the feasible region.

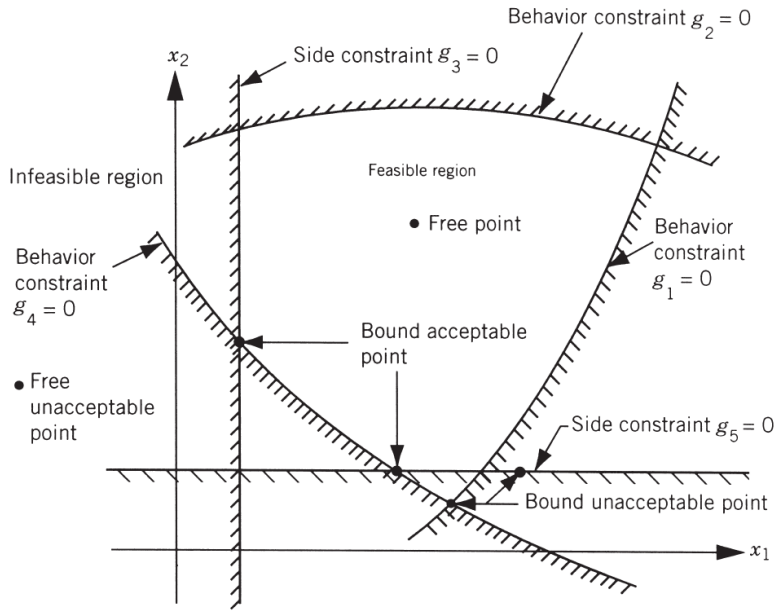

Figure 13: The constraint surfaces in a hypothetical two-dimensional space [111]

Objective function

The desired outcome of an optimisation problem is to minimise or maximise a certain parameter of the system under consideration. The function that defines these parameters in relation to the controllable variables is known as the criterion, merit or objective function [113]. Some optimisation problems might have more than one objective function that would need to be solved simultaneously. Such problems are called multi-objective programming problems, and might result in conflicting parameters, as all functions attempt to achieve their specific objective. This is resolved by expressing the various objective functions as a set of linear objective functions represented by a single objective function. The objective function for the energy optimisation of a mine or industrial cooling system would consist of the sum of the energy consumption of the various system components.

For a trivial, hypothetical two-dimensional optimisation problem, as shown in Figure 14, it is clear that the objective function contours could be present inside and outside the allowable constrained region with the acceptable optimal point as shown [111].

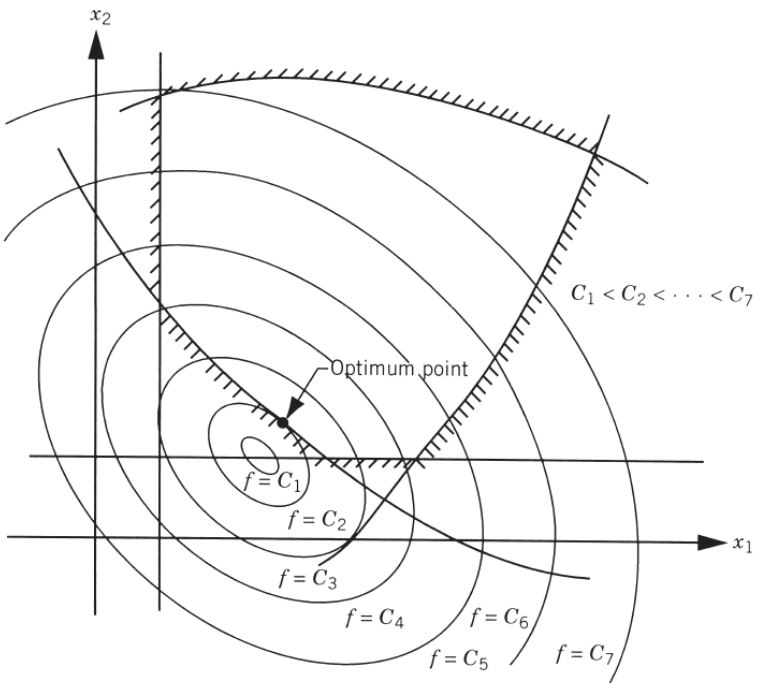

Figure 14: The objective function contours with constraint surfaces [111]

Non-linear global optimal solution and test functions

Non-linear optimisation functions often lead to multiple peaks in the functions, as shown in Figure 15, for a function with a single variable, resulting in various local minima or maxima [113]. It is also shown how the feasible region defined by certain constraint functions, would influence the optimum point relative to the objective function as discussed earlier.

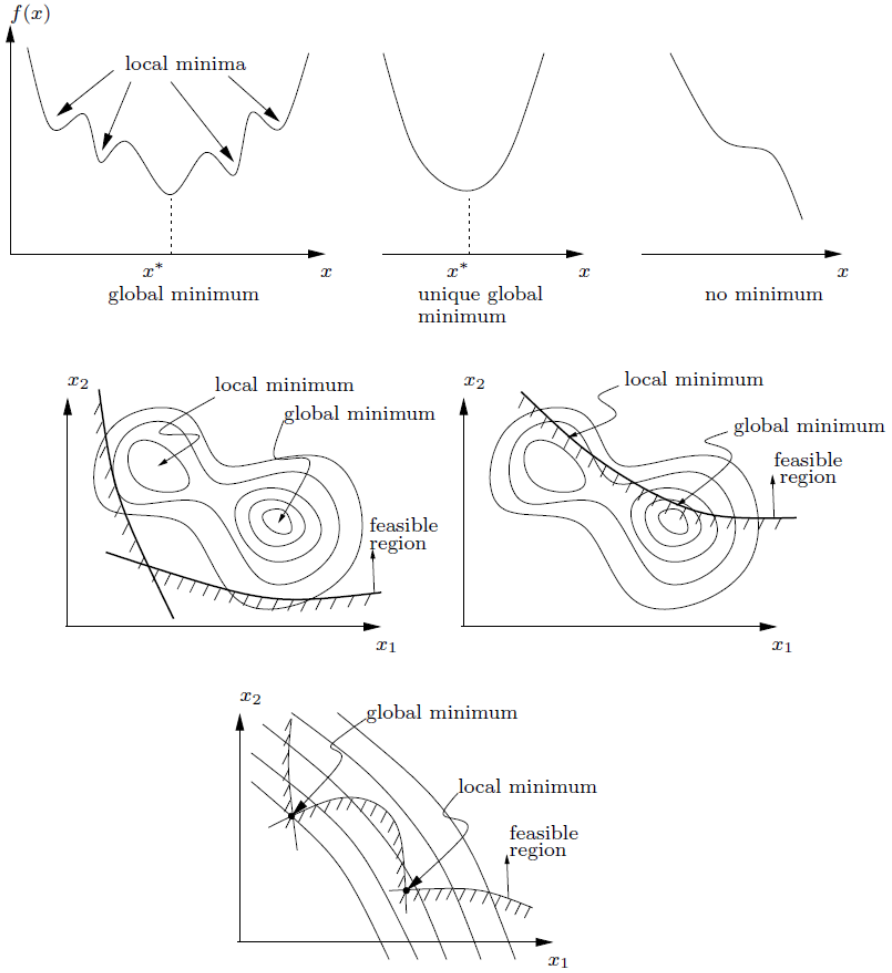

Figure 15: The global and local minima [113]

These local and global minima and maxima could furthermore be subdivided into strong and weak local and global minima and maxima as shown in Figure 16 [110]. Here a discontinuity such as point *C* is problematic, as $f'(x) = 0$ would not be valid for this point. It is therefore important to ensure that all functions are continuous and twice-continuously differentiable.

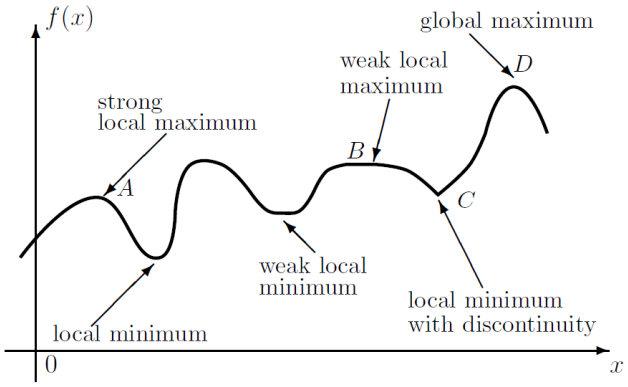

Figure 16: The strong and weak local and global minima and maxima [110]

The same is true for non-linear functions of multiple variables. The three-dimensional function in Figure 17 has many local minima and maxima [110]. The objective and constraint functions for problems with more than two or three variables might not be easily presented graphically, and in some cases not at all, and would therefore rely purely on the mathematical solution [111].

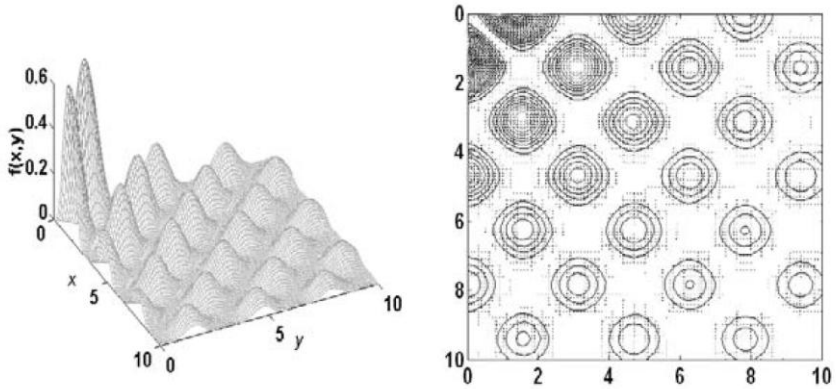

Figure 17: The surface variation of a non-linear, three-dimensional test function presented in Equation (27) [110]

Due to these reasons, extensive research and numerous approaches have been conducted, suggested and implemented to obtain global optimisation results [114–120]. Some studies have conducted in-depth reviews and comparisons between various optimisation algorithms and platforms available in the market-place [114, 116–117]. Gathering from these studies, it is no easy task to evaluate and determine which platform continuously performs the best.

Various test functions are suggested whereby the robustness of a given platform could be evaluated and confirmed [110, 115, 118]. For the purposes of the current study, a few arbitrarily selected test functions are considered to validate the optimisation platform that would be utilised for energy minimisation of the cooling system. These functions will be introduced later in this document.

2.6.3 Commercially available optimisation platforms

Many commercial non-linear optimisation platforms are available today. An extensive list of both freeware and, proprietary software is available online [121]. It should be noted that many of these platforms and algorithms are cross-integrated with reference to each other. This suggests that some platforms borrow algorithms from each other to solve unique optimisation problems, while each platform retains its unique user interface with the cross-platform integration conducted in the background.

It could often be a daunting task to select the correct or most appropriate platform, as more than one could suitably satisfy the optimisation problem at hand [114]. For this reason, platform selection is often dictated by the organisation or research institution where the work is being conducted with regard to licences that are already in place or licences that are granted by the vendor for research purposes. One should also consider which platform will provide the simplest integration with the method through which the problem was formulated.

In a review study, the performance of numerous global optimisation solvers were compared based on software performing a complete search to solve the global optimal solution to constraint problems [114]. It is suggested that several dozen solvers claim to solve global optimisation problems through a complete search. For this reason, the review study uses a large sample set of over a thousand problems, with the primary performance criteria being the number of times the solver correctly attains the global optimum. It was found that the OptQuest non-linear programming (OQNLP) Premium Solver obtained the most satisfying results for global optimisation problems with around 100 variables. The OQNLP solver is based on the principles of tabu search and scatter search and requires upper and lower bounds on all variables [122]. Scatter search works on a set of reference points which systematically

generates linear combinations of reference points to create new points. The new points each maps into an associated point that yields integer values. From here tabu search is superimposed to manage the reference points. Tabu search in turn uses a memory base of search history to drive the process and therefore avoids reinvestigating solutions that have been considered before.

The OQNLP solver stops and return a result either through the user stopping it or when it exceeds one of the set limits via the solver engine input options being the maximum time, iterations or to stop when the objective hasn't improved. This engine has a further auto stop function whereby it stops automatically when it is making weak progress. This is based on a set value of iterations resulting in an improvement of the objective function of less than a given convergence limit, set to a default of 100 iterations and variance of $1.0E-06$.

2.7 Mine cooling system and simulation

To investigate and quantify the additional identified saving opportunities would require a suitable research instrument, consisting of a holistic understanding of the mine cooling system under consideration, as well as the construction of a computer-based simulation model that would be used to mimic the system's thermal hydraulic behaviour and subsequent energy performance.

Many mathematical models of various cooling system components have been developed and are well documented in the literature. In order to simulate the holistic cooling system, adequate system component models have to be coupled together so that the system's integrated effect could be modelled, whereby the consequence of varying any system component parameter will yield results on the energy consumption of the system as a whole.

Facilitating integrated system optimisation would require the various component models to be expressed by smooth and continuous explicit functions that do not require iterative computation to arrive at a solution.

The following chapter systematically introduces the research instrument that consists of the mine cooling system, and subsequently the simulation model, as used for this study.

2.8 Conclusion

It was established that mine cooling systems based on vapour compression refrigeration cycles have been in use for the last century. Furthermore, it is concluded that the demand for cooling in deep-level mines continues to rise due to the increasing depths of mining operations. As mine cooling systems currently account for around 25% of a typical deep level mine's total energy consumption, it is of significant value to consider the further energy efficiency and possible optimal operational strategies of these systems to ensure the minimum energy consumption to satisfy the cooling demand.

Mine cooling systems include installed refrigeration cooling capacities of up to 30 MW*c*, typically cooling a few hundred litres of water every second from pre-cooled temperatures of around 14 °C to roughly 3 °C. The major components that are responsible for energy consumption in the range of 25 kW to 3.5 MW include chillers, cooling towers, pumps and fans.

By reviewing the state of the art, it was established that numerous cooling system modelling approaches, as well as several optimisation studies, had previously been considered. From these, none were found where an integrated mine cooling system was optimised through an explicit component-based modelling approach.

The energy consumption of the major components in their respective positions in the integrated cooling system was identified. Subsequently, energy-saving strategies through flow control were recognised. The effect of the energy consumption of the various components, based on variations in process flow and philosophies of operation, was also identified.

The energy consumption response to variations in flow was mostly found to be non-linear. It can therefore be concluded that suitable non-linear models would be required to model each of the components that could subsequently be coupled together to model the integrated system.

This would therefore enable a suitable simulation model that could accurately simulate the thermal hydraulic behaviour and the corresponding energy consumption accordingly.

A brief overview and background on mathematic optimisation was considered. Various considerations for choosing a suitable optimisation platform when conducting optimisation calculations were identified and discussed. Thereafter, various test functions used to verify the stability of an optimisation algorithm were presented as these would be considered later in the study to verify the integrity of the chosen optimisation platform.

3 Case study – mine cooling system and simulation

3.1 Preamble

In this chapter, the mine cooling system considered for the case study in this investigation is briefly presented. Major energy-consuming devices are identified. To facilitate energy consumption optimisation, component models for an integrated dynamic simulation model are developed and described. A combination of data formulated, as well as first-principle equation sets are considered and used through various methods of regression, along with equations obtained in the literature. These are used to evaluate the thermal hydraulic and energy-consuming behaviour of a typical mine cooling system at various inlet and boundary conditions. All major energy-consuming devices are calibrated with system data obtained from the case study mine.

3.2 Cooling system overview

The Kopanang deep-level gold mine, which was considered for this study, is situated on the moderate cold eastern plateau interior of South Africa at an altitude of 1 336 m. The American Society of Heating, Refrigeration and Air Conditioning Engineers (ASHRAE) design summer weather conditions for this location is shown in Table 4 [123].

Table 4: Ambient design summer weather conditions [123]

Parameter	Unit	Value
Ambient air pressure	kPa	86.11
Dry bulb temperature	°C	33.1
Wet bulb temperature	°C	17.4

The mine has a typical cooling system layout, which is schematically represented in Figure 18. It consists of a refrigeration plant and two main water loop systems. The first water loop systems (blue lines in the figure) passes water through the mine, pre-cooling towers (PCT), the evaporators of the refrigeration plant and the BACs. The second water loop system (red lines in the figure), passes through the condensers of the refrigeration plant and the condenser cooling towers (CCTs).

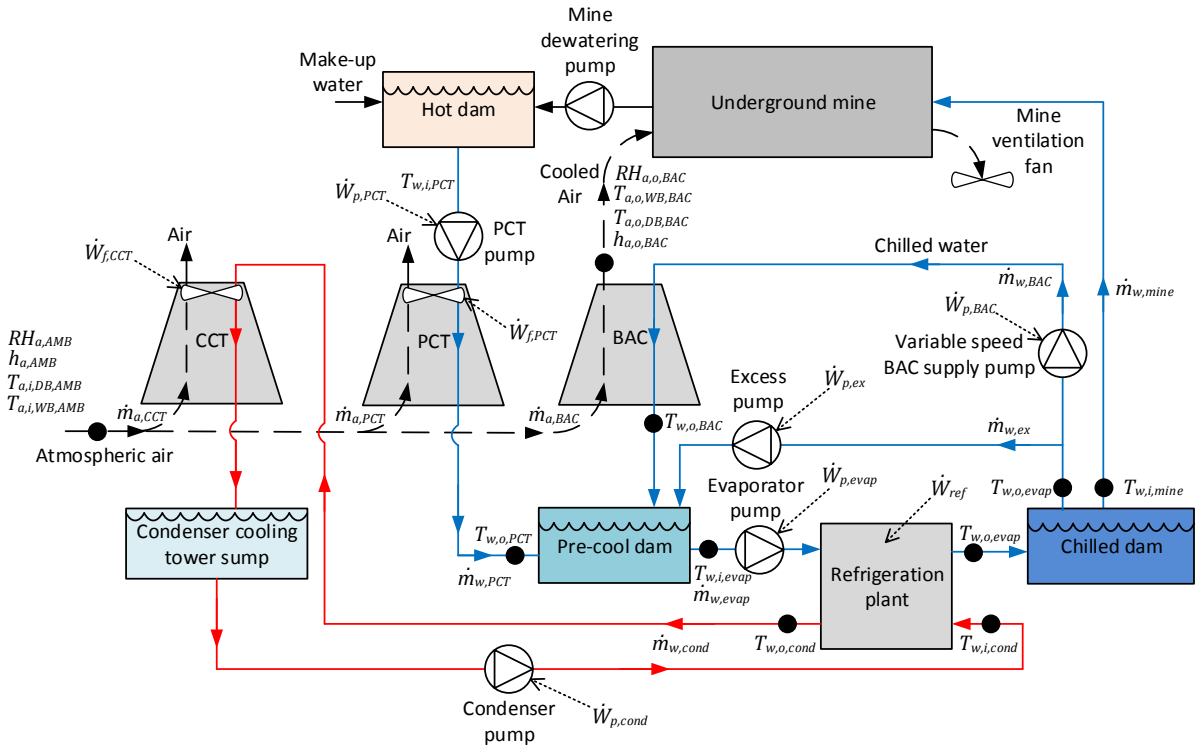

Figure 18: The case study mine cooling system layout

Refrigeration plant

The refrigeration plant consists of six refrigeration machines, each operated as a simple vapour compression cycle. The parallel configuration of the chiller machines inside the refrigeration plant is shown in Figure 19. The combined rated power input to the refrigeration machines, $\dot{W}_{ref}$, is 7 092 kW at a design cooling capacity of 39 000 kWc. This suggests a design COP of 5.5. The compressors are centrifugal compressors with inlet guide vane control for partial cooling operation. The evaporators and condensers are shell and tube heat exchangers with the refrigerant (R134a) flowing through the shell and water flowing in the tubes. The water flow through the evaporators is used to service the cooling needs of the mine, while the water flow through the condenser is used to transport heat to the condenser cooling towers for rejection into the atmosphere. Each of the six chillers operate in conjunction with its dedicated evaporator pump, condenser pump and associated condenser cooling tower as a set. The chillers are manually started and stopped by the operator based on the total demand, typically observed as the chilled water flow rate and temperature supplied to underground as well as the flow rate and chilled water temperature supplied to the BACs.

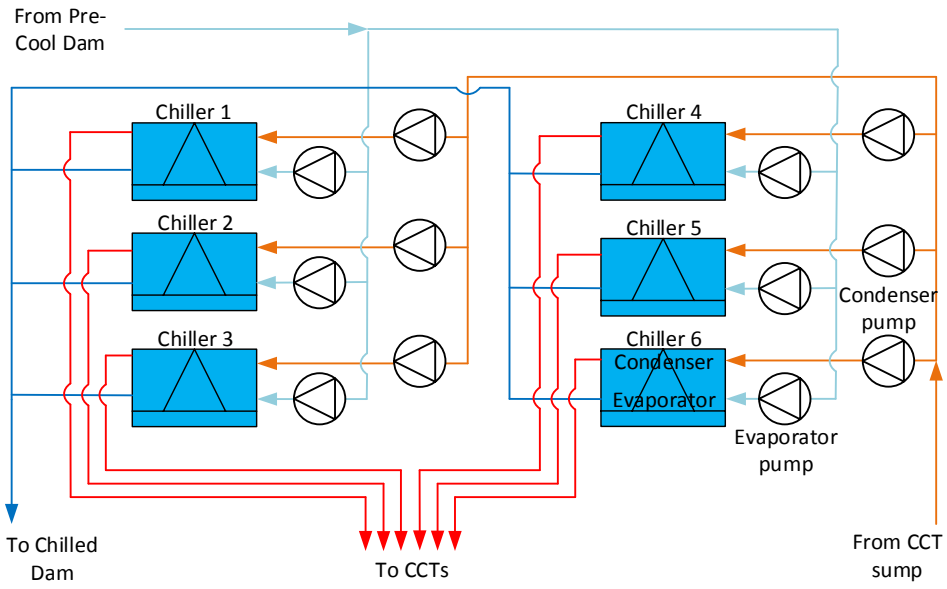

Figure 19: The refrigeration plant's parallel chiller schematic layout

Water circuit passing water through the mine

The first water-loop system (see Figure 18) contains an above-ground hot-water dam that stores relatively warm water at a design temperature of 30 °C, after extracting it from underground and before re-cooling it. Fresh make-up water is supplied to the hot-water dam to maintain a water balance in the system. The water of the hot dam is pumped at a variable flow rate through two parallel connected PCTs at a combined design water flow rate ($\dot{m}_{w,PCT}$) of 360 kg/s and a combined design operating air flow rate ($\dot{m}_{a,PCT}$) of 720 kg/s. The pumps and fans of the PCTs consume electrical energy ($\dot{W}_{p,PCT}$ and $\dot{W}_{f,PCT}$) for which the installed capacities are 140 kW and 210 kW respectively. The water inlet and outlet temperatures of the PCTs are presented by $T_{w,i,PCT}$ and $T_{w,o,PCT,}$ which have design state values of 30 °C and 24 °C, respectively.

Even though there is a net water addition in the hot-water dam and a net water loss in the underground mine, it is assumed for simplicity that the water flow rate through the PCTs is equal to the chilled-water flow rate supplied to the underground section. This governing flow rate is presented by $\dot{m}_{w,mine}$ in the figure. After the PCTs, the water is passed to the pre-cooling dam with a design temperature of 9 °C. The temperature in the pre-cooling dam is obtained through a mixture of water from the PCTs, return water from the BACs, and recirculated excess water. From here, the water is pumped via variable speed pumps through the evaporators of

the six parallel connected refrigeration machines at a design water flow rate ($\dot{m}_{w,evap}$) of 1 250 kg/s, an inlet temperature of $T_{w,i,evap}$ and a design outlet temperature, $T_{w,o,evap}$, of 3 °C. The cooled water is stored in the chilled-water dam. The variable speed evaporator pumps have a combined installed power rating ($\dot{W}_{p,evap}$) of 660 kW at a maximum combined design water flow rate of 1500 kg/s ($\dot{m}_{w,evap}$). The actual combined water flow rate, ($\dot{m}_{w,evap}$) is controlled to maintain a set chilled-water dam level as part of the mine's original flow control strategy.

From the chilled-water dam, water is simultaneously supplied to the mine at a mass flow rate of $\dot{m}_{w,mine}$ (as mentioned) and to the BACs at a combined mass rate of $\dot{m}_{w,BAC}$. Any excess water is recirculated back to the pre-cooling dam at a mass rate of $\dot{m}_{w,ex}$. The water flowing to the mine and the BACs is assumed to be the same temperature as the evaporator outlet. Thus, $T_{w,i,mine} = T_{w,i,BAC} = T_{w,o,evap}$. The excess water pump (rated at 80 kW) has a power consumption of $\dot{W}_{p,ex}$.

The BACs consist of three direct-contact (wet) units connected in parallel and are designed for a combined water flow rate of 750 kg/s supplied from the common water supply line. Outlet water from the BAC is discharged back into the pre-cooling dam at a design temperature ($T_{w,o,BAC}$) of 9 °C. The associated water pumps have an installed power capacity of 225 kW. The design-state combined air flow rate supplied to the mine ($\dot{m}_{a,BAC}$) is 1 250 kg/s. The original water flow control strategy for the BACs had the objective of maintaining a constant air outlet enthalpy. This was not successfully maintained, as will be evident in the baseline simulation that is presented in Chapter 5. Because the BAC fans are controlled to satisfy the ventilation requirements of the mine, their power consumption is not considered in the system analysis for this investigation. The water from the BACs is returned to the pre-cooling dam.

All pipes, valves, sumps, pumps and dams are assumed to be adiabatic with no heat gain or loss introduced to the system through these devices. This results in the assumption that the PCT water outlet temperature equals the water inlet temperature of the pre-cooling dam from the PCT. Also resulting from this assumption is the fact that the water inlet temperature of the chilled-water dam equals the water outlet temperature of the refrigeration plant.

Water circuit passing water through the condensers

Heat rejection from the refrigeration plant is realised through water-cooled condensers (see Figure 19). Each condenser is serviced by a separate direct-contact (wet) condenser cooling tower (CCT), which results in six condensers and six cooling towers. All six CCTs discharge into a common CCT sump from where the water is pumped back to each condenser by means of six dedicated condenser pumps associated with each condenser. The combined water and air mass flow rates through the CCTs are $\dot{m}_{w,cond}$ and $\dot{m}_{a,CCT}$, and the design-state flow rates for these are 2 700 kg/s and 1 350 kg/s respectively. The inlet and outlet water temperature at the CCTs are $T_{w,i,cond}$ and $T_{w,o,cond}$, and the design-state temperatures for these are 32 °C and 27 °C respectively. The condenser pumps and fans consume electrical energy ($\dot{W}_{p,CCT}$ and $\dot{W}_{f,CCT}$) at installed capacities of 960 kW and 495 kW respectively. The fans are operated at a constant speed, while the pump speeds are controlled to maintain a 5 °C temperature differential across the condenser.

3.2.1 Plant control and measuring and data capturing system

The refrigeration plant is controlled by various programmable logic controllers which are programmed to control and operate as described above. Each of the controllers interface with the mine's supervisory control and data acquisition (SCADA) system from where set-points as well as various maxima and minima values of the plant operation could be adjusted and monitored.

Several operating data values are logged on the SCADA system as part of the cooling system's operation. Some of the measured quantities are included in the system flow network, as indicated in Figure 18. These quantities are the following:

1) The combined compressor power input ($\dot{W}_{ref}$), which is calculated by the SCADA system via the current drawn by each of the six compressor's motors as measured at the motor control centre of each chiller machine, as well as the refrigerant inlet guide vane position, measured as a percentage representing the chiller's part-load capacity.

2) The PCT, BAC, condenser, evaporator, circulation and underground water flow rates of the mine ($\dot{m}_{w,PCT}$, $\dot{m}_{w,BAC}$, $\dot{m}_{w,cond}$, $\dot{m}_{w,evap}$, $\dot{m}_{w,ex}$, $\dot{m}_{w,mine}$). These parameters are measured by means of water flow meters connected in the flow pipes in series with each component.

3) The PCT, condenser and evaporator water inlet and outlet temperatures ($T_{w,i,PCT}$, $T_{w,o,PCT}$, $T_{w,i,cond}$, $T_{w,o,cond}$, $T_{w,i,evap}$, $T_{w,o,evap}$), measured before and after the various components via temperature probes typically installed in welded thermocouple sockets.

4) The PCT and CCT fan power as well as the PCT, BAC, condenser, evaporator and circulation pump power ($\dot{W}_{f,PCT}$, $\dot{W}_{f,CCT}$, $\dot{W}_{p,PCT}$, $\dot{W}_{p,BAC}$, $\dot{W}_{p,cond}$, $\dot{W}_{p,evap}$ and $\dot{W}_{p,cir}$), which are included in the total plant power.

The total combined power consumption of the cooling system, $\dot{W}_{plant,}$ is also recorded on the SCADA system as measured from the main electrical feeder to the plant. The status (on/off) of all components is also recorded.

A weather station is used to measure the ambient weather conditions. It measures the ambient dry bulb temperature and relative humidity ($T_{a,DB,AMB}$ and $RH_{a,AMB}$), respectively. The ambient enthalpy ($h_{a,AMB}$) is calculated and fed to the SCADA system along with the other parameters. A similar weather station device is used downstream of the BACs to measure the air outlet conditions ($T_{a,o,DB,BAC}$, $RH_{a,o,BAC}$ and $h_{a,o,BAC}$). During the mine's normal operation, its SCADA system continuously logs data in three-minute intervals, which results in 480 data points for each 24-hour day. The accuracy of the relevant measuring instrumentation is summarised in Table 5.

Table 5: Measuring instrumentation of the mine cooling system

Parameter	Instrument	Unit	Accuracy
Water temperature	Wika Model TC40 Type T thermocouple [124]	ºC	± 0.5 ºC
Water flow rate	Krohne UFM 3030 in-line ultrasonic flowmeter [125]	kg/s	± 0.5 %
Air temperature	Testo 6682 with 6616 probe [126]	ºC	± 0.15 ºC
Air relative humidity	Testo 6682 with 6616 probe [126]	%	± 1 %

3.3 Modelling approaches

There are two possible approaches in system modelling. The model's desired outcome and purpose determine the approach to be used. As mentioned earlier, these are known as the forward or classical approach and the data-driven or inverse approach. [123]. These are also referred to as white box and black box approaches. The two types of modelling approaches could also be integrated, resulting in what is called a grey-box model [39, 40].

The primary advantage of the forward approach is that the system does not need to be physically built to model its performance. BLAST, DOE-2 and EnergyPlus use this approach. [123]. These types of models are considered to be more generic in their application, although this comes at the cost of accuracy [40].

Data-driven models, on the other hand, are formulated by measured system data. This is achieved by deriving relations for various parameters by means of regression models for the measured data. Data-driven modelling is often simpler to use, and in many cases, more accurate in modelling the behaviour of the specific system being examined as opposed to forward models [123, 39].

A heat exchanger designer might want to use a detailed tube-by-tube analysis of the various heat transfer phenomena, including convection and conduction, as well as flow phenomena inside and outside the tubes. The designer would therefore benefit from a forward model. On the other hand, an energy analyst would only require an explicit model with fewer parameters based on the boundary performance of some of the system components, and would therefore rather consider a data-driven model.

For the purposes of this study, a combination of forward and data-driven models was used to describe the energy consumption of the various identified major components of the cooling system. This combination is examined and discussed in sections 3.4 to 3.6.

3.4 Cooling towers as direct contact heat exchangers

In typical mine cooling systems, the BACs, PCTs and CCTs are commonly direct-contact heat exchangers. A suitable model that is capable of predicting the performance of these components, with the restrictions of not requiring iterative computation, being smooth and continuous, would be required.

From the literature considered in Section 2.4.2, it was concluded that most cooling tower models found in the literature require iterative computation to arrive at a solution. As this would deteriorate the optimisation application, these models would not be ideally suited for the current study. Arndt [98] presented a suitable model that was adopted for the current study.

The proposed cooling tower modelling method consists of forward and first-principle methods that are based on energy balance and heat transfer fundamentals. In terms of this, the following assumptions are made:

1. Water loss due to evaporation is negligible.
2. The heat transfer surface area remains constant.
3. The saturation enthalpy is assumed to be linear in relation to the wet bulb temperature.
4. The specific heat of the water remains constant for the considered temperature range.

In terms of Assumption 1, Chargui *et al*. [85] suggest that the omission of water loss due to evaporation has resulted in modelling inaccuracies of about 1 °C. The accuracy of the water temperature probes used for the current study is ±0.5 °C, and the marginal error due to omitting the water loss through evaporation was deemed acceptable. In terms of Assumption (3), Lombard [127] showed that for temperatures between 7 °C and 20 °C, the saturation enthalpy behaves linearly and suggests that the linearity of the saturation curve can be extended to 40 °C for cooling tower applications where the temperature range is relatively small. As these ranges are relevant to the current study, this simplification was adopted. Regarding Assumption 4, the maximum and minimum temperatures under consideration typically range from 3 °C to 32 °C. The specific heat of the water at 5 °C is 4.205 kJ/kgK and at 30 °C it is 4.178 kJ/kgK [29]. This range suggests a variance of 0.64% relative to the average value of 4.192 kJ/kgK, and is therefore deemed acceptable.

See Figure 20 for the mass flow rates and boundary thermodynamic properties of interest for a typical mine cooling tower. The known system parameters include the water inlet temperature ($T_{w,i}$) the water mass flow rate ($\dot{m}_w$), the air inlet dry bulb temperature ($T_{a,i}$), the air inlet enthalpy ($h_{a,i}$) and the air mass flow rate ($\dot{m}_a$). In order to analyse the thermal performance of the cooling tower mathematically for optimisation purposes, the cooling tower's air outlet enthalpy ($h_{a,o}$) and the water outlet temperature ($T_{w,o}$) need to be determined explicitly from the known inlet conditions and mass flow rates. In addition to this, as stated previously, the equations used to construct the model should be continuous functions without step changes.

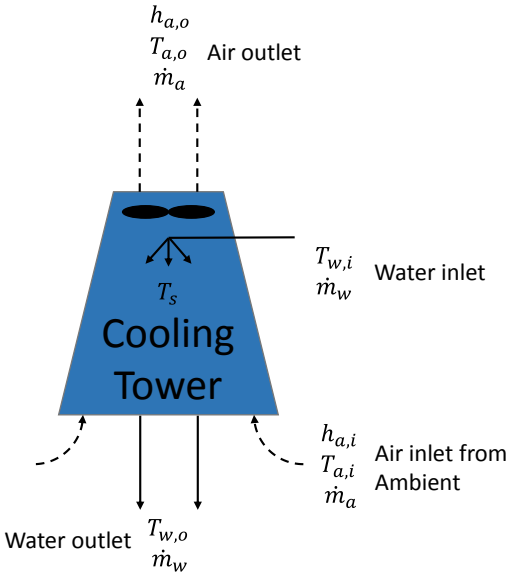

Figure 20: The cooling tower schematic

Based on the heat balance principle and heat transfer rate fundamentals, it is possible to express the steady-state air and water outlet conditions of a cooling tower in terms of the air and water inlet conditions by using Equations (7) to (10) [98].

$$h_{a,o} = \frac{(1-\Gamma)}{(\zeta-\Gamma)} h_{a,i} + \frac{(\zeta-1)h_s}{(\zeta-\Gamma)T_s} T_{w,i} \tag{7}$$

$$T_{w,o} = \frac{\frac{(\zeta-1)\Gamma}{(\zeta-\Gamma)} h_{a,i} T_s}{h_s} + \frac{(1-\Gamma)}{(\zeta-\Gamma)} T_{w,i} \quad (8)$$

with:

$$\zeta = \exp\left(-\beta\left(\frac{h_s}{C_{p,w}\dot{m}_w T_s} - \frac{1}{\dot{m}_a}\right)\right) \quad (9)$$

and,

$$\Gamma = \frac{\dot{m}_a h_s}{C_{p,w}\dot{m}_w T_s} \quad (10)$$

Here, $C_{p,w}$ represents the specific heat of the water. Furthermore, h_s denotes the saturated air enthalpy at the average water droplet temperature in the cooling tower (T_s) calculated, as the arithmetic average of the design water inlet and outlet temperatures. β is the specific cooling tower parameter and characterises the inverse of the effective overall thermal resistance of the cooling tower under consideration [98].

This system parameter can be determined either from the manufacturer's data or from a set of measured performance data. This could be accomplished by minimising the squares of the error of the simulated water outlet temperature values relative to the manufacturer's data or relative to the measured system performance data, as represented in Equation (11).

$$\beta_{min} = MIN \sum_{n=1}^{N} \left(T_{w,o,calc,n} - T_{w,o,real,n}\right)^2 \quad (11)$$

Here, *N* refers to the number of data points in the comparative set. $T_{w,o,calc,n}$ is the calculated water outlet temperature from Equation (8), based on β, while $T_{w,o,real,n}$ is the measured cooling tower water outlet temperature for each data point (n) respectively.

With the air outlet enthalpy known, it is possible to determine the air outlet temperature with Equation (12). This is true based on the assumption that the saturation enthalpy is linear with respect to the wet bulb temperature and can therefore be linearly interpolated [98, 127].

$$T_{a,o} = \frac{(T_{a,i} - T_{w,i})}{(h_{a,i} - \phi T_{w,i})} h_{a,o} + T_{a,i} - \frac{(T_{a,i} - T_{w,i})}{(h_{a,i} - \phi T_{w,i})} h_{a,i} \quad \textbf{(12)}$$

3.5 Water-cooled chillers

Centrifugal compressor chiller machines are most frequently used in the mining industry, as discussed earlier. The cooling load is most often controlled by compressor inlet guide vanes, which control the refrigerant mass flow through the compressor. Modelling the chiller's energy consumption, as required for this study, would require a suitable model that would consider variations in the system's operational parameters, as determined in the previous chapter. In summary, these include variations in the evaporator and condenser water flow rates, as well as the inlet and outlet temperatures of these components.

The component model to be considered for a chiller would also be subject to the limitations of being explicit so that there would be no requirement for iterative computation as well as remaining smooth and continuous for optimisation applications.

From the literature considered in Section 2.5, it is suggested that the maximum cooling a chiller could perform depends, *ceteris paribus*, on the average evaporator and condenser temperatures [19, 102]. This parameter is considered important, as it would be required as a constraint for optimisation purposes. A simplified black box relation for determining the maximum cooling or cooling capacity is given in Equation (13). This simplistic approach, which is based only on a linear relation between the cooling capacity and the evaporator and condenser water

temperatures, was compared to another empirical approach where non-linear relationships that require nine coefficients, instead of three, is used [102]. There was only a 0.86% variation in the average error for the prediction of the cooling capacity. Thus, the more simplistic approach was adopted.

$$CC = c_1 T_{w,avg,evap} + c_2 T_{w,avg,cond} + c_3 \quad \textbf{(13)}$$

In Equation (13), the system-specific constants c_1, c_2 and c_3 could be determined either the manufacturer's data or by a set of measured system performance data. Similar to the cooling tower coefficient, these could be determined by minimising the squares of the errors between the predicted cooling capacity and the measured cooling capacity for each data point. The expression given in Equation (14) could be used for this purpose. In this equation, $CC_{calc,n}$ represents the predicted or calculated cooling capacity, while $CC_{real,n}$ represents the measured value or that provided by the manufacturer.

$$([c_1, c_2, c_3]^T)_{min} = MIN \sum_{n=1}^{N} \left(CC_{calc,n} - CC_{real,n}\right)^2 \quad \textbf{(14)}$$

With the cooling capacity fully defined, the next step would be to express the chiller's energy consumption through the compressor's work input, $\dot{W}_{ref}$. From thermodynamic fundamentals, it is known that the energy input to a refrigeration system is proportional to the cooling that is achieved, and is inversely proportional to the machine's (COP) [102]. The compressor work input could be expressed as follows:

$$\dot{W}_{ref} = \frac{\dot{Q}_{w,evap}}{COP} \quad \textbf{(15)}$$

From Equation (15), it is furthermore known that the cooling performed ($\dot{Q}_{w,evap}$) could be expressed as follows:

$$\dot{Q}_{w,evap} = \dot{m}_w C_p (T_{w,i,evap} - T_{w,o,evap}) \quad (16)$$

It is thus evident that the COP would have to be determined for any set of operational parameters in order to determine the electrical energy required to satisfy the said cooling load. The COP is a function of the cooling performed by the chiller, as well as the condenser and evaporator water inlet temperatures, and could be expressed empirically (see Equation (17)). This is acceptable if the expansion devices are successful in controlling the vapour compression cycle, and if the phase-change heat transfer mechanisms in the condensers and evaporators are not significantly influenced by the possible variation in the refrigerant mass flow rate (especially when the flow is throttled) and the condensing and evaporating wall temperatures. Equation (17) was found in the literature as part of a review of various empirical expressions for determining a chiller's COP [39]. The other forms are included in Appendix A so that other systems could be considered from where the most suitable one could be used. The multivariate polynomial regression model selected here was found to be the most accurate for the typical deep-level mine chillers considered in this study. For this model, an RMSRE value of 0.0114 was obtained, while the other models varied between RMSRE values of 0.0124 and 0.0528.

$$\begin{aligned} COP = {} & \sigma_0 + \sigma_1 \dot{Q}_{w,evap} + \sigma_2 T_{w,i,evap} + \sigma_3 T_{w,i,cond} + \sigma_4 \dot{Q}_{w,evap}{}^2 + \sigma_5 T_{w,i,evap}{}^2 \\ & + \sigma_6 T_{w,i,cond}{}^2 + \sigma_7 T_{w,i,evap} \dot{Q}_{w,evap} + \sigma_8 T_{w,i,cond} \dot{Q}_{w,evap} \\ & + \sigma_9 T_{w,i,cond} T_{w,i,evap} \end{aligned} \quad (17)$$

Since the water mass flow rates through the evaporator and the condenser directly impact on the relevant heat transfer rates, the presence of the heat transfer rates in Equation (17) indirectly represents the impact of the mass flow rate and subsequently includes the effect of part-load operation as a result. In Equation (17), the coefficients σ_0 to σ_9 are system-specific constants that could be derived from the chiller manufacturer's data or system data. These could be obtained through the method of least square errors, as discussed previously, for other components and as given in Equation (18).

$$([\sigma_1, \dots, \sigma_9]^T)_{min} = MIN \sum_{n=1}^{N} \left(COP_{calc,n} - COP_{real,n}\right)^2 \quad \textbf{(18)}$$

Here $COP_{calc,n}$ represents the calculated COP and $COP_{real,n}$ represents the actual measured system's COP.

3.6 Pumps and fans

The energy-saving potential identified earlier is related to variable flow strategies with additional savings achievable through reduced water and air flow. It would therefore necessitate the inclusion of relevant pump and fan energy consumption expressions to the simulation model.

From Equations (5) and (6), the pump and fan power rates are functions of the pressure differential, mass flow rate, fluid density and motor efficiency. The pressure differential could be determined through a simplified version of the Darcy Weishbach equation in Equation (19) to arrive at the simplified Equation (21) [123].

$$\Delta P = \left(\frac{10^6 f L}{D_h} + \sum C\right)\left(\frac{\rho V^2}{2}\right) \quad \textbf{(19)}$$

By replacing the average velocity (V) with $\frac{\dot{m}}{\rho A}$, the equation can be rewritten as Equation (20).

$$\Delta P = \left(\frac{10^6 f L}{D_h} + \sum C\right)\left(\frac{\dot{m}^2}{2\rho A^2}\right) \quad \textbf{(20)}$$

Equation (20) can be simplified by assuming constant values for the friction factor f, characteristic length L, characteristic diameter (D_h) and the flow passage cross-sectional area A^2 for each subsystem containing a pump or fan. The assumption of a constant friction factor was found acceptable, since the typical variance of this value for the flow ranges considered

during this study was found to be less than 0.1% [35]. By doing so, Equation (20) reduces to Equation (21)

$$\Delta P = k\frac{\dot{m}_{w/a}^2}{\rho} \tag{21}$$

In Equation (21), the only system-specific parameter that needs to be determined is the flow admittance value (k), which could be obtained from a single-point measurement or from manufacturer's data. From here Equations (5) and (6) could subsequently be rewritten as given in Equation (22), resembling the electrical power input $\dot{W}_{p,f}$ for pumps and fans respectively.

$$\dot{W}_{p,f} = k\frac{\dot{m}_{w/a}^3}{\rho^2 \cdot \eta_{p,f}} \tag{22}$$

Here, $\dot{m}_{w/a}$ is the mass flow rate of the fluid (whether it is water for a pump or air for a fan), ρ is the average fluid density, and $\eta_{p,f}$ is the efficiency of the complete pump or fan arrangement, including the motors, and would typically be obtained from the manufacturer's information.

3.7 Simulation model parameter determination and verification

In order to construct a thermodynamic model of a mine cooling system installation, the various component parameters first need to be determined and verified. In this study, this was done from data obtained for the case study mine for a one-week period in February, which represents a typical summer design period for the particular location. The results are presented in sections 3.7.1 to 3.7.3, from where they would be further developed as required for optimisation purposes as introduced below and executed in Chapter 5.

The one week's data in February that is considered for parameter determination, referred to as Dataset A in this document, was isolated so that the weekends before and after were excluded, as mining operations might be reduced during weekends. Similarly, Dataset B, which contains data from a period one month after that of Dataset A, was isolated to exclude the two weekends

before and after that period. Dataset B was used to validate the integrated simulation model outside the training data of Dataset A.

A further validation was conducted to confirm the applicability of the simulation model and the parameters determined with Dataset A by simulating a typical week in August (Dataset C), which was six months after the training dataset in order to determine if the model's accuracy would remain relatively unchanged for a period significantly later than that of the training dataset. It should be noted that Datasets A, B and C consist of data in the three-minute intervals, as recorded by the SCADA system. Due to computational constraints, especially when computing the minimum energy consumption via the optimisation platform, and the intention to simulate and optimise a whole year's data, Datasets A, B and C were thereafter also considered in hourly average data formats as Datasets D, E and F for the validation. Finally, the annual calculation of hourly average data was performed for an entire year and represented by Dataset G. This dataset was used to perform energy minimisation in order to confirm the hypothesis that the energy minimum operation of the system could be determined by using an integrated system simulation along with the corresponding optimisation. The typical measurement ranges of Dataset A to Dataset G are shown on Table 15 in Appendix C.

Only the chiller and cooling tower models are considered as part of the subsystem model verifications, while the pump and fan power are included in the integrated simulation model (see Section 4.2). The motivation for this approach is that the power consumption of the pumps and fans were not logged individually on the SCADA system, but rather included as part of the main feeder energy measurements that were recorded. The component-specific parameters are presented without a correlation to measured data, as these were determined by single-point the measurement's and manufacturer name-plate data where applicable.

The accuracies of the parameter determination correlations are interpreted with the RMSRE method as an index of the error, and can be calculated with Equation (23) [65]. It is furthermore suggested that RMSRE values below 0.1 are deemed acceptable for engineering applications. In addition, the average percentage error, as well as the percentage of time that the correlations remain inside a certain error margin, is considered.

$$RMSRE = \sqrt{\frac{\sum_{n=1}^{N}\left(\frac{D_{real,n}-D_{sim,n}}{D_{real,n}}\right)^2}{N}} \quad (23)$$

Where D_{real} and D_{sim} denote the measured and calculated or simulated value for the same parameter respectively.

3.7.1 Cooling towers

Dataset A was used to calibrate and determine the cooling tower parameters β_{PCT}, β_{BAC} and β_{CCT} for the PCTs, BACs and CCTs respectively. The sections to follow briefly discuss the parameters and the correlations obtained. For these determinations, Equations (7) to (12) were used to simulate the water and air outlet temperatures. The system's design operational parameters are presented in Table 6.

Table 6: PCT, BAC and CCT design operational parameters

Parameter	Unit	PCT	BAC	CCT
Water mass flow rate	kg/s	360 (maximum)	750 (maximum)	2 700 (maximum)
Water inlet temperature	°C	30	3	32
Water outlet temperature	°C	24	9	27
Air mass flow rate	kg/s	720 (fixed)	1 250 (maximum)	1 350 (fixed)
Air inlet wet bulb temperature	°C	18 °C	18 °C	18 °C
Air inlet specific enthalpy	kJ/kg	50 kJ/kg	50 kJ/kg	50 kJ/kg
Air outlet wet bulb temperature	°C	N / A	7 °C	N / A
Air outlet specific enthalpy	kJ/kg	N / A	27 kJ/kg	N / A

Pre-cooling tower

The PCT model parameter was obtained as β_{PCT} = 655.12 W/K with the correlation between the simulated and measured data that achieves an RMSRE value of 0.0651 on the water outlet temperature. The calculated water outlet temperature remained in a ± 1 °C error margin for 66.24% of the time, while it remained in a ± 2 °C error margin for 89.61% of the time. The

average absolute error achieved was 0.87 °C, which was deemed acceptable, since the accuracy of the temperature measuring instrumentation is ± 0.5 °C.

The parameter determination verification is graphically presented in the form of a correlation between the measured and calculated water outlet temperatures, as shown in Figure 21, which includes the ± 1 °C and ± 2 °C error margins considered above. See Figure 22 for the superimposed graphs displaying the temperatures for the week of Dataset A.

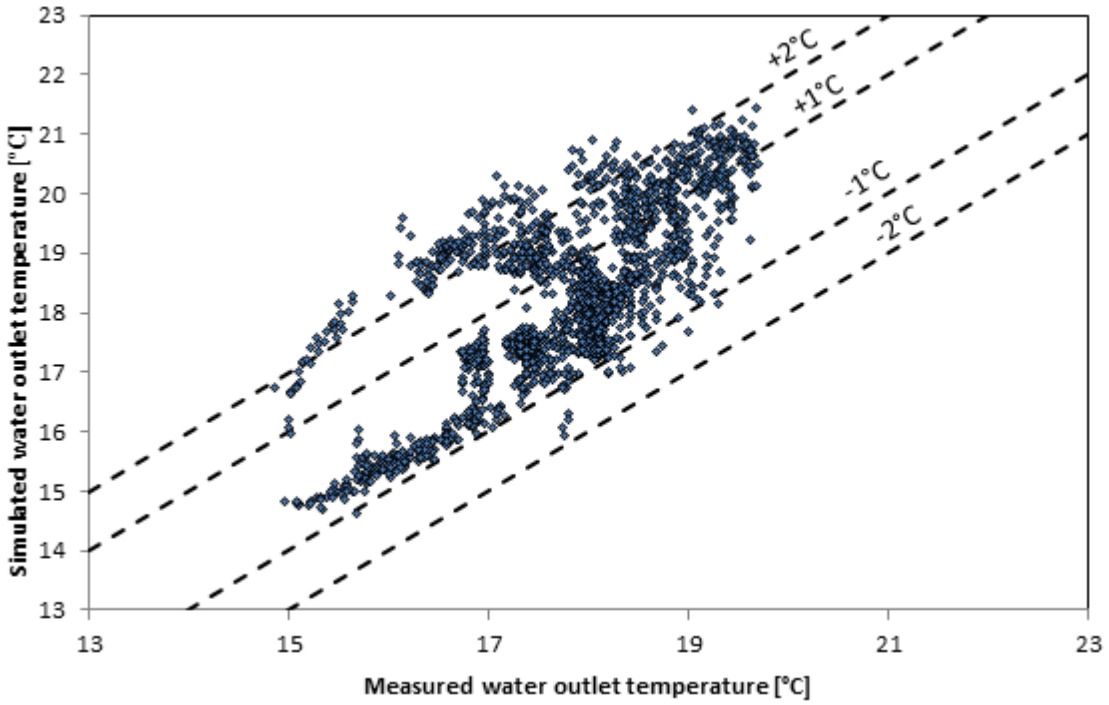

Figure 21: The PCT parameter determination water outlet temperature correlation for Dataset A

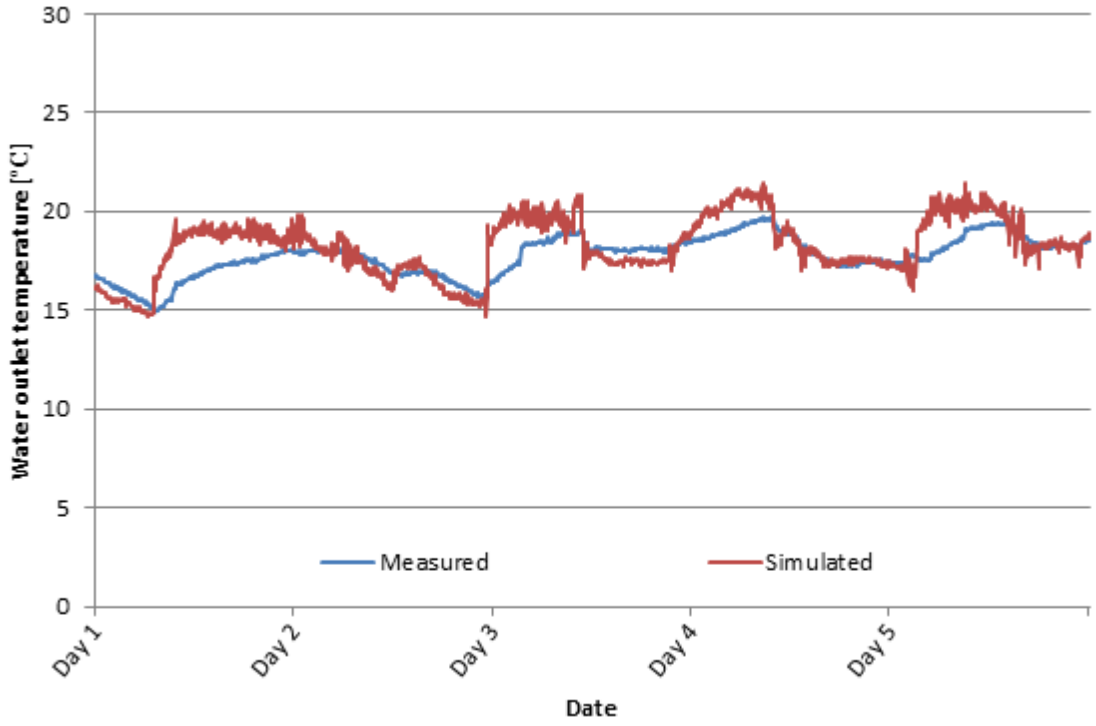

Figure 22: The PCT simulated and measured water outlet temperature for Dataset A

Bulk air cooler

Dataset A was used to determine the BAC's parameter. Before this could be achieved, the water outlet temperature, $T_{w,o,BAC}$ and air flow rate, $\dot{m}_{a,BAC,}$ of the BAC had to be calculated, as these were not directly measured and included in the data logged on the SCADA system. These values were calculated by means of a mass and energy balance across the BAC and pre-cooling dam.

The energy balance considered across the pre-cooling dam is presented in Equation (24). The following assumptions apply for the energy balance:

1. The specific heat of the water remains constant for the temperature range considered.
2. There is no water loss due to evaporation, as the dam is enclosed.
3. The pre-cooling dam is covered and considered adiabatic.
4. All pumps and pipes connecting to and from the dam are adiabatic.

$$T_{w,o,BAC} = \frac{\dot{m}_{w,evap} \cdot T_{w,i,evap} - \dot{m}_{w,mine} \cdot T_{w,o,PCT} - (\dot{m}_{w,evap} - \dot{m}_{w,mine} - \dot{m}_{w,BAC}) \cdot T_{w,o,evap}}{\dot{m}_{w,BAC}} \quad \textbf{(24)}$$

Following from the water outlet temperature determined in Equation (24), the BAC's air flow rate $\dot{m}_{a,BAC}$ can be determined by means of the energy balance through the BAC, as presented in Equation (25).

$$\dot{m}_{a,BAC} = \frac{C_{p,w} \cdot \dot{m}_{w,BAC}(T_{w,o,BAC} - T_{w,o,evap})}{h_{a,AMB} - h_{a,o,BAC}} \quad \textbf{(25)}$$

The BAC's parameter determination was subsequently calculated as β_{BAC} = 835.19 W/K with the correlation between the simulated and measured water outlet temperature achieving a RMSRE value of 0.0648. The simulated water outlet temperature remained in a ± 1 °C error margin for 81.58% of the time and an average absolute error of 0.5 °C, again remaining inside the measuring accuracy range of 1 °C. It was therefore deemed acceptably accurate.

The parameter determination verification is included in the form of a correlation of the simulated and measured water outlet temperatures, as shown in Figure 23, which includes the ± 1 °C error margin considered. The temperatures for the period of Dataset A are superimposed in Figure 24.

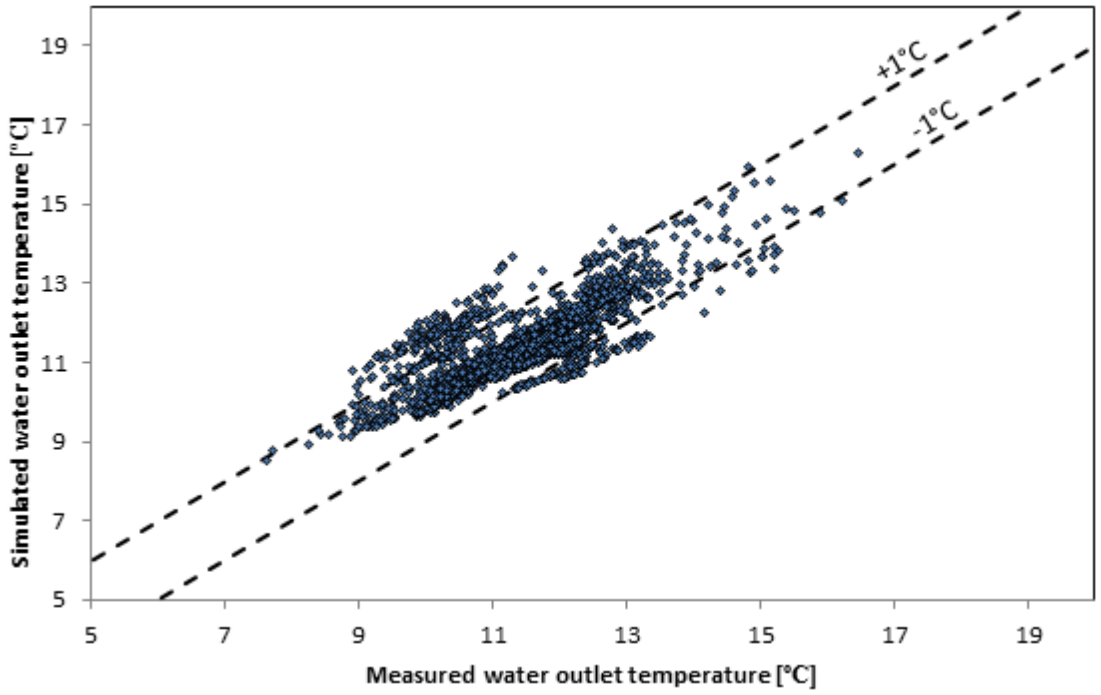

Figure 23: The BAC's parameter determination water outlet temperature correlation for Dataset A

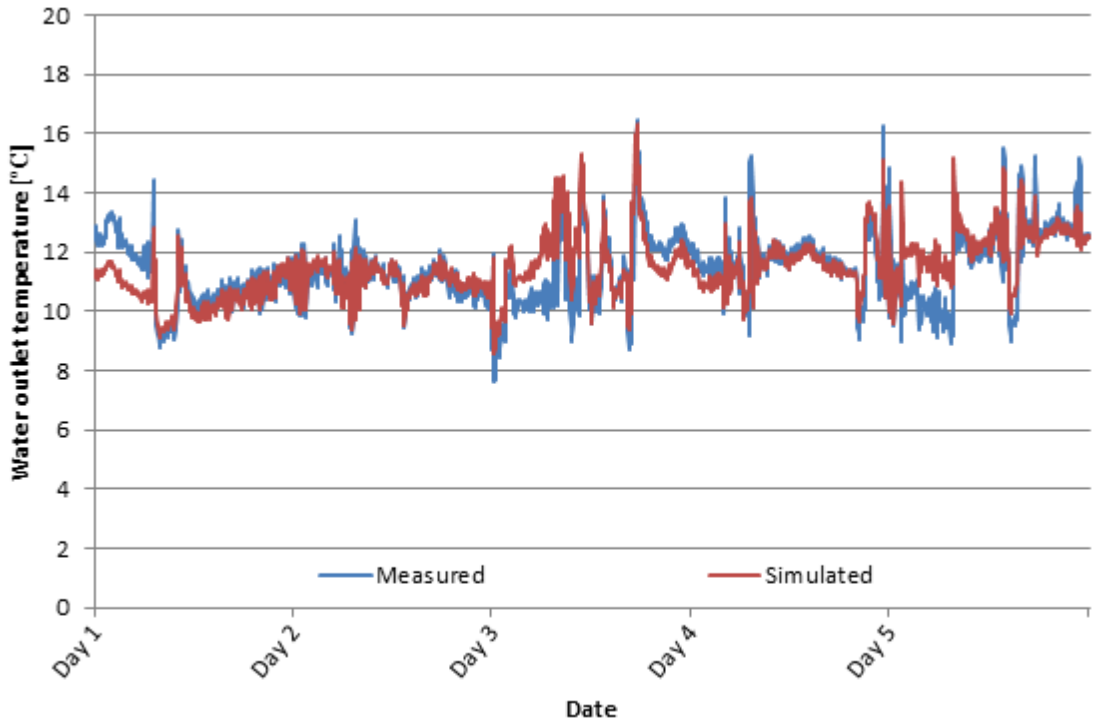

Figure 24: The BAC's simulated and measured water outlet temperature for Dataset A

It would be beneficial for the potential savings opportunity relating to the BAC described earlier to consider the model behaviour for variations in the operational parameters, especially the air outlet conditions (as the air outlet enthalpy), as the objective of the BAC is to condition the ambient air for underground use. This is only considered for the BAC, as the air outlet conditions of the PCT and CCT are not considered important and are therefore not relevant to the current investigation. With the suggested model and the calculated system parameter (β), the expected behaviour of the BAC for different operating conditions can be predicted. Figure 25 gives the outlet air enthalpy of the BAC for different air mass flow rates and air inlet temperatures, while the water mass flow rate remains constant at the design value of 650 kg/s and the ambient relative humidity (RH) remains constant at the design value of 50%. Figure 26 gives the outlet air enthalpy for variations in the water mass flow rate at various air inlet temperatures, while the air mass flow and RH remain constant at the design rates of 1 250 kg/s and 50% respectively.

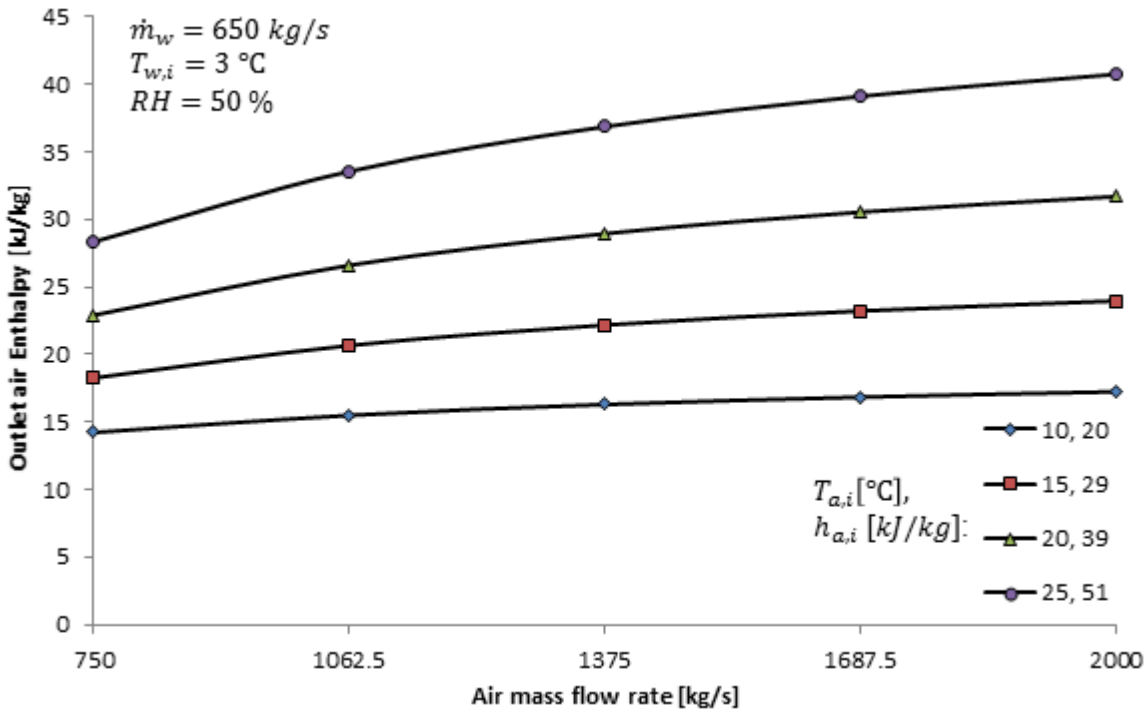

Figure 25: The BAC's air outlet enthalpy behaviour by varying air mass flow rate

From Figure 25, it can be seen that the air outlet enthalpy increases non-linearly as the air flow rate increases with a constant water flow rate and a constant RH. This corresponds with the expected behaviour described by Lemouari *et al*. [72]. This proposes that lower air enthalpies can be maintained during reduced air flow requirement periods, which results in the opportunity to reduce water consumption as the water flow can also be reduced during these periods, as long as acceptable air outlet conditions are maintained. From Figure 25, it can also be seen that the air outlet conditions behave more linearly with a smaller gradient as the air inlet temperature drops. This indicates that the air outlet conditions are less sensitive to air flow variations for lower air inlet temperatures.

From Figure 26, it can be seen that the air outlet enthalpy decreases non-linearly as the water flow rate is increased, while the air flow rate and RH remain constant. From this graph, it can also be seen that the reduction converges as the flow rate increases, which results in the opportunity to reduce the water flow rate fractionally when operating in the higher end of the water flow rate range, while maintaining nearly the same air outlet conditions. The water flow rate can be reduced further for lower air inlet temperatures, as the air outlet conditions behave nearly linear with a smaller gradient at lower air inlet temperatures.

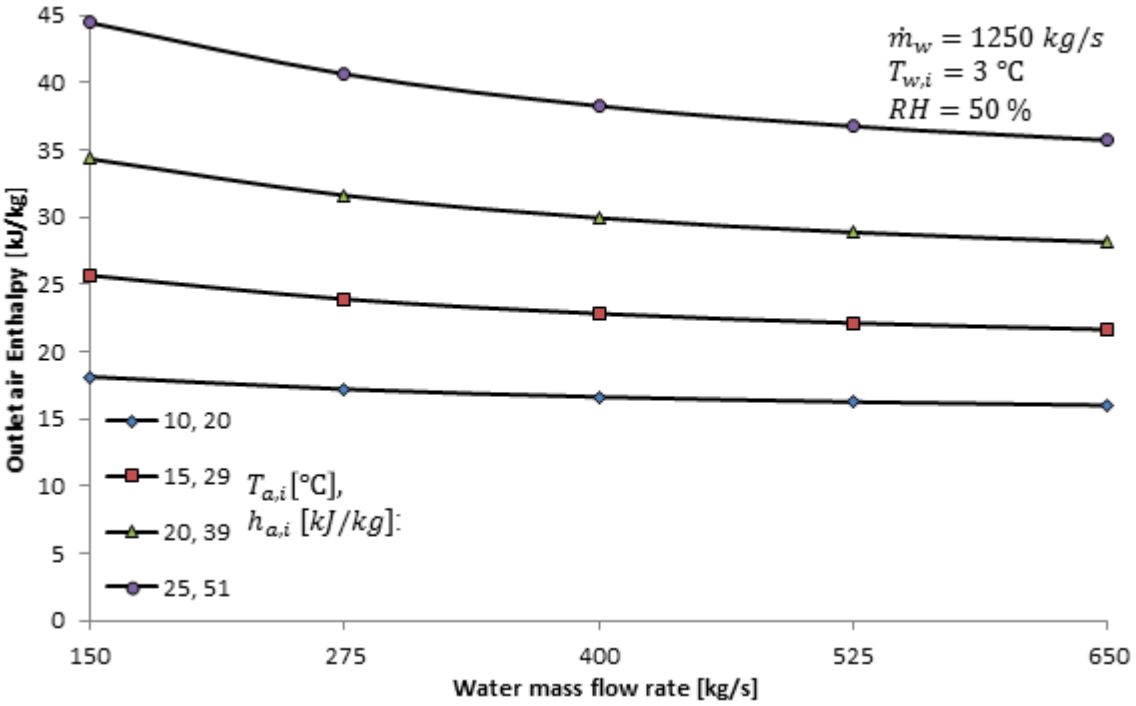

Figure 26: The BAC's air outlet enthalpy behaviour by varying the water mass flow rate

The behaviour of the model obtained above assumed a constant ambient RH of 50%. In order to determine the model's behaviour for other ambient RH values, a few aspects will now be considered. Firstly, the highest allowed ambient RH for which the system can sustain the required cooling rate at fixed air and water mass flow rates should be determined. Secondly, this activity is repeated for variations in the air mass flow rate. This is finally repeated for variations in the water mass flow rate. In Figure 27, the highest allowed RH for fixed mass flow rates of $\dot{m}_a$ = 1250 kg/s and $\dot{m}_w$= 650 kg/s are shown for different air inlet temperatures, which would yield an air outlet enthalpy of 35 kJ/kg. It should be noted that a target air outlet enthalpy of 35 kJ/kg was used, as it corresponds to the BAC's air outlet enthalpies found in the literature [22]. From Figure 27, it can be seen that the maximum RH satisfying this requirement commences at 100% up to an air inlet temperature of around 17 ºC, from where the highest allowed RH starts decreasing, suggesting that, for air inlet temperatures greater than 17 ºC, the cooling tower will not be able to cool the ambient air far enough to obtain the desired air outlet enthalpy should the air inlet RH remain higher than the curve shown in the graph.

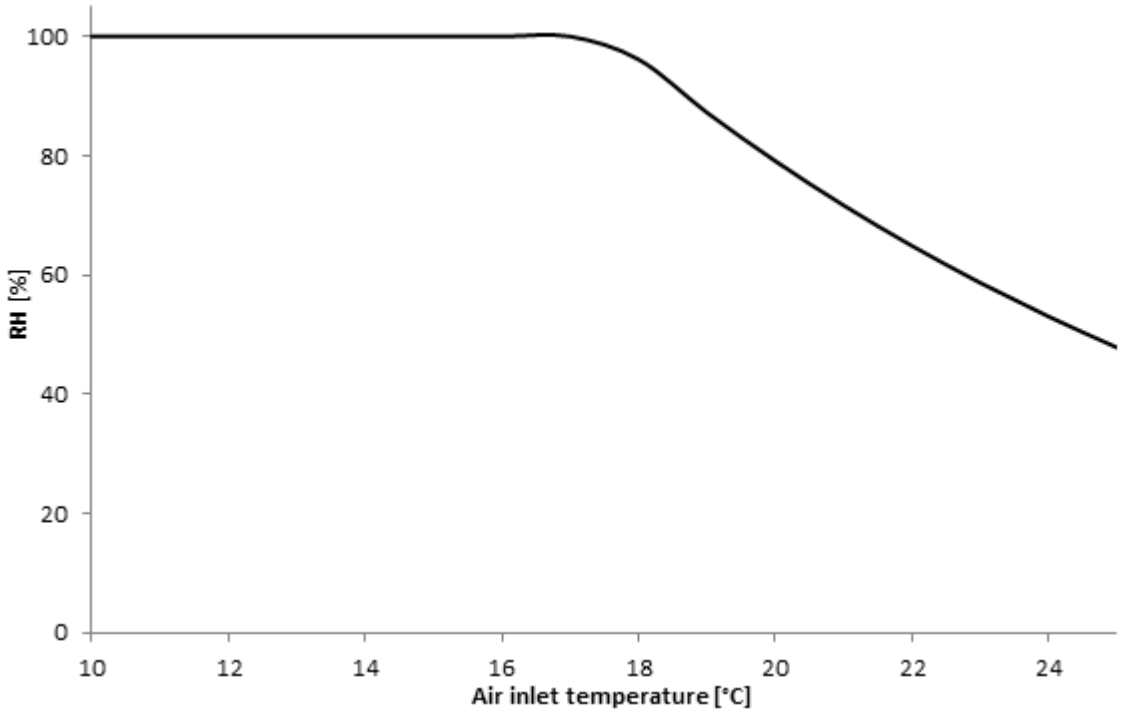

Figure 27: The BAC's maximum air inlet RH for a given air inlet temperature at design water and air mass flow rates

Next, the impact on the model's behaviour in terms of variances in the air inlet RH and temperature were determined for cases where the air and water mass flow rates were varied. Figure 28 shows the maximum air inlet RH values at which the BAC will be able to maintain the desired outlet conditions for variances in the air mass flow rate and air inlet temperature, while the water mass flow rate remains constant at the design rate of 650 kg/s. Figure 29 similarly shows the maximum air inlet RH values for variances in the water mass flow rate and air inlet temperature, while the air mass flow rate remains constant at the design rate of 1 250 kg/s.

From Figure 28, it can be seen that the maximum air inlet RH decreases as the air flow rate increases. It is also evident that the magnitude of variance decreases as the air flow rate increases, suggesting that the maximum air inlet RH is less sensitive to air flow variances at higher air flow rates than at lower air flow rates.

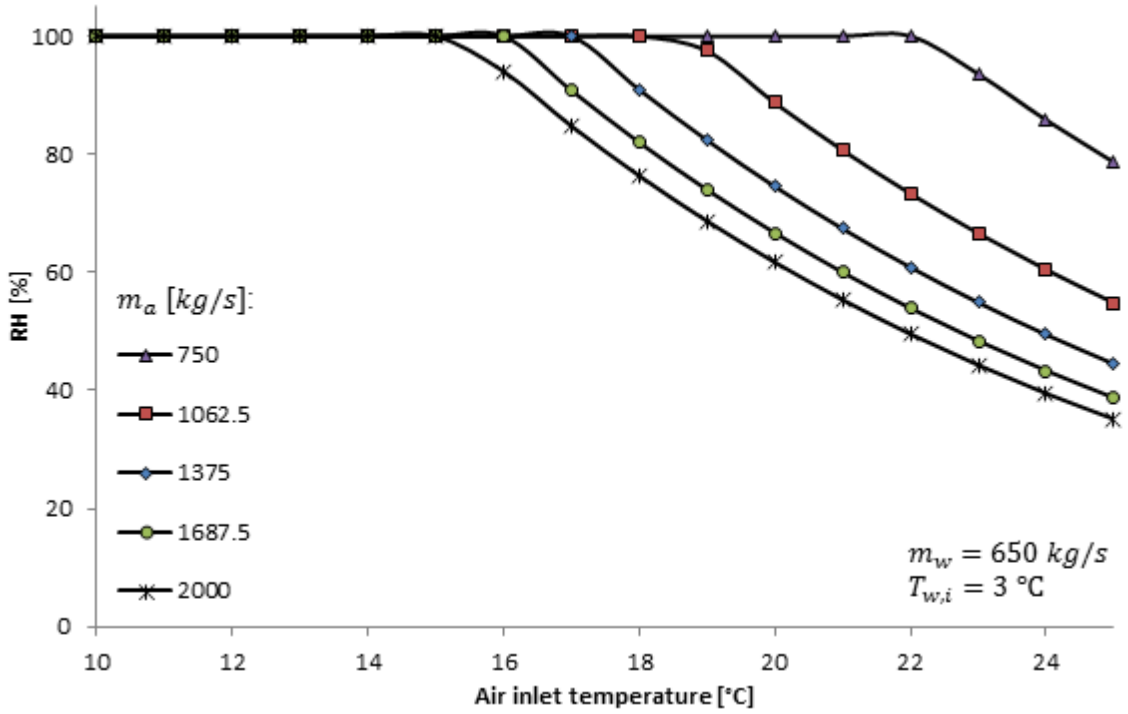

Figure 28: The BAC's maximum air inlet RH for given air inlet temperatures with varying air mass flow rates

From Figure 29, it can be seen that the maximum air inlet RH decreases as the water flow rate decreases. Furthermore, it can be seen that the variance in the maximum RH increases as the water flow rate decreases, which suggests that the maximum air inlet RH is more sensitive to water flow variances when operated at reduced water flow rates.

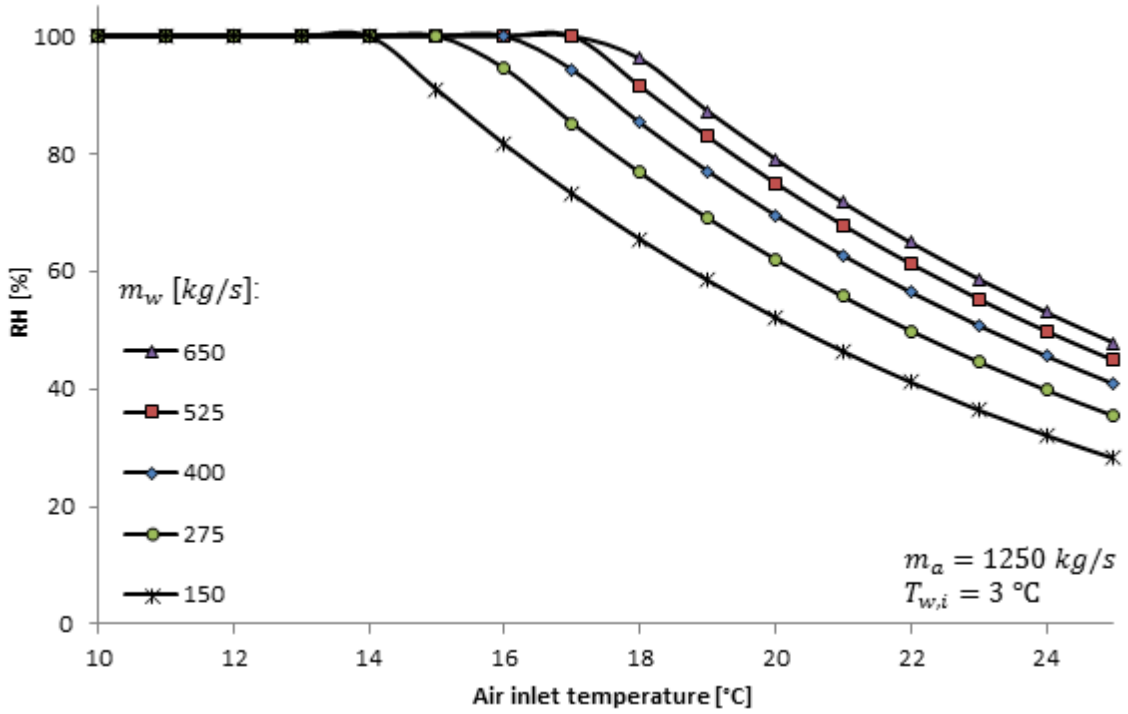

Figure 29: The BAC's maximum inlet air RH for the given air inlet temperature with varying water mass flow rates

Condenser cooling tower

The CCT model parameter was the last cooling tower model considered and was determined as β_{CCT} = 234.98 W/K. For this determination, the correlation between the simulated and measured water outlet temperature achieved an RMSRE value of 0.0246 with the error remaining inside a ± 1 °C error margin for 90.07% of the time. The average absolute error that was obtained was 0.48 °C, which is again inside the instrumentation accuracy range of 1 °C and therefore considered acceptably accurate.

This parameter's determination verification is also graphically presented, as shown in the correlation between the calculated and measured water outlet temperatures in Figure 30, which includes the ± 1 °C error margins considered as described above. These temperatures are also superimposed as displayed on the graphs in Figure 31 for the week of Dataset A.

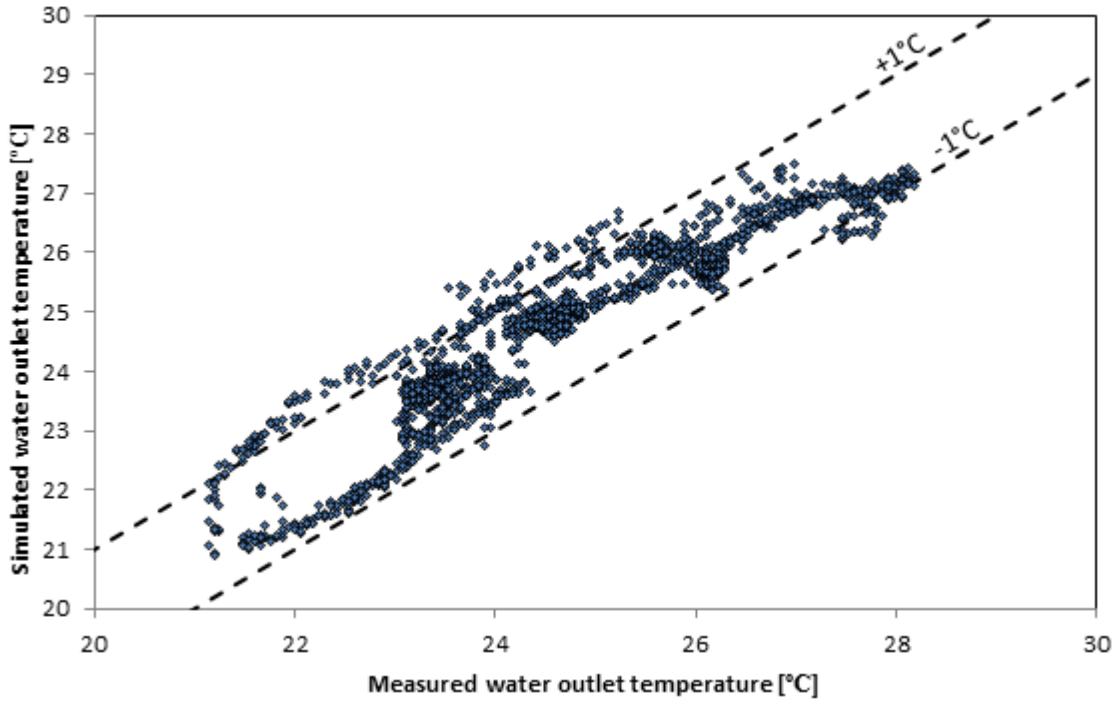

Figure 30: The CCT's parameter determination water outlet temperature correlation for Dataset A

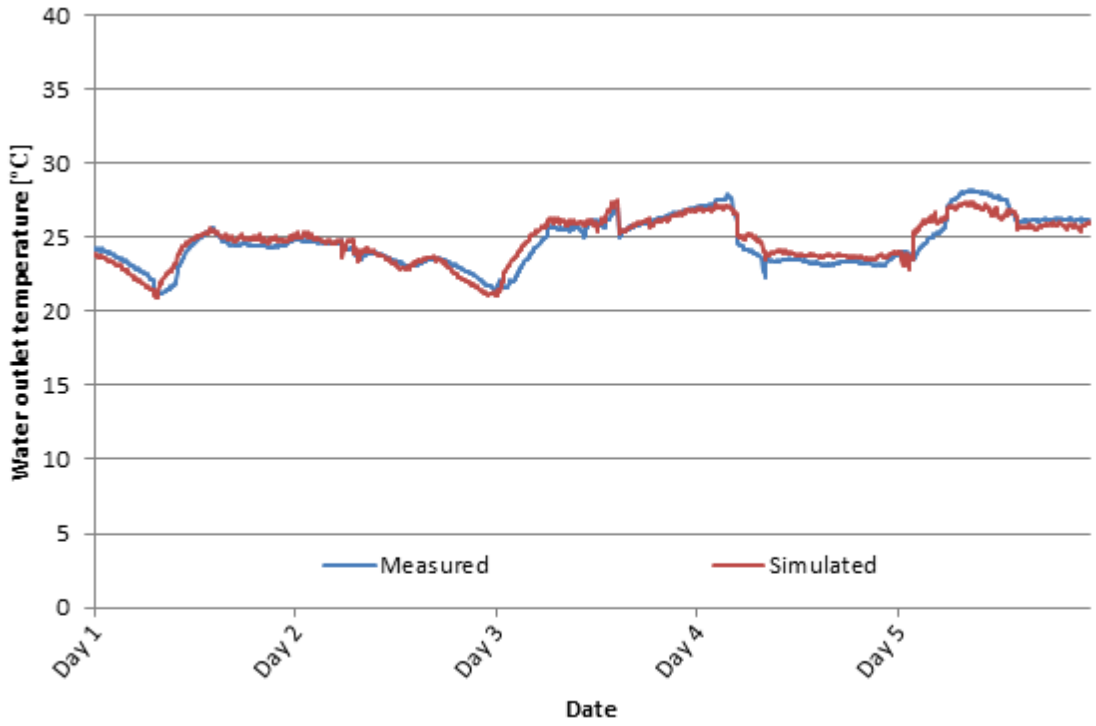

Figure 31: The CCT's simulated and measured water outlet temperature for Dataset A

3.7.2 Chiller

Similar to the cooling towers, Dataset A was used to determine and verify the chiller machines' cooling capacity (CC) model parameters (c_1, c_2 and c_3), as well as the COP model parameters (σ_0 to σ_9). Equations (13) to (18) were used for this purpose. For the CC model's parameters, the data had to be filtered to only include instances where the chiller operated at full capacity to capture the maximum capacity fluctuations, as the water temperatures and flow rates of the evaporator and condenser varied. This was achieved by isolating data from Dataset A, where the vane position of the chiller is above 98% to ensure near-full load operation only. To determine of the COP parameters, all the elements in Dataset A were used, which includes both full load and part-load operations.

For these parameter determinations, the correlation accuracies are considered based on the RMSRE value that was obtained, as well as the percentage of time that the simulated values remained in ± 5% and ± 10% error margins respectively. The model parameters, as well as the accuracies achieved, are summarised for the CC and COP in Table 7 and Table 8 respectively.

Table 7: The chiller CC model parameters and correlation accuracies achieved

CC parameter	Value	RMSRE	Average error	Error ≤ 10%	Error ≤ 5%
c_1	$9.562E+03$	0.0197	1.49%	All data points	97.9% of data points
c_2	$4.052E+02$				
c_3	$-2.067E-02$				

Table 8: The chiller COP model parameters and correlation accuracies achieved

COP parameter	Value	RMSRE	Average error	Error ≤ 10%	Error ≤ 5%
σ_0	$3.251E+01$	0.0114	0.75%	All data points	99.4% of data points
σ_1	$-2.573E-03$				
σ_2	$1.674E-02$				
σ_3	$-1.393E+00$				
σ_4	$3.639E-08$				
σ_5	$5.435E-03$				
σ_6	$1.585E-02$				
σ_7	$3.721E-05$				
σ_8	$8.615E-05$				
σ_9	$-1.546E-02$				

The CC and COP parameter determination verifications are presented graphically in Figure 32 and Figure 33, which also indicate the error margins of ± 5% and ± 10% that were considered earlier and reported in Table 7 and Table 8. The simulated and measured CC and COP are furthermore superimposed in Figure 34 and Figure 35 for Dataset A.

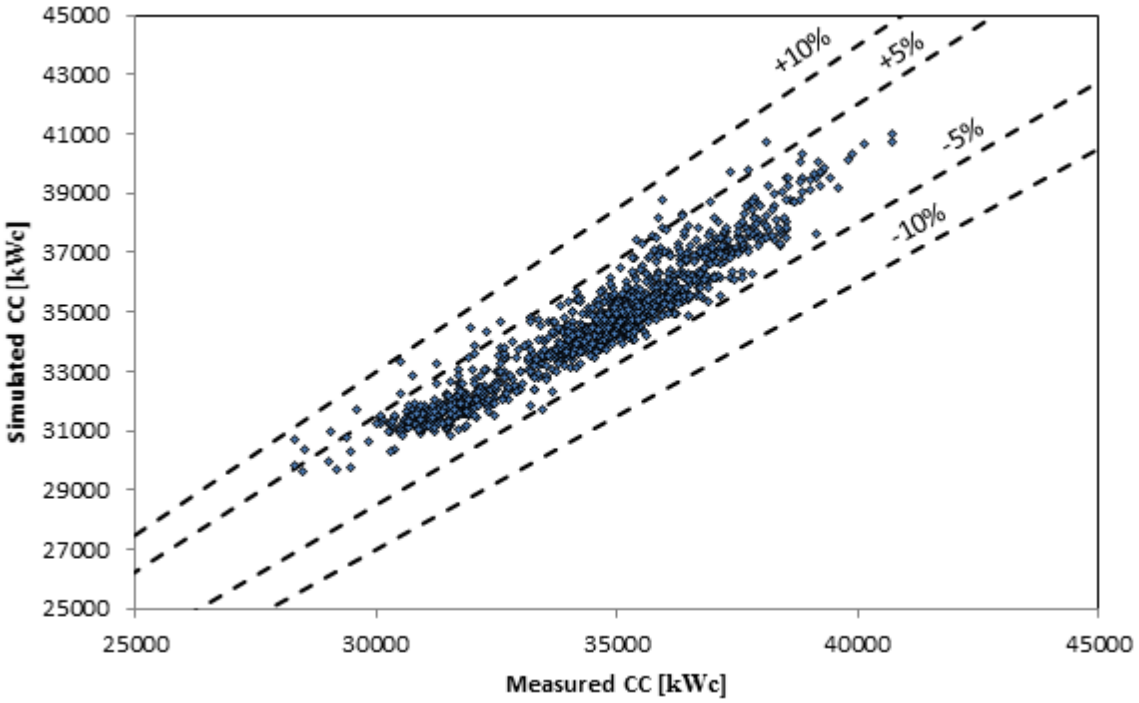

Figure 32: The chiller's CC parameter determination correlation for Dataset A

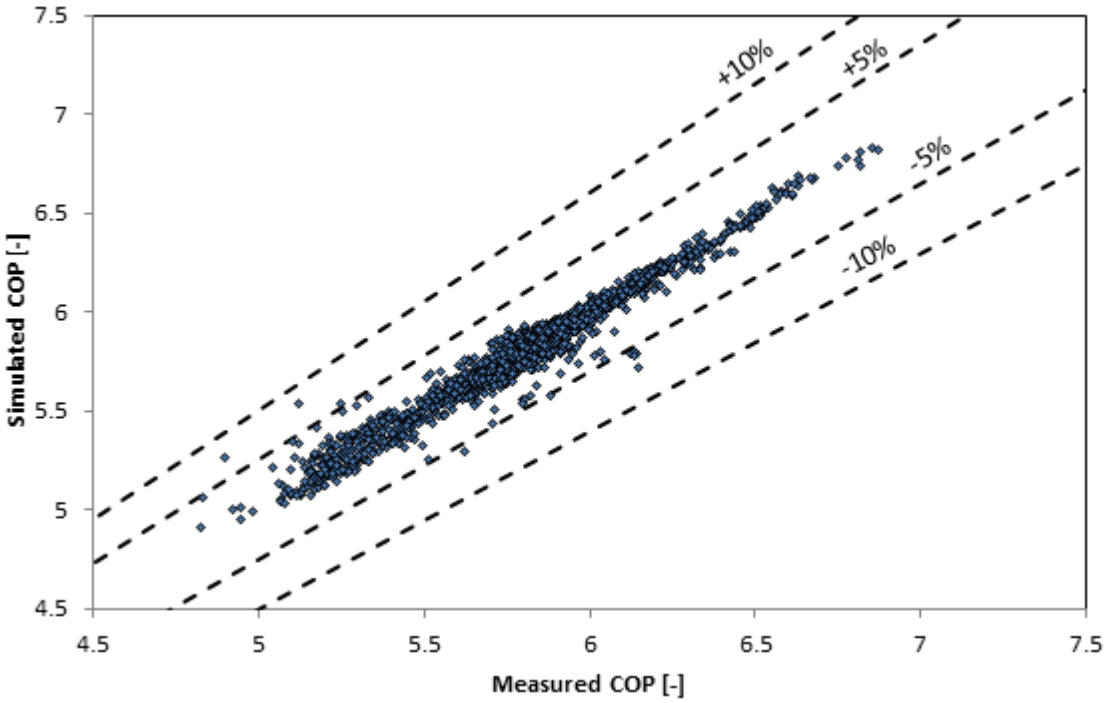

Figure 33: The chiller's COP parameter determination correlation for Dataset A

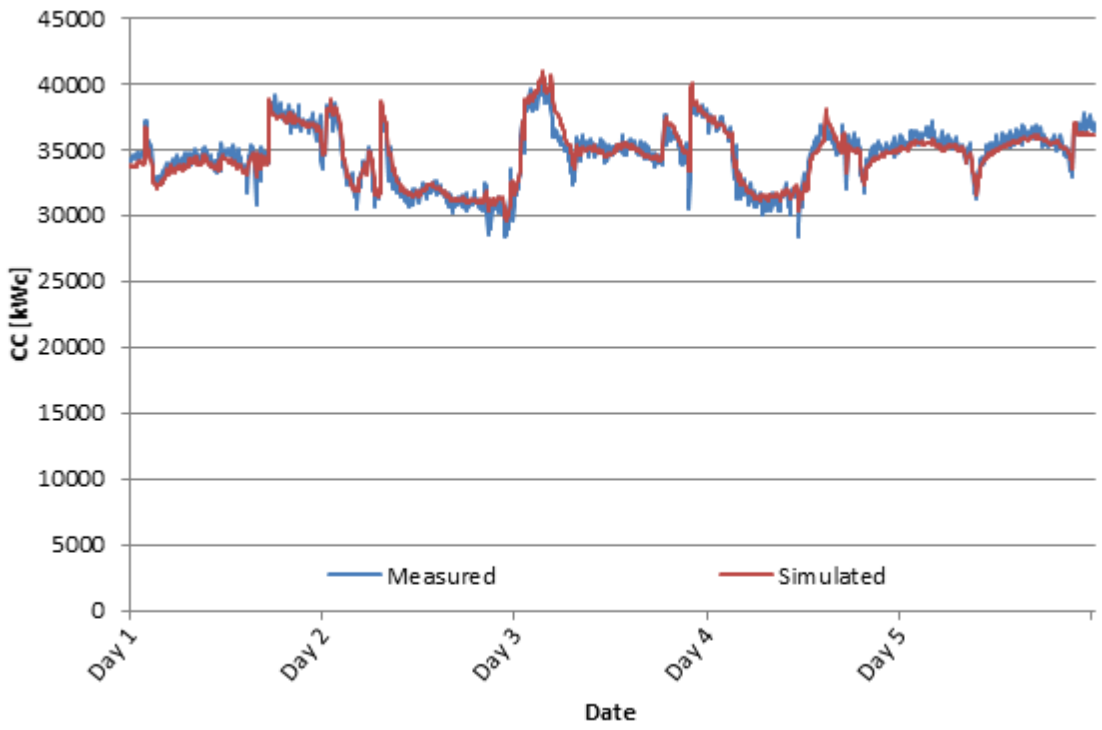

Figure 34: The chiller's simulated and measured CC for Dataset A

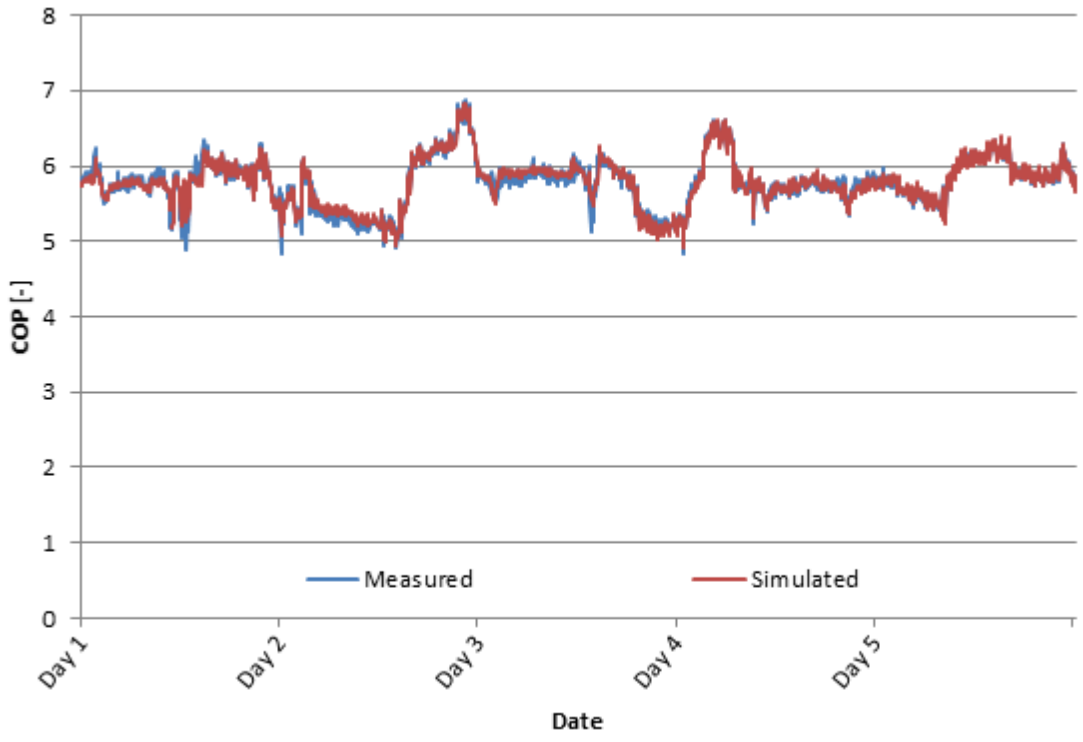

Figure 35: The chiller's simulated and measured COP for Dataset A

3.7.3 Pumps and fans

The pumps and fans were not individually measured and logged on the mine's SCADA system, as stated earlier. For these components, Equations (21) and (22) were used to determine the pressured differential and admittance values of each based on the manufacturer's name plate information. Table 9 summarises the pumps and fans that were considered, along with the parameters as determined.

Table 9: The pressure differentials and flow admittance values of the pumps and fans

Component	Pressure differential, ΔP [kPa]	Admittance value, k [m^4]
Evaporator pump	352	5.63
Pre-cooling tower pump	311	2.40
Pre-cooling tower fan	0.3	4.22E-07
BAC pump	240	3.84
Excess pump	178	1.37
Condenser pump	284	1.40
Condenser fan	0.28	5.49E-06

3.8 Conclusion

The mine cooling system considered as part of the current study was presented and discussed based on the system's installed capacities and design operational parameters. This was assisted by a schematic layout of the cooling system, which indicates all the components, as well as the relative parameters and power inputs. The SCADA system capturing the mine's data was briefly described along with the typical measuring instrumentation accuracies.

Suitable component models for the mine cooling system were identified through an extensive literature survey. These models were based on first-principle expressions and data-driven models, which resulted in a combination of the two methods, known as a grey-box model once integrated.

The simulation model's component parameters were subsequently determined, based on one week's data isolated as a typical summer week and labelled Dataset A. The various operational parameters for each of the major components were determined with correlation accuracies ranging between RMSRE values of 0.0114 and 0.0651. Cooling tower water outlet

temperatures obtained average absolute errors ranging between 0.48 °C and 0.89 °C. These are deemed acceptable since the typical temperature measuring error was ± 0.5 °C.

These models will ultimately form part of an integrated simulation model once they are all coupled together. The outlet of one component will become the inlet condition to the next. The implementation and validation this model is presented in Chapter 4, where the simulation models identified in this chapter are integrated to simulate the existing operation of the cooling system as the baseline.

4 Case study – baseline simulation

4.1 Preamble

The cooling system of the Kopanang deep - level gold mine, which is described in Section 3.2, was simulated based on the actual operational parameters measured by the SCADA system to establish and validate a baseline integrated simulation model. This model's energy consumption is compared to cooling system's actual measured energy consumption, suggesting the simulation model's overall accuracy.

Datasets A to G, as described in Section 3.7, were considered as part of the baseline simulation to validate the simulation model's performance on data extracted from different parts of the year and different time periods away from the training data, as well as to confirm the performance of variations in the dataset measuring increments.

4.2 Baseline simulation and validation

For the purpose of the current study, the integrated simulation model was constructed by coupling the component models identified in Chapter 3 with Microsoft (MS) Office Excel due to its ease of use via the graphical user interface and regular availability. The automation of the simulation was therefore conducted through Visual Basic for Applications (VBA) code programmed in the background of MS Office Excel. This typically included sweeping through the data sets and setting up the simulation model for various dataset entries.

The integrated cooling system's power consumption was simulated based on the same thermal hydraulic parameters measured by the mine's SCADA system. This was achieved by assigning the inlet and outlet conditions of each component based on the measured data, and simulating the mass flows, as well as inlet and outlet temperatures accordingly. The simulated results, as shown in Equation (26), were then compared to the measured total system power to determine the accuracy of the energy consumption prediction of the simulation model.

$$\dot{W}_{plant} = \sum_{j=1}^{6} \dot{W}_{ref,j} + \sum_{j=1}^{2} \dot{W}_{p,PCT,j} + \sum_{j=1}^{2} \dot{W}_{f,PCT,j} + \sum_{j=1}^{3} \dot{W}_{p,BAC,j} + \sum_{j=1}^{6} \dot{W}_{f,CCT,j} + \sum_{j=1}^{6} \dot{W}_{p,cond,j} + \sum_{j=1}^{6} \dot{W}_{p,evap,j} + \dot{W}_{p,ex,n} \quad (26)$$

4.2.1 Dataset A baseline simulation

Dataset A consists of the same dataset used to calibrate the simulation model through parameter determination. The simulated and measured integrated system power for the one-week period is shown in Figure 36. From this figure, it is evident that the simulated power follows the measured power consumption relatively accurately.

The simulation achieved an RMSRE value of 0.0498 and an absolute average error of 3.52%, which compared well with the simulation accuracies achieved previously, where average errors between 4.1% and 4.3% were achieved [20, 96]. For clarity and justification of the step changes in the power consumption, the number of chiller machines in operation is included on the secondary axis of Figure 36. From this figure, it is evident that the simulation model tends to over-predict the power consumption for instances where more chiller machines are running, while the opposite is true for fewer chillers in operation.

4.2.2 Dataset B baseline simulation

Dataset B was taken one month after the parameter determination period of Dataset A to determine the accuracy of the model for a period relatively near, but outside the parameter determination dataset. The simulated and measured integrated cooling system power for this dataset is shown in Figure 37. From this figure, it can be seen that the simulated power closely represents the measured power.

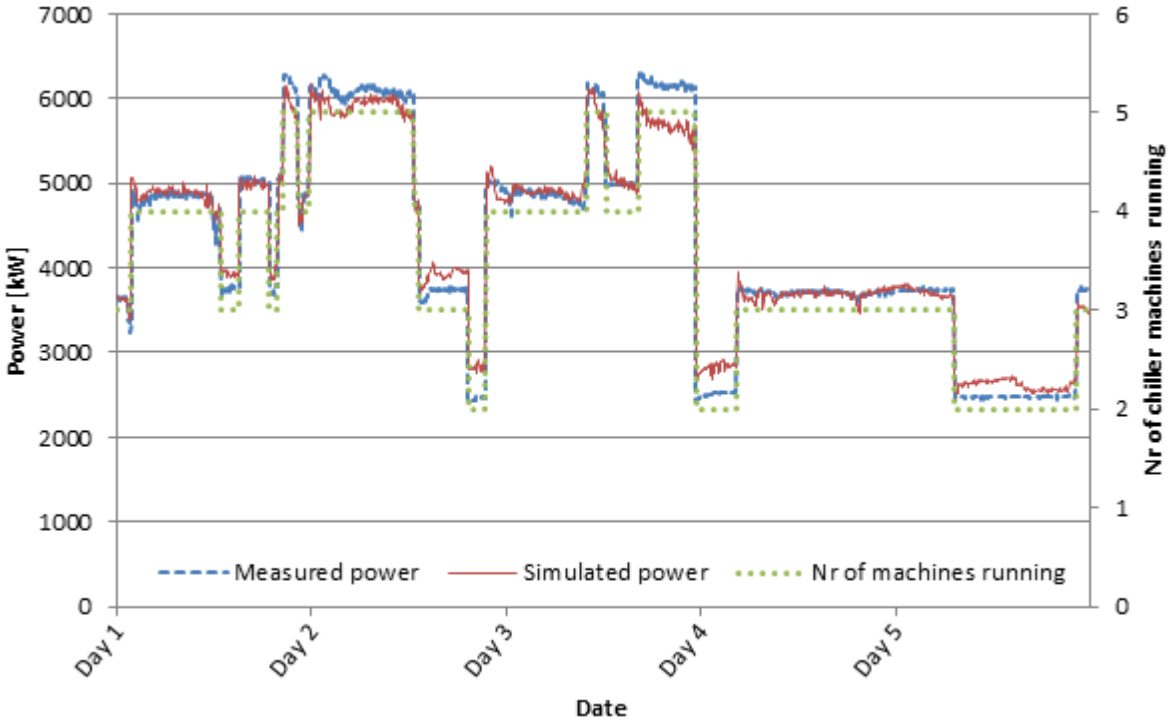

Figure 36: The simulated and measured cooling system's power consumption for Dataset A

This simulation for Dataset B achieved an RMSRE value of 0.0375 and an average absolute error of 2.53%. It is suggested that the increase in accuracy when compared to Dataset A could be due to less variations in the number of chillers in operation for the period of Dataset B as opposed to that of Dataset A. The step changes in the power consumption could again be justified by the number of chiller machines in operation, as indicated on the secondary axis. From Figure 37, it is evident that the simulation also slightly over-predicted the power consumption for cases of higher power consumption and vice versa for cases of lower power consumption, as was the case for the simulation of Dataset A.

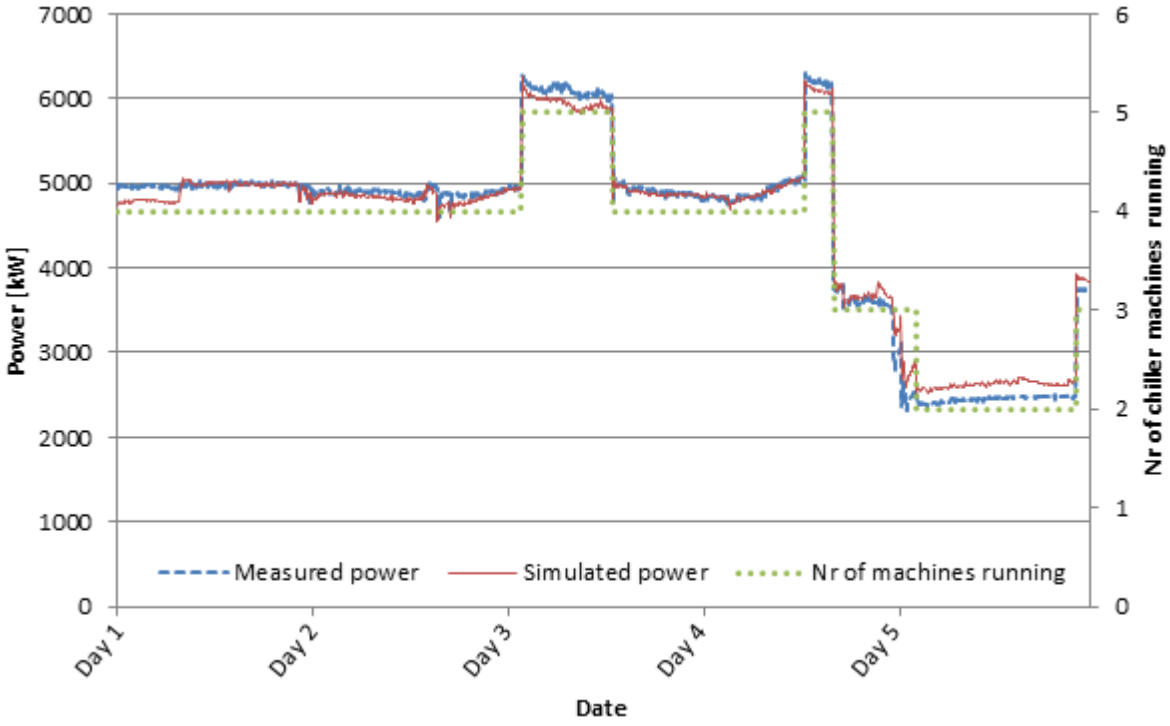

Figure 37: The simulated and measured cooling system's power consumption for Dataset B

4.2.3 Dataset C baseline simulation

Dataset C was used to perform a simulation validation for a period six months after the training period. The total simulated and measured cooling system power rates are presented in Figure 38. From this figure, it can be seen that the simulated power closely follows the measured power, even for data six months away from the parameter determination period.

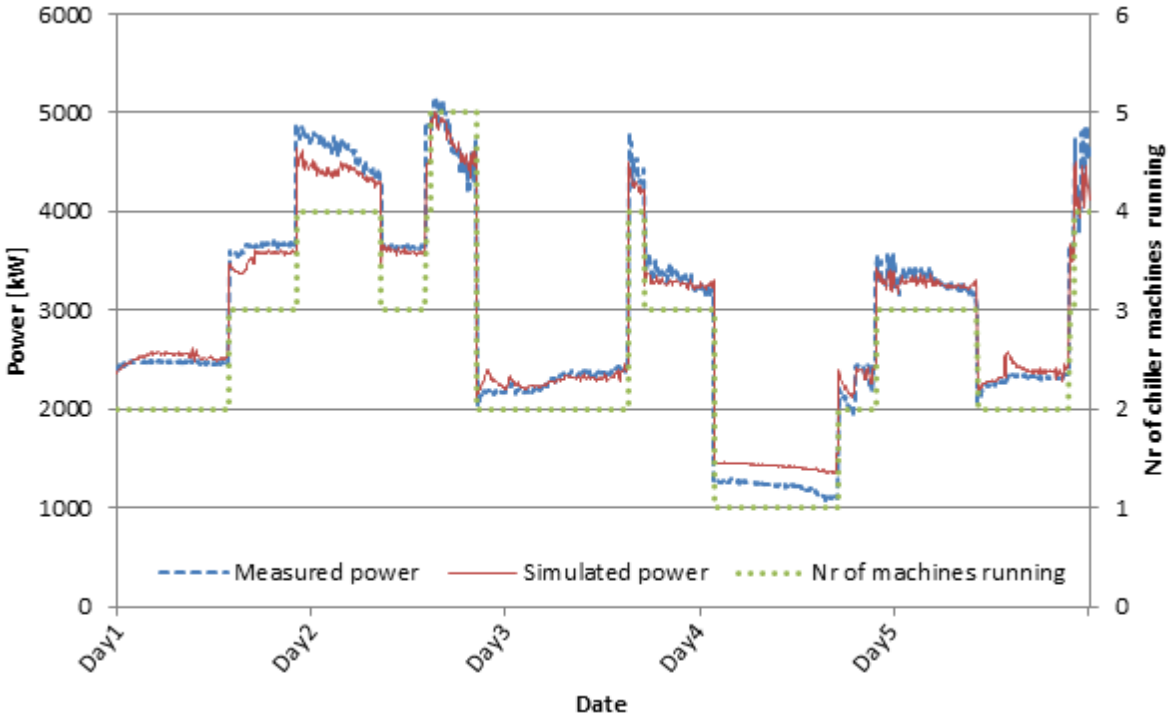

Figure 38: The simulated and measured cooling system's power consumption for Dataset C

An RMSRE value of 0.0704 and an absolute average error of 4.61% were achieved for this dataset. Similar to Datasets A and B, it can be seen that the simulation model tends to over-predict for instances where more chiller machines are in operation, while it under-predicts for fewer chillers. Although the correlation accuracy has deteriorated marginally for Dataset C, it could still be considered acceptable, since the RMSRE value is less than 0.1. Similar to the previous two datasets, it could be seen that the step changes in power are due to the number of chiller machines in operation, as shown on the secondary axis of Figure 38.

4.2.4 Dataset D baseline simulation

Dataset D was used to validate the simulation model's accuracy when simulated with hourly average data instead of the three-minute intervals in which the data was captured. The simulated and measured integrated cooling system's power is shown in Figure 39. From this figure, it is evident that the trend closely reflects what is found in the baseline simulation of Dataset A in Figure 36, with the reduction in resolution noticeable.

Figure 39: The simulated and measured cooling system's power consumption for Dataset D

The simulation considered for Dataset D achieved a RMSRE value of 0.0452 with an average absolute error of 3.15%. The correlation results obtained for the hourly dataset very closely reflects what was achieved by the three-minute data of Dataset A, with a variance in the RMSRE value of only 0.0046 and 0.37% on the absolute average error. It was therefore deemed acceptable to consider the hourly average data for simulation inside the parameter determination dataset.

4.2.5 Dataset E baseline simulation

Dataset E was used to perform the validation to the average hourly data of Dataset B. The simulated and measured integrated cooling system's power, as obtained, is shown in Figure 40. It could again be seen that the trend closely replicates what was obtained by the simulation of Dataset B in Figure 37 with the reduction in data resolution.

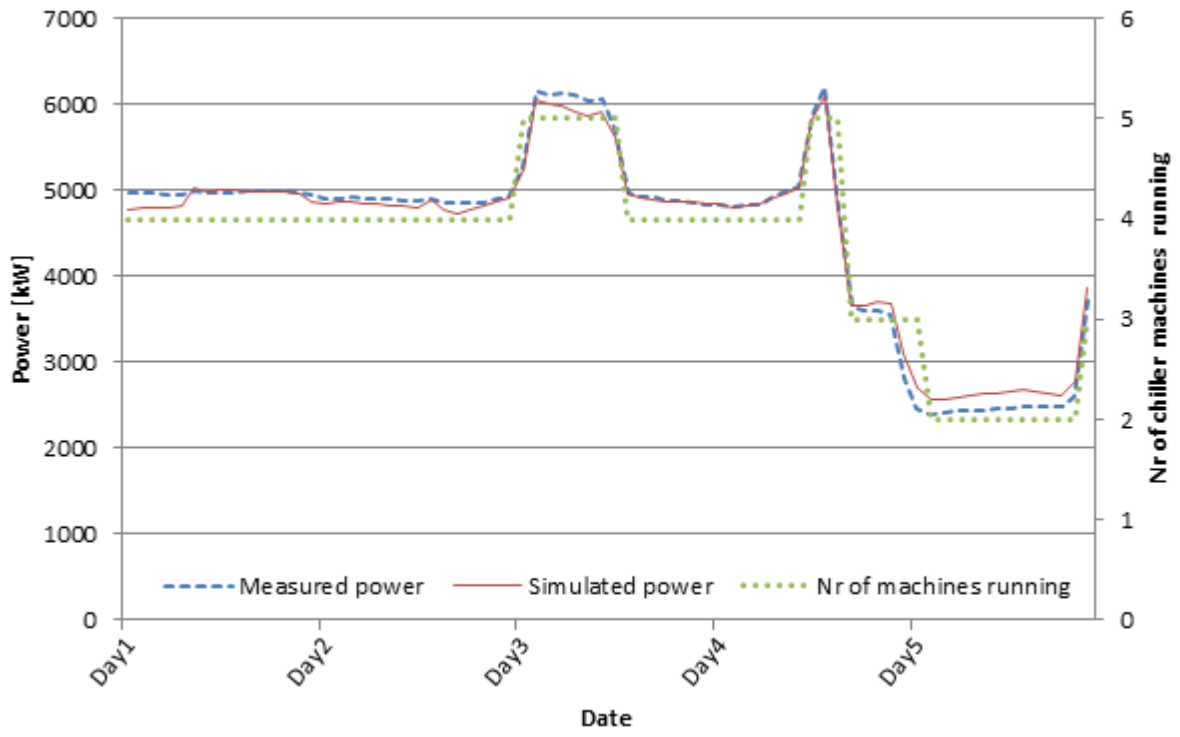

Figure 40: The simulated and measured cooling system's power consumption for Dataset E

An RMSRE value of 0.0362 was achieved for this simulation, while the average absolute error was found to be 2.44%. Similar to Dataset D, the results obtained for the hourly data of Dataset E correlates closely to what was achieved for Dataset B with only a 0.0013 variance between the RMSRE values and 0.09% difference between the average absolute errors. It is therefore suggested that the hourly average data for periods outside, but relatively near the parameter determination dataset yields similar accuracy to that of the three-minute data.

4.2.6 Dataset F baseline simulation

Dataset F considered the period six months after the period used for the parameter determination, but for hourly average values of the mine data. Figure 41 shows the simulated and measured integrated cooling system's power consumption. Similar to Datasets D and E, it is evident that the trend obtained here correlates well with the results attained for Dataset C, with a similar reduction in resolution due to the data consisting of hourly increments.

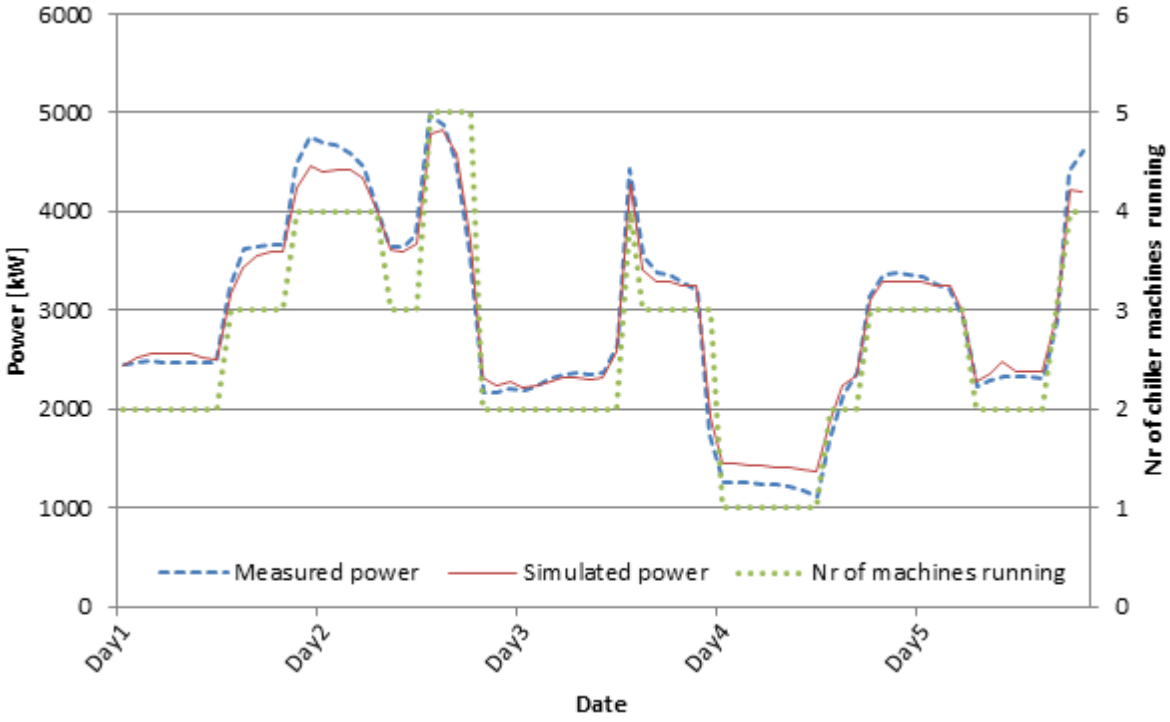

Figure 41: The simulated and measured cooling system's power consumption for Dataset F

An RMSRE value of 0.0659 and an average absolute error of 4.45% were achieved as part of this validation. This correlates closely with the results obtained for Dataset C with a 0.0045 variance in the RMSRE value and a 0.16% difference between the absolute average errors. Based on these results, it is suggested that hourly average simulation results for periods six months away from the parameter determination are in an acceptable accuracy range. For this reason, it was deemed acceptable to consider only hourly data for the annual baseline simulation of Dataset G.

4.2.7 Dataset G baseline simulation

Dataset G is the last baseline simulation to be considered. It consists of hourly data for the entire year. The annual baseline simulation was only considered for hourly data due to computational constraints. As demonstrated earlier, it was deemed adequate that the hourly average simulations all achieved satisfactory simulation accuracies when compared to the measured data. Figure 42 presents the total simulated and measured cooling system's power for the year and Figure 43 shows the correlation. From Figure 42, it is evident that the simulated

results maintain a relatively close correlation to that of the measured data. From the correlation in Figure 43, it can be seen that the simulated results predict the measured power consumption in a 10% error band relatively well. The simulated data remains inside the 10% error margin for 83.9% of the time.

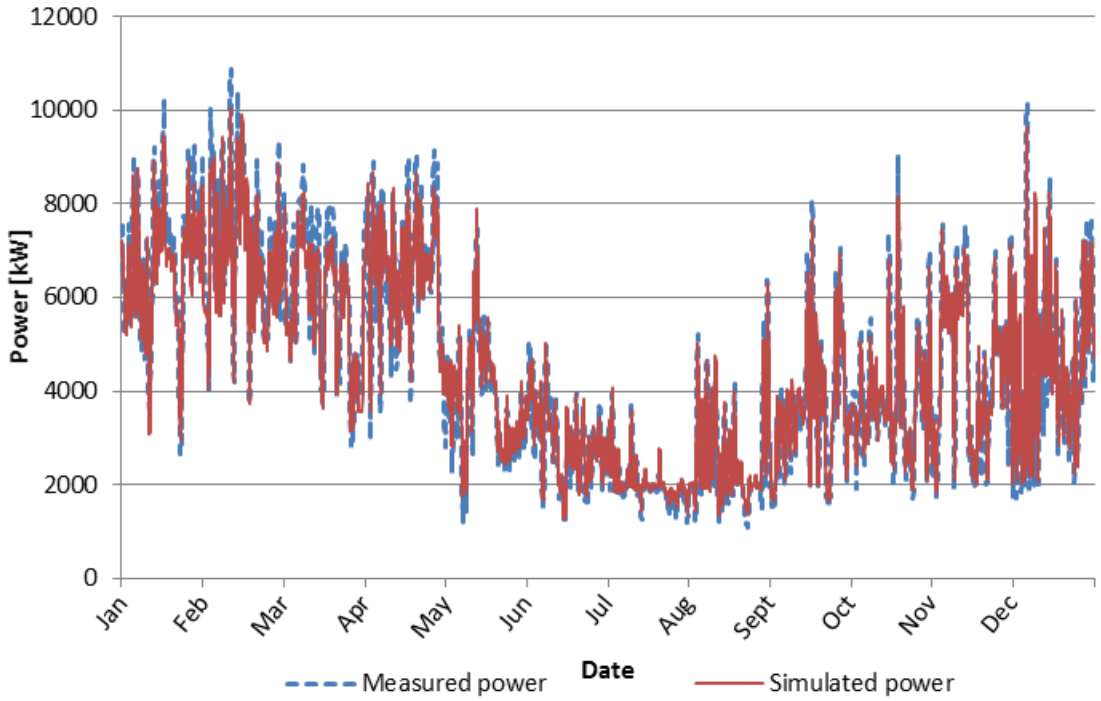

Figure 42: The simulated and measured cooling system's power consumption for Dataset G

Due to the significant number of data points on the hourly graph, it was found useful to present the same results in a daily, continuously integrated average fashion in order to observe the trend easier. These will be referred to as the *daily average* graphs for the purposes of annual considerations from here onwards. Figure 44 shows the daily average simulated and measured total power of the cooling system. From this figure, it can be seen that the simulated power consumption closely follows the measured value.

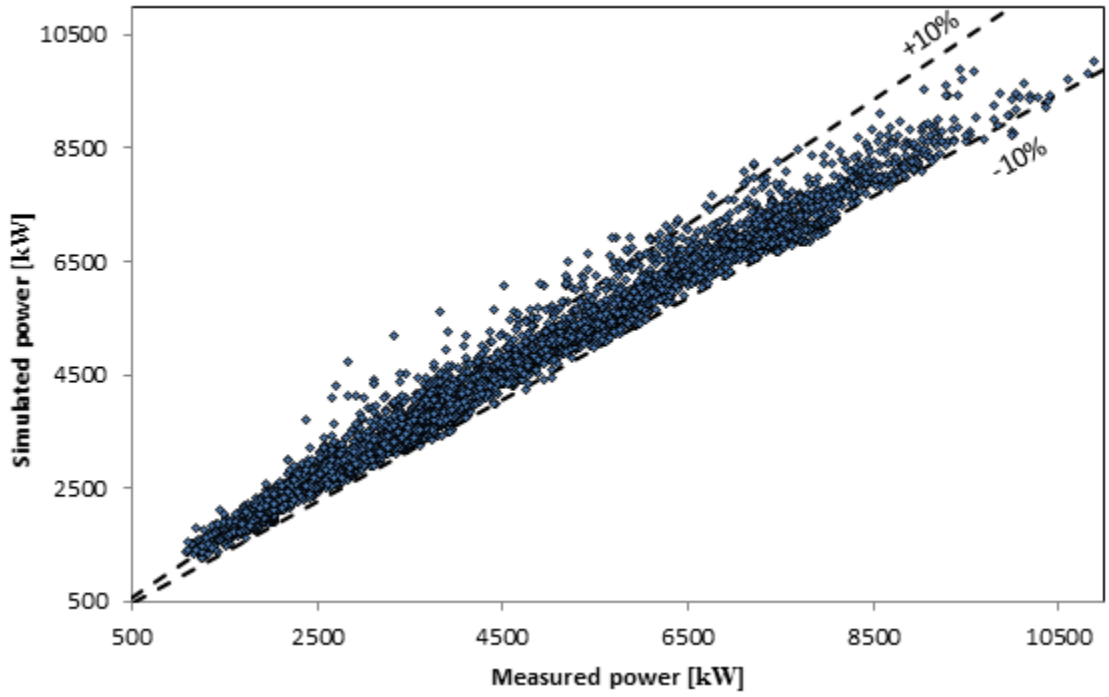

Figure 43: The simulated and measured cooling system's power consumption correlation for Dataset G

An RMSRE value of 0.086 with an average absolute error of 6.22% was achieved for the annual simulation of Dataset G. These results suggest an RMSRE value deterioration of only 0.0201 and an increase in the average absolute error of 1.77% when compared to the week's data of Dataset F. When compared to the hourly model training data of Dataset D, a reduction in the RMSRE value of 0.0408 is obtained with an increase of 3.07 % on the average absolute error.

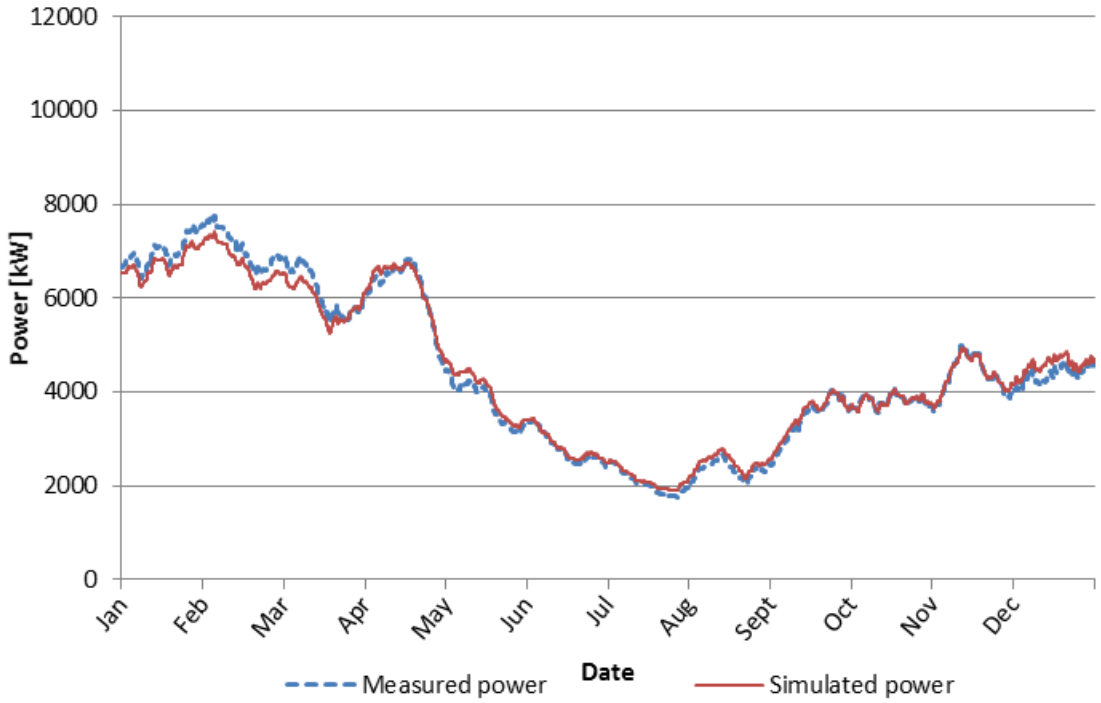

Figure 44: The daily average simulated and measured cooling system's power consumption for Dataset G

The results obtained for the annual baseline simulation correlates well with typical accuracies for cooling system energy consumption simulations that were conducted previously, where an overall average error of 7% was achieved [20, 61]. This suggests an improvement of 0.78% on the average absolute error for the proposed simulation model compared to similar models found in the literature.

4.3 Optimisation

The complete baseline simulation and validation allows the optimisation application. Achieving this requires a suitable optimisation algorithm, as most of the suggested system component models are based on non-linear equations. It is therefore noticeable that this requirement would form part of what would be required when procuring a suitable optimisation platform, along with verifying its suitability in order to ensure that the results suggested by the system could be accepted.

The simulation model would furthermore need to be coupled to the optimisation platform, as seamless integration between these systems greatly assists the integrated optimisation application.

The integration of the simulation model and a suitable optimisation platform ultimately facilitate the confirmation of the hypothesis that the minimum energy operational parameters could be determined using an integrated system simulation and corresponding optimisation for variations in system demands and constraints. This could be obtained by applying the optimisation to the mine cooling system described and comparing the results to those of the current system.

4.4 Conclusion

The integrated cooling system's simulation model was constructed from the calibrated components models established in the previous chapter with a subset of mine data isolated. Thereafter, various datasets (Datasets A to G) were used to validate the simulation models' performance for data inside and outside the training dataset. The model consistency for variations in the dataset frequency were also determined for the various datasets to establish the accuracy when hourly data is considered for the annual data of Dataset G. RMSRE values ranging between 0.0362 and 0.0860 were obtained for the various datasets, suggesting that all scenarios remained below 0.1 and were therefore deemed acceptable.

The fully developed integrated simulation model allows coupling with an optimisation platform to determine the minimum energy system operation, subsequent system behaviour and associated energy consumption.

5 Case study – optimisation

5.1 Preamble

The commercially available Analytic Solver Platform optimisation toolbox developed by Frontline Systems Inc. was used for the optimisation application and case study. Frontline made this software available via a student licence for the purposes of this study. The primary driver for the selection of this platform was its ease of integration with the simulation model as it is coupled to MS Office Excel by means of an add-on toolbox which ensures seamless interaction between the solver and the simulation model. Secondly, from the literature considered, it was concluded that this solver provides satisfactory global optimal solutions to non-linear optimisation problems when compared to other available solvers. Lastly, it complied with the relevant optimisation algorithm classifications, as identified in the literature and confirmed later in the current chapter.

A further requirement before energy minimisation would be to verify the optimisation platform chosen by means of test functions as suggested in Section 2.6.2. This was achieved by introducing the selected test functions and solving them with the proposed optimisation platform, and comparing the results obtained to those obtained in the literature.

The simulation model was subsequently coupled to the optimisation platform in order to simulate the energy-optimised operational parameters of the cooling system. This was based on certain operational and system constraints, as well as variables established from the energy-saving opportunities identified earlier. The optimisation was subsequently performed for the hourly annual data of Dataset G.

5.2 Optimisation platform

5.2.1 Optimisation platform verification

As most of the equations used for the cooling system simulation model are non-linear, it is obvious that the first requirement of a suitable optimisation algorithm would be for it to fall under the non-linear classification. As mine cooling systems are subject to certain physical and

environmental limitations, such as maximum and minimum fluid flow rates, cooling demand variations based on operational parameters, and ambient weather conditions, the second requirement would be to cater for constraints, so it should fall under the constraint optimisation classification described earlier.

As the intention of the current study is to minimise the overall electrical consumption of the integrated cooling system, the objective function could therefore be defined as the sum of all the components' electrical energy consumption. Adding all these values to a single value that represents the overall system's energy consumption, as described earlier, suggests that the optimisation problem at hand could furthermore be categorised as a single objective problem.

Four different arbitrarily chosen test functions, found in the literature, that meet the optimisation classification requirements as identified were considered to verify the optimisation platform used. This is presented in the sections that follow.

5.2.2 Test functions from the literature

The test functions that are considered, as referred to in Section 2.6.2, together with their objectives and constraints, are briefly presented below in Equations (27) to (35).

The first test function is known as the Keane function, with multiple peaks (see Figure 17). It is represented by Equation (27) [110]. The objective is to globally maximise $f(x, y)$.

$$f(x,y) = \frac{sin^2(x-y)sin^2(x+y)}{\sqrt{x^2+y^2}} \quad \textbf{(27)}$$

With bound constraints, as shown in Equation (28).

$$0 \leq x \leq 10; 0 \leq y \leq 10 \quad \textbf{(28)}$$

Without any further constraints, this function is symmetric with two global maximum values at $f(0, 1.39325)$ and $f(1.39325, 0)$ respectively. The constraints presented in Equation (29) are subsequently added.

$$x + y \leq 15;\ xy \geq \frac{3}{4} \tag{29}$$

From Figure 17, it can be seen that the function is nearly symmetrical about $x = y$ with peaks occurring in pairs where one is typically slightly higher than the other, suggesting multiple local minima and maxima. The optimised global maximum is suggested to be at $f(1.593, 0.471) \approx 0.365$.

The second test function is shown in Equation (30) [118]. The objective here is to find a numerical solution to the variables x and y that yield the minimum least square error to the set of equations. The least square error function is graphically presented in Figure 45.

$$\begin{aligned} &e^{x-y} + \sin(2x) - \cos(y) = 0 \\ &4x - e^{-y} + 5\sin(6x - y) + 3\cos(3xy) = 0 \end{aligned} \tag{30}$$

Constraint to Equation (31)

$$-2 \leq x \leq 2;\ -1 \leq y \leq 3 \tag{31}$$

From Figure 45, one can see that the global minimum point cannot be easily predicted graphically as there are various weak local minima where the gradients are substantially flat. The optimised global minimum value is suggested to be $g(-0.4363, 2.3525) \approx 0$, where $g(x, y)$ represents the least square error function.

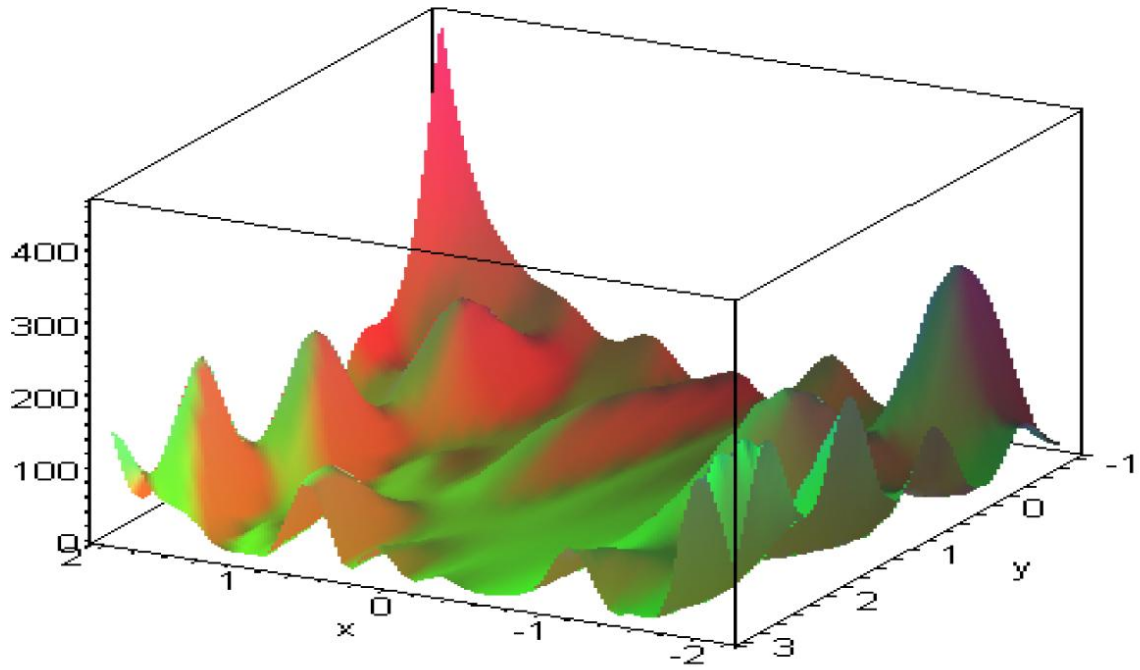

Figure 45: The least square error function for the test problem presented in Equation (30) [118]

Another test function considered is the one presented in Equation (32), which consists of a multimodal objective. Here the objective is to find the global minimum of $h(x, y)$ subject to the constraints presented in Equation (33) [118].

$$h(x,y) = (\sin(2x^2 + xy^2)^2 + (\sin(4y + x^2 - 12xy))^2 \quad \textbf{(32)}$$

$$\log(1 + x^4) + 8\sin(x^2 - y) \leq 0.01; -2 \leq x \leq 3;\ -4 \leq y \leq 2 \quad \textbf{(33)}$$

The graphic representation of this test function is shown in Figure 46. It is evident that this test function consists of multiple local maxima and minima. The suggested global minimum of this function is $h(0.10157e-9, 1.57079) \approx 0.14908e-18$.

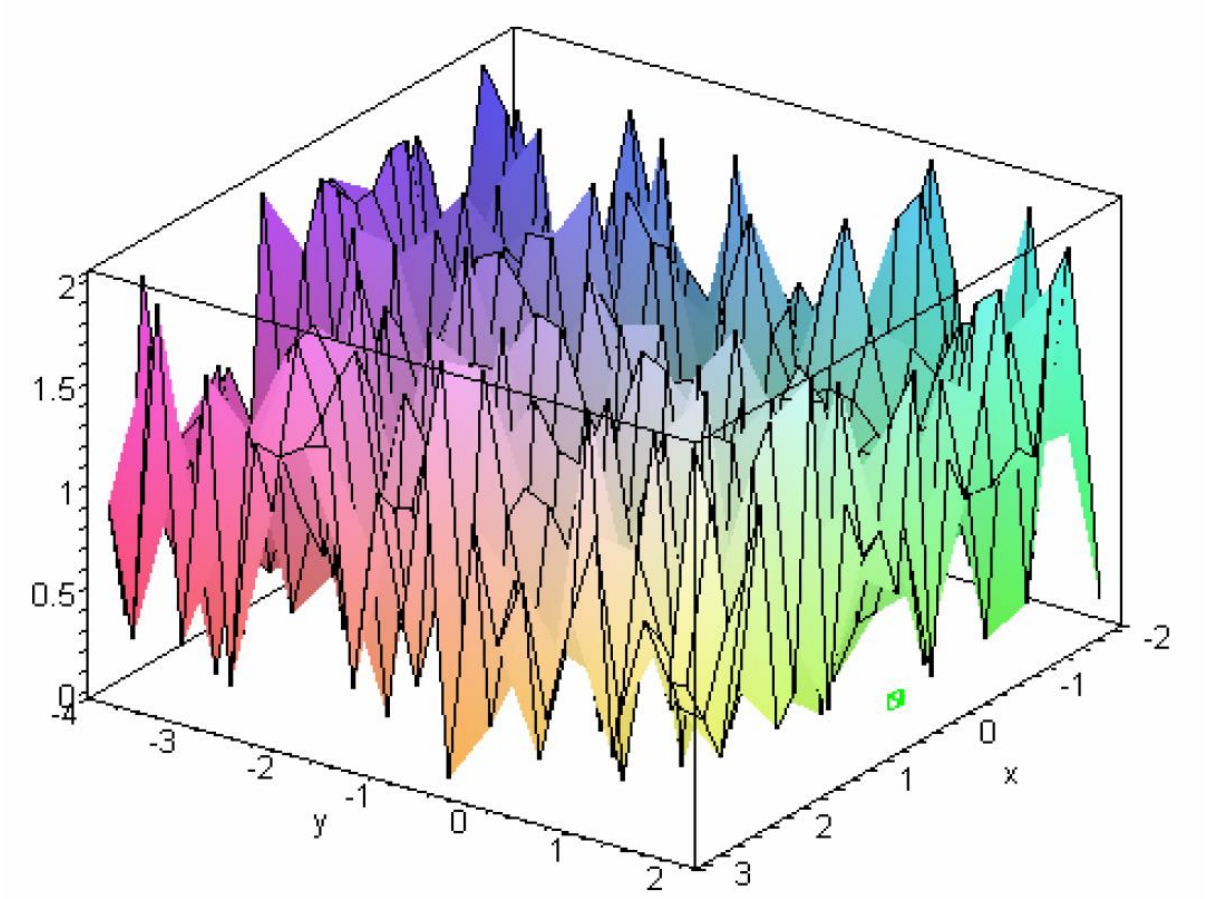

Figure 46: The surface variation of a non-linear three-dimensional test function is presented in Equation (32) [118]

The final test function considered is a third order polynomial with four variables. This is considered to be a system affected by interval uncertainty [115]. The objective is to find the global minimum of k among the variables k, x, y and z, which satisfies the system of equations presented in Equation (34). This function could not be visually constructed in a single three-dimensional plot like the other test functions due to the variables exceeding the three axes available to construct such a graph.

$$\begin{aligned} &10y^2z^3 + 10y^3z^2 + 200y^2z^2 + 100y^3z + 100yz^3 + xyz^2 + xy^2z \\ &\quad + 1000yz^2 + 8xz^2 + 6xyz - x^2 + 60xz + 60xy - 200x \\ &\quad \leq 0; 800 - 800k \leq x \leq 800 + 800k; 4 - 2q \leq y \\ &\quad \leq 4 + 2q; 6 - 3q \leq z \leq 6 + 3q \end{aligned} \tag{34}$$

And the bound constraints, as shown in Equation (35):

$$-10\,000 \leq q \leq 10\,000;\ -10\,000 \leq x \leq 10\,000;\ -10\,000 \leq y \leq 10\,000;\ -10\,000 \leq z \leq 10\,000 \tag{35}$$

When solved, the suggested global minimum value of $q = 0.34174$ with $x, y, z = (1073.4, 3.3165, 4.9748)$ is obtained.

5.2.3 Test function application

The test functions presented were incorporated into the Analytic Solver Platform provided by Frontline Systems Inc. This was implemented by programming the test functions into MS Office Excel, after which the objective functions and constraints were included and solved.

Test function 1

The first test function considered is the one presented by Equation (27), with constraints bounding the feasible region as shown in Equation (28). The minimisation was performed multiple times by sweeping through the variations of initial conditions in the bound constraints, in increments of 1, to verify the robustness of the optimisation platform.

For this test function, the Analytic Solver Platform obtained the same maximum value of $f(1.587, 0.472) \approx 0.379$ for all 120 permutations of initial conditions. At first glance, this appears to be a marginally larger value than the one suggested by Yang [110] of 0.365. Although, upon closer inspection, the actual maximum obtained by the suggested values for the variables is approximately the same as that obtained by the Analytic Solver Platform to the value of 0.379. It is therefore suggested that this discrepancy could be due to the number of significant values considered in the text of the book referenced.

Figure 47 shows the surface variations of the test function, as obtained by MS Office Excel. It is evident that it compares well with the one suggested in Figure 17.

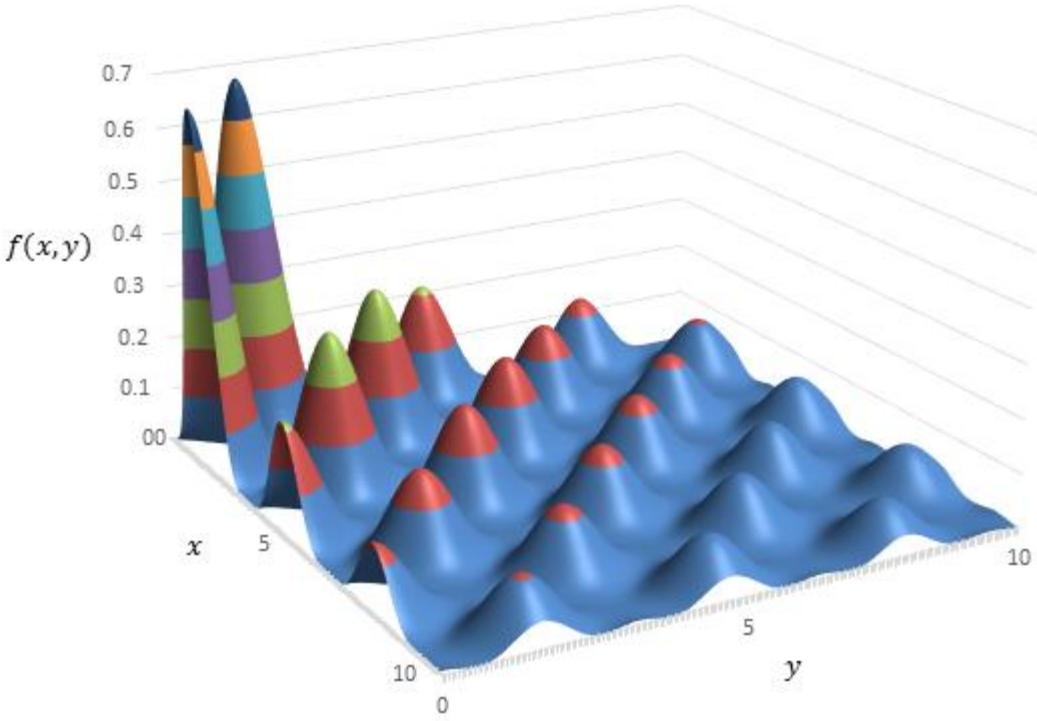

Figure 47: The surface variations of test problem 1

Test function 2

The second test function, represented by the least square error function in Equation (30) and constraints of Equation (31), was used to verify the Analytic Solver Platform. For this function, initial conditions were swept through between boundary constraints in increments of 0.5, resulting in 81 permutations of the initial conditions.

For this test function, the Analytic Solver Platform obtained four variations of minimum values, as summarised in Table 10. From these variations, it is evident that one variation, as shown by Nr. 4, resulted in similar values to those suggested by Pintér, Linder and Chin [118] of $g(-0.4363, 2.3525) \approx 0$. It should be noted that the other three sets of minimum results suggested are lower than the suggested global minimum, and therefore suggest that $g(-0.4363, 2.3525)$ is not the ultimate or only global minimum of this problem.

Table 10: Test function 2 result variations

Nr.	x	y	$g(x,y)$
1	-0.08423	-0.21863	1.4E-17
2	-0.20749	1.84977	3.43E-17
3	0.068883	1.019413	1.36E-19
4	-0.43631	2.35254	1.32E-14

The variation to the proposed result is suggested to be due to the significant weak local minima that are present and visible in Figure 48. This figure was again constructed from the surface variations, as obtained in MS Office Excel and closely correlates to those of Figure 45.

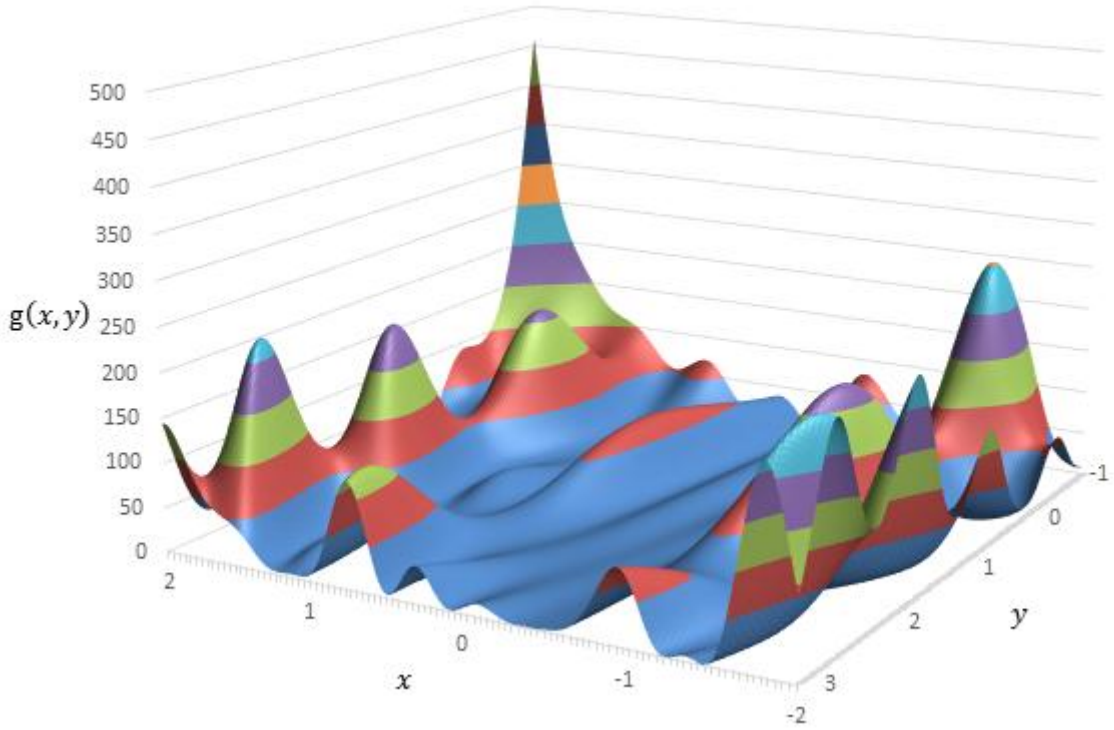

Figure 48: The surface variations in the least square error function of test problem 2

Test function 3

The third test function considered is the one reflected in Equation (32) with bound constraints, as shown in Equation (33). For this test function, initial conditions were swept through in increments of 0.5 between the bound constraints, which resulted in 143 permutations of optimisation. Two variations of the minimum solution were obtained, as shown in Table 11.

Table 11: Test function 3 result variations

Nr.	x	y	$h(x,y)$
1	6.12E-17	1.570796	4.07E-28
2	6.12E-17	0.785398	6.46E-30

The results obtained here lead to an improvement to the suggested result by Pintér *et al*. [118] of $h(0.10157e-9, 1.57079) \approx 0.14908e-18$. The reason for the discrepancy could again be ascribed to variances between the suggested models' number of significant values considered. The surface variations of this test function are shown in Figure 49, as constructed in MS Office Excel.

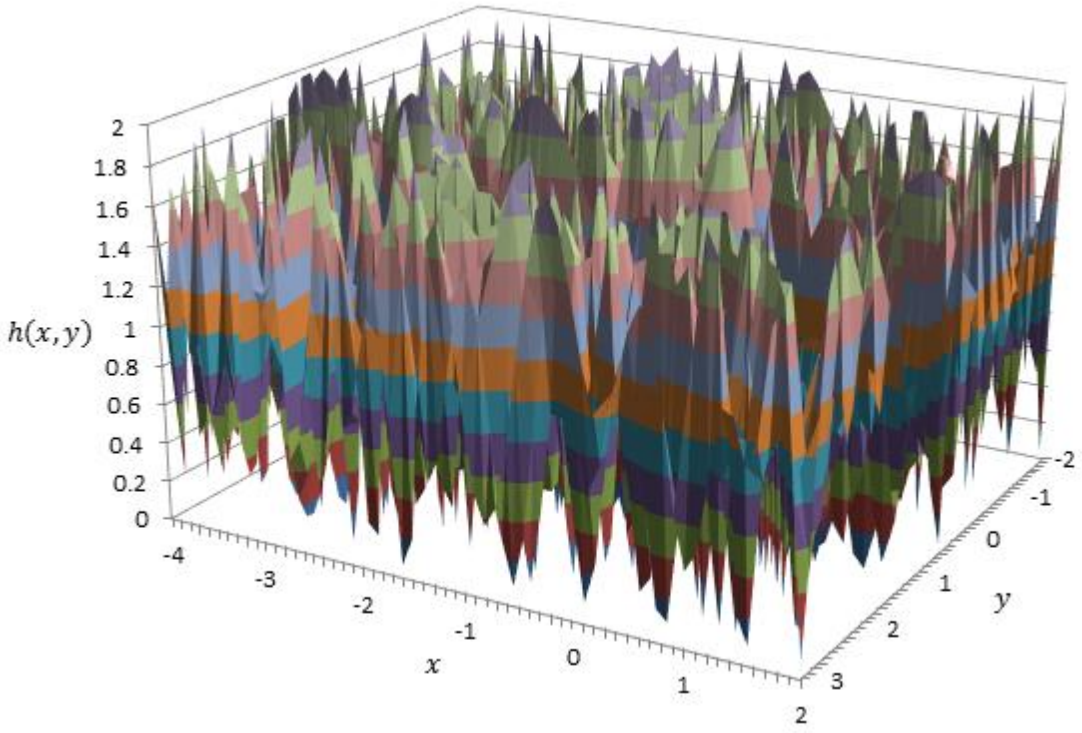

Figure 49: The surface variations of test function 3

Test function 4

The fourth and final test function considered to verify in the Analytic Solver Platform is the one presented in Equation (34) with bound constraints described in Equation (35). As this function consists of four variables and a significantly larger feasible region bounded by the boundary constraints, it was not feasible to perform an incremental sweep through all the

variable permutations, as was done for the first three test functions. Instead, initial conditions were generated randomly for each variable individually inside the feasible region for 100 permutations to allow for a similar size test set than the other test functions.

For this test function, all permutations of initial conditions obtained the same minimum value of $q = 0.34174$ with $(x, y, z) = (1073.39164, 3.31652, 4.97478)$, which reflects the same results Henrion [115] obtained earlier.

5.3 Optimisation application and results

The fully developed and successfully integrated simulation model and optimisation platform allow the optimisation of the mine cooling system. As stated earlier, due to computational limitations, only Dataset G was considered for optimisation.

Table 12 repeats some of the system design flow rates presented earlier, along with additional parameters that are included as part of the optimisation application. The bound constraints are presented, as well as operational constraints imposed on each of the components.

Table 12: The mine cooling system variables and constraints for optimisation

Parameter	Unit	Chiller	BAC	PCT	CCT
Design air flow rate	kg/s	N / A	1250	720	1 350
Minimum air flow rate	kg/s	N / A	0	0	0
Maximum air flow rate	kg/s	N / A	1 250	720	1 350
Design water flow rate	kg/s	1 500	750	360	2 700
Minimum water flow rate	kg/s	150	0	0	450
Maximum water flow rate	kg/s	1 500	750	360	2 700
Control variables	kg/s	$\dot{m}_{w,evap}$	$\dot{m}_{w,BAC}$	$\dot{m}_{a,PCT}$	$\dot{m}_{w,CCT}$, $\dot{m}_{a,CCT}$
Uncontrolled variables	kg/s	N / A	$\dot{m}_{a,BAC}$	$\dot{m}_{w,PCT}$	N / A
Bound constraints		$T_{w,o,evap}$ = Mine data	$h_{a,o,BAC}$ = 35 kJ/kg or Mine data if > 35 kJ/kg	$\dot{m}_{w,PCT}$ = Mine data	20 °C < $T_{w,o,cond}$ < 32 °C

The energy-saving strategies identified in Section 2.5 were implemented via the integrated simulation model, coupled to the optimisation platform. This suggests that the optimisation platform becomes the control system controller. This method of control is referred to as an optimal control system [128]. A schematic flow diagram of the information flow between the input data from the SCADA which includes the constraints, control variables and power consumption feedback of the optimisation is shown in Figure 50.

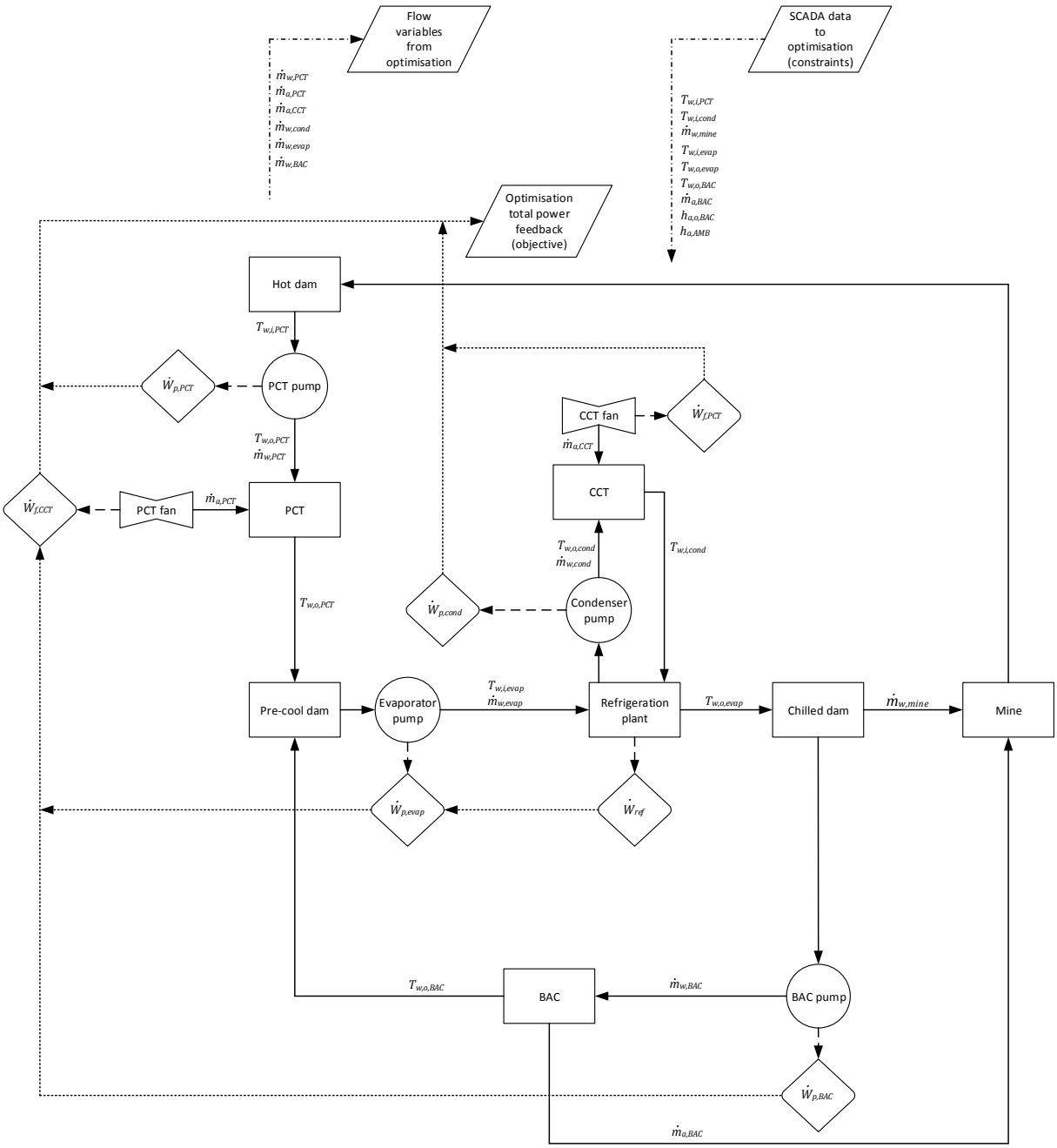

Figure 50: Optimisation schematic flow diagram

A new set of data is passed between the input from the SCADA and the optimisation simulation model for each time step of Dataset G. The optimisation is then performed from where the outputs are obtained and stored.

It should be noted that, for a valid comparison of the optimised results to those of the baseline system, it was deemed necessary to include certain additional optimisation constraints. These include the constraint imposed on the evaporator water outlet temperature, which suggests that the optimisation set point temperature should follow the temperature measured on the mine cooling system, instead of the system design temperature of 3 °C. The motivation for this is that it was found in many instances that the evaporator water outlet temperature was above this value, suggesting that, if the optimisation temperature was set according to the system design, instead of the measured values, it would result in increased energy consumption and therefore unfairly penalise the optimised system.

The BAC air outlet enthalpy was treated similarly by dynamically varying the optimisation set point according to the air outlet enthalpy measured for all cases where the air outlet enthalpy was larger than the ideal 35 kJ/kg. This set point was furthermore controlled in such a way as to clip the air outlet enthalpy at 35 kJ/kg, as this value is deemed acceptable for underground mining, as stated earlier. This suggests that, in instances where the measured air outlet conditions were lower, the acceptable value was adopted and used as the set point for the optimisation model. This method suggests that the BAC will be turned off for instances where the ambient enthalpy is found to be below the desired 35 kJ/kg.

The optimisation objective was to minimise the overall system's energy consumption subject to the system constraints presented in Table 12. The objective function could therefore be expressed as given in Equation (36). With the control strategy used and the ability to maintain a water balance through the variable evaporator flow control, it was no longer deemed necessary to utilise the back-pass valve that circulates chilled water back to the pre-cooling dam, so this pump does not form part of the optimised cooling system, and would be decommissioned if the strategy was to be implemented.

$$\left(\dot{W}_{plant}\right)_{min} = MIN \sum_{n=1}^{N} \left[\left(\sum_{j=1}^{6} \dot{W}_{ref,j} \right)_n + \left(\sum_{j=1}^{2} \dot{W}_{p,PCT,j} \right)_n + \left(\sum_{j=1}^{2} \dot{W}_{f,PCT,j} \right)_n \right.$$
$$+ \left(\sum_{j=1}^{3} \dot{W}_{p,BAC,j} \right)_n + \left(\sum_{j=1}^{6} \dot{W}_{f,CCT,j} \right)_n + \left(\sum_{j=1}^{6} \dot{W}_{p,cond,j} \right)_n \quad (36)$$
$$\left. + \left(\sum_{j=1}^{6} \dot{W}_{p,evap,j} \right)_n \right]$$

5.3.1 Baseline and optimised total system power consumption and saving

The overall integrated cooling system power consumption for the baseline is shown in Figure 51, along with the optimised power consumption. The daily average baseline and optimised integrated power consumption is shown in Figure 52. The optimised system achieved an average saving of 17.9% on the overall energy consumption for the year relative to the simulated baseline. This translates to a total annual consumption of 32.3 GWh for the optimised system compared to 39.4 GWh on the baseline system, suggesting an annual saving of 7.1 GWh.

With the saving of 29.3% obtained through the previous flow control, it is suggested that the mine cooling system would have obtained an integrated saving of 41.9% if the integrated optimisation had been implemented on the original system before the previous flow control strategies were implemented. As this saving formed part of the strategy in operation during the current study, it was included as part of the baseline.

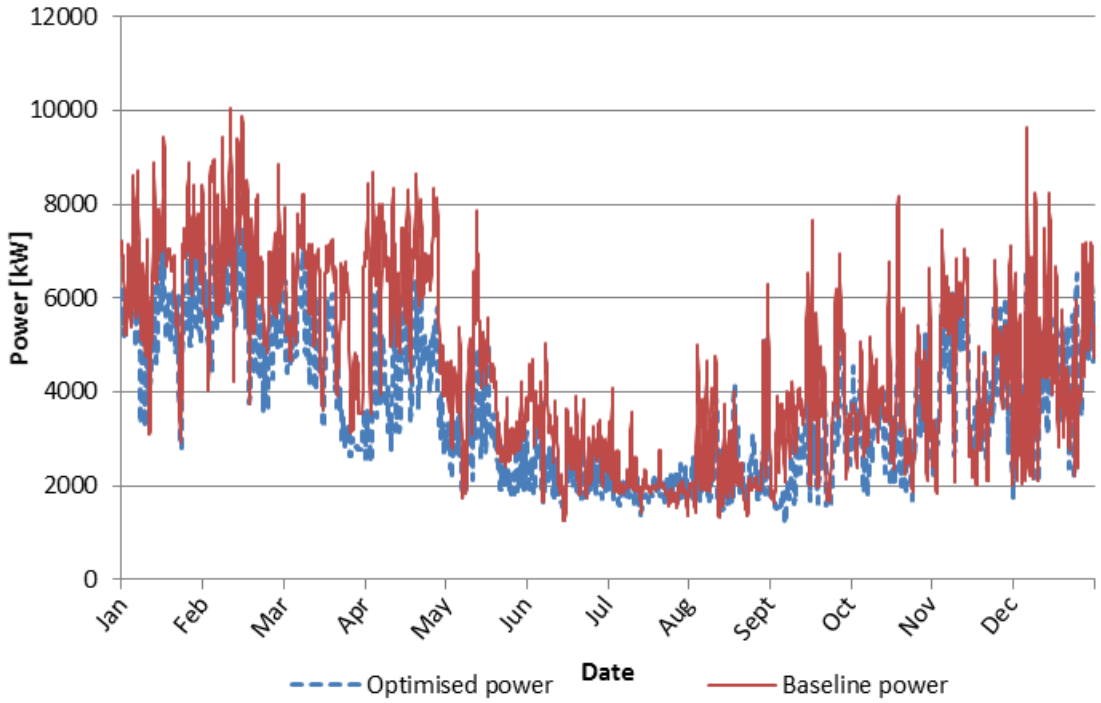

Figure 51: The baseline and optimised integrated cooling system's power consumption

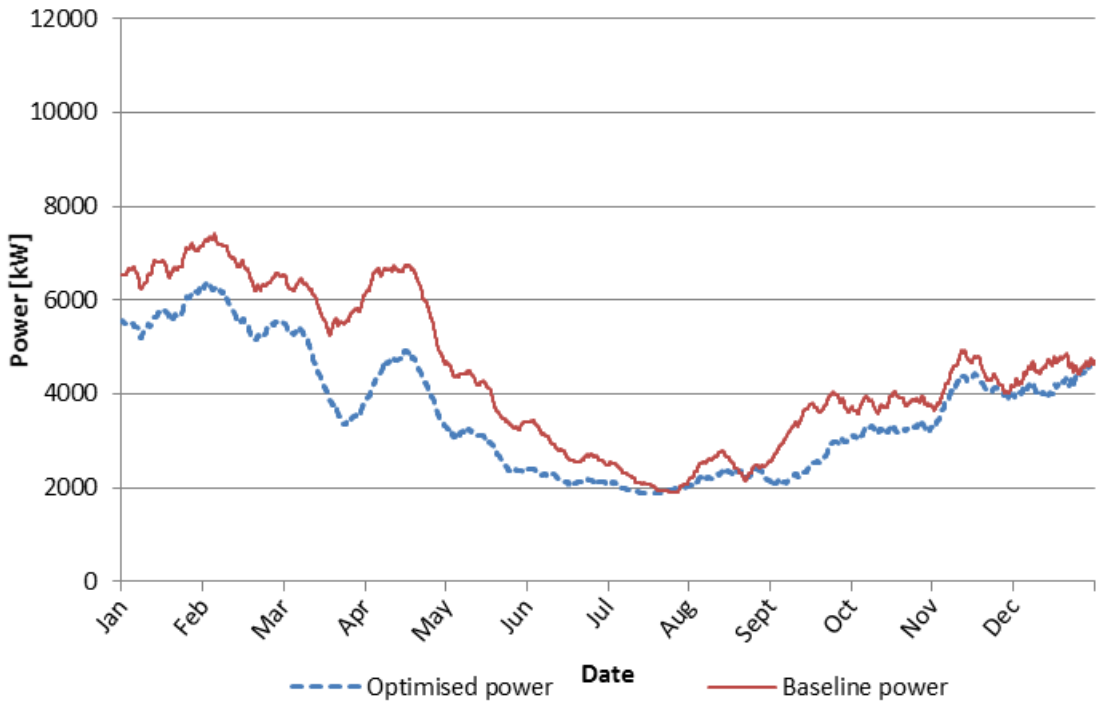

Figure 52: The daily average baseline and optimised integrated cooling system's power consumption

5.3.2 Component baseline and optimised power consumption and saving

The various major energy-consuming components, as identified earlier, along with their respective baseline and optimised power consumptions, are presented in the sections to follow. This assists the quantification of the individual components' contribution towards the energy consumption, as well as the saving contribution, each of which is presented in Section 5.3.3.

Pre-cooling tower

Figure 53 shows the power consumption of the PCT's pumps, and Figure 54 shows the daily average consumption. From these figures, it is evident that the PCT's pump power of the optimised system follows the baseline exactly, as the water flow through the PCT is directly related to the chilled-water demand for underground use and is, as mentioned before, not a controllable variable. The flow associated with the pump power in Figure 53 and Figure 54 is included in Appendix B.

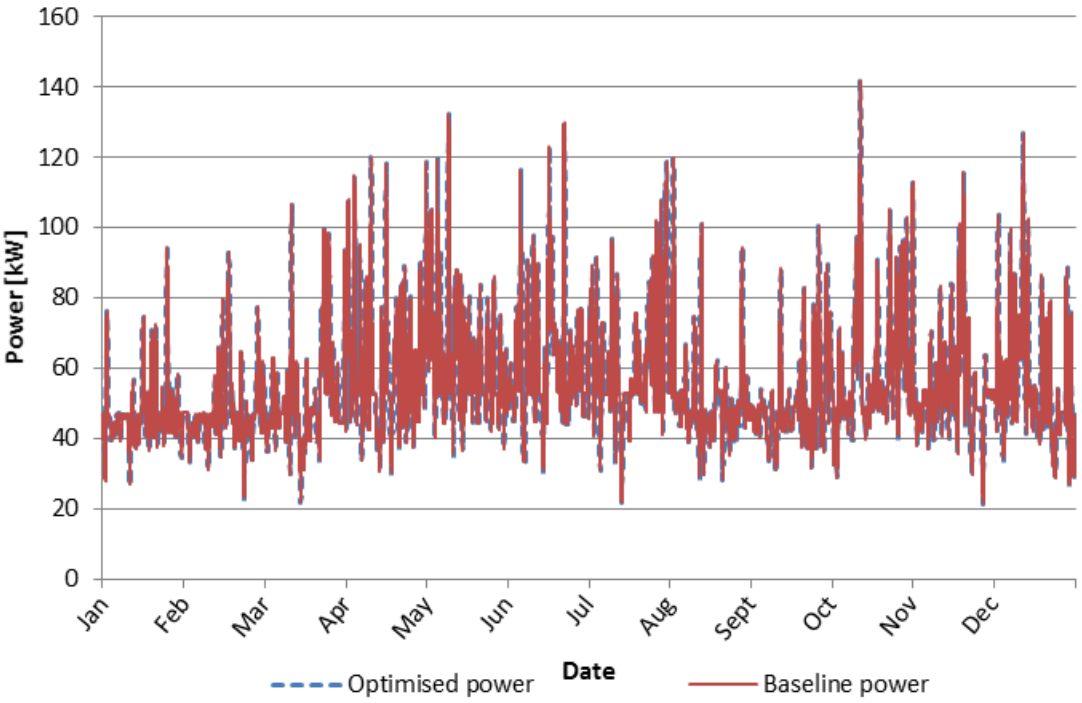

Figure 53: The PCT pump's baseline and optimised power consumption

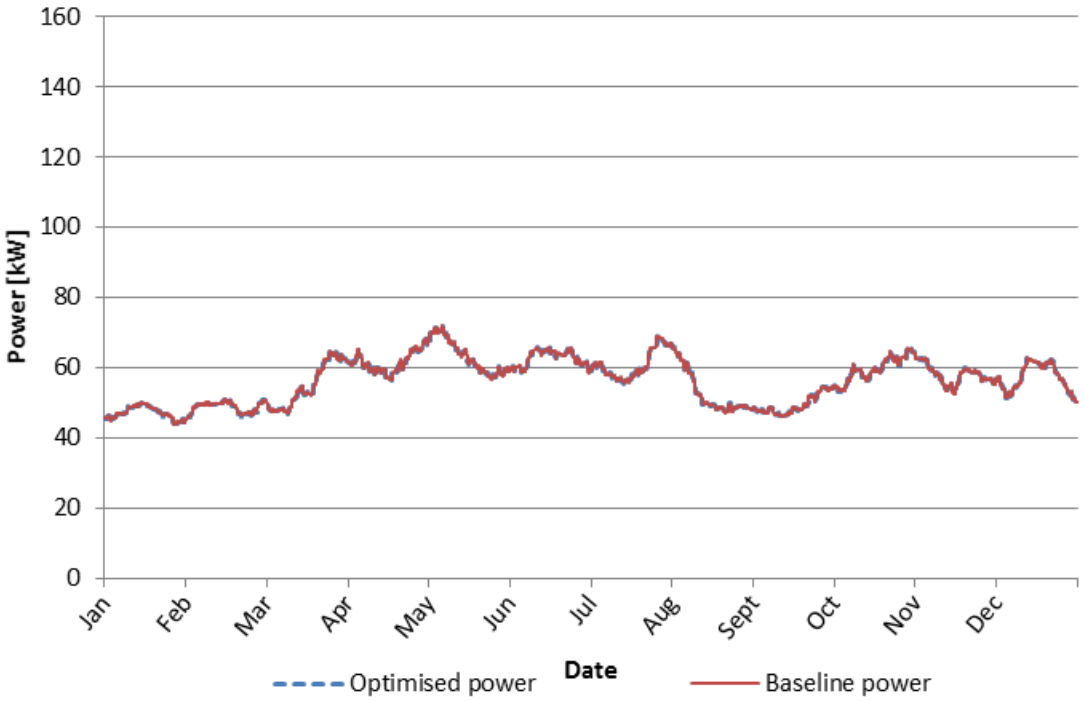

Figure 54: The daily average PCT pump's baseline and optimised power consumption

The baseline and optimised PCT fan power are shown in Figure 55 with the daily average values shown in Figure 56. From these figures, it can be seen that the optimisation suggests significant reductions in the air flow of the PCT's fan when compared to the constant flow strategy of the baseline. With the ambient enthalpy superimposed on Figure 56, it is clear that the optimisation tends to utilise the potential of the PCT more by increasing the fan power and subsequent air flow as the ambient air enthalpy reduces, suggesting that more significant cooling could be performed at a given increase in fan power. This results in the suggested integrated optimised trade-off between chiller power and fan power on the PCT for variations in the ambient enthalpy.

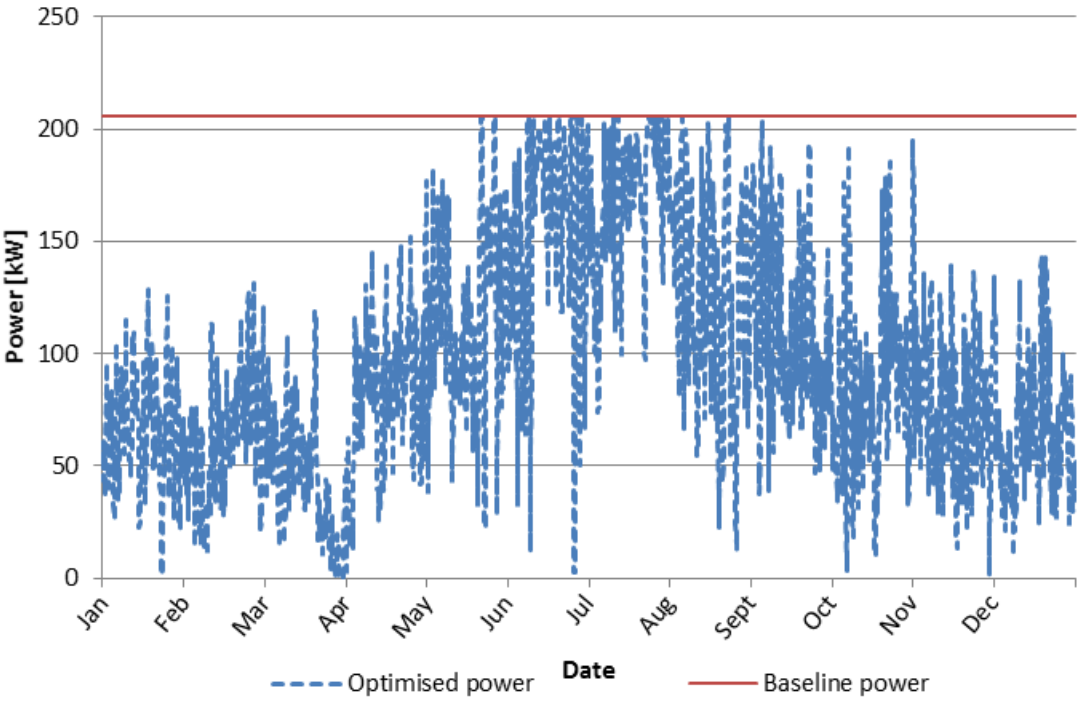

Figure 55: The PCT fan's baseline and optimised power consumption

Figure 56: The daily average PCT fan's baseline and optimised power consumption

The PCT's water outlet temperature of the baseline and optimised scenarios are presented in Figure 57, with the daily average shown in Figure 58. It can be seen that the optimisation suggests that higher PCT water outlet temperatures result in an overall reduction in energy. This is achieved through fan savings as presented earlier and relates closely to the literature, which suggests that increased evaporator inlet temperatures would lead to increased chiller efficiencies. Additional tendencies on the optimised PCT control will be discussed in the sections to follow.

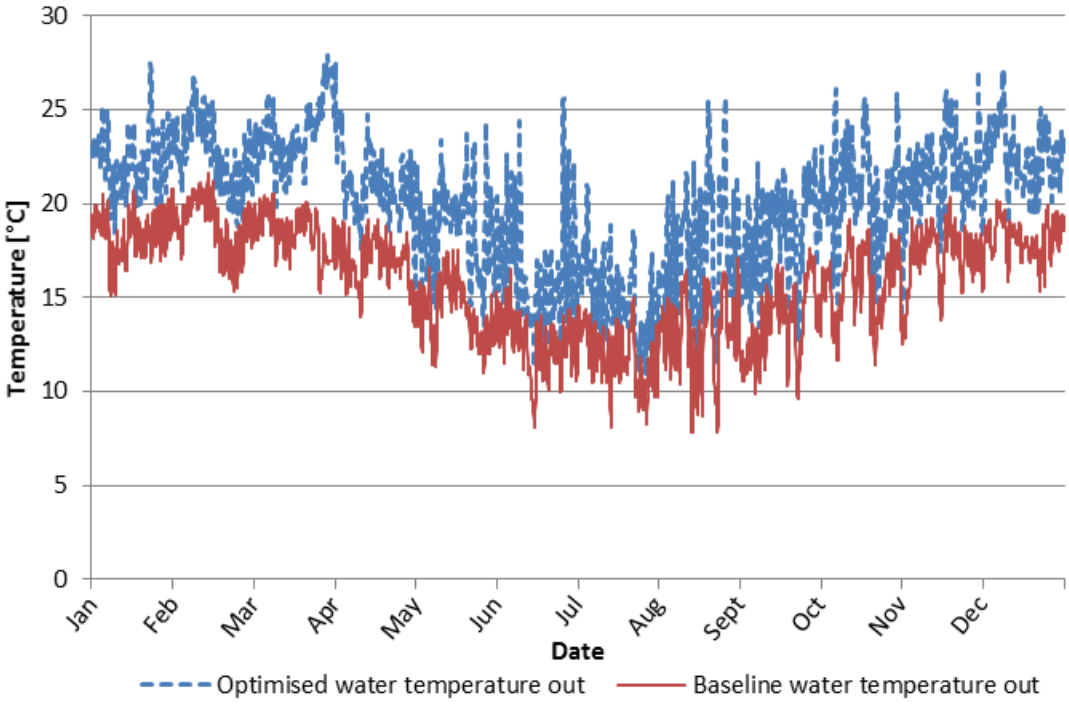

Figure 57: The PCT's baseline and optimised water outlet temperature

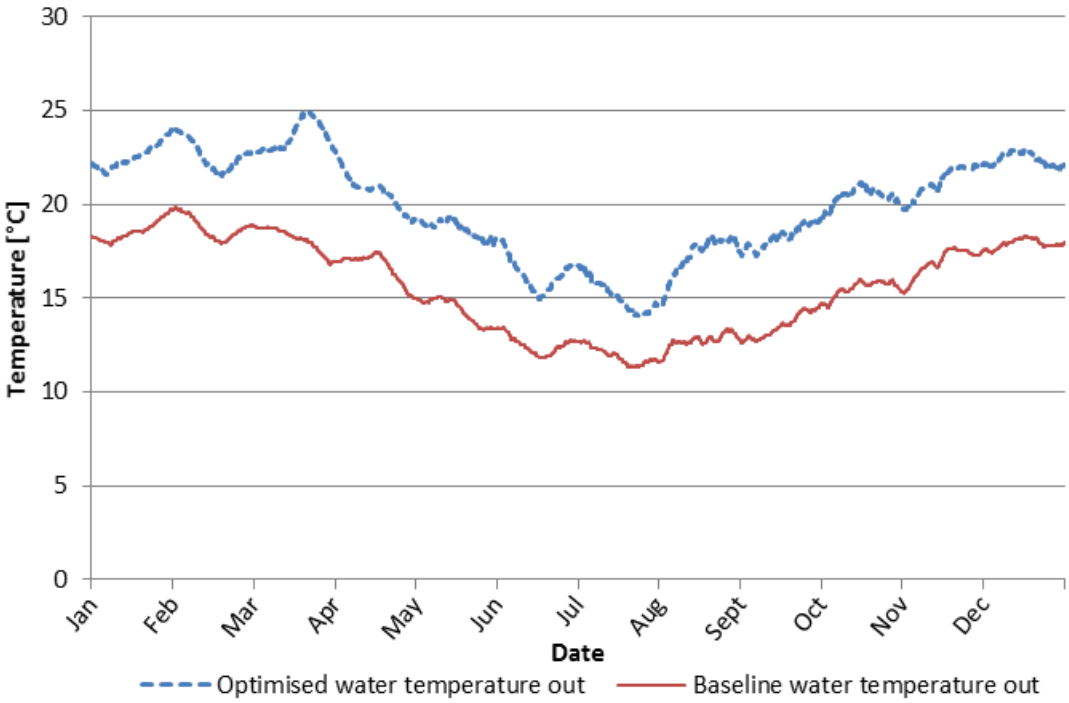

Figure 58: The daily average PCT's baseline and optimised water outlet temperature

Bulk air cooler

Figure 59 shows the BAC pump's baseline and optimised power consumption, while the daily average values of these consumptions are shown in Figure 60. It is clear from these figures that the BAC was off with no chilled-water flow supplied to it during the period from the end of March to the beginning of April, as well as during the winter from the end of June to August. The reason for the BAC being off at the end of March is unclear and could have been due to maintenance or a breakdown. The mine personnel were unfortunately not available for consultation to confirm the reason behind the identified method of operation.

When considering the ambient air enthalpy, which is also included on the secondary axis of Figure 60, it is evident that the ambient enthalpy decreased during March, although it only decreased to around 43 kJ/kg. This suggests that BAC cooling there should ideally have been introduced to the air. This reinforces the suggestion that the downtime during this period was perhaps due to other reasons.

It is evident from Figure 60 that the optimised BAC required reduced pumping power relating to reduced chilled water supply, which suggests both a noticeable saving on the BAC's pump power from the figure and a further saving due to a reduction in chilled-water consumption. The saving due to the reduced chilled-water consumption would be included as part of the power consumption of the evaporator pump and the chiller. These components will be discussed later on. The water flow associated with the pump power in Figure 59 and Figure 60 is included in Appendix B.

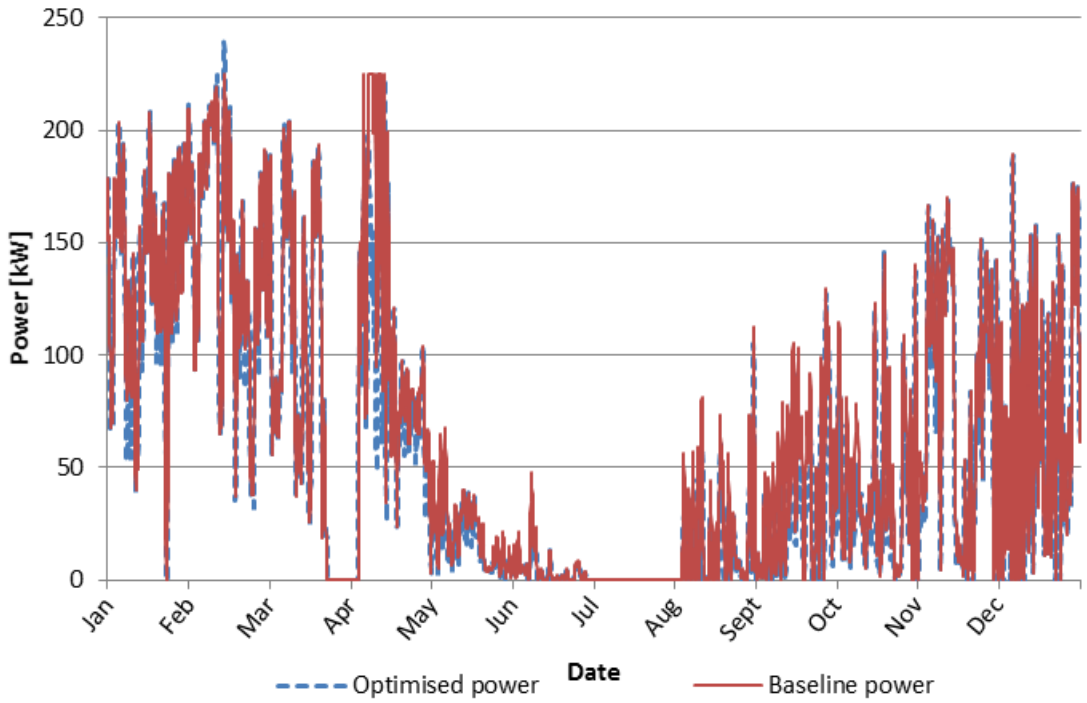

Figure 59: The BAC pump's baseline and optimised power consumption

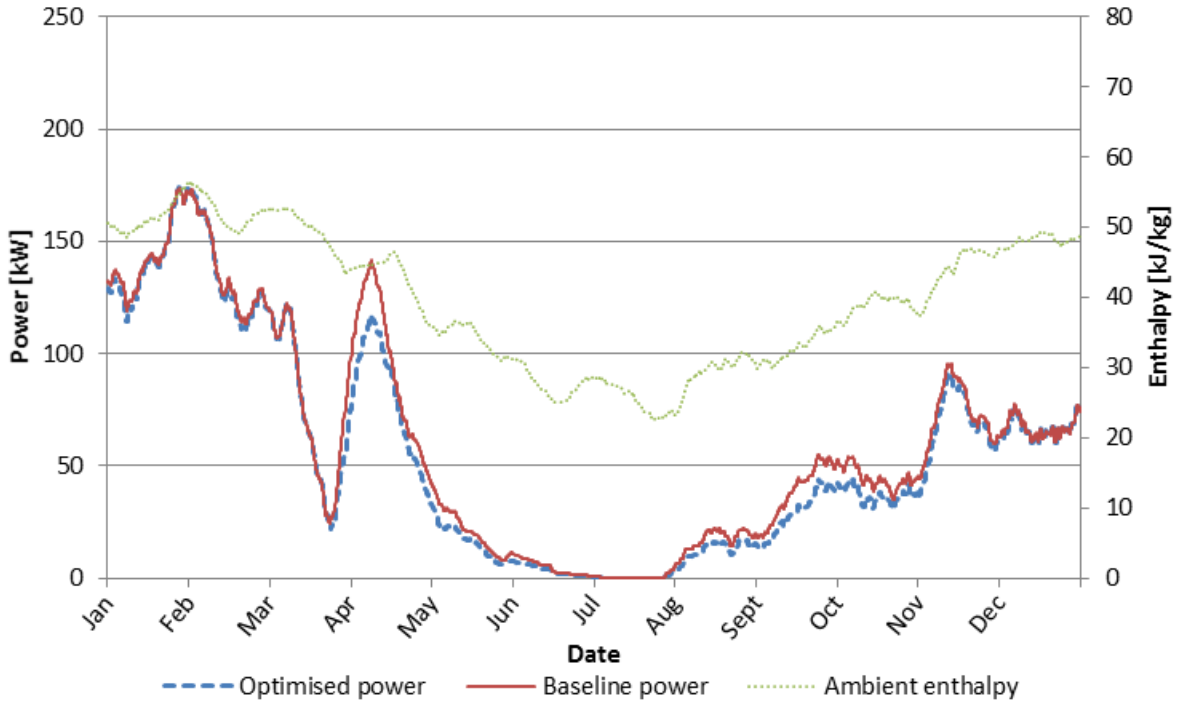

Figure 60: The daily average BAC pump's baseline and optimised power consumption

Figure 61 shows the BAC's air outlet enthalpy for the baseline and optimised scenarios, while the daily average values are shown in Figure 62. From Figure 62, where the ambient enthalpy is superimposed, it can be seen that the BAC's air outlet enthalpy converges to the ambient enthalpy during the winter period, as well as momentarily during the time that the BAC is off around the end of March. It can also be seen that the BAC's behaviour is closely coupled to the ambient conditions, as can be expected.

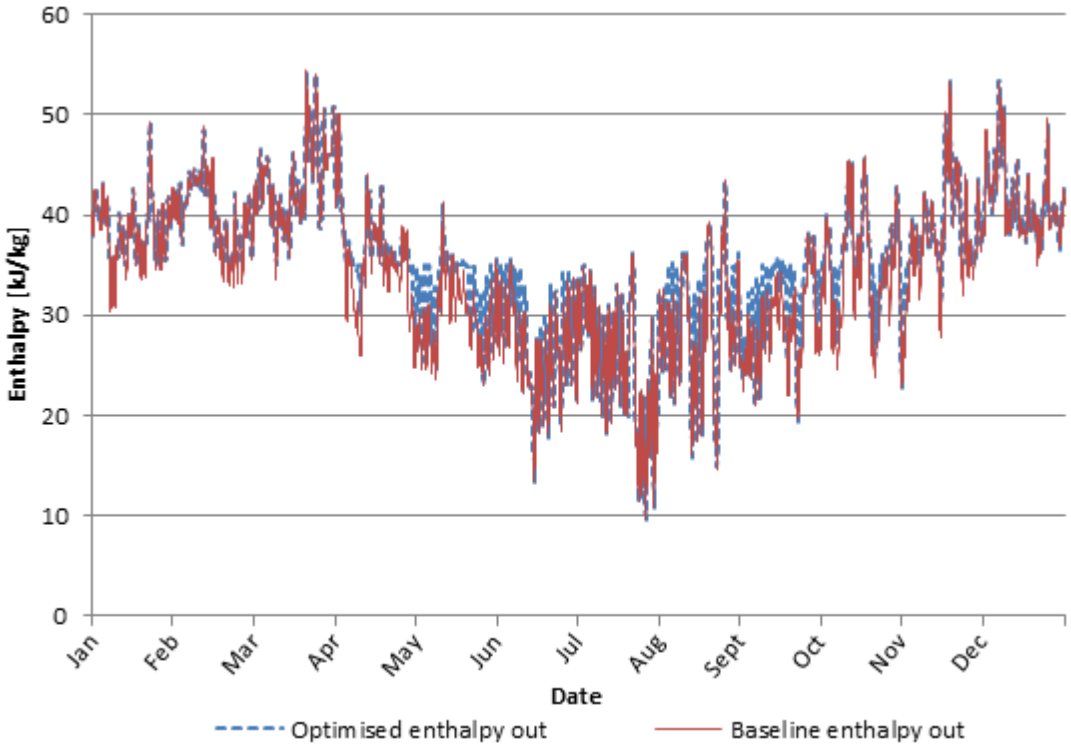

Figure 61: The BAC's baseline and optimised air outlet enthalpy

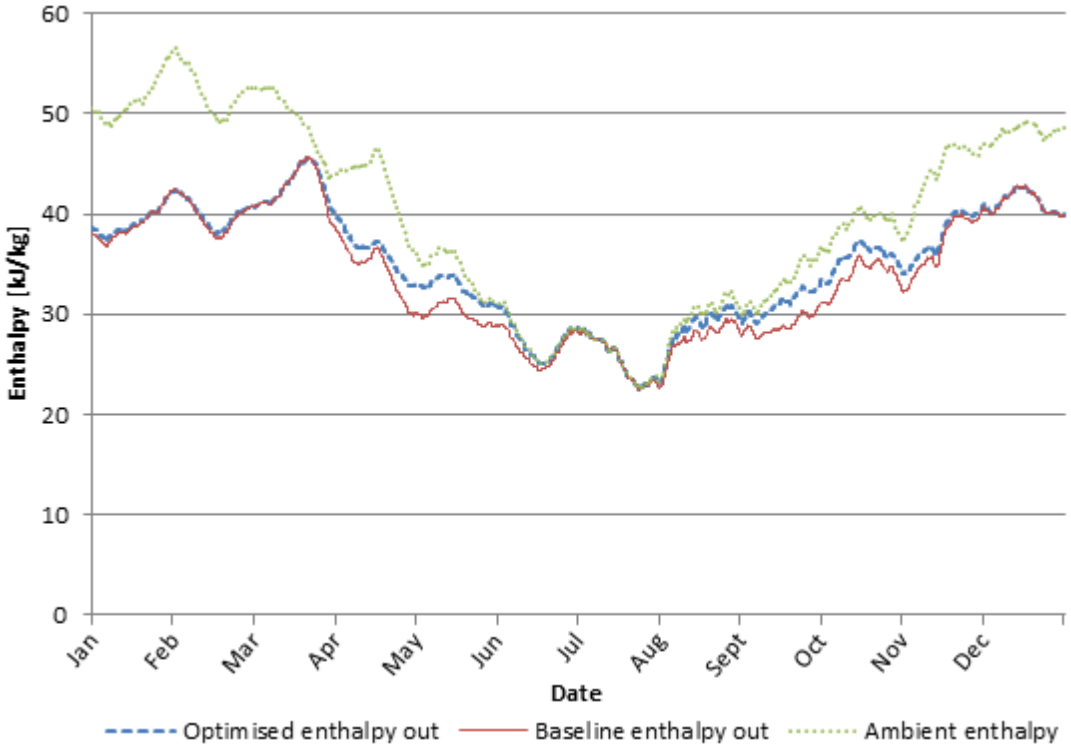

Figure 62: The daily average BAC's baseline and optimised air outlet enthalpy

In order to observe the result of the optimisation on the BAC air outlet enthalpy, a more refined graph of a typical day is required, which only shows the daily trend. For this purpose, two typical days in April were chosen to highlight the behaviour. In Figure 63 and Figure 64, the clipping effect of the optimised BAC is visible as the water flow is controlled to cool the ambient air to a minimum enthalpy of 35 kJ/kg. It is evident from these figures that the baseline case performed more cooling than required, as the BAC's outlet enthalpy is lower than the required value.

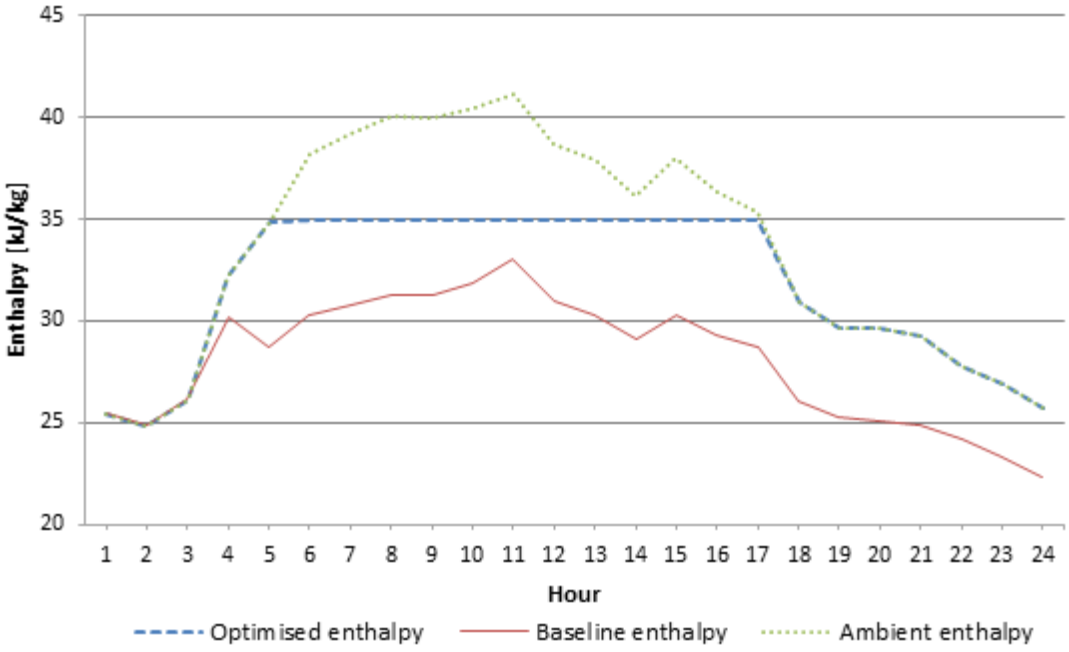

Figure 63: The BAC's outlet enthalpy of a typical day in April

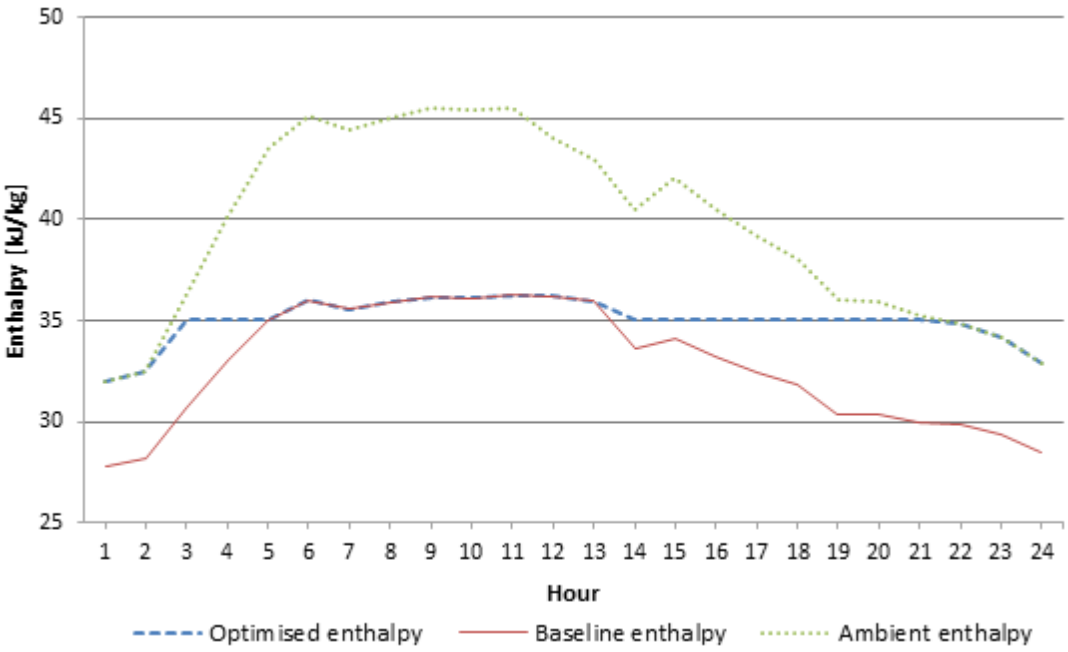

Figure 64: The BAC's outlet enthalpy of another typical day in April

The periods between hours 5 and 13, where the optimised BAC air outlet enthalpy in Figure 64 is above the set point of 35 kJ/kg, reflects the BAC air outlet enthalpy simulated as part of the baseline model, which is in accordance with the original system operations. This suggests that the mine accepted higher outlet enthalpies during those periods. As mentioned earlier, this method of control was adopted to avoid unfairly penalising the optimisation application. Finally, it is worth mentioning that the instances where the BAC outlet enthalpy of the optimised system drops below 35 kJ/kg reflect times when the ambient enthalpy is below the set point, which results in no chilled water being supplied to the BAC. The air inlet condition therefore becomes the outlet condition.

Evaporator

Figure 65 shows the total power consumption of the evaporator pump for the baseline, as well as the optimised system with the daily average values shown in Figure 66. From these graphs the optimisation suggests significant savings on the power consumption of the evaporator pump. This is due to the significantly reduced flow through the evaporators suggested by the optimisation. The water flow associated with the pump power presented in Figure 65 and Figure 66 is shown in Appendix B.

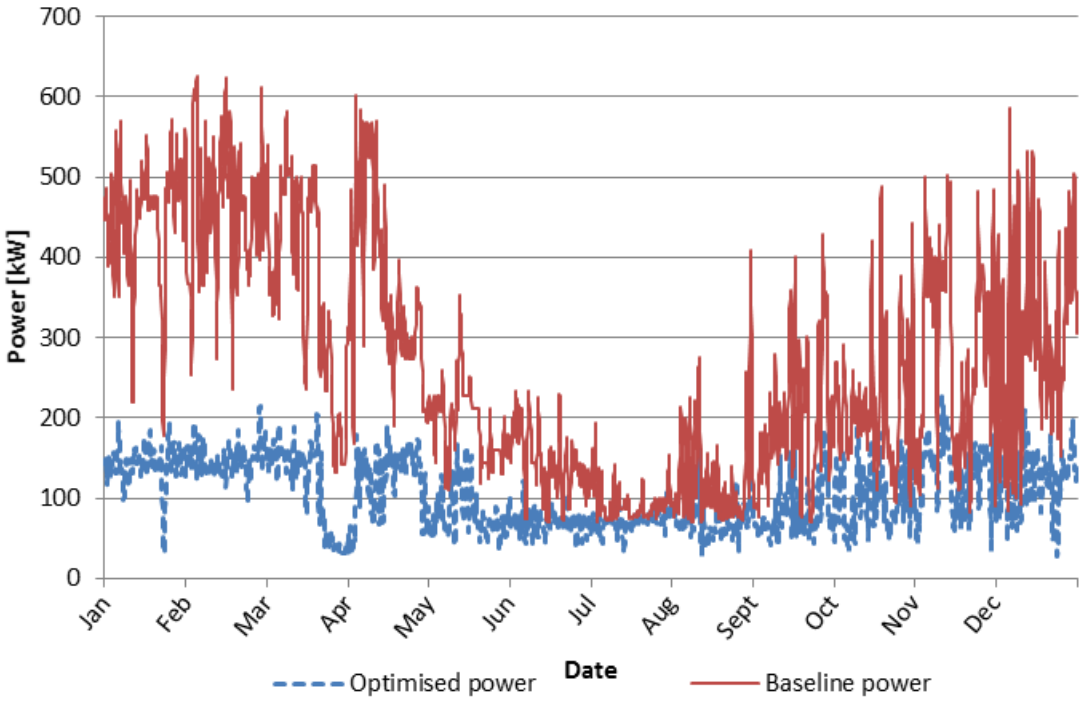

Figure 65: The evaporator pump's baseline and optimised power consumption

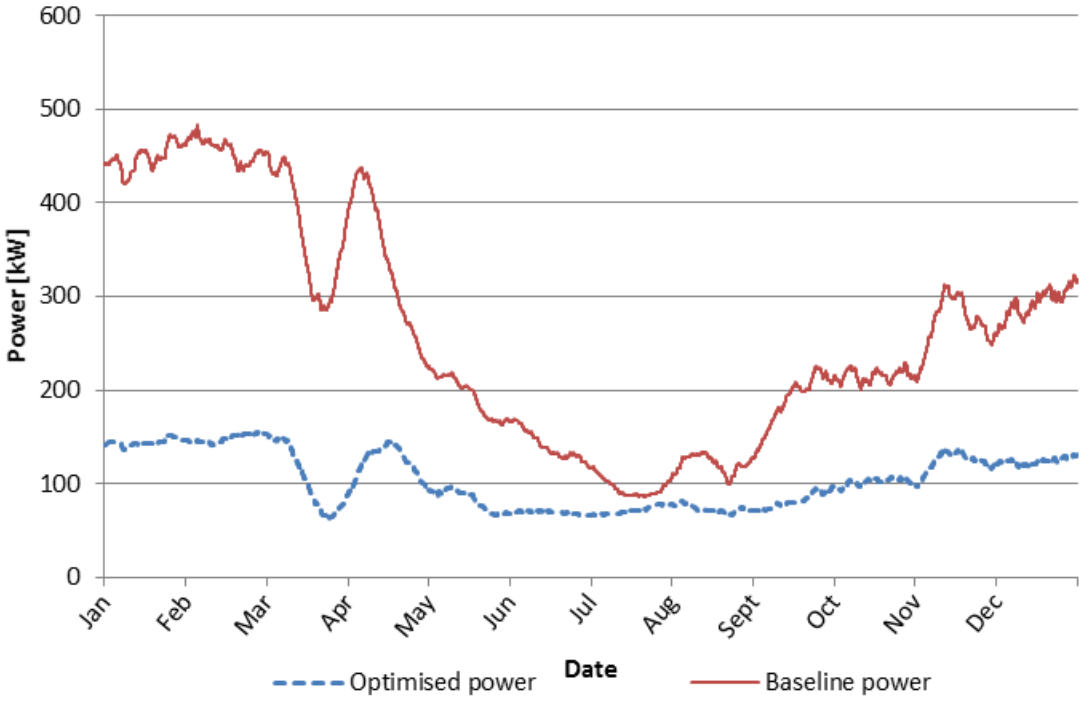

Figure 66: The daily average evaporator pump's baseline and optimised power consumption

Reduced evaporator flow rates suggests that larger temperature differences could be achieved on the reduced volume of water flowing through the evaporator. Figure 67 and Figure 68 shows the increased evaporator water inlet temperatures due to the pre-cool dam water temperature of the optimised system. In Figure 69 and Figure 70 it can be seen that the same evaporator water outlet temperature is maintained for both the baseline and optimised systems. The increased water inlet temperature of the evaporator for the optimised system is due to a higher PCT water outlet temperature, as discussed earlier, as well as reduced water flow through the BAC during certain periods, and finally the decommissioning of the back-pass valve that used to circulate chilled water from the chilled-water dam back to the pre-cooling dam.

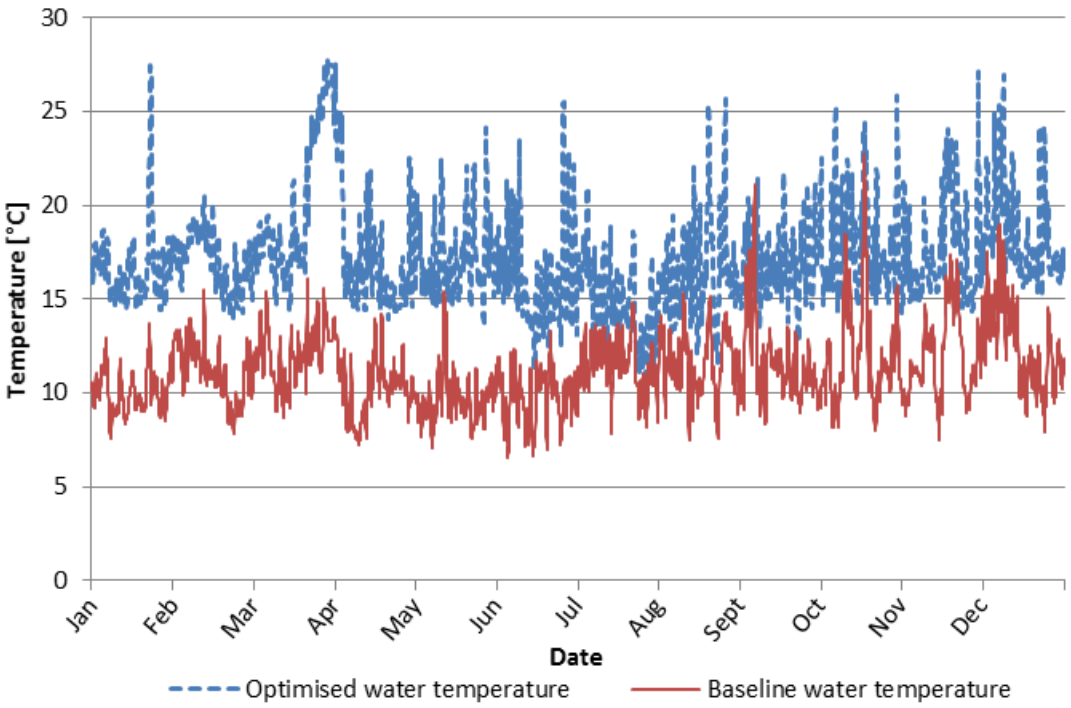

Figure 67: The evaporator's baseline and optimised water inlet temperature

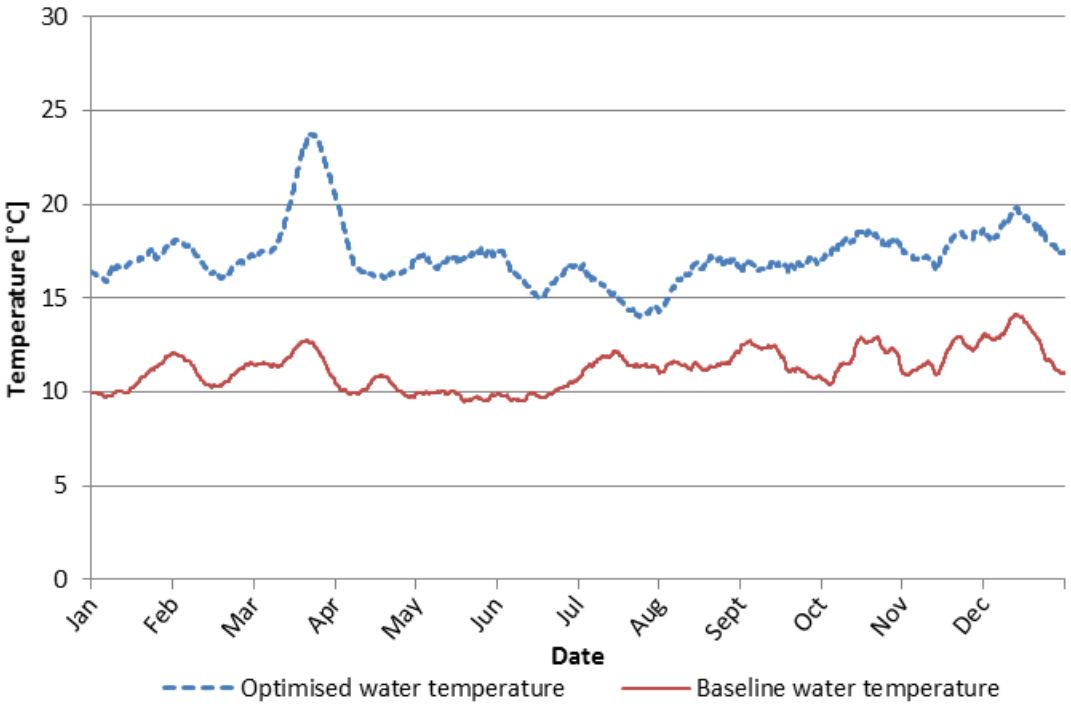

Figure 68: The daily average evaporator's baseline and optimised water inlet temperature

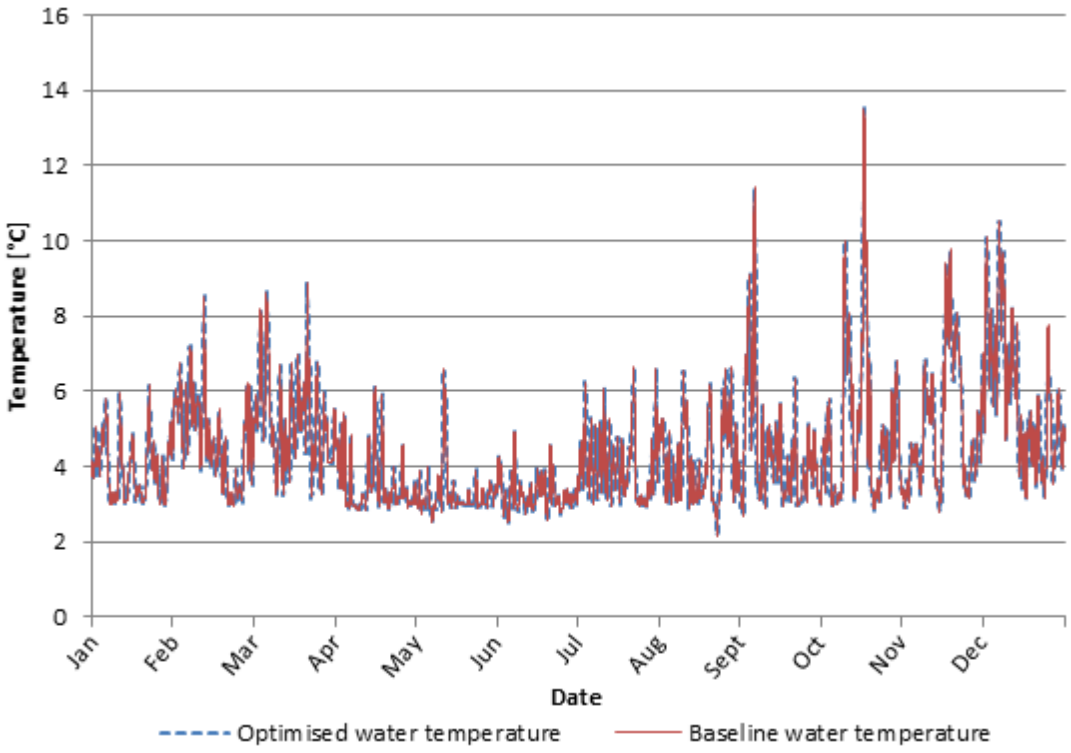

Figure 69: The evaporator's baseline and optimised water outlet temperature

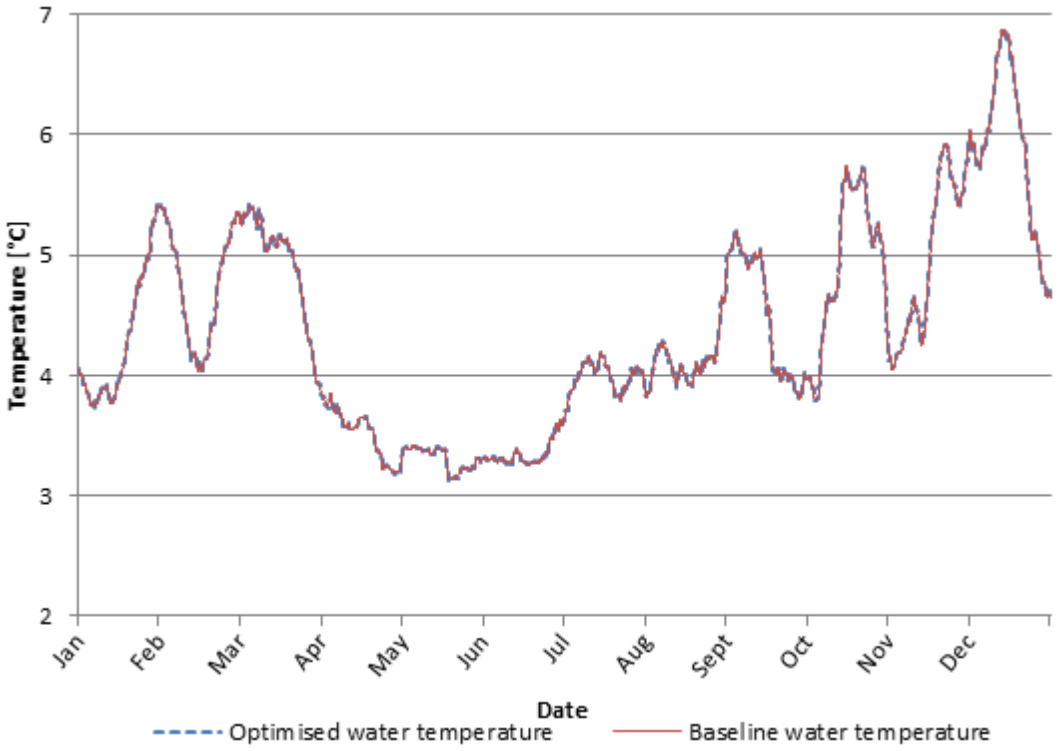

Figure 70: The daily average evaporator's baseline and optimised water outlet temperature

When considering Figure 66, it is evident that the water flow through the evaporator decreased significantly for both the baseline and the optimised systems around the middle of March. This reduction is directly related to the BAC being periodically switched off, as discussed earlier. This is also reflected in Figure 68, where the water inlet temperature of the evaporator increases during this time. This increase is again due to lower overall flow requirements due to the BAC being switched off, as well as the BAC outlet water not contributing to the pre-cooling.

The sudden increase in evaporator flow early in November, as is evident in Figure 66, relates to increase in the BAC's flow, as can be seen in Figure 60. The gradual increase in evaporator flow from the start of September is due to the same reason.

Figure 69 and Figure 70, show the outlet temperatures of the evaporator water for the baseline and optimised models. From these graphs, it is clear that the optimisation followed the baseline outlet temperature exactly, which is expected, due to the constraint imposed to avoid unfairly penalising the optimised model, as discussed earlier. When comparing the inlet temperature of

the evaporator water in Figure 68 to the outlet temperature of the evaporator water in Figure 70, one can also see that higher inlet temperatures were typically found during increased water outlet temperature periods, as can typically be seen during October. It is also evident that the period during March, experienced a slight increase in the water outlet temperature when the BAC was off.

Condenser

The condenser control depends on the condenser pump flow rates, as well as the air flow rates of the CCT's fan. Figure 71 shows the power consumption of the condenser pump and Figure 72 shows the daily average. From these figures, it is evident that the optimised condenser strategy achieved additional pump savings when compared to the baseline. In Figure 72 it can be seen that the optimised power is higher than the baseline power for the condenser in some instances. This is suggested to be due to larger savings that were obtained in the CCT fan power consumption requiring additional condenser water flow to maintain sufficient heat rejection from the system. This phenomena will be considered as part of a comparison in Figure 83. The total cooling performed by the refrigeration plant is superimposed in Figure 72. From this figure, it is evident that the optimised condenser water flow correlates closely to the cooling load imposed on the refrigeration plant. The water flow associated with the pump power of Figure 71 and Figure 72 is included in Appendix B.

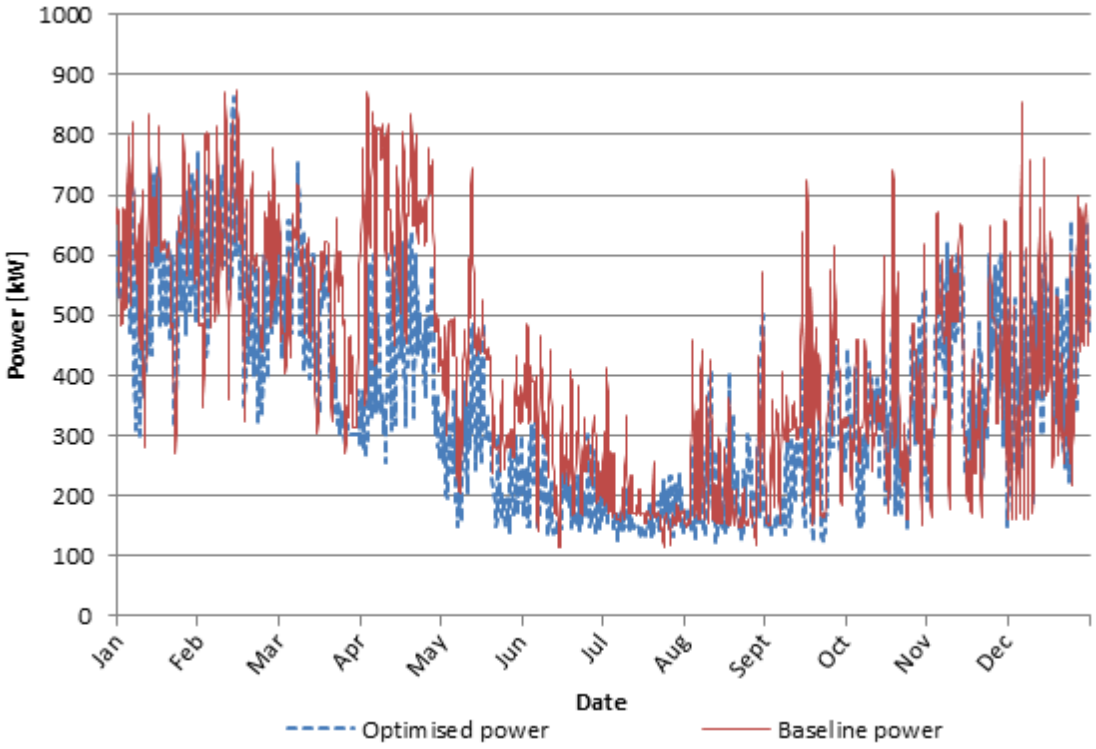

Figure 71: The condenser pump's baseline and optimised power consumption

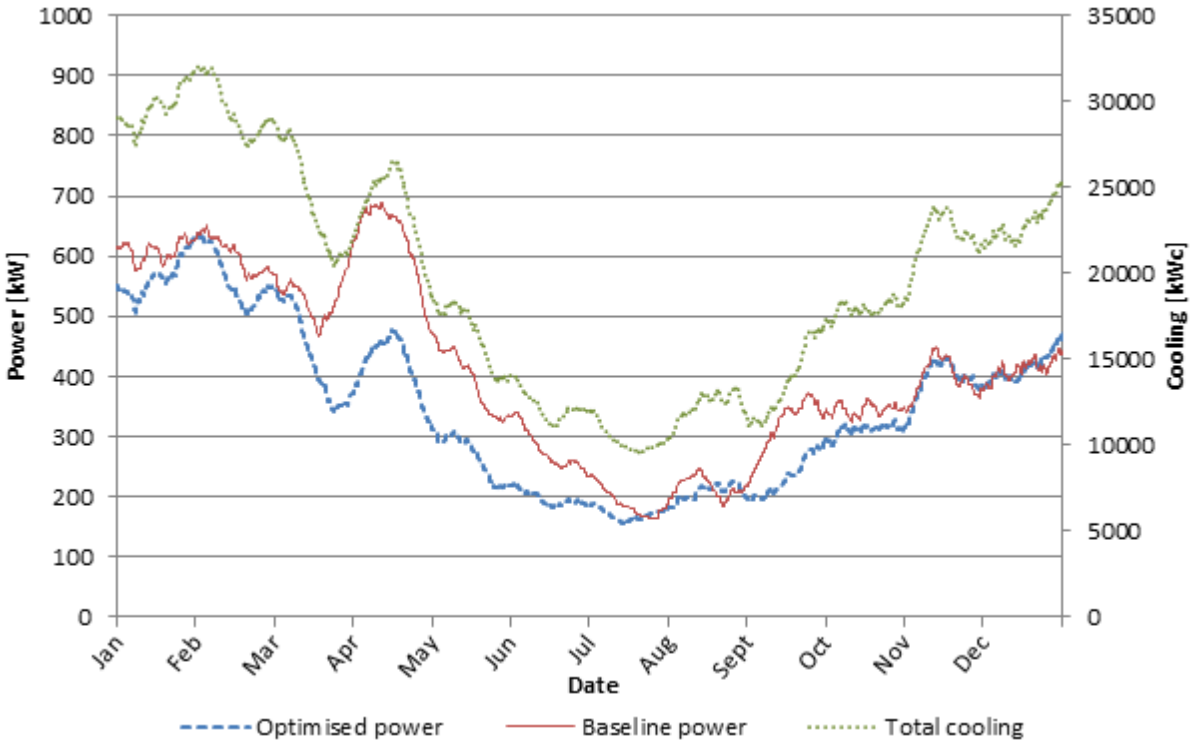

Figure 72: The daily average condenser pump's baseline and optimised power consumption

Figure 73 shows the power consumption of the CCT's fan for the baseline and optimised scenarios, with the daily average values shown in Figure 74. From these figures, the optimisation suggests significant fan power savings when compared to the baseline. With the ambient air enthalpy superimposed on Figure 74, it is evident that the power consumption of the optimised CCT's fan follows the trend of the ambient air. This is in contrast to what was seen for the PCT and suggests that the CCT fan's power had a more significant contribution to the saving potential when considering the integrated system. The reduction in CCT air flow results in higher condenser water temperatures, as can be seen in Figure 75 to Figure 78, which show the baseline and optimised condenser water inlet and outlet temperatures. Additional figures are included in Appendix B, showing both the inlet and outlet temperatures for the baseline and optimised cases.

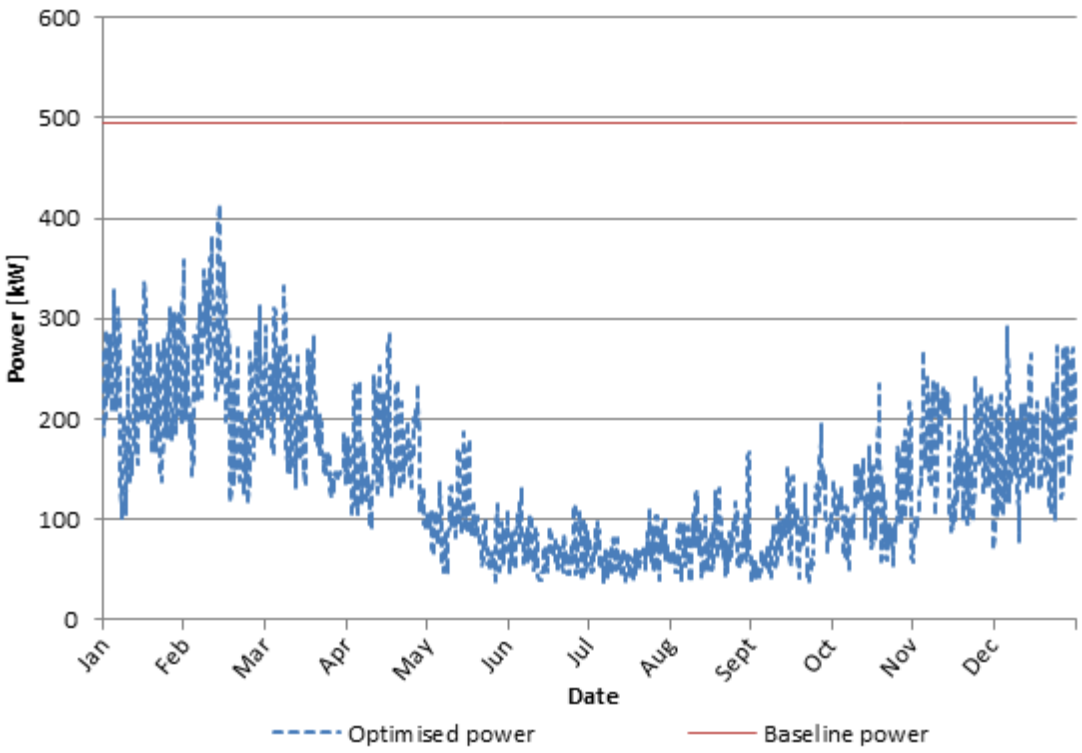

Figure 73: The CCT's baseline and optimised fan power consumption

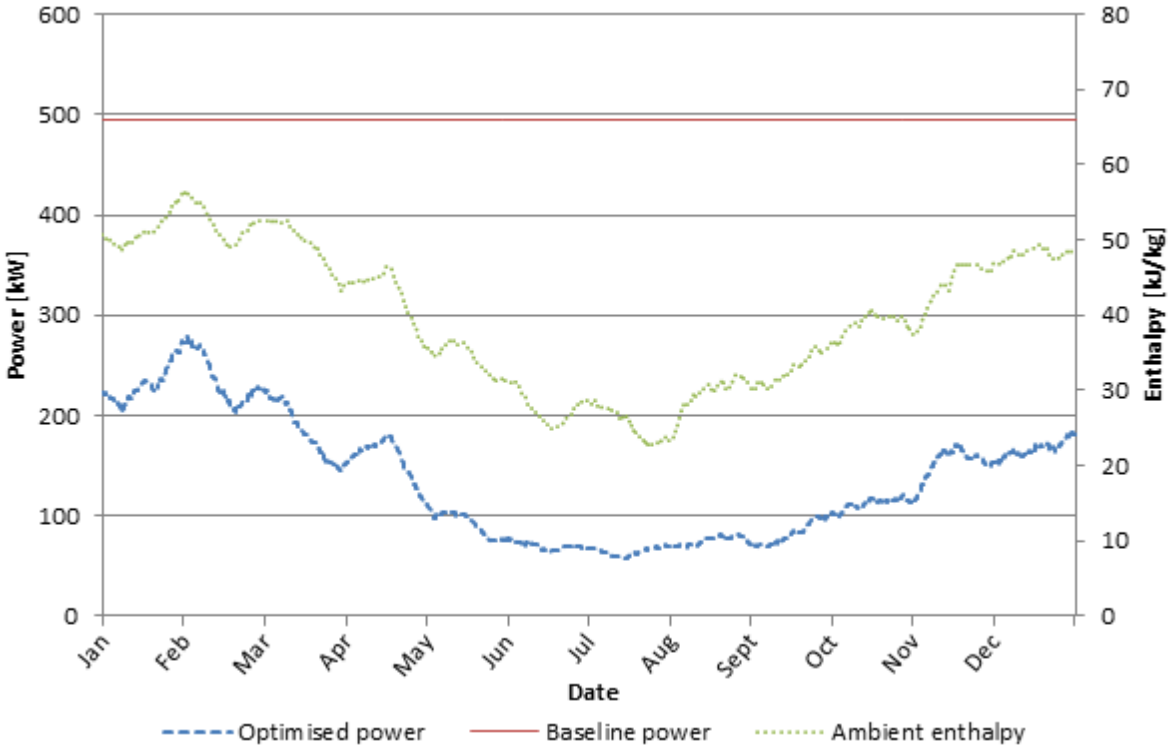

Figure 74: The daily average CCT's baseline and optimised fan power consumption

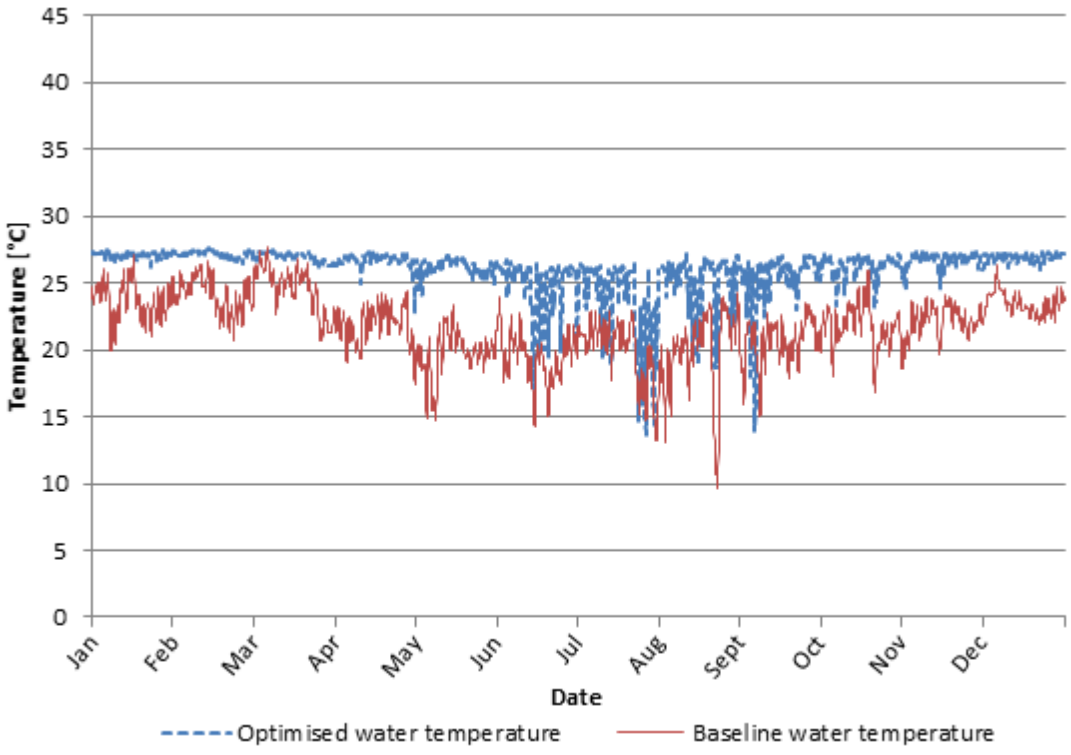

Figure 75: The condenser's baseline and optimised water inlet temperature

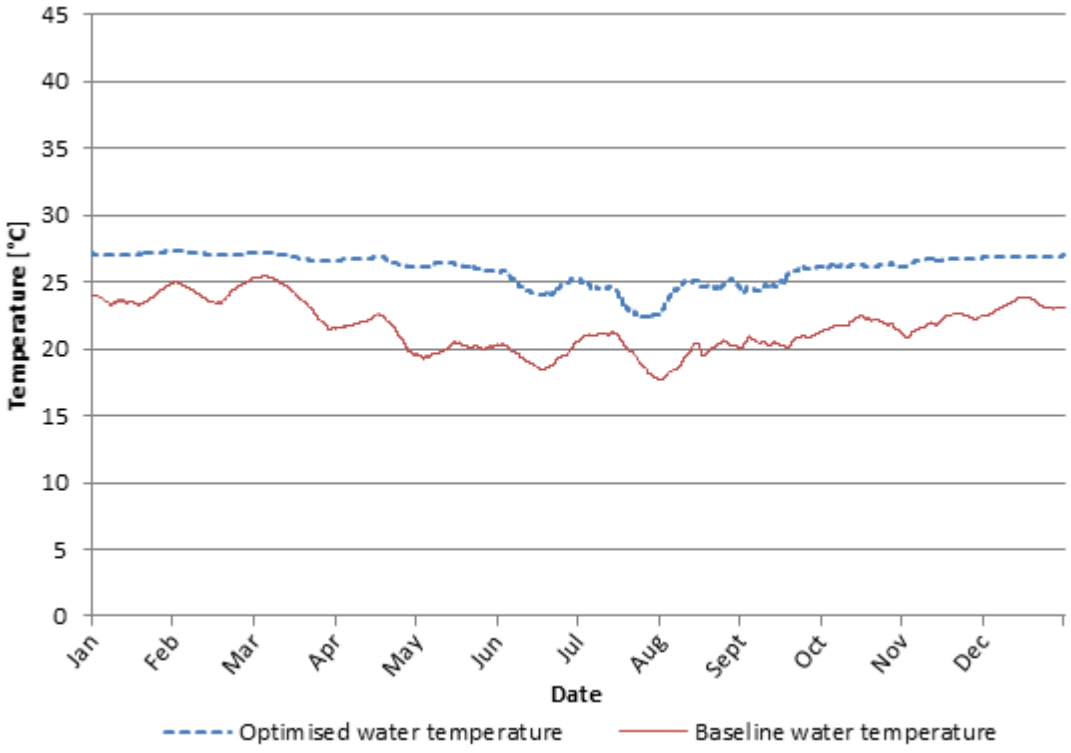

Figure 76: The daily average condenser's baseline and optimised water inlet temperature

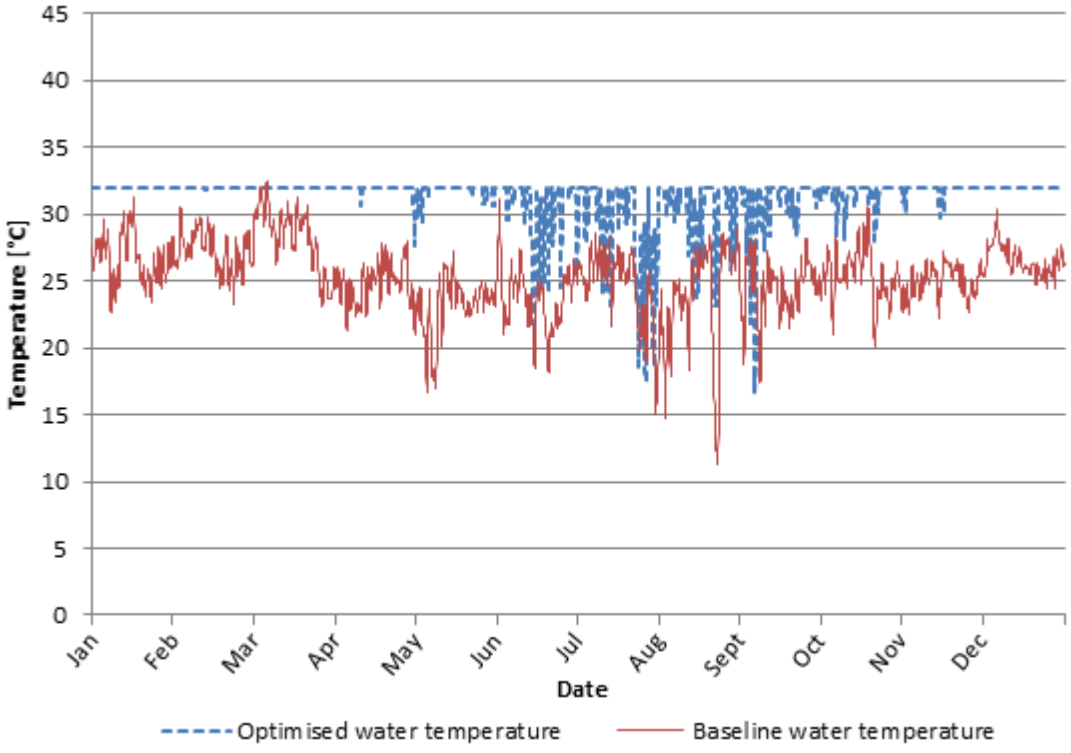

Figure 77: The condenser's baseline and optimised water outlet temperature

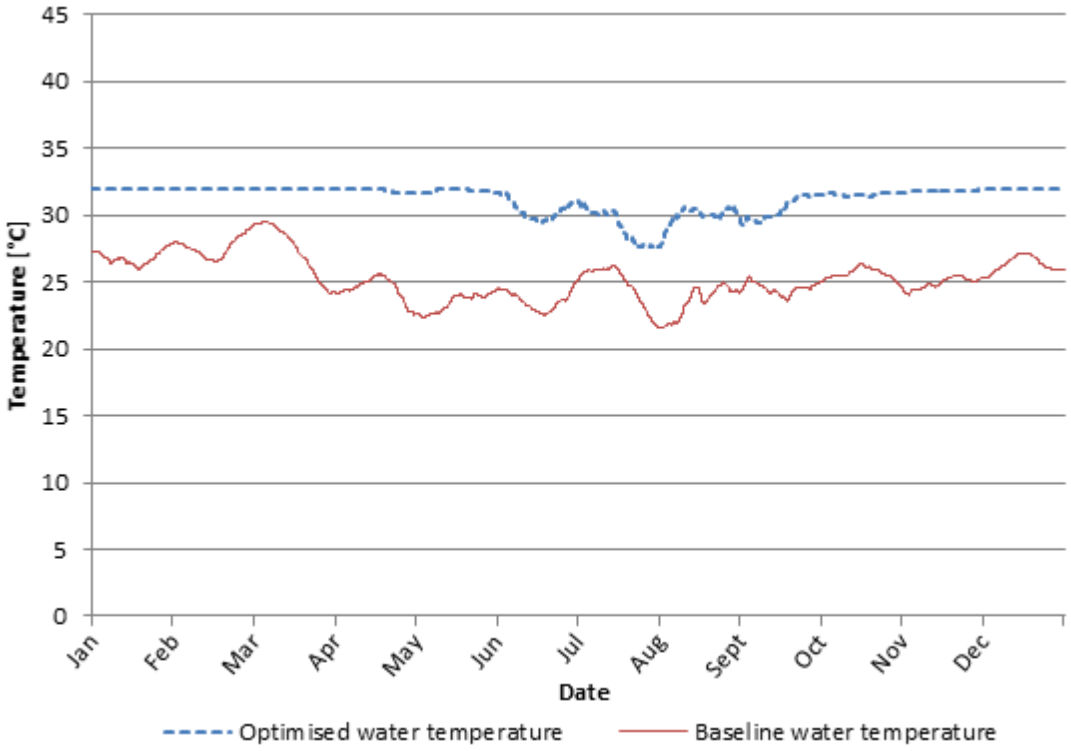

Figure 78: The daily average condenser's baseline and optimised water outlet temperature

When these phenomena are compared to the literature of Section 2.5.2, it is noted that the opposite of the suggested saving strategy is realised, as the condenser temperature has increased instead of decreasing. However, as noted in the literature, cases could occur where a slight increase in the energy consumption of one component could result in a larger decrease in the energy consumption of another component. This seems to be the case here, as the optimisation controller favoured the saving realised on the CCT's fan, as opposed to the possible saving that lower condenser temperatures would have made to power consumption of the chiller's compressor.

Chiller

Figure 79 shows the total chiller power for the baseline and optimised cases, with the daily average values shown in Figure 80. From these figures, it can be seen that the chiller obtained energy savings mostly during the change-of-season periods, when the BAC flow was reduced. The significant saving in March is suggested to be due to the BAC being switched off, as well

as the decommissioning of the back-pass valve, which could have resulted in a significant overall cooling load during that period.

Figure 81 shows the overall chiller's baseline and optimised COP, with the daily average values shown in Figure 82. From these figures, it is clear that the chillers maintained an improved overall COP. This is primarily suggested to be due to the increased water inlet temperature of the evaporator relating, relating to an increase in the chiller COP values, as suggested in the literature.

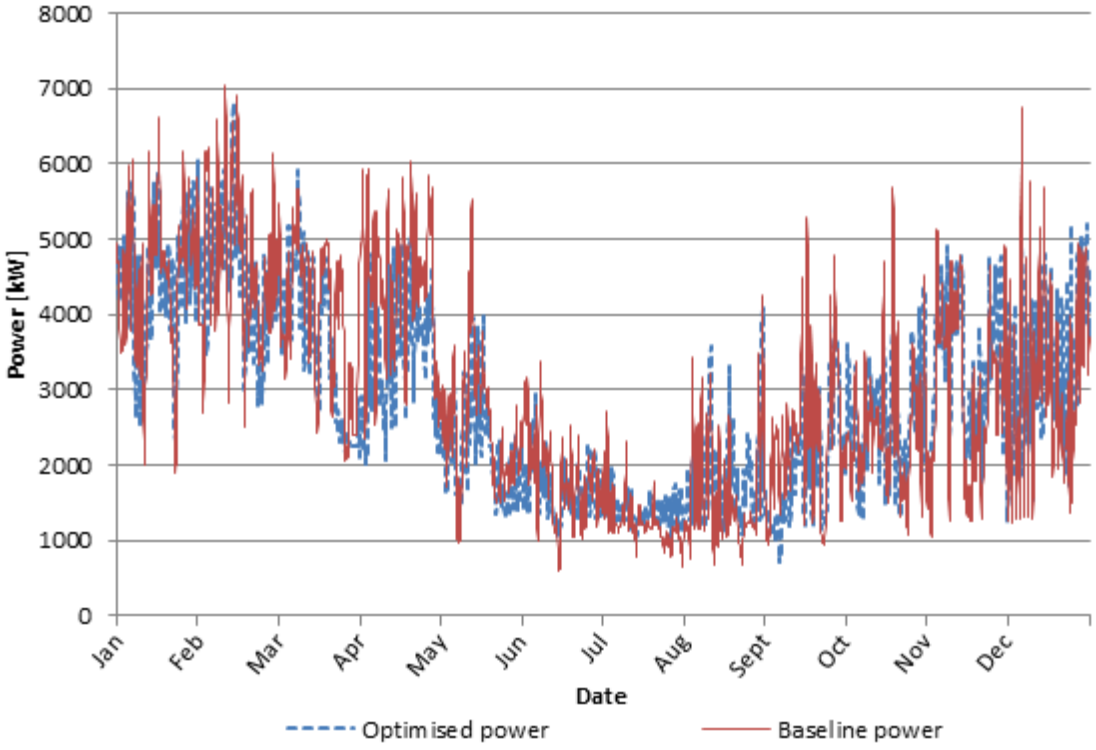

Figure 79: The chiller's baseline and optimised power consumption

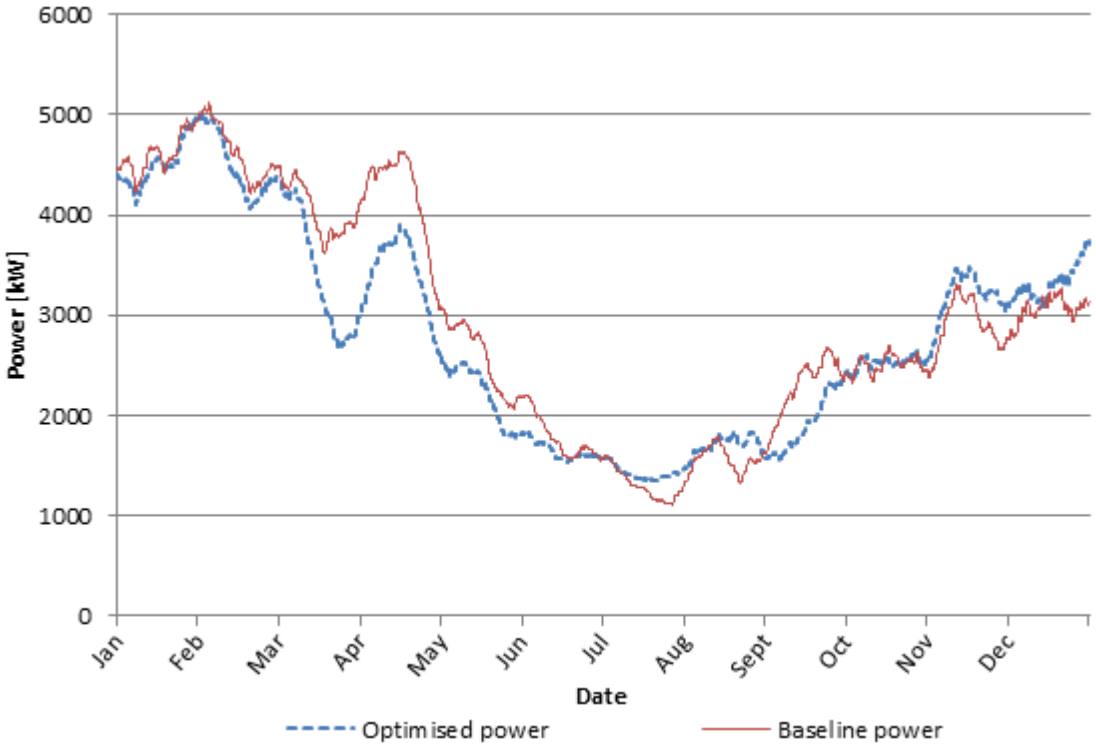

Figure 80: The daily average chiller's baseline and optimised power consumption

From Figure 80, it is also evident that there are instances where the optimised chiller consumed more energy than the baseline chiller. For these instances, it is suggested that the CCT fan's power saving was greater than the increased power consumption by the chiller, still providing a net saving. To confirm this conclusion, the power savings obtained by the chiller, CCT fan and condenser pumps are included on an area graph in Figure 83, where the savings contribution due to each component can be compared. From this comparison, it is clear that the net result yields a saving most of the time and when the chiller contributes to what seems to be a negative saving, as can be seen in Figure 80, which is then overweighed with the increased saving from the CCT's fan and condenser pump. It is only at the end of November, the beginning of December, and the last part of December that the net effect of these components together does not seem to provide any saving. It is therefore suggested that any saving achieved on the integrated system is contributed by components other than the ones considered here.

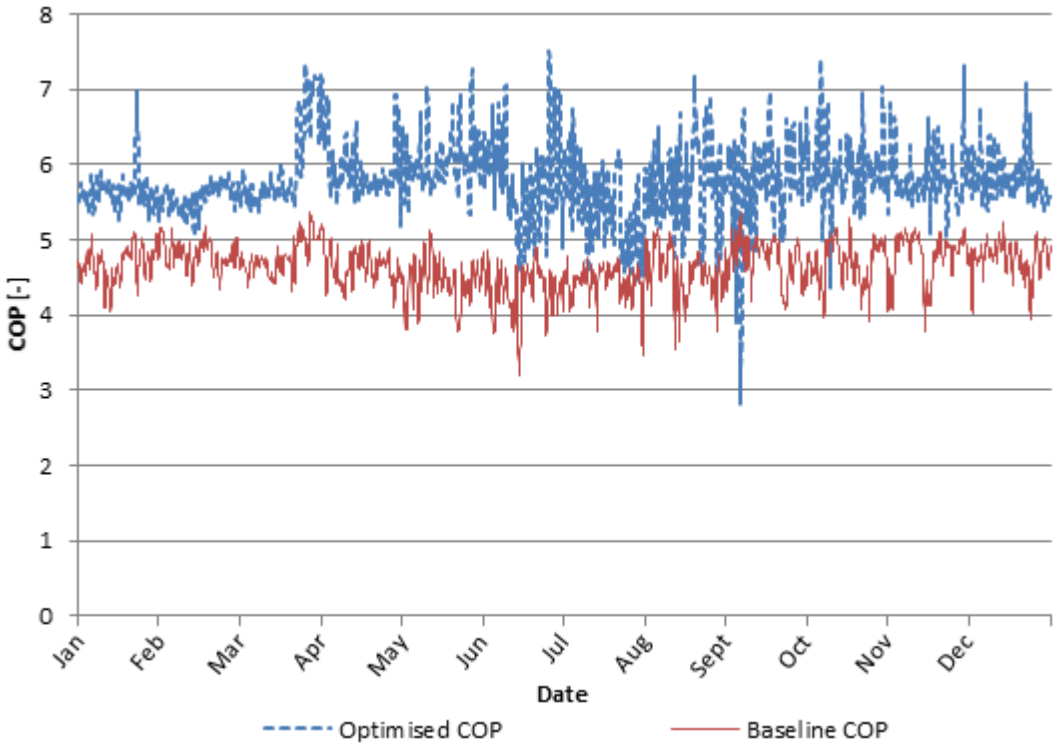

Figure 81: The chiller's baseline and optimised COP

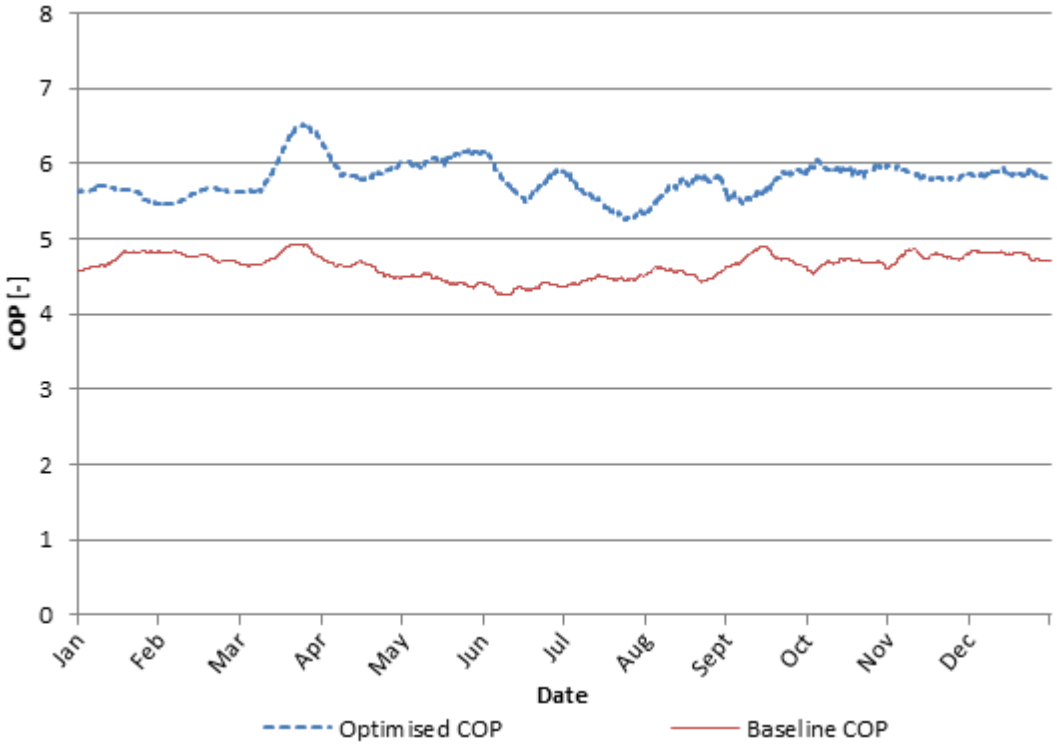

Figure 82: The daily average chiller's baseline and optimised COP

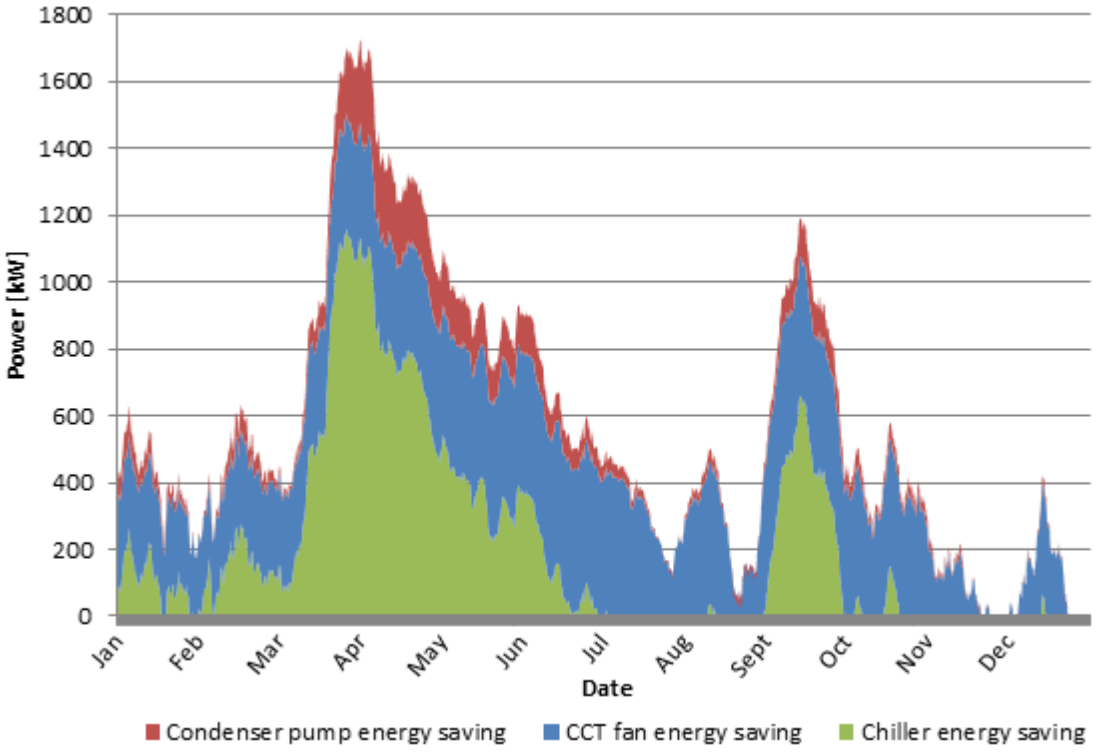

Figure 83: The daily average optimised chiller, condenser pump and CCT fan's energy savings

5.3.3 Component and integrated savings

In order to fully quantify the saving contribution realised through each of the components, various graphs were constructed as area graphs where the saving contribution of each component could be seen. Various similar subcomponents, such as the pumps and fans, were first grouped together for comparison, as shown in Figure 84 and Figure 85, after which all the major energy-consuming components were added to indicate the overall saving as shown in Figure 86. The combined total pump power and total fan power of all the pumps and fans is included in Appendix B.

From Figure 86, it is evident that the integrated system achieved satisfying overall savings. The importance of an integrated simulation model for the application of overall energy minimisation is highlighted where it can be seen that certain components could have more significant savings for somewhat reduced savings on other components, or even slight increases in some components for a more substantial saving elsewhere.

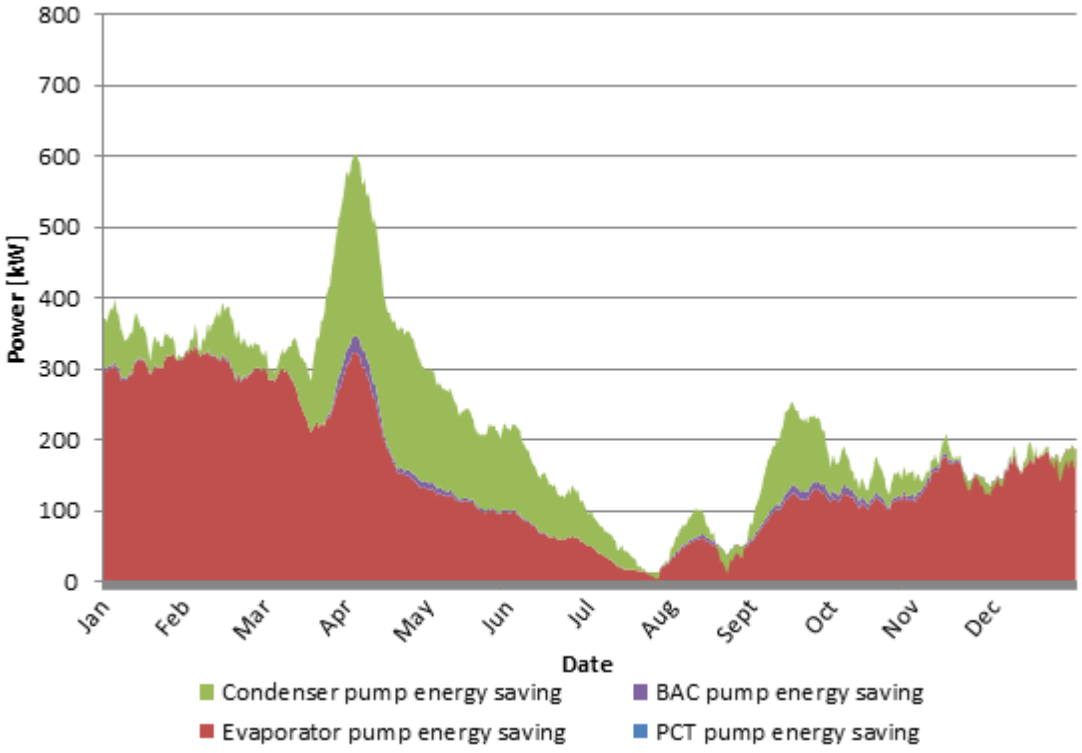

Figure 84: The condenser, evaporator, BAC and PCT pumps' energy savings

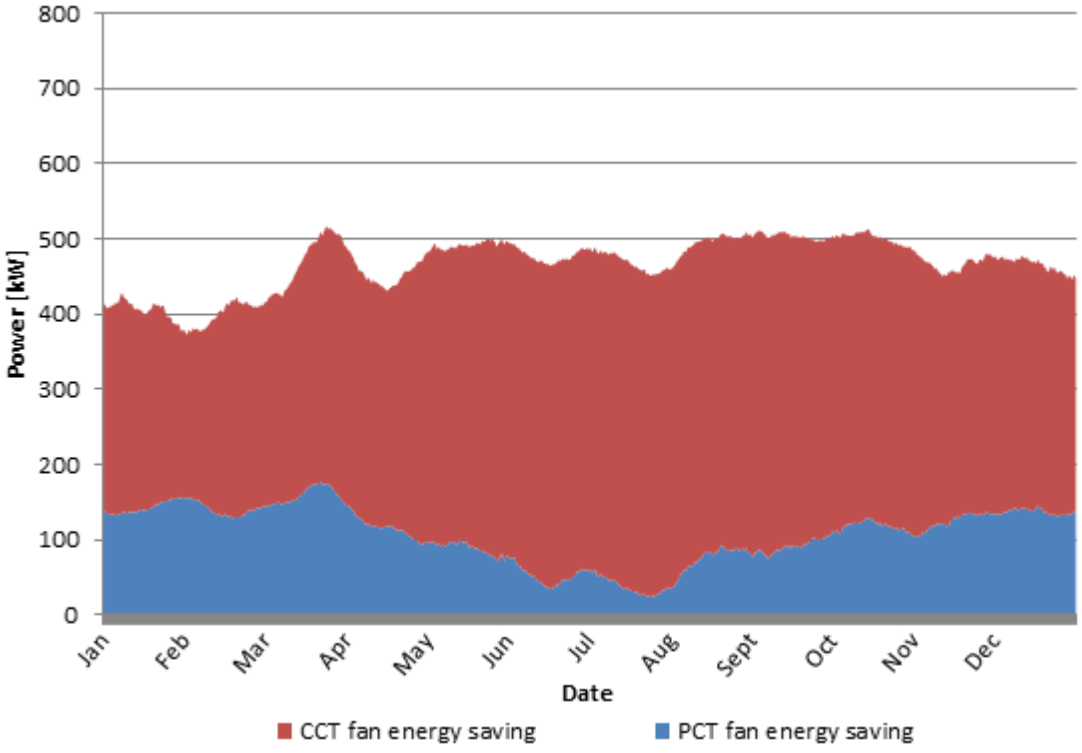

Figure 85: The CCT and PCT fans' energy savings

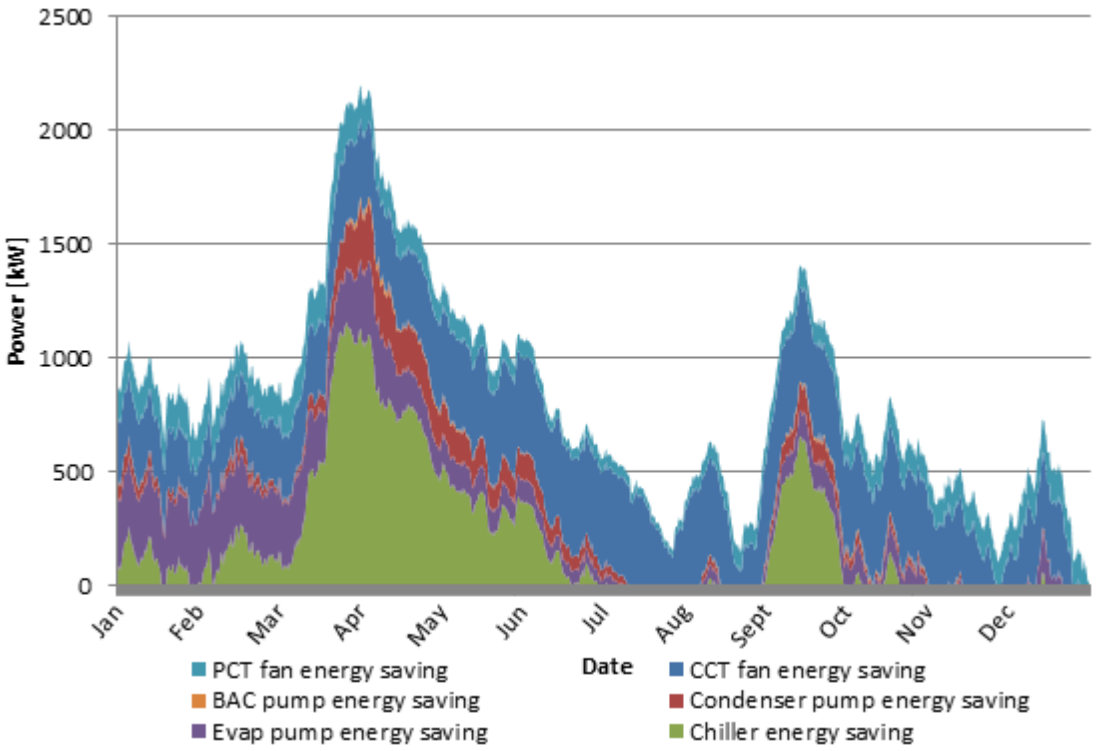

Figure 86: The component-based total integrated system's energy savings

The contribution of the energy savings for the various major energy-consuming components suggested by the optimisation model are summarised in Table 13. From these results, it is evident that the most significant contribution to the overall savings was realised by the CCT's fan, evaporator pumps and chiller in decreasing order.

Table 13: The component-based annual energy savings

Component	Energy saving (kWh)	Percentage of total saving	Percentage point contribution to 17.9% saving
Evaporator pump	1 409 760.67 kWh	19.89%	3.58%
Condenser pump	524 529.42 kWh	7.40%	1.33%
BAC pump	37 402.55 kWh	0.53%	0.09%
PCT fan	954 708.83 kWh	13.47%	2.42%
CCT fan	3 120 741.94 kWh	44.04%	7.92%
Chiller	1 038 962.67 kWh	14.66%	2.64%
Total	**7 086 106.07 kWh**	**100%**	**17.99%**

5.3.4 Optimisation computational load

The integrated system optimisation was performed on a computer with the specifications as listed in Table 14. The average hourly annual optimisation of Dataset G required an average of 7 minutes and 39 seconds to solve each time step with the computer specified. The total annual optimisation of the system therefore required roughly 46.6 days to optimise the cooling system simulation model's energy consumption for the year of Dataset G.

Table 14: Simulation and optimisation computer specifications

Computer component	Specification
System Type	X64 based PC
Processor	Intel® Core™ i7-4600U CPU @ 2.1Ghz, 2701 Mhz, 2 Cores, 4 Logical Processors
Installed Physical Memory	16.0 GB
Operating System	Microsoft Windows 7

5.4 Conclusion

The integration of the optimisation platform with the simulation model was briefly discussed. This was achieved by constructing a simulation model in MS Office Excel to which the Analytic Solver Platform integrates by means of an add-on toolbox. This arrangement ensured seamless integration between the simulation model and the optimisation platform.

In order to ensure acceptable results from the optimisation platform considered, it was necessary to verify the platform by means of test functions typically found in the literature, which were suitable for testing constraints in non-linear global optimisation problems. This was achieved by programming each of the test functions into MS Office Excel, after which the objective functions were optimised subject to the various constraints imposed. It was generally found that the Analytic Solver Platform achieved equal or better results to those suggested in the literature. This provided confidence that the optimisation platform solved these types of optimisation problems with acceptable consistency.

Various system and boundary constraints were imposed on the optimisation to allow the system to remain in the system-installed capacities and achieve the intended potential savings. With

this arrangement, the optimisation platform was deemed to be the system controller, and was known as an optimal control system.

The optimised system achieved an average saving of 17.9% for the year considered. This resulted in an overall reduction in energy consumption of 7.1 GWh for the year. The behaviour of the various major energy-consuming devices was considered on an hourly and integrated daily average basis to assist in observing trends with greater ease. The integrated effect of variations to certain components' parameters and their effect on other components in the system were identified and discussed. Most importantly, it was confirmed that the mine chilled-water temperature and flow rates supplied underground were maintained, while the BAC's air outlet conditions were maintained at acceptable levels through the optimisation.

6 Conclusion

6.1 Introduction and literature

A brief overview of the current state and sector distribution of electrical energy consumption in South Africa was considered. From this, it was established that the mining sector is the largest single energy user on a percentage per user scale and that the energy requirements of mining have increased four-fold from 1970 to 2001. The mining sector accounted for 14.3% of the total electrical energy supplied by Eskom in 2016. It was furthermore established that roughly 25% of a typical deep-level mine's energy consumption is attributed to the cooling system.

Various previous efforts were made, as alluded to in the study, to reduce energy consumption and implement load-shifting strategies to relieve the strain on the South African energy utility, Eskom, as well as to provide financial relief on the cost of energy to the mines. Of these strategies, some included cooling system flow control, resulting in energy savings of around 30%. It was found that these comprised trial-and-error energy improvements and therefore created the opportunity for possible further reductions by implementing integrated optimisation to ensure a global minimum energy consumption.

An extensive literature survey was conducted to identify the most typical mine cooling systems and their operational ranges, as well as previously implemented energy-saving strategies. From the literature, the opportunity was identified to construct an integrated mine cooling system simulation model suitable for optimisation. This led to the integration of the simulation model with an optimisation platform to determine the minimum energy operational parameters of the integrated cooling system. The cooling system's state of the art was considered, where it was determined that no optimisation-friendly simulation model or explicit optimisation application had been constructed before, which allowed a component-level quantification of the system's operation, savings potential and subsequent contribution.

Thereafter, various mine cooling system flow-control energy-saving opportunities were identified. These included PCT and CCT air and water flow control, as well as BAC and

evaporator water flow control. All these factors have an impact on the energy consumption of the PCT and CCT fans, BAC, evaporator and condenser pumps, as well as power consumption of the chiller compressor.

The literature was concluded with an overview of optimisation, considering constraints in non-linear global optimisation. Four test functions were identified for the verification of the optimisation platform.

6.2 Mine cooling system and simulation

The mine cooling system considered for the current study was presented. The typical system operation and installed capacities were identified, and subsequently. the parameters for energy optimisation were identified. The mine's SCADA system was introduced next, stipulating the parameters that are monitored and logged, as well as the measuring instrumentation accuracies.

Thereafter, the simulation models for the various major energy-consuming components were identified and described. These included models for the cooling towers, chillers, pumps and fans. These models were all smooth and continuous functions to facilitate optimisation applications and were furthermore all based on system-side operational parameters relating to the energy consumption of each component. These models were then integrated to model the whole cooling system.

One week's data was isolated for calibration of the various component models, from which the various model parameters were determined. These achieved RMSRE values in the range of 0.0114 and 0.0651. The integrated cooling system was then constructed by coupling all the components with the inlets and outlets of the various components assigned according to the system's thermal hydraulic flow of the. Various weekly datasets were used to validate the simulation model. For these validations, RMSRE values in the range of 0.0375 to 0.0704 were obtained. Hourly data was subsequently considered for the same datasets to evaluate the accuracy when compared to the measured time-step data that was measured in three-minute intervals. This was required due to the intention of applying the optimisation to an annual dataset that was considered on an hourly basis due to computational constraints. For these

validations, RMSRE values in the range of 0.0362 to 0.0659 were achieved. The hourly annual dataset obtained a RMSRE value of 0.086.

6.3 Optimisation and results

The test functions identified as part of the optimisation literature were used to verify the Analytic Solver Platform provided by Frontline Systems Inc. For this purpose, four different test functions were used, for which the optimisation platform obtained similar or better global optimal solutions. It was therefore established that the optimisation platform was suitable for solving non-linear global optimisation problems.

The optimisation platform was subsequently coupled to the integrated simulation model. The energy-saving strategies were then implemented by assigning the various variables and constraints according to the system's design parameters and installed capacity limitations. These included PCT and CCT fan air flow control, as well as evaporator, condenser and BAC water flow control. The most important consideration was to ensure that the same chilled-water outlet temperature and demand water flow rate was maintained.

The optimisation was performed for the same annual hourly data used to construct the annual baseline model and subsequently compared to the baseline. An average saving on the energy consumption of 17.9% was suggested by the optimisation. This saving relates to an energy saving of 7.1 GWh for the year.

All the components that experienced variations in fluid flow through the optimisation process were analysed on their thermal hydraulic behaviour for both the baseline and optimised scenarios. Various conclusions, as well as the integrated effects of variations to various components, were discussed and highlighted. It was found that, for some instances, a slight increase in one component's energy consumption could potentially reduce another component's energy consumption more significantly than the increase to the initial component. This phenomenon highlights the importance of considering the optimisation in an integrated approach instead of considering components in isolation.

The hypothesis that there is an energy minimum that can be determined through integrated simulation and optimisation was thus satisfied, as the annual energy minimum points of operation were successfully determined for the mine cooling system under consideration.

6.4 Recommendations

Although extensive time and effort was afforded to the current study, some recommended further studies could be considered as discussed below.

Limitations were encountered during the course of the study due to various constraints. It is for these reasons that it could be recommended to consider the annual optimisation through a reduced time-step frequency to determine the accuracy of the optimisation when time steps of less than an hour are considered. The computing power at the disposal of the current study did not allow for this, as the optimisation becomes increasingly computationally intense as the time-step durations are reduced. Even though the current increments provided a holistic view with acceptable accuracy when compared to similar studies, it is worth evaluating the significance of the improvement in accuracy when considering refined time steps.

The current cooling tower model assumes a constant heat transfer surface area. In reality, the effective heat transfer surface area will decrease as water and air flow rates are reduced. It is suggested that the effects thereof could be investigated in future studies from where the implication to the overall simulation accuracy could be quantified.

Further studies could be conducted in an attempt to improve the simulation model's accuracy by including local heat loss through components such as pumps, valves, piping, dams and sumps, as these were all assumed to be adiabatic for the purposes of the current study. Notwithstanding the fact that the current study provided suitable results, the effect of this assumption on the overall accuracy could be investigated.

Periodic recalibration could be considered where the simulation model is frequently recalibrated. This could be incorporated as part of the annual simulation and optimisation in

order to determine the increase in accuracy for a given frequency of recalibration. For the purpose of the current study, only one calibration period was considered.

The practical implementation of an optimisation strategy, as simulated for this study could be considered. Various options could be investigated, including, but not limited to, implementing a real-time optimisation application where the actual system is coupled to an optimisation controller. This strategy would ultimately require adequate computing power to ensure that the optimisation could be computed sufficiently in order to meet the system response times. An alternative approach that could be followed when constrained computing power is available would be to derive tables of optimal operational parameter sets for all the components of the system for pre-defined ranges of demand and climate data. These sets would typically be constructed by means of an integrated simulation model coupled to an optimisation platform, as proposed in the current study. This will allow a more robust and simplistic control method whereby the optimal values could be derived from the tables, as the demand and/or climate fluctuates. Periodic recalibration could be implemented to ensure the accuracy of the optimised parameter sets as the system changes through time and degradation of the components' performance.

7 References

[1] A. J. Schutte, "Demand-side energy management of a cascade mine surface refrigeration system," M-Eng dissertation, North-West University, Potchefstroom, South Africa, 2007.

[2] Eskom, "Eskom Integrated Report," 2016. [Online]. Available: www.eskom.co.za. [Accessed: 09 September 2016]

[3] H. Winkler, O. Davidson, A. Kenny, G. Prasad, J. Nkomo, D. Sparks, M. Howells, T. Alfstad, S. Mwakasonda, B. Cowan and E. Visagie, Energy policies for sustainable development in South Africa - options for the future, Energy Research Centre, University of Cape Town, Cape Town, South Africa, 2006.

[4] Gold Fields, "Gold Fields Annual Report," 2010. [Online]. Available: www.goldfields.co.za. [Accessed: 25 March 2014]

[5] M. Levesque, D. Millar and J. Paraszczak, "Energy and mining – the home truths," *Journal of Cleaner Production*, vol.84, pp. 1–23, 2014.

[6] R. Els, "Potential for load shifting in ventilation and cooling systems," M-Eng dissertation, University of Pretoria, Pretoria, South Africa, 2000.

[7] J. Vosloo, L. Liebenberg, and D. Velleman, "Case study : Energy savings for a deep-mine water reticulation system," *Applied Energy*, vol. 92, pp. 328–335, 2012.

[8] J. van Rensburg, A. Botha and G. Bolt, "Energy efficiency via optimisation of water reticulation in deep mines," *Proceedings of the 8th Conference on the Industrial and Commercial Use of* Energy, pp. 124–132, 2011.

[9] RCW Webber-Youngman, "An integrated approach towards the optimisation of ventilation, air cooling and pumping requirements for hot mines," PhD thesis, North-West University, Potchefstroom, South Africa, 2005.

[10] J. W. Fourie, "Power savings by impeller replacement for main fan stations in the South African Gold mining industry," *Proceedings of the 9th Conference on the Industrial and Commercial Use of Energy*, 2012.

[11] B. K. Belle, "Energy savings on mine ventilation fans using 'Quick-Win' hermit crab technology – a perspective," *North American Mine Ventilation Symposium*, vol. 12, pp.

427–434, 2008.

[12] B. P. Kazakov, A. V. Shalimov, and A. S. Kiryakov, "Energy-saving mine ventilation," *Journal of Mining Science*, vol. 49, no. 3, pp. 475–481, 2013.

[13] W. C. Kukard, "Research on reducing costs of underground ventilation networks in South African mines," M-Eng dissertation, North-West University, Potchefstroom, South Africa, 2006.

[14] UNEP, "Electrical Energy Equipment: Cooling Towers," *Energy Efficiency Guide for Industry in Asia*, 2006. [Online]. Available: www.energyefficiencyasia.org.

[15] A. Hassan, K. Ouahada, T. Marwala and B. Twala, "Optimization of the Compressed Air-Usage in South African mines," *IEEE Africon*, no. 18656, 2011.

[16] R. Joubert, "Cost and time effective DSM on mine compressed air systems," M-Eng dissertation, North-West University, Potchefstroom, South Africa, 2010.

[17] H. P. R. Joubert, J. F. van Rensburg, and R. Pelzer, "Energy efficiency opportunities resulting from splitting a compressed air ring," *Proceedings of the 8th Conference on the Industrial and Commercial Use of Energy*, 2011, pp. 75–81.

[18] G. E. du Plessis, L. Liebenberg and E. H. Mathews, "Case study: The effects of a variable flow energy saving strategy on a deep-mine cooling system," *Applied Energy*, vol. 102, pp. 700–709, 2013.

[19] W. Bornman, "Improved mine cooling system performance through the control of auxiliary systems," M-Eng dissertation, North-West University, Potchefstroom, South Africa, 2012.

[20] G. E. du Plessis, D. C. Arndt and E. H. Mathews, "The development and integrated simulation of a variable water flow energy saving strategy for deep-mine cooling systems," *Sustainable Energy Technologies and Assessments*, vol. 10, pp. 71–78, 2015.

[21] D. Roux, "Energy recovery from high pressure cold water in mines," *Proceedings of the 9th Conference on the Industrial and Commercial Use of Energy*, pp. 28–32, 2012.

[22] G. E. du Plessis, "A variable water flow strategy for energy savings in large cooling systems," PhD thesis, North-West University, Potchefstroom, South Africa, 2013.

[23] M. J. McPherson, "Refrigeration plant and mine air conditioning systems," *Subsurface*

ventilation and environmental engineering, Dordrecht: Springer Netherlands, pp. 651–738, 1993.

[24] R. E. Noble, C. E. Gulledge, H. J. McKew, K. C. Peet, M. Norm, M. P. Modera and J. P. Pennington, *ASHRAE Handbook - HVAC Applications*, Atlanta, GA: ASHRAE, pp. 29.1–29.13, 2011.

[25] L. Mackay, S. Bluhm and J. van Rensburg, "Refrigeration and cooling concepts for ultra-deep platinum mining," *The International Platinum Conference*, pp. 285–292, 2010.

[26] G. E. du Plessis, L. Liebenberg, E. H. Mathews and J. N. du Plessis, "A versatile energy management system for large integrated cooling systems," *Energy Conversion Management* vol. 66, pp. 312–325, 2013.

[27] G. E. du Plessis, L. Liebenberg and E. H. Mathews, "The use of variable speed drives for cost-effective energy savings in South African mine cooling systems," *Applied Energy*, vol. 111, pp. 16–27, 2013.

[28] H. Grollius, C. Meyer and M. Rautenberg, "Computer modelling of the performance of centrifugal water chillers in mine refrigeration installations," *International Journal of Refrigeration*, vol. 10, pp. 49–52, 1987.

[29] Y. A. Çenegal, *Heat and Mass Transfer – A Practical Approach*, 3rd ed., New York, NY: McGraw-Hill, pp. 609–645, 2006.

[30] K. Shan, S. Wang, D. Gao and F. Xiao, "Development and validation of an effective and robust chiller sequence control strategy using data-driven models," *Automation in Construction*, vol. 65, pp. 78–85, 2016.

[31] DAIKIN, "Centrifugal chiller fundamentals," 2015. [Online]. Available: www.daikinapplied.com. [Accessed: 06 August 2016].

[32] B. Bergsten, "Evaporative Cooling Tower and Chilled Beams Evaporative," PhD thesis, Chalmers University of Technology, Göteborg, Sweden, 2009.

[33] G. Pingye and C. Chen, "Field experimental study on the cooling effect of mine cooling system acquiring cold source from return air," *International Journal of Mining Science and Technology*, vol. 23, no. 3, pp. 453–456, 2013.

[34] R. Al-Waked and M. Behnia, "Enhancing performance of wet cooling towers," *Energy Conversion and Management*, vol. 48, no. 10, pp. 2638–2648, 2007.

[35] F. M. White, "*Fluid mechanics*," 6th ed., New York, NY: McGraw-Hill, pp. 751–798, 2008.

[36] R. W. Shortridge, "Lester Pelton and His Water Wheel," *Hydro Review*, vol. 8, pp. 22–26, 1989.

[37] F. J. Nadaraju, "Study to evaluate the economic feasibility of replacing a pressure reducing valve with a pressure-reducing turbine for a specific case study," M-Eng dissertation, University of the Witwatersrand, Johannseburg, South Africa, 2011.

[38] C. A. Noble, D. A. John, T. M. Lawrence, R. E. Lindemann, H. M. Sheinman and F. S. Yount, *ASHRAE Handbook – HVAC systems and equipment*, Atlanta, GA: ASHRAE, p. 44.1–44.16, 2012.

[39] T. S. Lee and W. C. Lu, "An evaluation of empirically-based models for predicting energy performance of vapor-compression water chillers," *Applied Energy*, vol. 87, no. 11, pp. 3486–3493, 2010.

[40] A. Afram and F. Janabi-shari, "Review of modeling methods for HVAC systems," *Applied Thermal Engineering*, vol. 67, no. 1/2, pp. 507–519, 2014.

[41] J. A. Romero, J. Navarro-Esbrí and J. M. Belman-Flores, "A simplified black-box model-oriented to chilled water temperature control in a variable speed vapour compression system," *Applied Thermal Engineering*, vol. 31, no. 2–3, pp. 329–335, 2011.

[42] K-P. Lee and T-A. Cheng, "A simulation–optimization approach for energy efficiency of chilled water system," *Energy and Buildings*, vol. 54, pp. 290–296, 2012.

[43] J. Hu and P. Karava, "A state-space modeling approach and multi-level optimization algorithm for predictive control of multi-zone buildings with mixed-mode cooling," *Building and Environment*, vol. 80, pp. 259–273, 2014.

[44] Z. Ma and S. Wang, "An optimal control strategy for complex building central chilled water systems for practical and real-time applications," *Building and Environment*, vol. 44, no. 6, pp. 1188–1198, 2009.

[45] X. Li, Y. Li, J. E. Seem, and P. Li, "Dynamic modeling and self-optimizing operation of chilled water systems using extremum seeking control," *Energy and Buildings*, vol. 58, pp. 172–182, 2013.

[46] Z. Lei and M. Zaheeruddin, "Dynamic simulation and analysis of a water chiller refrigeration system," *Applied Thermal Engineering*, vol. 25, no. 14–15, pp. 2258–2271, 2005.

[47] N. Liang, S. Shao, C. Tian and Y. Yan, "Dynamic simulation of variable capacity refrigeration systems under abnormal conditions," *Applied Thermal Engineering*, vol. 30, no. 10, pp. 1205–1214, 2010.

[48] M. Ali, V. Vukovic, M. H. Sahir and G. Fontanella, "Energy analysis of chilled water system configurations using simulation-based optimization," *Energy and Buildings*, vol. 59, pp. 111–122, 2013.

[49] T. T. Chow, K. F. Fong, A. L. S. Chan, R. Yau, W. H. Au, and V. Cheng, "Energy modelling of district cooling system for new urban development," *Energy and Buildings*, vol. 36, no. 11, pp. 1153–1162, 2004.

[50] A. Aravelli and S. S. Rao, "Energy optimization in chiller plants: A novel formulation and solution using a hybrid optimization technique," *Engineering Optimization*, December 2014, pp. 1–17, 2012.

[51] V. Vakiloroaya, Q. P. Ha and B. Samali, "Energy-efficient HVAC systems: Simulation-empirical modelling and gradient optimization," *Automation in Construction*, vol. 31, pp. 176–182, 2013.

[52] Y. Li, J. Wu and S. Shiochi, "Modeling and energy simulation of the variable refrigerant flow air conditioning system with water-cooled condenser under cooling conditions," *Energy and Buildings*, vol. 41, no. 9, pp. 949–957, 2009.

[53] N. Nassif, "Modeling and optimization of HVAC systems using artificial neural network and genetic algorithm," *Building Simulations*, vol. 7, no. 3, pp. 237–245, 2013.

[54] Z. X. Jing, X. S. Jiang, Q. H. Wu, W. H. Tang and B. Hua, "Modelling and optimal operation of a small-scale integrated energy based district heating and cooling system," *Energy*, vol. 73, pp. 399–415, 2014.

[55] G. L. Ding, "Recent developments in simulation techniques for vapour-compression refrigeration systems," *International Journal of Refrigeration*, vol. 30, no. 7, pp. 1119–1133, 2007.

[56] R. N. N. Koury, L. Machado and K. A. R. Ismail, "Numerical simulation of a variable speed refrigeration system," *International Journal of Refrigeration*, vol. 24, pp. 192–200, 2001.

[57] T. T. Chow, G. Q. Zhang, Z. Lin and C. L. Song, "Global optimization of absorption chiller system by genetic algorithm and neural network," *Energy and Buildings*, vol. 34, pp. 103–109, 2002.

[58] K. F. Fong, V. I. Hanby and T. T. Chow, "HVAC system optimization for energy management by evolutionary programming," *Energy and Buildings*, vol. 38, no. 3, pp. 220–231, 2006.

[59] F. W. Yu and K. T. Chan, "Modelling of the coefficient of performance of an air-cooled screw chiller with variable speed condenser fans," *Building and Environment*, vol. 41, no. 4, pp. 407–417, 2006.

[60] V. Vakiloroaya, M. Khatibi, Q. P. Ha, and B. Samali, "New Integrated Hybrid Evaporative Cooling System for HVAC Energy Efficiency Improvement," *International Symposiom on System Integration*, pp. 772–778, 2011.

[61] D. Monfet and R. Zmeureanu, "Ongoing commissioning of water-cooled electric chillers using benchmarking models," *Applied Energy*, vol. 92, pp. 99–108, 2012.

[62] Y. Yao, Z. Lian, Z. Hou and X. Zhou, "Optimal operation of a large cooling system based on an empirical model," *Applied Thermal Engineering*, vol. 24, no. 16, pp. 2303–2321, 2004.

[63] W. Bornman, J. Dirker, D. C. Arndt and J. P. Meyer, "Operational energy minimisation for forced draft, direct-contact bulk air cooling tower through a combination of forward and first-principle modelling, coupled with an optimisation platform," *Energy*, vol. 114, pp. 995–1006, 2016.

[64] R. Al Waked and M. Behnia, "CFD simulation of wet cooling towers," *Applied Thermal Engineering*, vol. 26, pp. 382–395, 2006.

[65] G. Y. Jin, W. J. Cai, L. Lu, E. L. Lee and A. Chiang, "A simplified modeling of mechanical cooling tower for control and optimization of HVAC systems," *Energy Conversion and Management*, vol. 48, no. 2, pp. 355–365, 2007.

[66] S. K. Wang, "*Handbook of air conditioning and refrigeration*," 2nd ed., New York, NY: McGraw-Hill, pp. 10.1-10.58, 2000.

[67] E. Hajidavalloo, R. Shakeri and M. A. Mehrabian, "Thermal performance of cross flow cooling towers in variable wet bulb temperature," *Energy Conversion and Management*, vol. 51, no. 6, pp. 1298–1303, 2010.

[68] M. Lemouari and M. Boumaza, "Experimental investigation of the performance characteristics of a counter flow wet cooling tower," *International Journal of Thermal Sciences*, vol. 49, no. 10, pp. 2049–2056, 2010.

[69] J. A. Queiroz, V. M. S. Rodrigues, H. A. Matos and F. G. Martins, "Modeling of existing cooling towers in ASPEN PLUS using an equilibrium stage method," *Energy Conversion and Management*, vol. 64, pp. 473–481, 2012.

[70] M. Serna-González, J. M. Ponce-Ortega and A. Jiménez-Gutiérrez, "MINLP optimization of mechanical draft counter flow wet-cooling towers," *Chemical Engineering Research and Design*, vol. 88, pp. 614–625, 2010.

[71] R. V Rao and V. K. Patel, "Optimization of mechanical draft counter flow wet-cooling tower using artificial bee colony algorithm," *Energy Conversion and Management*, vol. 52, no. 7, pp. 2611–2622, 2011.

[72] M. Lemouari, M. Boumaza, and I. M. Mujtaba, "Thermal performances investigation of a wet cooling tower," *Applied Thermal Engineering*, vol. 27, pp. 902–909, 2007.

[73] E. Rubio-Castro and M. Serna-González, "Heat and Mass Transfer – modeling and simulation," Rijeka: InTech, pp. 117–142, 2011.

[74] B. A. Qureshi and S. M. Zubair, "A complete model of wet cooling towers with fouling in fills," *Applied Thermal Engineering*, vol. 26, pp. 1982–1989, 2006.

[75] T. Pan, S. Shieh, S. Jang, W. Tseng, C. Wu and J. Ou, "Statistical multi-model approach for performance assessment of cooling tower," *Energy Conversion and Management*, vol. 52, no. 2, pp. 1377–1385, 2011.

[76] J-G. Wang, S-S. Shieh, S-S. Jang, D. S-H. Wong, and C-W. Wu, "Data-driven modeling approach for performance analysis and optimal operation of a cooling tower," *Journal of the Taiwan Institue of Chemical Engineers*, vol. 45, pp. 180–185, 2014.

[77] G. Heidarinejad, M. Karami and S. Delfani, "Numerical simulation of counter-flow wet-cooling towers," *International Journal of Refrigeration*, vol. 32, no. 5, pp. 996–1002, 2009.

[78] J. Wang, S. Shieh, S. Jang and C. Wu, "Discrete model-based operation of cooling tower based on statistical analysis," *Energy Conversion and Management*, vol. 73, pp. 226–233, 2013.

[79] M. A. Al-Nimr, "Dynamic thermal behaviour of cooling towers," *Energy Conversion and Management*, vol. 39, no. 7, pp. 631–636, 1998.

[80] X. Wen, C. Liang and X. Zhang, "Experimental study on heat transfer coefficient between air and liquid in the cross-flow heat-source tower," *Building and Environment*, vol. 57, pp. 205–213, 2012.

[81] J. Khan, B. A. Qureshi and S. M. Zubair, "A comprehensive design and performance evaluation study of counter flow wet cooling towers," *International Journal of Refrigeration*, vol. 27, pp. 914–923, 2004.

[82] G. F. Cortinovis, J. L. Paiva, T. W. Song, and J. M. Pinto, "A systemic approach for optimal cooling tower operation," *Energy Conversion and Management*, vol. 50, no. 9, pp. 2200–2209, 2009.

[83] G. Ge, F. Xiao, S. Wang and L. Pu, "Effects of discharge recirculation in cooling towers on energy ef fi ciency and visible plume potential of chilling plants," *Applied Thermal Engineering*, vol. 39, pp. 37–44, 2012.

[84] H. Sayyaadi and M. Nejatolahi, "Multi-objective optimization of a cooling tower assisted vapor compression refrigeration system," *International Journal of Refrigeration*, vol. 34, no. 1, pp. 243–256, 2010.

[85] R. Chargui, H. Sammouda and A. Farhat, "Numerical simulation of a cooling tower coupled with heat pump system associated with single house using TRNSYS," *Energy Conversion and Management*, vol. 75, pp. 105–117, 2013.

[86] M. N. A. Hawlader and B. M. Liu, "Numerical study of the thermal-hydraulic performance of evaporative natural draft cooling towers," *Applied Thermal Engineering*, vol. 22, pp. 41–59, 2002.

[87] M. S. Söylemez, "On the optimum performance of forced draft counter flow cooling towers," *Energy Conversion and Management*, vol. 45, no. 15–16, pp. 2335–2341, 2004.

[88] E. Rubio-Castro, M. Serna-González, J. M. Ponce-Ortega and M. A. Morales-Cabrera, "Optimization of mechanical draft counter flow wet-cooling towers using a rigorous model," *Applied Thermal Engineering*, vol. 31, no. 16, pp. 3615–3628, 2011.

[89] A. Klimanek and R. A. Bia, "Solution of heat and mass transfer in counter flow wet-cooling tower fills," *International Communications in Heat and Mass Transfer*, vol. 36, pp. 547–553, 2009.

[90] J. C. Kloppers and D. G. Kröger, "A critical investigation into the heat and mass transfer analysis of counterflow wet-cooling towers," *International Journal of Heat and Mass Transfer*, vol. 48, pp. 765–777, 2005.

[91] J. C. Kloppers and D. G. Kröger, "Loss coefficient correlation for wet-cooling tower fills," *Applied Thermal Engineering*, vol. 23, pp. 2201–2211, 2003.

[92] Q. Zhang, J. Wu, G. Zhang, J. Zhou and Y. Guo, "Calculations on performance characteristics of counterflow reversibly used cooling towers," *International Journal of Refrigeration*, vol. 35, no. 2, pp. 424–433, 2011.

[93] Z. Huang, Y. Pan and G. Wu, "Emulation based optimal control of chiller plants," in *International Mechanical Engineering Congress amd Exposition*, 2010.

[94] D. J. Brake, "Design of the world's largest bulk air cooler for the Enterprise mine in northern Australia," *North American Mine Ventilation Symposium*, 2002.

[95] Z. K. Xue and S. Y. Li, "Multi-model modelling and predictive control based on local model networks," *Control and Inteligence Systems*, vol. 34, no. 2, pp. 105–112, 2006.

[96] X. Wei, G. Xu and A. Kusiak, "Modeling and optimization of a chiller plant," *Energy*, vol. 73, pp. 898–907, 2014.

[97] S. P. Fisenko, A. I. Petruchik and A. D. Solodukhin, "Evaporative cooling of water in a mechanical draft cooling tower," *International Journal of Heat and Mass Transfer*, vol.

47, no. 1, pp. 165–177, 2004.

[98] D. Arndt, "Integrated dynamic simulation of large thermal systems," PhD thesis, University of Pretoria, Pretoria, South Africa., 2000.

[99] F. W. Yu and K. T. Chan, "Modelling of a condenser-fan control for an air-cooled centrifugal chiller," *Applied Energy*, vol. 84, no. 11, pp. 1117–1135, 2007.

[100] F. W. Yu and K. T. Chan, "Optimizing condenser fan control for air-cooled centrifugal chillers," *International Journal of Thermal Sciences*, vol. 47, no. 7, pp. 942–953, 2008.

[101] F. W. Yu and K. T. Chan, "Part load performance of air-cooled centrifugal chillers with variable speed condenser fan control," *Building and Environment*, vol. 42, no. 11, pp. 3816–3829, 2007.

[102] W. F. Stoecker and J. W. Jones, *Refrigeration and air conditioning*, 2nd ed., New York, NY: McGraw-Hill, pp. 205–295, 1982.

[103] F. W. Yu and K. T. Chan, "Improved energy performance of air cooled centrifugal chillers with variable chilled water flow," *Energy Conversion and Management*, vol. 49, no. 6, pp. 1595–1611, 2008.

[104] P. Bahnfleth and B. Peyer, "Varying Views om Variable-Primary Flow," *Chilled Water Engineering*, March, pp. 5–9, 2004.

[105] Y. Kwak, D. Kong, S. Cheon, R. Kwak and J. Huh, "Condensing temperature control through energy management system simulation for a large office building," *Conference of the International Building Performance Simulation Association*, pp. 2619–2626, 2011.

[106] B. Mu, Y. Li, J. E. Seem, and B. Hu, "A multi-variable Newton-based Extremum Seeking Control for Condenser Water Loop Optimization of Chilled Water Plant," *Journal of Dynamic Systems, Measurement and Control*, vol. 137, pp. 1–10, 2015.

[107] F. W. Yu and K. T. Chan, "Tune up of the set point of condensing temperature for more energy efficient air cooled chillers," *Energy Conversion and Management*, vol. 47, no. 15–16, pp. 2499–2514, 2006.

[108] M. Schwedler, "Condenser water system savings," 2008. [Online]. Available: www.trane.com. [Accessed: 09 August 2016].

[109] T. R. Doll, "Energy Saving Potential Of Solid-State AC drives In VAV systems," 1983. [Online]. Available: https://www.rockwellautomation.com. [Accessed: 12 September 2016].

[110] X. Yang, *Introduction to mathematical optimization*, 1st ed., Cambridge, Cambridge International Science Publishing, pp. 104–106, 2008.

[111] S. S. Rao, *Engineering Optimization*, 4th ed., New Jersey, NJ: Wiley, pp. 1–480, 2009.

[112] U. Dikwekar, *Introduction to applied optimization*, 2nd ed., Illinois: Springer, pp. 41–72, 2002.

[113] J. A. Snyman, *Practical mathematical optimisation*, Pretoria: University of Pretoria, pp. 1–93, 2004.

[114] A. Neumaier, O. Shcherbina, W. Huyer, and T. Vinkó, "A comparison of complete global optimization solvers," *Mathematical Programming Series B*, vol. 356, pp. 335–356, 2005.

[115] D. Henrion, "A review of the Global Optimization Toolbox for Maple," *IEEE Control Systems Magazine*, Apr, pp. 106–110, 2006.

[116] J. D. Pintér, "Continuous Global Optimization: An Introduction to Models, Solution Approaches, Tests and Applications," 1999. [Online]. Available: www.informs.org/Pubs/ITORMS/Archive/Volume-2/Volume-2-No.-2-Pinter. [Accessed: 25 September 2016].

[117] J. D. Pintér, "Continuous global optimization software: A brief review," *Optima*, vol. 52, Halifax, December, 1996.

[118] J. D. Pintér, D. Linder and P. Chin, "Global optimization toolbox for maple : An introduction with illustrative applications," *Optimization. Methods Software*, vol. 21, no. 4, pp. 565–582, 2006.

[119] Maplesoft, "Global and non-smooth optimization," 2006. [Online]. Available: www.maplesoft.com. [Accessed: 26 September 2016].

[120] T. Coleman, M. A. Branch and A. Grace, *Optimization toolbox for use with MATLAB*. Natick: The MathWorks, 1999.

[121] "Commercial optimization platforms." [Online]. Available:

https://en.wikipedia.org/wiki/List_of_optimization_software. [Accessed: 22 September 2016].

[122] "V12 Plug-in Solver Engines User Guide." [Online]. Available: www.solver.com. [Accessed: 16 July 2014].

[123] C. Callaway, J. D. Aswegan, J. A. Connell, P. Simmonds, J. J. Traylor and D. P. Yuill, "*ASHRAE Handbook Fundamentals*," Atlanta, GA: ASHRAE, p. 14.1–22.21, 2013.

[124] WIKA, "WIKA cable thermocouple Model TC40 datasheet." [Online]. Available: http://www.wika.co.za/upload/DS_TE6540_en_co_2045.pdf. [Accessed: 17 July 2014].

[125] Khrohne, "Krohne UFM 3030 techinical datasheet." [Online]. Available: http://cdn.krohne.com/dlc/TD_UFM3030_en_060424.pdf. [Accessed: 7 September 2014].

[126] Testo, "Testo 6682 instruction manual." [Online]. Available: https://www.testo.org/resources/media/global_media/produkte/testo_6682/Testo_6682_Ex_-_Manual.pdf. [Accessed: 9 July 2014].

[127] C. Lombard, "Two-Port Simulation of HVAC Systems and Object Approach," PhD thesis, University of Pretoria, Pretoria, South Africa, 1996.

[128] R. C. Dorf and R. H. Bishop, *Modern control systems*, 11th ed., New Jersey, NJ: Pearson Education, pp. 781–791, 2008.

Appendix A

This appendix summarises the empirical chiller COP models suggested by Lee and Lu [39] as referred to in Section 3.5.

Simple linear regression model

$$COP = \sigma_1 \dot{Q}_{w,evap} + \sigma_2 T_{w,i,evap} + \sigma_3 T_{w,i,cond} \tag{37}$$

Bi-quadratic regression model

$$\begin{aligned} \frac{1}{COP} = {} & \sigma_0 + \sigma_1 \frac{1}{\dot{Q}_{w,evap}} + \sigma_2 \dot{Q}_{w,evap} + \sigma_3 \frac{T_{w,i,cond}}{\dot{Q}_{w,evap}} + \sigma_4 \frac{{T_{w,i,cond}}^2}{\dot{Q}_{w,evap}} \\ & + \sigma_5 T_{w,i,cond} + \sigma_6 \dot{Q}_{w,evap} T_{w,i,cond} + \sigma_7 {T_{w,i,cond}}^2 \\ & + \sigma_8 \dot{Q}_{w,evap} {T_{w,i,cond}}^2 \end{aligned} \tag{38}$$

Multivariate polynomial regression model

$$\begin{aligned} COP = {} & \sigma_0 + \sigma_1 \dot{Q}_{w,evap} + \sigma_2 T_{w,i,evap} + \sigma_3 T_{w,i,cond} + \sigma_4 {\dot{Q}_{w,evap}}^2 + \sigma_5 {T_{w,i,evap}}^2 \\ & + \sigma_6 {T_{w,i,cond}}^2 + \sigma_7 T_{w,i,evap} \dot{Q}_{w,evap} + \sigma_8 T_{w,i,cond} \dot{Q}_{w,evap} \\ & + \sigma_9 T_{w,i,cond} T_{w,i,evap} \end{aligned} \tag{39}$$

Gordon-Ng universal model

$$\begin{aligned} & \frac{T_{w,i,evap}}{T_{w,i,cond}} \left(1 + \frac{1}{COP}\right) - 1 \\ & = \sigma_1 \frac{T_{w,i,evap}}{\dot{Q}_{w,evap}} + \sigma_2 \frac{T_{w,i,cond} - T_{w,i,evap}}{T_{w,i,cond} \dot{Q}_{w,evap}} + \sigma_3 \frac{\dot{Q}_{w,evap}}{T_{w,i,cond}} \left(1 + \frac{1}{COP}\right) \end{aligned} \tag{40}$$

Gordon-Ng simplified model

$$\frac{1}{COP} = -1 + \frac{T_{w,i,cond}}{T_{w,o,evap}} + \frac{1}{\dot{Q}_{w,evap}}\left[-\sigma_1 + \sigma_2 T_{w,i,cond} - \sigma_3 \frac{T_{w,i,cond}}{T_{w,o,evap}}\right] \quad \textbf{(41)}$$

Lee's simplified model

$$\frac{1}{COP} = -1 + \frac{T_{w,i,cond}}{T_{w,i,evap}} + \frac{1}{\dot{Q}_{w,evap}}\left[-\sigma_1 + \sigma_2 T_{w,i,cond} - \sigma_3 \frac{T_{w,i,cond}}{T_{w,i,evap}}\right] \quad \textbf{(42)}$$

Appendix B

Various additional fluid flow, temperature and power results were obtained for the various major energy-consuming devices as part of the mine cooling system optimisation. These are included here as additional information and were not included in the main text to avoid cluttering the results section. These were not found to be fundamental to the discussion on the results, but could be useful for consideration should the effect of these parameters be of interest to any reader or future research in this regard.

Figure 87 shows the hourly values of the PCT water flow rate of the baseline and optimised cases, while Figure 88 displays the daily average values. From these figures, it is evident that the water flow through the PCT remained unchanged during the optimisation.

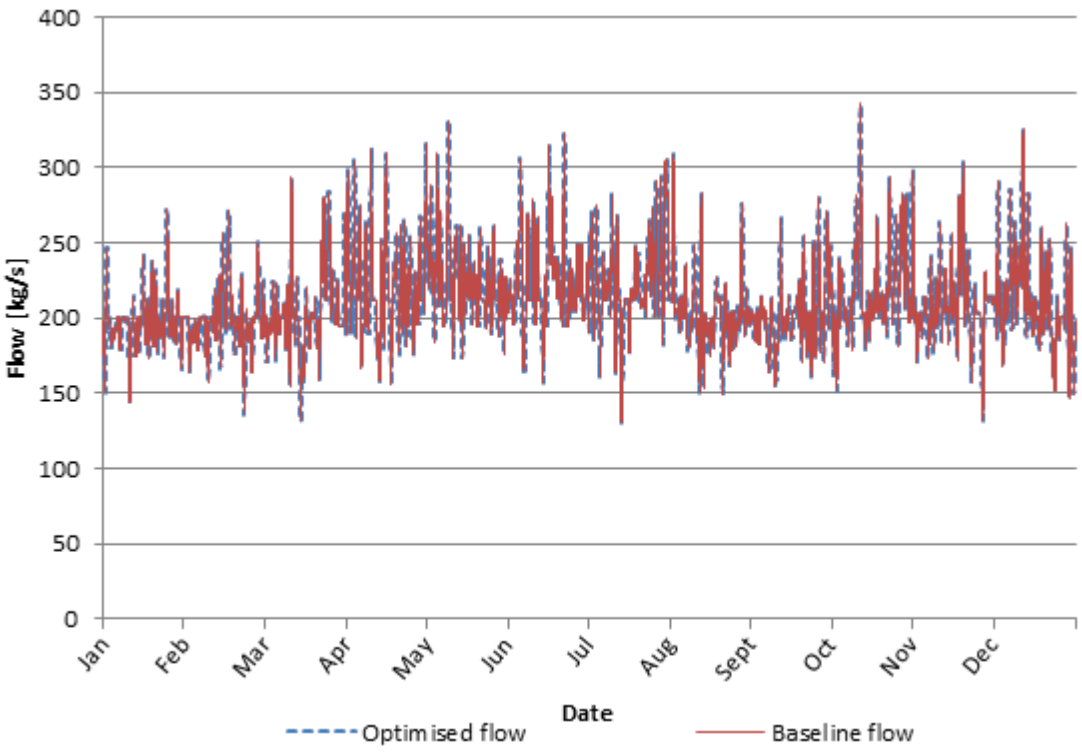

Figure 87: The PCT's baseline and optimised water flow

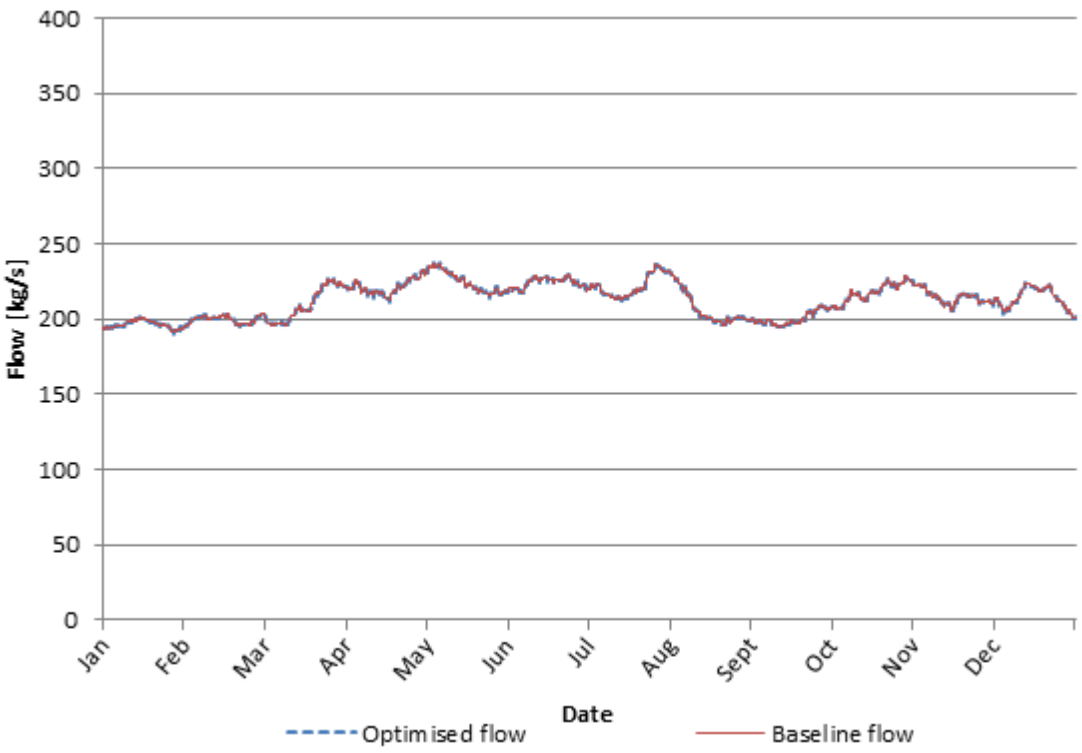

Figure 88: The daily average PCT's baseline and optimised water flow

Figure 89 and Figure 90 display the baseline and optimised water flow rates of the BAC both in hourly and daily average formats. It can be seen that the water flow correlates directly with the BAC's pump power of figures Figure 59 and Figure 60.

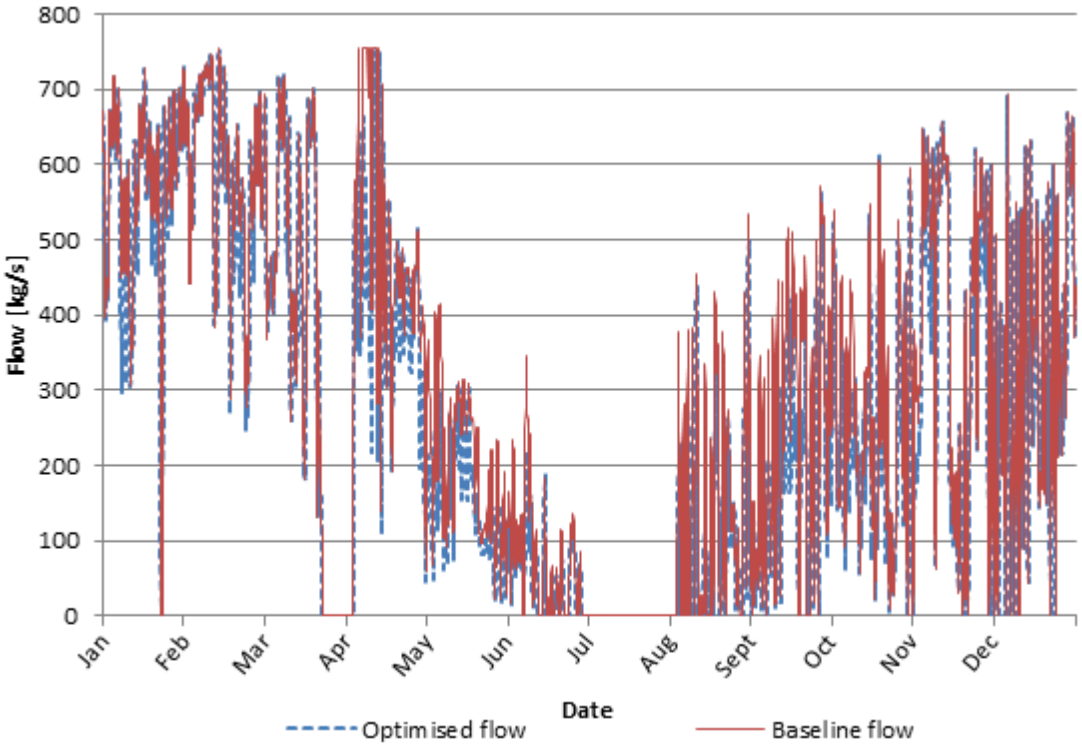

Figure 89: The BAC's baseline and optimised water flow

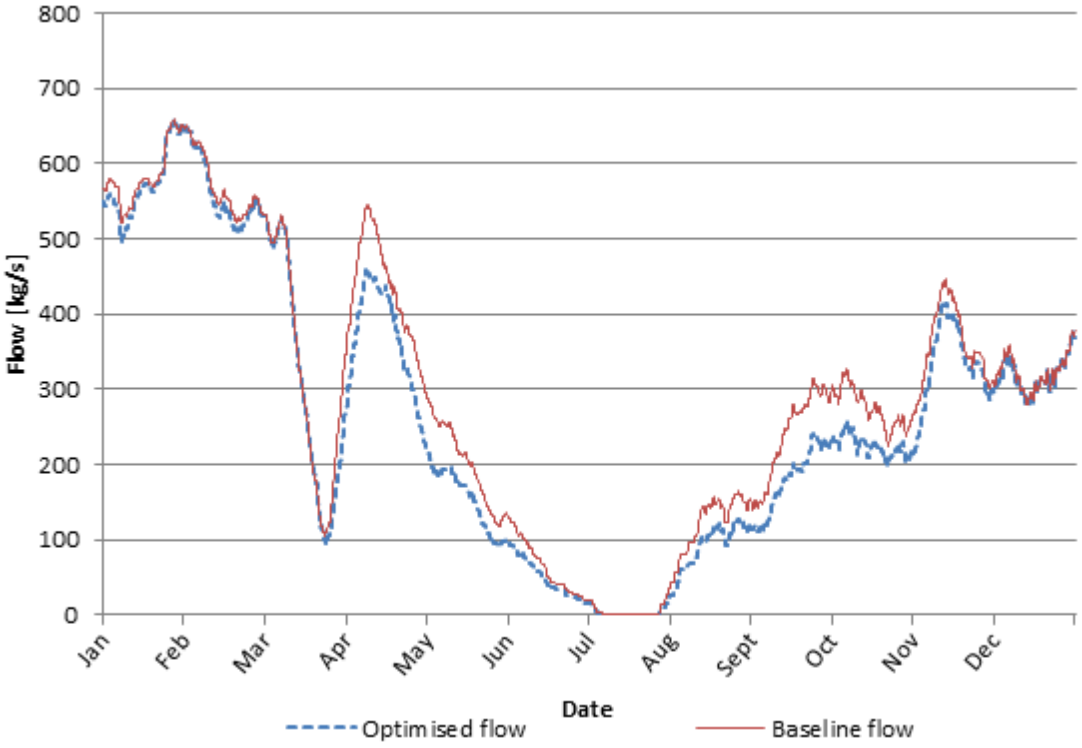

Figure 90: The daily average BAC's baseline and optimised water flow

The hourly evaporator water flow rate for the baseline and optimised scenarios are presented in Figure 91, while the daily average values are shown in Figure 92. It is evident that these follow the trend of the evaporator's pump power shown in Figure 65 and Figure 66.

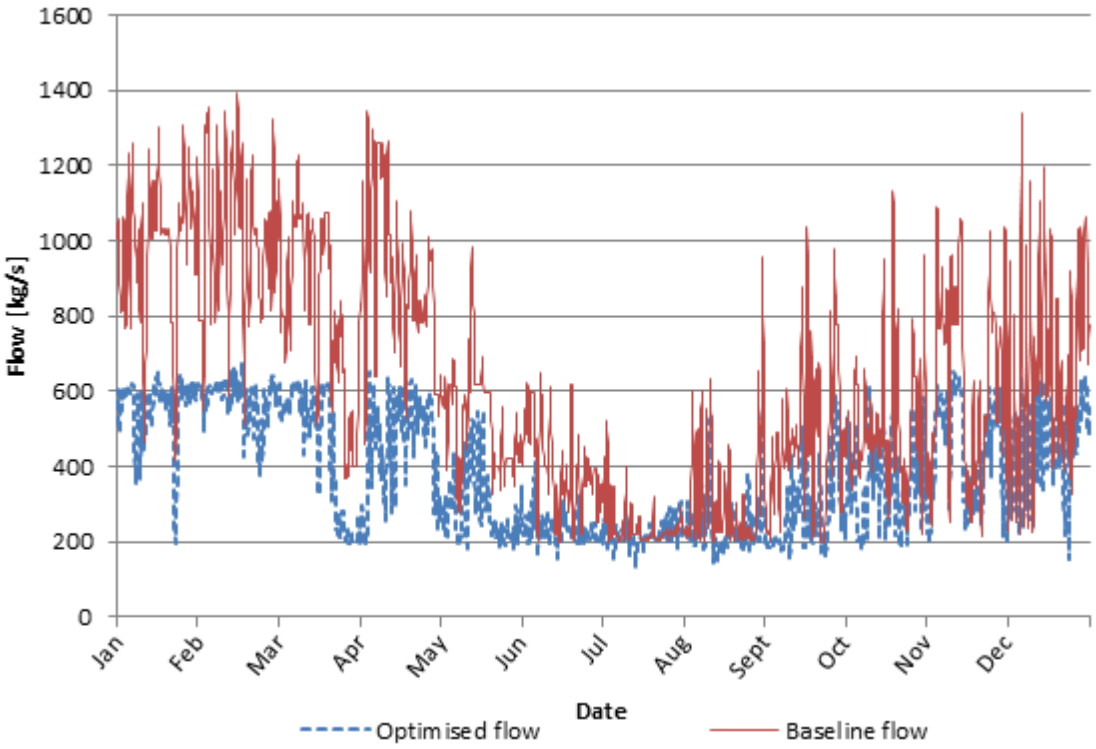

Figure 91: The evaporator's baseline and optimised water flow

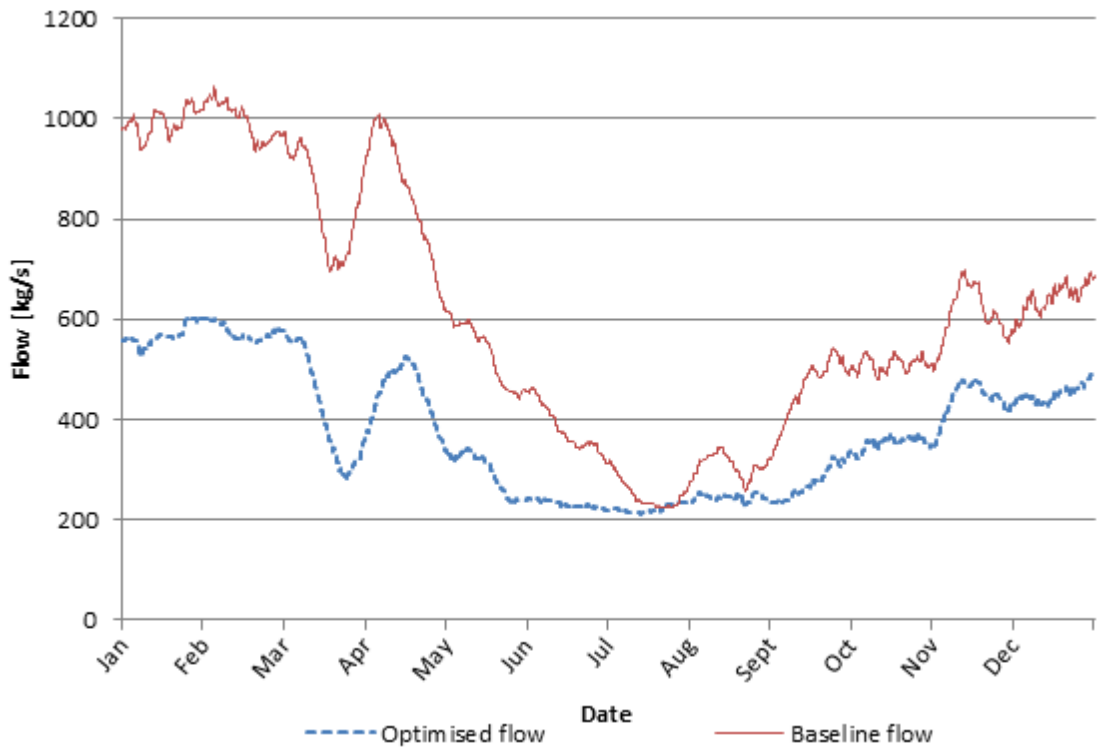

Figure 92: The daily average evaporator's baseline and optimised flow

Figure 93 and Figure 94 display the hourly and daily average values of the condenser water flow rate for both the baseline and optimised cases. Similar to the evaporator, it can be seen that these follow the trend of the condenser's pump power shown in Figure 71 and Figure 72.

The condenser's water inlet and outlet temperature for the baseline, as well as the optimised scenarios, are grouped together in Figure 95 to Figure 98, in hourly and daily average formats, to provide easy comparison of these temperature differences achieved individually for both the baseline and optimised cases.

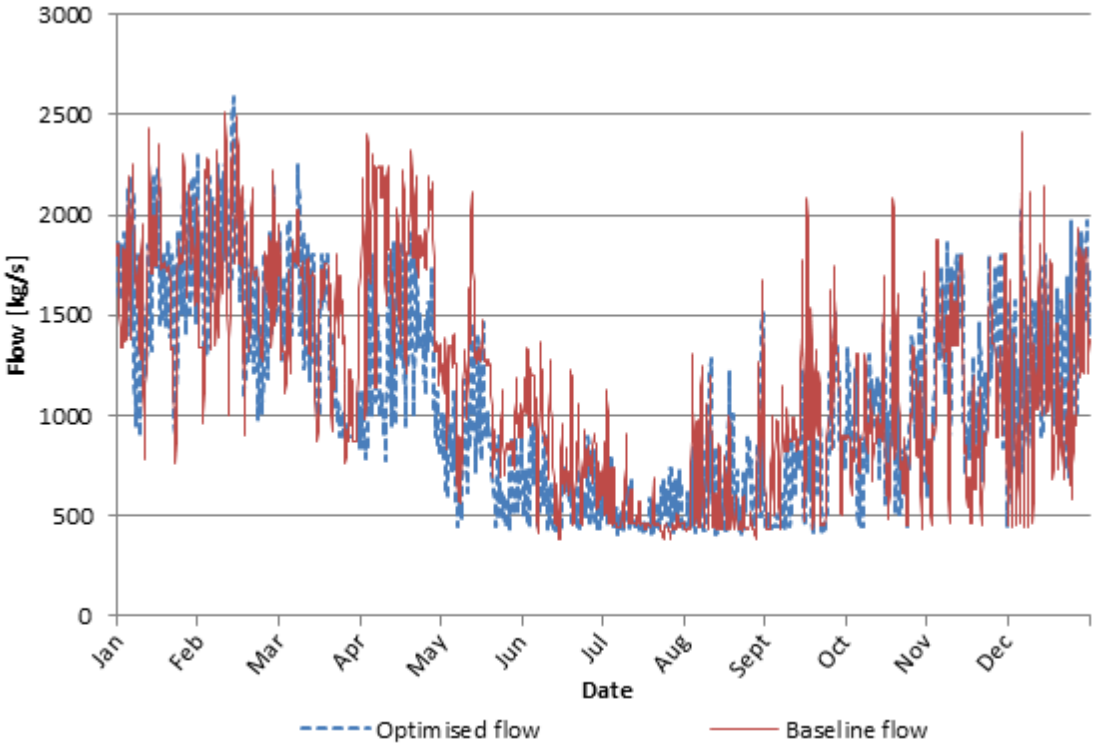

Figure 93: The condenser's baseline and optimised water flow

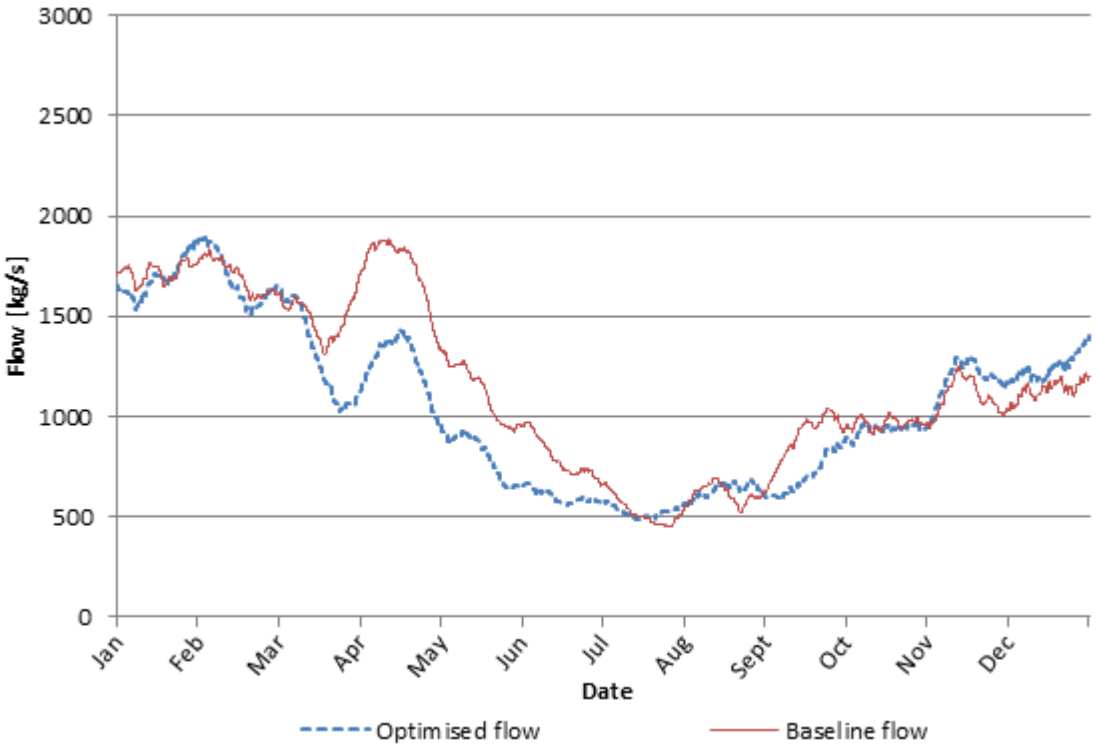

Figure 94: The daily average condenser's baseline and optimised water flow

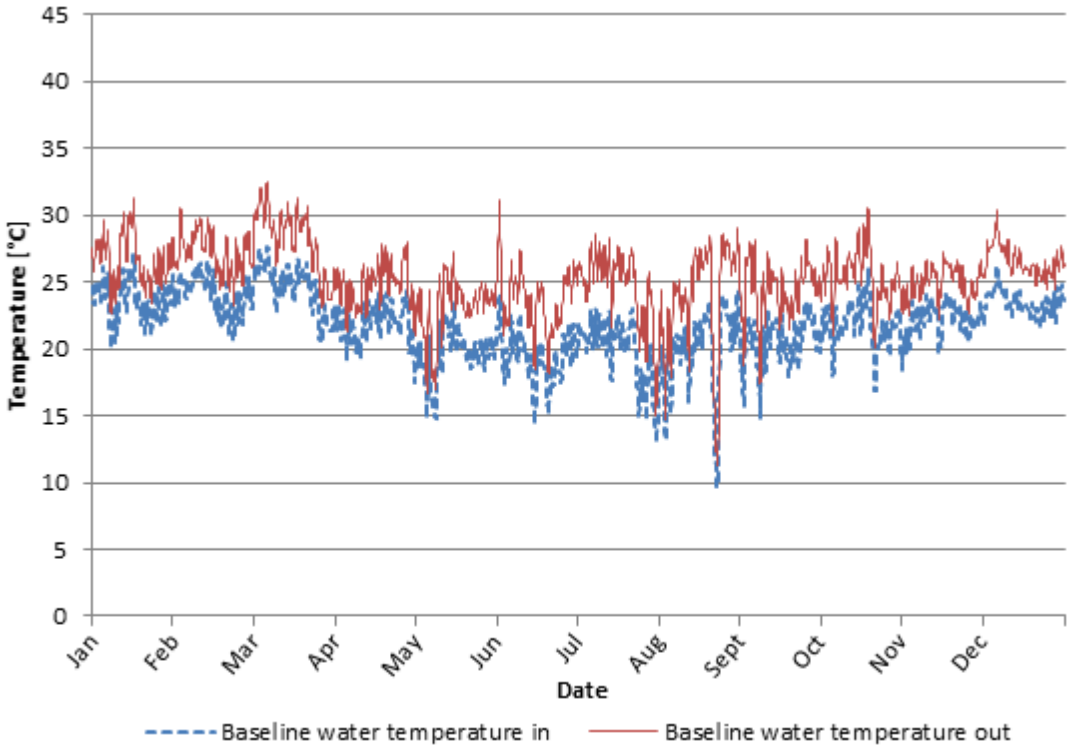

Figure 95: The condenser's baseline inlet and outlet water temperatures

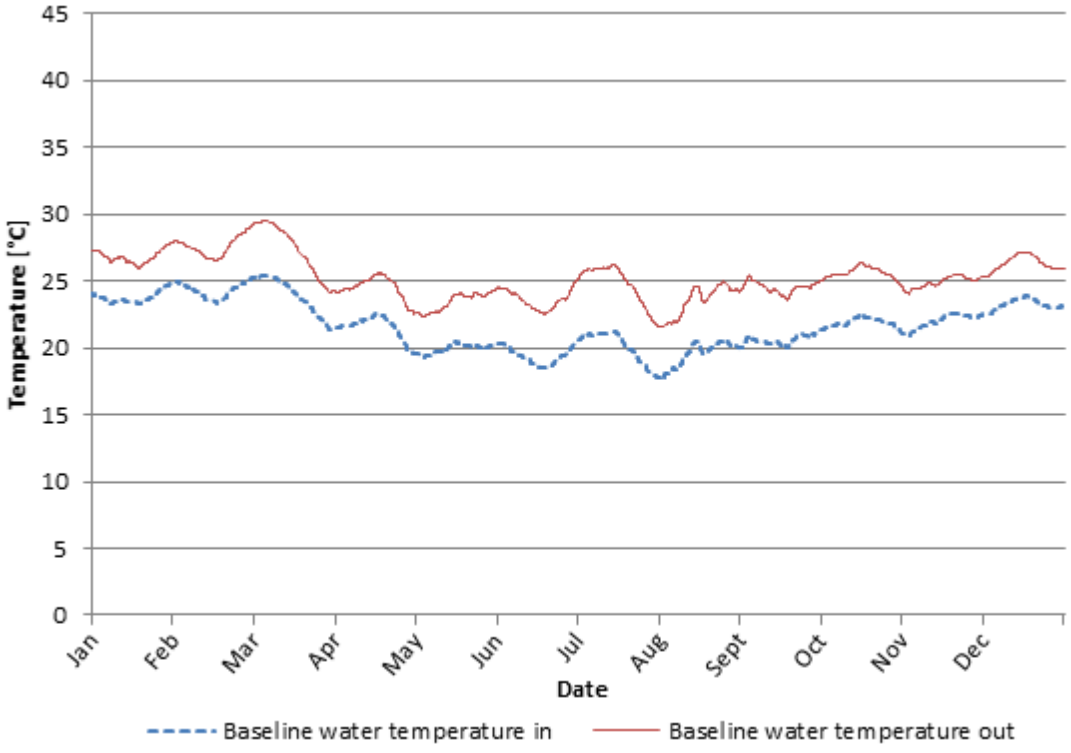

Figure 96: The daily average condenser's baseline inlet and outlet water temperatures

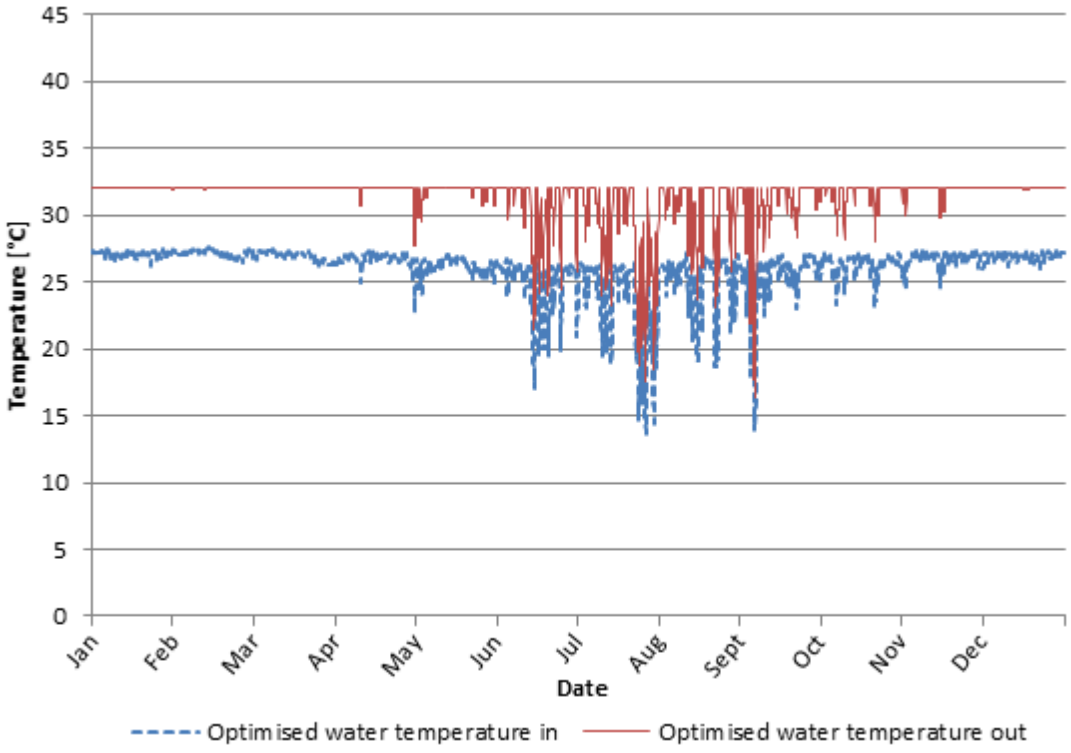

Figure 97: The optimised condenser's inlet and outlet water temperatures

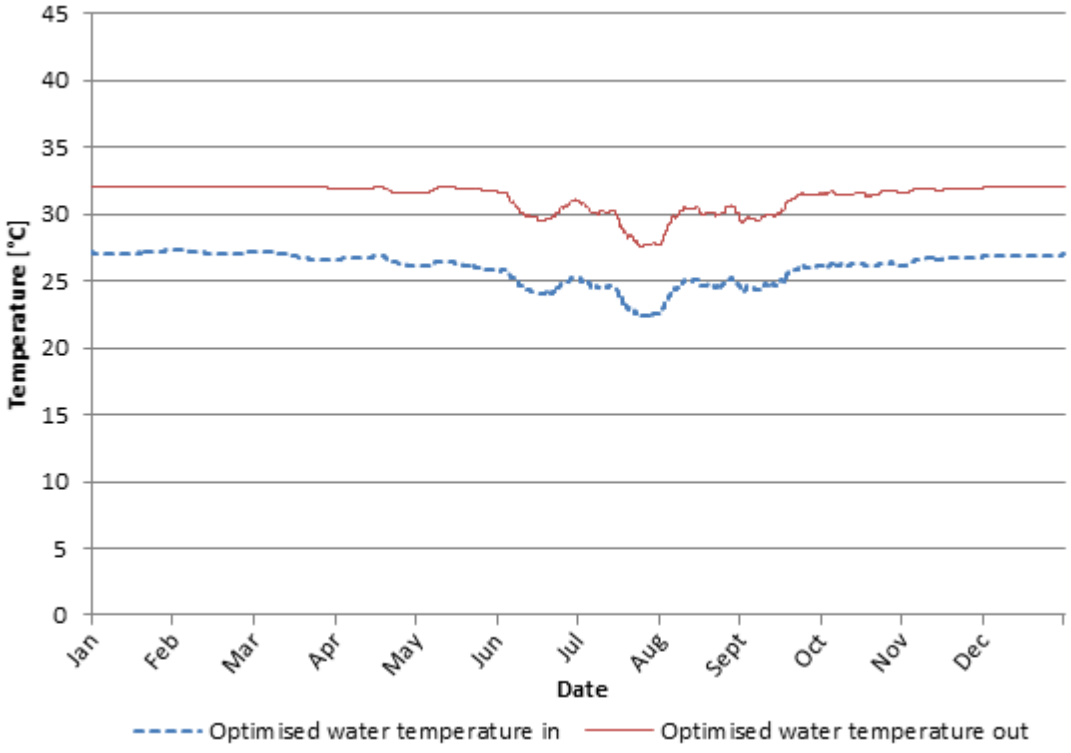

Figure 98: The daily average condenser's optimised inlet and outlet water temperatures

The baseline and optimised combined total pump power are shown in Figure 99 and Figure 100 in hourly and daily average formats.

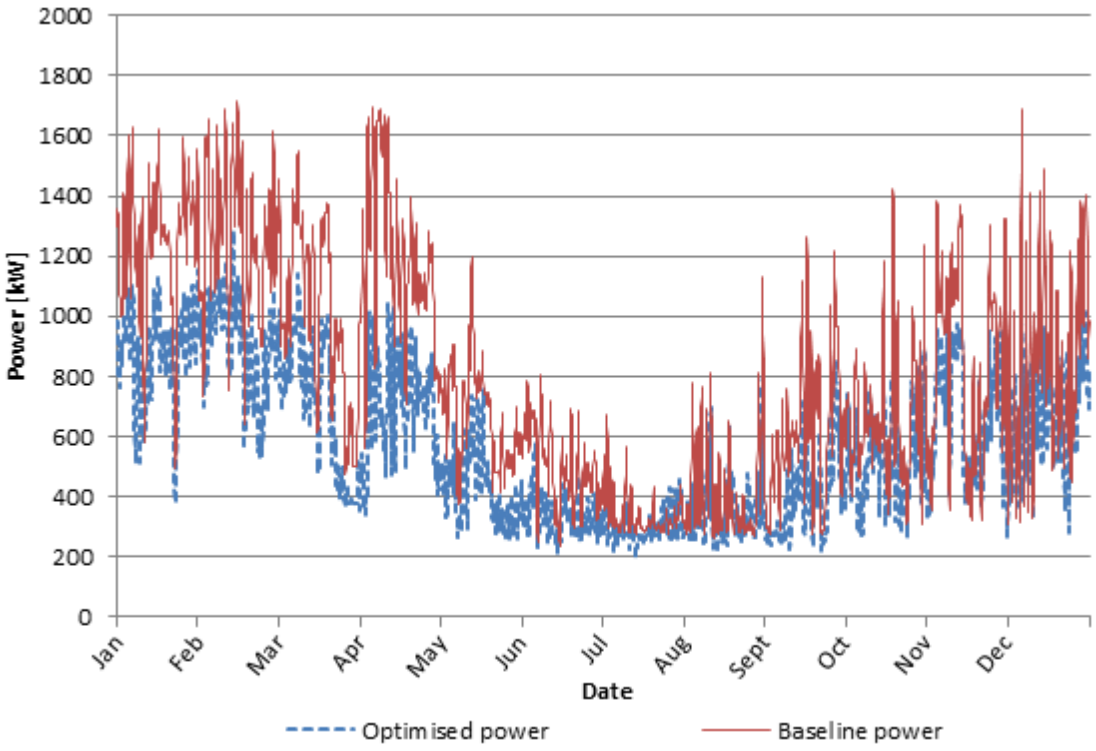

Figure 99: The baseline and optimised total pump power

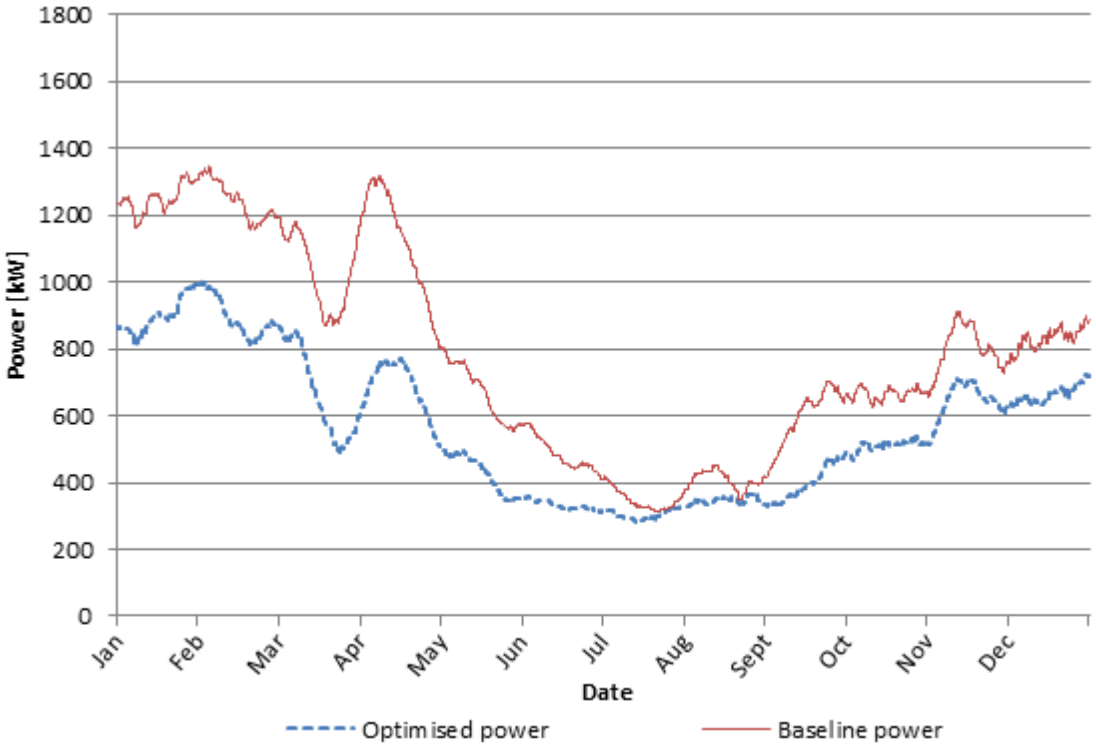

Figure 100: The daily average baseline and optimised total pump power

The hourly and daily average baseline and optimised total fan power is shown in Figure 101 and Figure 102.

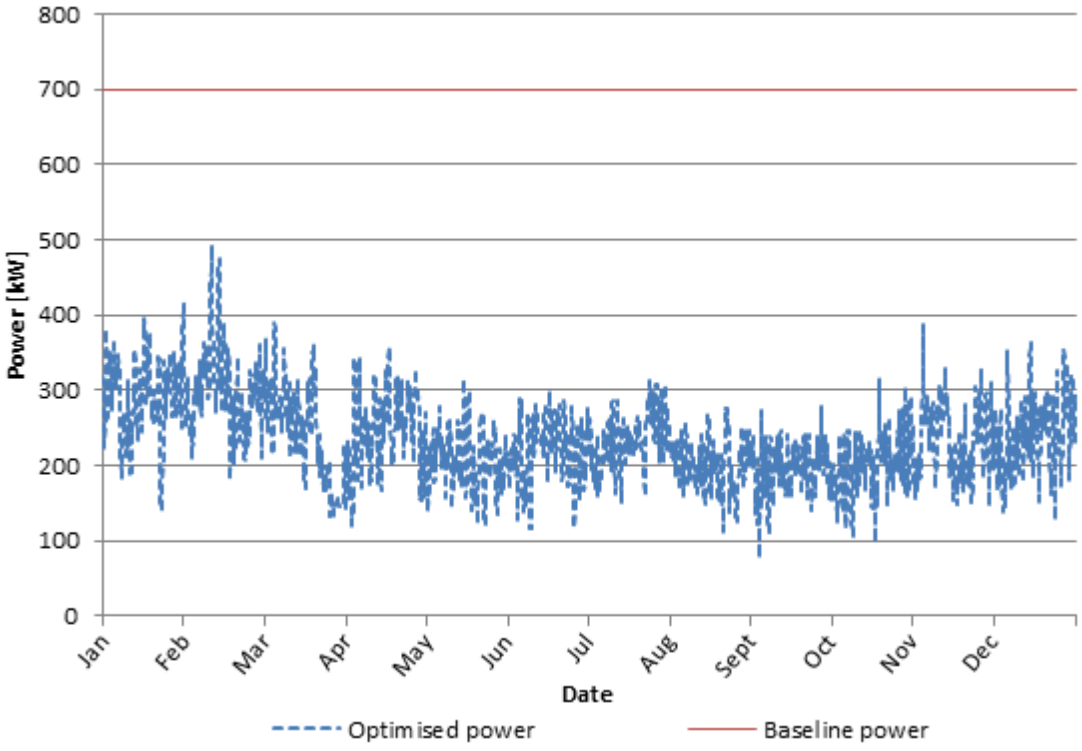

Figure 101: The baseline and optimised total fan power

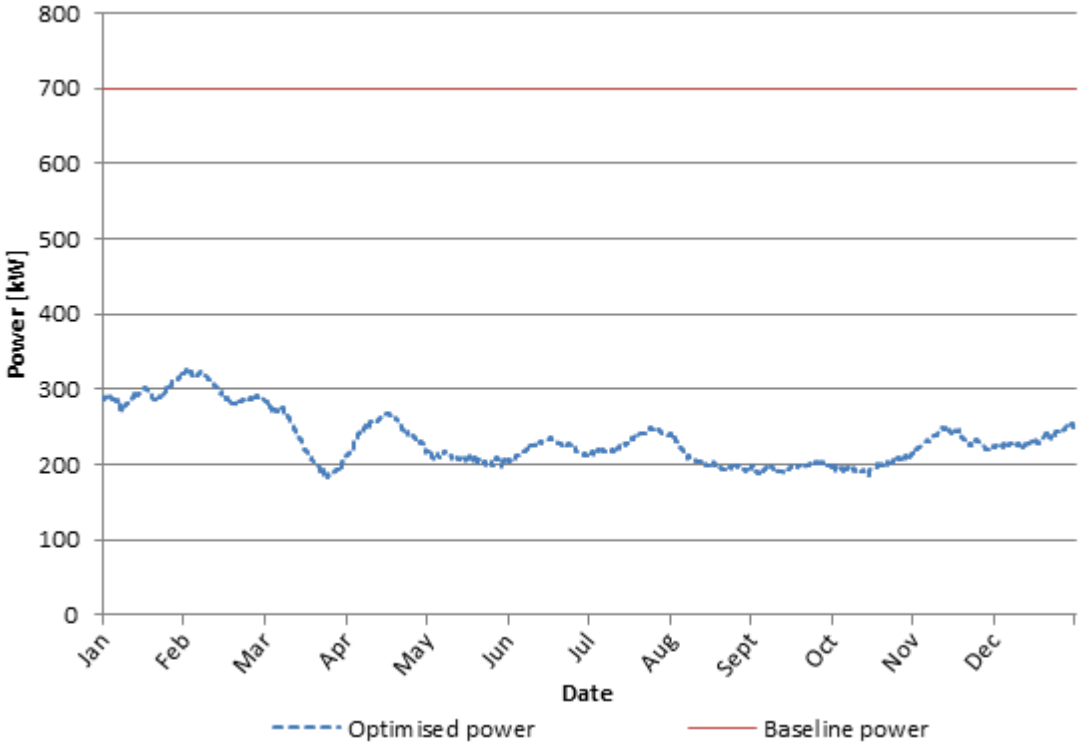

Figure 102: The daily average baseline and optimised total fan power

Appendix C

Table 15 contains a summary of the measuring ranges of the variables of Dataset A to Dataset G.

Table 15: Dataset A to G measured variable ranges

Variable	Unit	Dataset A	Dataset B	Dataset C	Dataset D	Dataset E	Dataset F	Dataset G
$T_{w,i,PCT}$	°C	27.3 – 29.4	26.1 – 29.8	27.6 – 29.2	27.6 – 29.3	26.4 – 29.7	27.9 – 29.1	19.1 – 30.3
$\dot{m}_{w,PCT}$	kg/s	17.8 – 374.3	193.5 – 401.7	17.9 – 398.6	17.9 – 295.6	194.6 – 241.8	176.2 – 243.1	12.5-415.9
$T_{w,o,PCT,}$	°C	15.2 – 20.4	14.4 – 21.5	12.1 – 18.9	16.3 – 20.3	14.6 – 21.3	12.3 – 18.8	9.6 – 22.8
$\dot{m}_{w,BAC}$	kg/s	0 - 675	208 – 675	0 - 576	293.8 – 654.6	264.3 - 675	0 – 514.9	0 - 756
$T_{w,i,BAC}$	°C	2.7 – 10.3	2.8 – 6.1	2.6 – 5.8	3.3 – 9.1	3.1 – 5.8	2.9 – 5.6	2.2 – 13.5
$T_{w,o,BAC}$	°C	4.9 – 17.9	7.9 – 13.2	5.1 – 11.5	10.9 – 17.6	8.4 – 13.1	5.6 – 11.4	1.6 – 21.4
$h_{a,o,BAC}$	kJ/kg	30.3 – 57.5	25.4 – 45.1	17.7 – 36.9	32.4 – 47.5	26.2 – 42.5	19.8 – 36.2	7.4 – 62.5
$\dot{m}_{w,cond}$	kg/s	852.5 – 2314.1	857.8 – 2190.8	425.8 – 2120.9	872.1 – 2233.2	862.6 – 218.2	429.5 – 2100.3	373.1 – 2714.2
$T_{w,i,cond}$	°C	25.1 – 32.7	18.5 – 27.1	16.7 – 23.3	26.5 – 30.4	18.8 – 26.9	16.9 – 22.9	8.4 – 33.1
$T_{w,o,cond}$	°C	28.8 – 35.7	21.1 – 30.7	20.1 – 26.6	30.8 – 35.4	21.7 – 30.6	20.6 – 26.3	10.4 – 36.4
$\dot{m}_{w,mine}$	kg/s	17.8 – 374.3	193.5 – 401.7	17.9 – 398.6	17.9 – 295.6	194.6 – 241.8	176.2 – 243.1	12.5 – 415.9
$\dot{W}_{ref}$	kW	2435.9 – 6298.2	2326.3 – 6307.1	1065.7 – 5132.1	2474.5 – 6190.9	2389.5 – 6200.3	1108.9 – 4976.7	1092.5 – 10877.1
$\dot{m}_{w,evap}$	kg/s	511 – 1345.8	521.6 – 1319.3	200.5 – 1065.1	514.5 – 1317.4	523.9 – 1315.7	201.7 – 1034.8	194.2 – 1598.9
$T_{w,i,evap}$	°C	8.3 – 15.9	6.9 – 12.4	8.5 – 14.7	9.4 – 15.5	8.1 – 11.8	8.8 – 14.5	4.8 – 26.3
$T_{w,o,evap}$	°C	2.7 – 10.3	2.8 – 6.1	2.6 – 5.8	3.3 – 9.1	3.1 – 5.8	2.9 – 5.6	2.2 – 13.5
$h_{a,AMB}$	kJ/kg	39.1 – 63.5	32.3 – 65.5	17.8 – 54.2	42.4 – 60.7	34.1 – 63.6	19.8 – 48.2	9.7 – 62.5